ENGINEERING THE PERFORMANCE OF MIXED MATRIX MEMBRANES FOR GAS SEPARATIONS

A Dissertation
Presented to
The Academic Faculty

By

Shu Shu

In Partial Fulfillment
Of the Requirements for the Degree
Doctor of Philosophy in the
School of Chemical & Biomolecular Engineering

Georgia Institute of Technology

December 2007

ENGINEERING THE PERFORMANCE OF MIXED MATRIX MEMBRANES FOR GAS SEPARATIONS

Approved by:

Dr. William Koros, Advisor
School of Chemical & Biomolecular Engineering
Georgia Institute of Technology

Dr. Christopher Jones
School of Chemical & Biomolecular Engineering
Georgia Institute of Technology

Dr. Dennis Hess
School of Chemical & Biomolecular Engineering
Georgia Institute of Technology

Dr. Carson Meredith
School of Chemical & Biomolecular Engineering
Georgia Institute of Technology

Dr. C. P. Wong
School of Material Science & Engineering
Georgia Institute of Technology

Date Approved: September 17, 2007

A Dedication to
My Dearest Parents

ACKNOWLEDGEMENTS

There are many people I would like to thank without whom I can never become the person who I am today. My parents, who give me the best family I could ever ask, always offer unconditional love, support and encouragement that have led me to every stage of my life. I can not find the words that truly describe how grateful I am to them. This degree is as much theirs as it is mine. My advisor Dr. William Koros, a brilliant and relentless researcher, sets a superb role model for me to follow. I feel grateful for his invaluable guidance, encouragement and trust, which inspired me to discover and fulfill things more than I thought I was capable of doing. My gratitude extends to all my committee members, Dr. Dennis Hess, Dr. Christopher Jones, Dr. Carson Meredith and Dr. C. P. Wong for their time and advice. Special thanks are attributed to Dr. Jones who has provided insightful technical suggestions along the way and Dr. Hess for his constant advice and encouragement.

I must also thank those who have helped my research in the past four years. Appreciation is credited to Dr. Brent Carter (XPS), Drs. Johannes Leisen and Les Gelbaum (NMR), Dr. Mukherjee (XRD) and Lingbo Zhu (SEM) for assistance with equipment techniques. Dr. Steve Miller (ChevronTexaco) and Dr. Sudhir Kulkarni (Medal) are appreciated for their helpful advices. The funding support from Medal L.P. is greatly acknowledged.

It has been a tremendous experience to work within Koros research group, where intellectual reciprocation and mutual assistance are highly respected and well conducted. Credit is due to past group members Rajiv Mahajan and Ted Moore for their excellent

work on mixed matrix membranes. Ted Moore and Alexis Hillock are specially thanked for teaching me around the lab and answering my questions with great patience. I must also acknowledge Shabbir Husain for generously sharing his discoveries and providing extensive technical opinions at any time. Jason Williams, Raymond Chafin, Adam Kratochvil, JR Johnson are always willing to lend a hand. There are many more to thank, too numerous to mention all, from whom I have received help and learnt substantially. Four years is far too short a time to work with such a team of excellent people. I wish the rich tradition of Koros family will continue to be passed down to future group members.

I am blessed with wonderful friends without whom graduate school would not have been much a joyful journey. Yeny Hudiono and Stephanie Barth, who I met in my first-year class and became best friends with since, are greatly acknowledged for their friendship. They are always there for me no matter at the happiest or saddest moments. I will also miss the pleasant time at the lunch, night outs and travel trips with Yeny, Stephanie, Mariefel and Suchitra. JR Johnson, who is a coworker as well as a great friend, owns my special gratitude. I'll certainly remember our nice dinners, enjoyable conversations and his help during my difficult time. In addition, Imona Omole, Ryan Adams, Mayumi Kiyono made grocery shopping a lot more fun with their accompany. Last but not the least, my friends in China, Kevin Chen, Xiang Kang and Jia Chen, thank you all for being life-long friends and care and encourage me over thousands of miles.

To those who have helped, impacted and inspired me, thank you so much for making my life an extraordinary venture so far. I truly wish you all have a wonderful life blessed with health and happiness.

TABLE OF CONTENTS

LIST OF TABLES

LIST OF FIGURES

SUMMARY

Mixed matrix membranes that comprise domains of organic and inorganic components are investigated in this research. Such materials effectively circumvent the polymeric 'upper bound trade-off curve' and show properties highly attractive for industrial gas separations. Nevertheless, lack of intrinsic compatibility between the organic polymers and inorganic fillers poses the biggest challenge to successful fabrication of mixed matrix membranes. Consequently, control of the nanoscale interface between the sieve and polymer has been the key technical challenge to the implementation of composite membrane materials. The overarching goal of this research was to devise and explore approaches to enhance the performance of mixed matrix membranes by properly tailoring the sieve/polymer interface.

In an effort to pursue the aforementioned objective, three approaches were developed and inspected: (i) use of silane coupling agents, (ii) hydrophobizing of sieve surface through alcohol etherification reactions, and (iii) a two-step modification sequence involving the use of a Grignard reagent. A comparison was drawn to evaluate these methodologies and the most effective strategy (Grignard treatment) was selected and further investigated.

Successful formulation and characterization of mixed matrix membranes constituting zeolite 4A modified via the Grignard treatment are described in detail. Membranes with impressive improvements in gas separation efficiency and mechanical properties were demonstrated. The basis for the improvements in polymer/sieve compatibility enabled by this specific process were proposed and investigated.

A key aspect of the present study was illuminating the detailed chemical mechanisms involved in the Grignard modification. Systematic characterization and carefully designed experiments revealed that the formation of distinctive surface structures is essentially a heterogeneous nucleation process, where $Mg(OH)_2$ crystals grow from the nuclei previously extracted from zeolites.

In addition to the main work, discovery of sonication-induced dealumination of zeolites was made during the systematic exploration of Grignard chemistry. The new procedure employing sonication can potentially be applied to prepare zeolites with a variety of Si/Al ratios under relatively mild conditions.

The last part of this thesis focused on development of a technique to generalize the highly specific Grignard treatment to inorganic materials other than zeolite 4A. This work delivered composite membranes with improved interfacial adhesion. Moreover, research revealed the effect of surface nuclei density on the ultimate morphology of deposited nanostructures and how different surface morphologies influence polymer/filler interaction in composite membranes. Methods were devised to tailor the morphologies of such structures in order to optimize adhesion enhancement. The acquired results demonstrated the potential of extending this modification process to a broad domain of materials and render it a general methodology for interfacial adhesion promotion.

CHAPTER 1
INTRODUCTION AND MOTIVATION

1.1 MEMBRANE-BASED GAS SEPARATION

Gas separation using membranes has emerged as a rapidly growing, commercially viable alternative to traditional methods of gas separation such as adsorption, absorption, and cryogenic distillation. In 1977, DuPont produced melt spun polyester hollow fibers with inside diameters of 36 μm for high pressure hydrogen applications.[1] Soon after DuPont's withdrawal from gas separation field, Permea (now a division of Air Products) launched its hydrogen-separating Prism membrane in 1980.[2] These are examples of the early large-scale industrial applications of gas separation membranes. Since then, membrane-based gas separation has grown into a $150 million/year business. Over the past decade or so, membranes have entered territories that were previously dominated by more traditional separation techniques, and substantial growth in the near future is very likely to take place. Even in many cases where membranes have not obsoleted conventional technologies, hybrid systems based on membranes combined with one of more traditional techniques are being accepted as attractive options.[3,4] Currently, the most widely practiced commercial gas separations using membranes involve a few major fields as will be introduced below.

1.1.1 Air Separation

The separation of air can be divided into two categories: nitrogen enriched air (NEA) and oxygen enriched air (OEA). Nitrogen-enriched air is used for inerting applications. For example, blanketing airline fuel tanks with nitrogen can virtually eliminate the chance of sparks igniting fuel vapors. Food industry uses nitrogen for purging, filling,

modified atmosphere packaging and controlled atmosphere storage. Selected applications of oxygen-enriched air include enhanced efficiency of high-temperature furnaces; life-support systems used in emergencies or long-term treatment of patients with respiratory disorders; conversion of hydrogen sulfide into sulfur oxide in Claus desulfurizing plants and intermittent catalyst regeneration in refineries.

Industrial membrane air separation is based primarily on the use of composite and asymmetric hollow fiber technology using polymers that permeate oxygen faster than nitrogen. In principle, it is possible to use membranes to produce both oxygen and nitrogen. In practice, with current membrane properties, it is much easier to produce high-purity nitrogen than high-purity oxygen since nitrogen already takes up 79% of air. Hence membranes have been confined largely to nitrogen production.[5] Cryogenic distillation and Pressure Swing Adsorption (PSA) dominate high purity production or where larger flow rates are required, while membranes are used to produce relatively low purity nitrogen (< ~99%).[6] In order to achieve broader penetration and growth (via higher purity or better economics), higher membrane selectivity, coupled with equal or greater productivity, is required.

1.1.2 Hydrogen Separation

Hydrogen is used in large quantities for petroleum refining and upgrading, petrochemical processes, chemical processes and production of alternate fuels. One of the first large-scale commercial implementations of membranes for gas separation was the separation of hydrogen from nitrogen, methane, and argon in ammonia purge gas streams, which is an ideal application for membranes.[5] Hydrogen is highly permeable compared to other gases so selectivities and fluxes are high. A similar application is

hydrogen/carbon monoxide ratio adjustment in syngas plants.[7] An even larger utilization of hydrogen-permeable membranes exists for hydrogen recovery in refineries. The demand for hydrogen in refineries is increasing because of increased environmental regulation and heavier crude. Nonetheless, fouling, plasticization and condensation of hydrocarbon vapors on the membrane surfaces pose challenges for applications of membranes in refineries. Also higher membrane selectivity, combined with equal or greater productivity is highly desirable.

1.1.3 Natural Gas Treatment

Raw natural gas varies substantially in composition from source to source. Methane is usually the major component, typically 75-90% of the total. In addition, the gas contains undesirable impurities: water, carbon dioxide, nitrogen, and hydrogen sulfide. Consequently, all natural gas requires some treatment, and about 20% requires extensive treatment before delivery to the pipeline.[8] Typical U.S. natural gas pipeline specifications are reported in Table 1.1. The opportunity for membranes lies in processing the gas to meet these specifications. The total worldwide market for new natural gas separation equipment is probably $5 billion/year, making natural gas purification by far the largest industrial gas separation application. Currently, membrane processes have less than 1% of this market, almost all for the removal of carbon dioxide. Nonetheless, the small foot prints of membrane units make them particularly attractive to small-scale applications such as off-shore gas separation platforms. One of the biggest problems in this field is that the presence of high partial pressures of carbon dioxide is known to cause plasticization of membranes. The development of plasticization resistant membrane

materials poses another technical challenge to widespread commercialization of such membranes.

Table 1.1 Composition specifications for natural gas for delivery to the U.S. national pipeline grid [9]

Component	Specification
carbon dioxide	<2%
water	<120ppm
hydrogen sulfide	<4ppm
C_{3+} content	950-1050 Btu/scf
total inert gases (N_2, CO_2, He, etc.)	<4%

There are certainly many other fields in which gas separation membranes can be potentially implemented, such as helium recovery from gas wells; dehumidification of various industrial streams such as air, nitrogen or hydrocarbons, etc. More detailed application list can be found elsewhere.[7]

1. 2 MEMBRANE MATERIALS

1.2.1 Polymeric Membranes

The ideal polymer for use as a gas separation membrane should be easily converted into cost-effective membrane forms that offer simultaneously high productivity, selectivity, and durability. These intrinsic qualities will dictate performance characteristics of the separation system. Early research on gas permeation in polymers focused on rubbery [10], semicrystalline[11,12], and a few glassy (with relatively low glass transition temperature, T_g) polymers[13]. Interest in rigid plastic containers like carbonated

beverage bottles during the late 1960s and early 1970s along with continued scientific curiosity fueled research on glassy polymers having relatively high T_g.[14-17] Today U.S. membrane-based gas separation systems employ several polymeric materials:[18] polysulfone, brominated polycarbonate, cellulose acetate, polydimethylsiloxane, ethylcellulose and polyimide.

The commonly used polymers are glassy with high T_g and can be spun into asymmetric hollow fibers to maximize the surface area to volume ratio as well as the flux through the membranes. Nonetheless, it was reported by Robeson in 1991 that the performance of polymers is limited by an upper-bound tradeoff curve as illustrated in Figure 1.1. The plot clearly shows the strong inverse relationship between permeability and selectivity. Development of improved membrane materials is a continuing topic of research, but movement of the upper bound has slowed considerably since 1991.

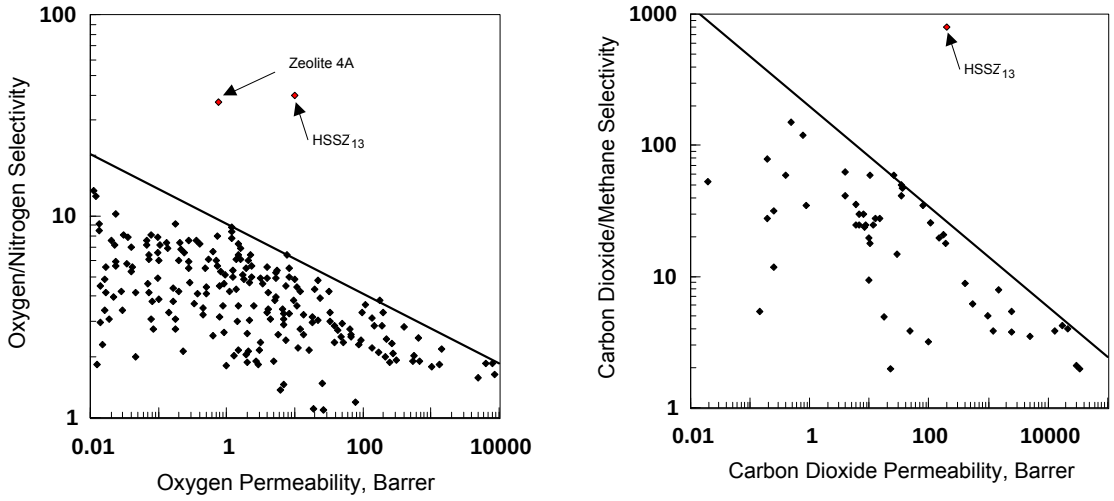

Figure 1.1 Upper-bound trade-off curves (1991) for the (a) oxygen – nitrogen and (b) carbon dioxide – methane gas pairs. Adapted from Ref.19. Also shown are the properties for the molecular sieving materials used in this work.

1.2.2 Zeolite Membranes

Zeolites are crystalline structures made up of "T-atoms" which are tetrahedrally bonded to each other with oxygen bridges. Because of the regularity of the crystalline structure and the pores with Ångstrom size dimensions, these crystals, when grown together to form a membrane, can operate as separation devices for gas and liquid mixtures. Diffusion in zeolites occurs by a pore 'window' moderated mechanism.[20] In general perfectly sized pores can provide a more selective discrimination than is possible to be exhibited by a polymer due to its random thermal fluctuations. The size or shape discrimination ability is the basic feature for gas molecules to preferentially transport through zeolites. The properties of commonly used zeolites are listed in Table 1.2.

Zeolite membranes have been shown to have exceptional selectivities for a number of important separations. In addition they have advantages over other types of membranes in that they are highly stable under thermal cycling, high temperatures, and harsh physical and chemical environments which other membranes cannot withstand. However, the poor mechanical properties of such membranes and the high cost of production limit the application of zeolites for large-scale industrial processes.

Table 1.2 Properties of commonly used zeolite types (adapted from Ref. 21)

Zeolite	Chemical Structure	Si/Al ratio	Pore Aperture (Å)	Dimension
LTA(3A, 4A, 5A)	$\{Na_{12}(Al_{12}Si_{12}O_{48}) \cdot 27H_2O\}_8$	1	3.2 – 4.3	3D
Silicalite	Pure silica from ZSM	>500	5.3 × 5.6 – 5.1 × 5.5	2D
ZSM-5	$Na_n(Al_nSi_{96}\text{-}nO_{192}) \cdot \sim 16H_2O$	10-500	5.3 × 5.6 – 5.1 × 5.5	2D
Faujasite (KY, 13X)	$(Na_2,Ca,Mg)_{29}[Al_{158}Si_{134}O_{384}] \cdot 240H_2O$	1.5-3	7.4	3D
Mordenite	$Na_8[Al_8Si_{40}O_{96}] \cdot 24H_2O$	5	6.5 × 7.0 – 2.6 × 5.7	2D

1.2.3 Mixed Matrix Membranes

The concept of mixed matrix membranes was proposed to effectively circumvent the Robeson upper bound trade-off curve. Mixed matrix membranes are composed of a molecular sieving phase, such as zeolites or carbon molecular sieves, dispersed in a continuous polymer matrix. The typical morphologies of a mixed matrix dense film and hollow fiber membrane are demonstrated in Figure 1.2. Such membranes are anticipated to combine the superb separation efficiency of zeolites with the low cost and ease of manufacturing of polymer membranes. Ideally, a mixed matrix membrane should have enhanced selectivity over the neat polymer phase. Nevertheless, previous researchers have discovered several undesirable morphologies at the polymer-sieve interface, which greatly affect the performance of composite membranes in undesirable ways.[22] Subsequent discussions will elaborate these non-ideal morphologies.

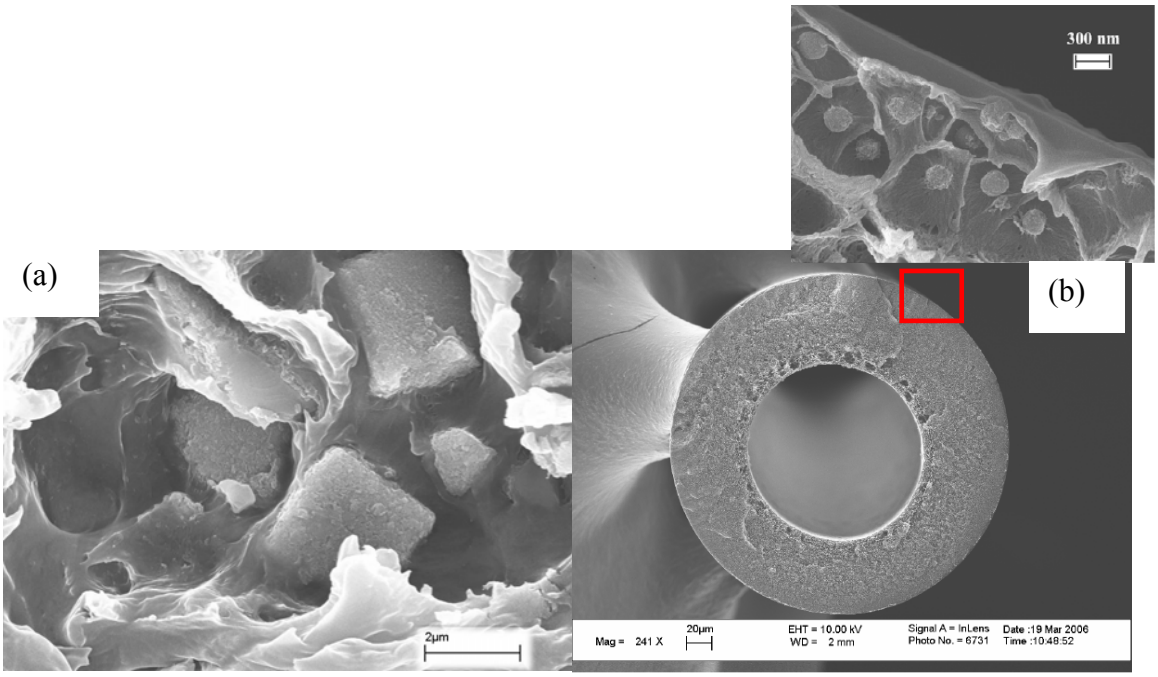

Figure 1.2 SEM micrographs of mixed matrix membranes: (a) Mixed matrix dense film of Ultem® containing zeolite 4A; (b) Mixed matrix hollow fiber of Ultem® with zeolite 4A dispersed in the skin layer.

1.3 NON-IDEALITIES IN MIXED MATRIX MEMBRANES

The inorganic-organic interface is clearly important in a composite material. Indeed the performance of a membrane could be greatly impacted by any change at the interfacial region due to the extremely small size of gas molecules and large percentage of interface present in a given membrane. Study has identified four undesirable morphologies at the polymer-sieve interface, which need to be overcome in order to create successful mixed matrix membranes. The signature gas transport properties of these non-idealities are described below and depicted in Figure 1.3.

1.3.1 Matrix Rigidification

Confinement of polymer chains to a solid surface is an important phenomenon that affects properties of organic-inorganic composites and is not accounted for in regular models. In mixed matrix membranes, this effect is characterized by reduced permeability at the interface and therefore decreased overall permeability of the whole membrane. It is believed to be caused by immobilization of polymer chains due to adsorption and/or chemical tethering on a solid surface. This morphology is undesirable because it negatively affects the productivity of a membrane; however, if it affects both penetrants in a similar manner, selectivity enhancement still occurs consistent with the expectation based on the Maxwell model.

1.3.2 Sieve in A Cage

The term ‘sieve-in-a-cage’ has been coined to describe the voids present at the polymer-sieve interface. The SEM image on the upper-left corner of Figure 1.3 depicts zeolite 4A dispersed in Ultem® (a polyether imide), which is an example of ‘sieve-in-a-cage’ morphology. This phenomenon is highly detrimental to the membrane performance

since the void is much more permeable than the zeolite and gas molecules bypass the zeolite by taking the path of least-resistance. The net result of such morphology is to cause a higher permeability than the neat polymer with an equivalent selectivity.

1.3.3 Leaky Interface

A 'leaky interface' is essentially a special case of 'sieve-in-a-cage' category, with an effective void or high free volume region of sufficient extent to enable partial and less selective bypass of the two gases. This non-ideality leads to actual loss of separation efficiency, since it adds a significant non-selective resistance that undesirably affects the most permeable component, as opposed to the negligible non-selective resistance present in the 'sieve-in-a-cage' situation. Knudsen diffusion or sorption-diffusion transport with extremely low selectivity is dominant at this dimension in the interfacial region. As a result, the overall membrane exhibits a somewhat higher permeability and lower selectivity than the neat polymer.

1.3.4 Plugged or Partially Plugged Sieves

This case is characterized by a permeability lower than the neat polymer with essentially no change in selectivity. It could be caused by the use of an impermeable zeolite (e.g. zeolite 3A) or by certain strongly held penetrants (e.g. water, organic solvents and silane coupling agents) that prevent the gas molecules from permeating through the internal pores of the sieves. Zeolites have lost selective ability under such circumstances and simply add an additional resistance to both penetrants. Gas sorption experiment is an excellent technique to probe this morphology by analyzing the dynamic rate and equilibrium sorption capacity of the molecular sieves.

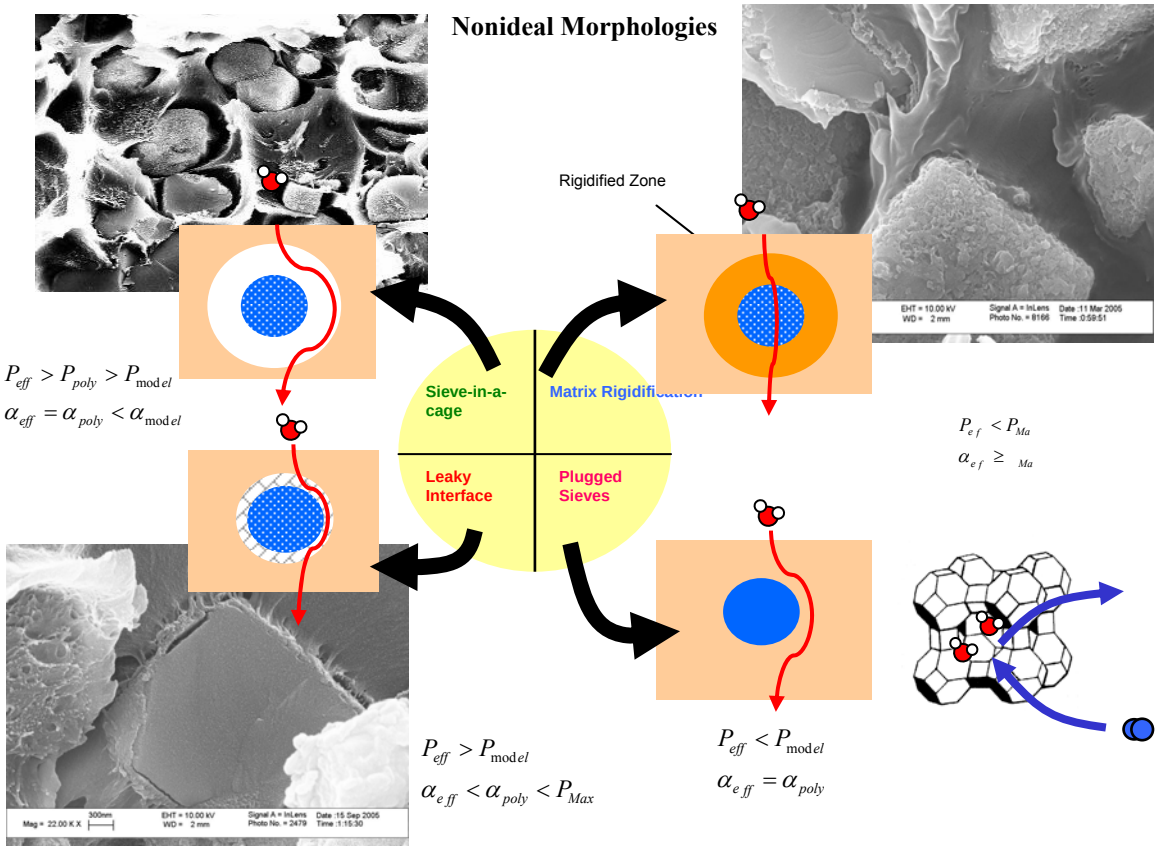

Figure 1.3 Illustration of the morphologies and gas transport properties of non-idealities in mixed matrix membranes

1. 4 RESEARCH OBJECTIVES

Among the non-idealities listed in the preceding discussions, the lack of interfacial compatibility is the most commonly encountered and thus most prominent challenge in mixed matrix membranes. Essentially, control of the nanoscale interface between the sieve and polymer in a composite membrane represents the key technical hurdle to be overcome in transitioning from a lab-scale to a large manufacturing scale. Therefore the overarching goal of this research is to ***devise and explore approaches to enhance the performance of mixed matrix membranes by properly tailoring the sub-optimal interface.*** Different strategies will be attempted and an optimal approach will be selected

and investigated in depth. This potential methodology will be extended and applied to different inserts to form a variety of mixed matrix membranes.

The objectives of the present work are:

1) Investigate different sieve surface modification strategies to promote interfacial adhesion in mixed matrix membranes and identify the most effective approach.
2) Inspect the most effective surface modification method with zeolite 4A and explore the underlying mechanisms for improvements in membrane performances.
3) Illuminate the detailed chemistry involved in the aforementioned zeolite surface treatment and propose methodologies to generalize this method.
4) Extend the surface modification technique to inorganic materials other than zeolite 4A to form a broader array of composite membranes with defect-free interfaces.

1.5 DISSERTATION OUTLINE

Chapter two provides theory and background essential to the understanding of gas transport through membranes. Chapter three summarizes materials and experimental procedures used throughout this work. Chapter four is dedicated to the variety of approaches developed in this research to promote interfacial adhesion in mixed matrix membranes. Chapter five presents the characterization results of mixed matrix membranes incorporated with zeolite 4A that are modified via the most effective Grignard treatment. Chapter six elucidates the underlying chemical mechanism involved in the complex Grignard surface treatment. Chapter seven features the discovery of how

sonication can induce the dealumination reaction of zeolites near room temperature. Chapter eight addresses the attempts to extend the Grignard surface treatment to inorganic materials other than zeolite 4A, hence render it a generalized methodology for inorganic surface modification. Finally, conclusions and recommendations for future research will be made in chapter nine.

1.6 REFERENCES

[1] C.R. Antonson, R.J. Gardner, C.F. King and D.Y. Ko, Analysis of gas separation by permeation in hollow fibers, *Ind. Eng. Chem., Proc. Des. Dev*. **1977**, *16*, 463.

[2] Maclean, D. L.; Bollinger, W. A.; King, D. E.; Narayan, R. S. *Recent Developments in Separation Science*; Li, N. N.; Calo, J. M. Eds.; CRC Press: Boca Raton, FL, 1986.

[3] Koros, W. J.; Flemming, G. K. *J. Membr. Sci*. **1993**, *83*, 1.

[4] Paul. D. R.; Yampol'skii, Y. P. *Polymeric Gas Separation Membranes*. CRC Press: Boca Raton, FL, 1994

[5] Baker, R. W. *Ind. Eng. Chem. Res.* **2002**, *41*, 1393.

[6] Baker, R. W. *Membrane Technology and Applications, 2nd edition*. John Wiley & Sons: Chichester, England, 2003.

[7] Lee, E.K.; Koros, W. J. *Membranes, synthetic, applications, in Encyclopedia of polymer science and technology*. Academic Press: New York, 2002.

[8] Tabe-Mohammadi, A. *Sep. Sci. Tech*. **1999**, *34*, 2095.

[9] Lee, A.L.; Feldkirchner, H. L.; Stern, S. A.; Houde, A. Y.; Gamez, J. P.; Meyer, H. S. *Gas Sepration Purification* **1995**, *9*, 35.

[10] Durgaryan, S. G.; Yampol'skii, Y. P. *Neftekhimia* **1983**, *23*, 579.

[11] Williams, M. L.; Landel, R. F.; Ferry, J. D. *J. Am. Chem. Soc*. **1955**, *77*, 3701.

[12] Simha, R. Boyer, R. F. *J. Chem. Phys.* **1962**, *37*, 1008.

[13] Koros, W. J.; Chern, R. T. in *Handbook of Separation Process Technology*, Rousseau, R. W. Wiley: New York, 1987.

[14] Lee, W. M. *Polym. Eng. Sci*. **1980**, *20*, 65.

[15] Maeda, Y.; Paul, D. R. *J. Polym. Sci. Part B Polym. Phys*. **1987**, *25*, 1005.

[16] Paul. D. R.; Maeda, Y. *J. Membr. Sci*. **1989**, *40*, 109.

[17] Petropoulos, J. *J. Membr. Sci*. **1990**, *53*, 229.

[18] Yampolskii, Y.; Pinnau, I.; Freeman, B. D. *Materials Science of Membranes for Gas and Vapor Separation*. John Wiley & Sons: Chichester, England, 2006.

[19] Robeson, L.M. *J. Membr. Sci*. **1991**, *62*, 165.

[20] Breck, D.W., *Zeolite Molecular Sieves: Structure, Chemistry, and Use*. Robert E. Krieger Publishing Co, Inc: Malabar, FL, 1974.

[21] Meier, W. M.; Olson, D. H. *Atlans of Zeolite Structure Types. 3rd edition*. London: Butterworths, 1992.

[22] Moore, T. T.; Koros, W. J. *J. Mole. Stru*. **2005**, *739*, 87.

CHAPTER 2
THEORY AND BACKGROUND

This chapter introduces concepts essential to understanding gas permeation through mixed matrix membranes. The first section briefly reviews basic membrane transport properties, diffusion and sorption of gas molecules through polymeric media as well as molecular sieves. Subsequent discussion will focus on strategies for modeling the complex behavior of mixed matrix materials. Further, the criteria to select appropriate materials for mixed matrix development will be outlined in a later section. Finally, a literature review on the studies to improve the performance of mixed matrix membranes will be provided to demonstrate the state-of-the-art and key challenges to be overcome.

2.1 FUNDAMENTAL TRANSPORT THEORY

The success of gas separation processes based on permselective membranes ultimately depends on the gas transport properties (notably permeability and intrinsic permselectivity) of the membrane material. This section intends to present the basic parameters of permeation, as well as the fundamental theories related to the sorption and diffusion of gas through polymeric and molecular sieving materials. These concepts build the basis for the understanding of membrane related gas separation.

2.1.1 Gas Permeation Parameters

In principle, gas separation can be performed using membranes functioning on one of three general transport mechanism: Knudsen diffusion, solution-diffusion, or molecular sieving.[1] As a practical material, however, solution-diffusion based gas transport through

polymeric membranes is used exclusively in current commercial devices. The 'solution-diffusion' model, formulated in the 19th century, is grounded in the works of J. K. Mitchell[2], T. Graham[3] and S. von Wroblewski[4], who demonstrated that the presence of microscopic open pores or capillaries was not a prerequisite for mass transfer through polymeric films, such as natural rubber. Currently the most widely accepted theory is that gas molecules at the high-concentration (high-pressure) side of the membrane dissolve in the membrane material and diffuse through the membrane along a concentration gradient to the low-concentration (low-pressure) side of the membrane. It is assumed that the gas phases on either side of the membrane are in thermodynamic equilibrium with their respective membrane interfaces, and that the interfacial sorption and desorption processes are rapid compared to the rate of diffusion through the membrane. The 'permeability' of penetrant *i* is a key parameter in membrane performance characterized via [5]:

$$P_i = \frac{Flux_i \cdot \ell}{\Delta p_i} \qquad (2.1)$$

Where the permeability, ***P***, is indicative of a material's productivity and is equal to the diffusive flux of a particular gas through a membrane normalized by the partial pressure driving force of the gas, Δp_i, and the thickness of the membrane, ℓ. Permeability is traditionally given in units of Barrer, where:

$$1 Barrer = 1 \times 10^{-10} \frac{cc(STP) \cdot cm}{cm^2 \cdot s \cdot cmHg} \qquad (2.2)$$

Permeability coefficients of common gases in polymers span a range of more than seven orders of magnitude, from 10^{-3} to 10^4 barrer or more.

When the downstream pressure is much less than the upstream pressure and Fickian diffusion is the rate limiting step in penetrant transport, permeability is written as[6]:

$$P_i = D_i \times S_i \qquad (2.3)$$

Where *S*, the apparent solubility coefficient, indicates how much gas can be taken up by the membrane at equilibrium with a given gas fugacity; and *D* is a measure of the mobility of the penetrant molecules in the membranes.[7] These two concepts will be discussed in detail in the subsequent session. Equation 2.3 emphasizes that high permeability coefficients can result from large *D* values, large *S* values, or both. For example, some so-called 'fast' (i.e. high-permeability) gases display (i) large diffusion coefficients (e.g. He or H_2), or (ii) high solubility coefficients (e.g. CO_2) or (iii) both (e.g. H_2O).

Another key characteristic of gas separation membranes is their selectivity which is a measure of a membrane's ability to differentiate between molecules of type A and type B. The ideal selectivity, $\alpha_{A/B}$, is defined as follows[8]:

$$\alpha_{A/B} = \frac{P_A}{P_B} \qquad (2.4)$$

Commonly, the more permeable gas is taken as A, so that the selectivity varies from 1 to infinity. A perfect molecular sieve would have an infinite selectivity. Many polymers are not very selective towards particular gas pairs and have selectivities near 1. When permeability is presented by equation (2.3), selectivity can be further expressed as:

$$\alpha_{A/B} = \left[\frac{D_A}{D_B}\right] \times \left[\frac{S_A}{S_B}\right] = \alpha_{AB}^{D} \alpha_{AB}^{S} \qquad (2.5)$$

The ratio (D_A/D_B) is referred to as the diffusivity selectivity α_{AB}^{D}, reflecting the different molecular sizes of the gases. The ratio (S_A/S_B) is viewed as solubility selectivity α_{AB}^{S},

primarily reflecting the relative condensabilities of the gases for cases of negligible nonspecific interactions between the gas and polymer.

When gas mixtures permeate across a membrane, the presence of one gas can, in some circumstances, influence the transport of other gases in the membrane. In such systems, the ideal selectivity, determined from pure-gas measurements, can be a rather crude (i.e. inaccurate) measure of the 'actual' selectivity, or separation factor, of a membrane. The separation factor, α^*_{AB}, determined from the ability of a membrane to separate a binary feed gas mixture, is defined as follows[8]:

$$\alpha^*_{AB} = \frac{y_A / y_B}{x_{A/} x_B} \qquad (2.\ 6)$$

Where y_A and y_B are the mole fractions of the components produced in the permeate, and x_A ad x_B are their corresponding mole fractions in the feed.

2.1.2 Gas Sorption

2.1.2.1 Sorption in Polymers

The equilibrium solubility coefficient of a gas in a polymer is the ratio of the concentration of gas dissolved in the polymer at equilibrium to the pressure of gas (or partial pressure in the case of mixtures) in the contiguous gas phase[9]:

$$S = \frac{C}{p} \qquad (2.\ 7)$$

The solubility coefficient *S* is evaluated at the upstream face of the membrane.

There are a large number of models to describe equilibrium sorption in glassy polymers presented in the literature; however, the most commonly used model is the dual mode sorption model.[10] The dual mode model is widely used because of its proven

performance in many penetrant/polymer systems, its mathematical simplicity, and its well-founded fundamental basis. The dual-mode sorption model considers the glassy solid to consist primarily of an equilibrium densified matrix with a small volume fraction of uniformly distributed nonequilibrium, molecular-scale packing disruption or gaps throughout the matrix. This model has proved to be very useful for interpreting a wide spectrum of phenomena including pure component and multi-component permeation and sorption and penetrant-induced dilation in gas–glassy polymer systems. The dual mode model can be written analytically for a penetrant indicated by subscript A, in terms of the sum of a Henry's law expression for C_D and a Langmuir expression for C'_H: [11]

$$C_A = C_{D,A} + C_{H,A} = k_{D,A} p_A + \frac{C'_{H,A} b_A p_A}{1 + b_A p_A} \qquad (2.8)$$

where k_D is the Henry's law coefficient characterizing sorption of the penetrant into the densified equilibrium matrix of the glassy polymer; C'_H is the Langmuir sorption capacity, which characterizes sorption into the non-equilibrium excess volume associated with the glassy state, and b is the Langmuir affinity parameter; p_A is the penetrant partial pressure. In this model, two 'populations' of sorbed species, in local chemical equilibrium with one another, are envisioned: those in long-lived, non-equilibrium free-volume elements and those dissolved in more densely packed regions within polymers.

In general, gas solubility increases with penetrant condensability[12]. In a series of penetrants, the critical temperature T_c, increases (roughly) as the size of the diffusing molecule increases, hence solubility coefficient often increases as the penetrant size increases. This provides the basis for the phenomenon that solubility selectivity often

favors larger, more condensable gas molecules, as opposed to diffusivity selectivity, which favors smaller penetrants. The latter will be elaborated in the next section.

2.1.2.1 Sorption in Zeolites

Sorption in molecular sieving materials is similar to the specific sorption in the microcavities of glassy polymers. These materials are rigid, and thus can only accommodate molecules within certain fixed sites. The simplest and most commonly used approach to describe sorption in these materials is based on the Langmuir isotherm[13]. The sorbed molecules are ideally assumed to be held at definite localized sites, each of which can accommodate only one molecule. The isotherm assumes dynamic equilibrium between the rates of adsorption and desorption. Thus the rate of sorption in zeolites is inversely proportional to the fractional coverage of these sites. Therefore, such materials show high sorption tendency at low concentrations (low fractional coverage) and lower sorption tendency at high concentrations (high fractional coverage). Once all the sites are saturated no more sorption occurs even with increasing concentration.

2.1.3 Gas Diffusion

2.1.3.1 Diffusion in Polymers

From the microscopic viewpoint, micromolecular diffusion is commonly regarded as a succession of random molecular jumps[14]. More specifically, a sorbed gas molecule is normally trapped in a certain position by the surrounding polymer segments (initial ground state); until such time as the said segments happen, as a result of thermal fluctuations, to be displaced in such a way that a hole of suitable size opens up for the gas molecule to jump to a new equilibrium position. The jump is completed by "closure" of

the hole left behind by the displaced gas molecule, so that the latter is now trapped in its new position (final ground state). A schematic of this mechanism is illustrated in figure 2.1.

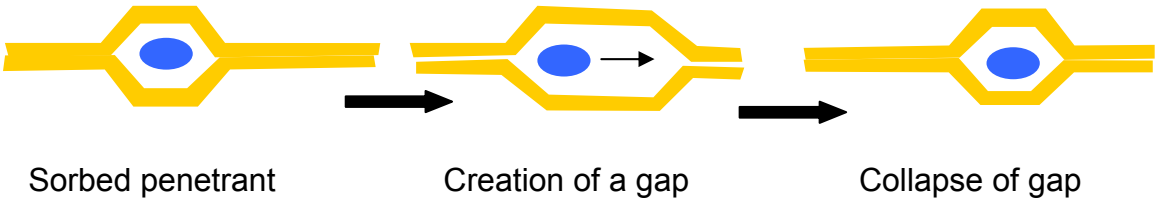

Figure 2.1 Schematic of a gas molecule's diffusion in a polymer matrix.

Consider a polymer (*P*)-penetrant (*A*) system at infinite dilution ($C \rightarrow 0$, $D=D_T=D_0$) and a given *T*, random walk theory yields[15]

$$D_0 = \kappa \nu \lambda^2 \qquad (2.9)$$

Where κ is a geometrical constant (=1/6 for a simple homogeneous random walk), λ is the mean jump length, and ν is the frequency of jumping, which corresponds to the frequency with which a hole of the minimum required size can open up in the polymeric medium at the appropriate location.

A larger penetrant molecule will find fewer opportunities to execute diffusional jumps because the probability of opening the gaps needed between molecules is reduced. Therefore, diffusion coefficients generally increase as gas molecule size decreases. Nonetheless, the size-sieving ability of polymers, can be quite different for polymers in the rubbery and glassy states. All other factors being equal, for polymers above their glass transition temperatures (T_g), *D* is often less sensitive to penetrant size than in traditional, stiff-chain, low-free-volume glassy polymers. This is because polymers with higher molecular chain mobility (i.e. lower T_g) tend to provide larger and more frequent availability of gaps of sufficient size to accommodate diffusion steps of both large and

small penetrant molecules, which is the basis of their weaker size-sieving ability (i.e. D depends weakly on penetrant size). Low-free-volume, rigid, glassy polymers have very restricted chain motion, which provides small free-volume elements, suitable for selective diffusion steps for small gases. The large disparity in the availability of free-volume elements suitable for small and large penetrants leads to strong size-sieving ability (i.e. a strong dependence of D on penetrant size). However, in addition to the influence of molecular mobility on diffusion coefficients and size-selectivity, there is a substantial influence of free volume on both D and diffusivity selectivity. Diffusivity selectivity increases as the mean size of free volume elements in the polymer decreases. These two effects (chain mobility, as characterized by T_g, and free volume) can oppose or complement one another in rigid packing inhibited glasses so that, for example, materials with higher T_g values, high diffusion coefficients and stronger size-sieving ability can be prepared.[15]

2.1.3.2 Diffusion in Molecular Sieves

Molecular sieving materials rely primarily on size differences to achieve separation. These materials are ultra-microporous, and are believed to be comprised of relatively large cavities interconnected by narrow channels. The penetrant molecules first sorb in the large cavities then continue to diffuse by making random jumps through the interconnecting channels. The diffusion mechanism is illustrated in Figure 2.2. Zeolites are able to discriminate even subtle differences in size and shape, which provides the basis for their superb gas separation efficiency. When one gas molecule is able to traverse the pore structure while the other is precluded due to oversize, the selectivity could ideally reach infinity. Even in cases where both penetrants can enter the micropores, the

larger one may have to forgo some degrees of rotational freedom in order to transit through the well defined crystalline structure, thereby yielding an additional 'entropic selectivity'.[16]

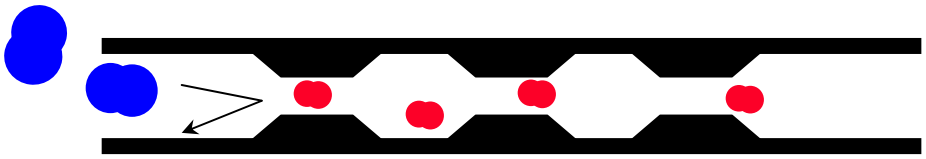

Figure 2.2 Illustration of gas molecules' diffusion through a molecular sieve material.

2.1.4 Polymeric Upper Bound Curve

As mentioned in Chapter 1, the motivation of creating mixed matrix platform is to surpass the polymeric upper bound trade-off curve. From a qualitative viewpoint, the existence of permeability/selectivity trade-off relations is most easily understood from a free-volume standpoint. The most typical way to significantly enhance the permeability of glassy polymers, such as those commonly considered as gas separation polymers, is to change the chemical structure by introducing packing-disrupting units into the polymer backbone, thereby increasing the free volume.[17] As mentioned in the preceding discussions, increasing the free volume usually strongly increases the diffusion coefficients and tends to reduce the diffusivity selectivity, accordingly.[18] The increase in diffusion coefficients increases permeability while the reduction in diffusivity selectivity reduces the overall permselectivity. On the other hand, low free volume polymers with densely packed chains offer relatively lower diffusion coefficients and higher diffusivity selectivity. A more theoretical investigation of the reverse relationship was carried out by Freeman and can be found elsewhere.[18]

2.1.5 Reverse-Selective Membranes

Unlike the aforementioned size-selective membranes, an unconventional membrane type which is called reverse-selective membranes is worth mentioning. It is characterized by selectively allowing larger molecules to permeate through faster than the smaller counterparts. Such performance is typically achieved by harnessing the much higher solubility of the larger component and selecting materials with very weak size-sieving properties, so that the diffusion selectivity, which will always favor the smaller molecule, is not so strong that the polymer is predominately selective for the smaller molecules.[19] In strongly size-sieving polymers (e.g. aromatic polyimides, polyamides, polysulfones, etc.), the diffusion selectivity is so high that it overwhelms the solubility selectivity. However, many rubbery and certain ultrahigh-free-volume glassy polymers have very weak size-sieving ability, thereby solubility selectivity dominates. An example is poly (4-methyl-2-pentyne), PMP, which is a reverse-selective glassy polymer.[20] Because of inherent chain packing characteristics, this material has an intrinsically high free volume. The high free volume reduces the importance of diffusivity selectivity, so that solubility selectivity becomes dominant for the overall separation process. As a result, PMP is more permeable to hydrocarbons relative to supercritical gases (e.g., air, nitrogen or methane).

2.2 MODELING MIXED MATRIX MEMBRANES

An appropriate theoretical description of the permeability of inorganic-polymer composite materials is needed for rational material design research. Such a description must predict the performances of mixed matrix membranes, in order to evaluate experimental results, and guide selections from various candidate materials for optimum

performance. This section addresses the modeling strategies for such composite materials.

2.2.1 The Maxwell Model

There have been substantial investigations in the literature with regard to selecting a proper theoretical model to predict the permeability of composite materials. Petropoulos gave a thorough comparative study of approaches applied to the permeability of binary composite polymeric materials.[21] The most widely employed model is the Maxwell model which was derived by James C. Maxwell in 1867 to analyze steady-state dielectric properties in a conducting dilute suspension of identical spheres.[22] The expression appears to have first been applied to transport properties by Michaels for semicrystalline polymers,[23] and it has been shown to work well for the permeability of two-phase membranes up to moderate dispersed phase loadings.[21, 24] The equation is expressed as:

$$P_{eff} = P_c\left[\frac{P_d + 2P_c - 2\Phi_d(P_c - P_d)}{P_d + 2P_c + \Phi_d(P_c - P_d)}\right] \qquad (2.\ 10)$$

Where P_{eff} is the effective permeability of the entire membrane, Φ_d is the volume fraction of sieves in a particular film, and the subscripts d and c refer to the dispersed phase (zeolites) and continuous phase (polymers), respectively.

This model is based on certain fundamental assumptions. In particular, it is hypothesized that in a dilute dispersion of spheres, inter-particle distances are sufficiently large to ensure that the flow-line pattern around any one sphere is practically undisturbed by the presence of the others. Thus the component phases form well-defined microscopic domains and do not interact with each other or with the penetrant. These assumptions greatly simplify the analysis yet still remain physically meaningful. On the other hand, the hypothesis intrinsically indicates limitations at high sieve volume fractions, since it

neglects interaction between the dispersed particles. However, Petropoulous has noted adequate applicability of this model through out the complete range of solid concentration.[24] Therefore, the Maxwell model provides a very useful theoretical point of reference.

2.2.2 Accounting for Non-Idealities in Modeling Mixed Matrix System

2.2.2.1 Three Phase Maxwell Model

As discussed in an earlier chapter, there are a number of non-ideal morphologies existing at the polymer/sieve interfaces in mixed matrix membranes. These non-idealities are obviously not accounted in the original form of the Maxwell model but need to be properly addressed to correct for the possible deviations from experimental results. In an effort to better predict the mixed matrix performances, Mahajan first proposed the modified form of the Maxwell model, the so-called three phase Maxwell model.[25] The basic concept is to regard the polymer, sieve and interface as a pseudo two-phase system with the matrix polymer being one continuous phase and the combined molecular sieve/interface constituting the other phase, as demonstrated in Figure 2.3. The combined sieve and interface can be envisioned as a 'pseudosieve' phase. The changes caused by the variety of interfacial morphologies are included in the interface properties and will be elaborated later.

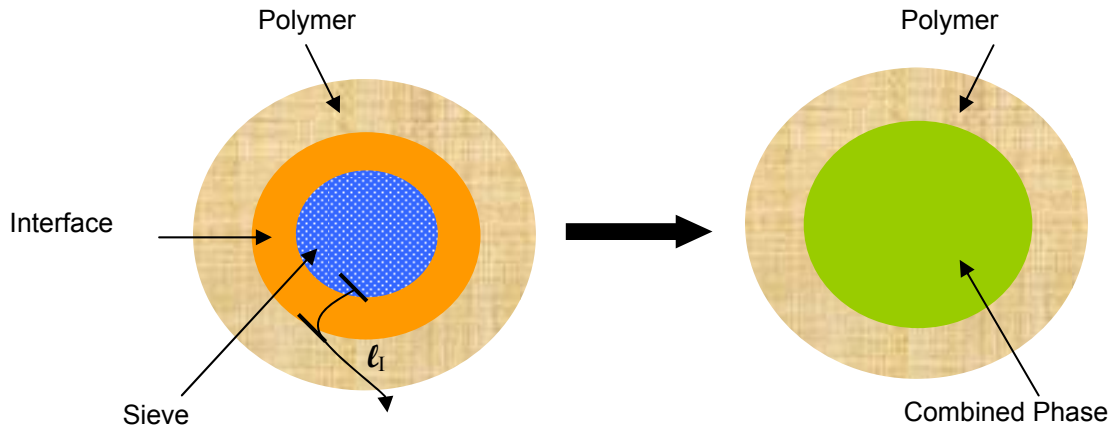

Figure 2.3 Schematic of the three phase system: polymer, interface and sieve are first treated individually; then a pseudo phase is formed by combining the sieve and interface together.

The three phase model involves applying the Maxwell model twice. First, the effective permeability of the 'pseudosieve' phase is calculated by considering the interface as the continuous phase and the molecular sieves as the dispersed phase:

$$P_{eff} = P_I \left[\frac{P_d + 2P_I - 2\phi_S (P_I - P_d)}{P_d + 2P_I + \varphi_S (P_I - P_d)} \right] \qquad (2.\ 11)$$

Where P_d is the permeability of the sieve phase, P_I is the permeability of the interface, and φ_S is the volume fraction of the sieve phase in the combined sieve/interface phase. The volume fraction φ_S is given by the following expression:[26]

$$\varphi_S = \frac{\varphi_d}{\varphi_d + \varphi_I} = \frac{r_d^{\,3}}{(r_d + \ell_I)^3} \qquad (2.\ 12)$$

Where φ_d and φ_I are the overall volume fractions in the membrane of the sieve phase and the interface, respectively; r_d is the dispersed sieve radius; and the interface thickness is denoted ℓ_I, as shown in Figure 2.3. The value of the combined permeability of sieve and

interface phase P_{eff} can be used along with the continuous polymer phase permeability P_c to obtain a predicted permeability P_{3MM} for three phase mixed matrix materials by applying the Maxwell equation a second time:

$$P_{3MM} = P_M \left[\frac{P_{eff} + 2P_c - 2(\varphi_d + \varphi_I)(P_c - P_{eff})}{P_{eff} + 2P_c + (\varphi_d + \varphi_I)(P_c - P_{eff})} \right] \qquad (2.\ 13)$$

Thus if the volume fraction and the permeability of the interface can be estimated, the Maxwell model can be easily extended to more complicated systems. The subsequent discussions will demonstrate how it can be applied to the non-ideal interfacial morphologies.

2.2.2.2 Application of Three Phase Maxwell Model to Sieve-in-a-cage

The permeability of the voids present in 'sieve-in-a-cage' is the product of effective diffusion and solubility coefficients. Assuming the penetrant in the void acts as an ideal gas, the solubility is fixed:[26]

$$S = \frac{C}{p} = \frac{\frac{n}{V}}{p} = \frac{1}{RT} = 0.012 \frac{cm^3 STP}{cm^3 \cdot cmHg} \qquad (2.\ 14)$$

Diffusion of gas through micron-sized void is assumed to fall within the Knudsen regime. Therefore the diffusivity of gas molecules through the void can be calculated using an empirical equation 2.15: [27]

$$D_{A,K} = 9.7 \times 10^{-5} \times r \times \sqrt{\frac{T}{M_A}} \qquad (2.\ 15)$$

where $D_{A,K}$ is the diffusion coefficient in cm^2/s, r is the pore radius in Å (half of the hydraulic diameter), T is the absolute temperature, and M_A is the molecular weight of the penetrant (g/mol).

When the void size decreases to the order of the gas molecules, a special phenomenon referred to as 'leaky interface' dominates the transport properties.[28] It is manifested as permeabilities higher than neat polymers, with selectivities even lower than the polymeric phase. Unlike the micron-sized voids present in typical 'sieve-in-a-cage', these nano-sized voids add a *non-selective* resistance to the flow of gas. In other words, as the permeability of the material increases from that of the pure polymer for both penetrants, the increase in permeability is *relatively more* for the slow gas (nitrogen) than the fast gas (oxygen), leading to lower selectivities. Under this situation, the above expression must be modified to account for the finite size of the penetrant:[29]

$$D_{A,K} = 9.7 \times 10^{-5} \times r \times \sqrt{\frac{T}{M_A}} \times \left[1 - \frac{d_g}{2r}\right] \qquad (2.16)$$

This is the modified form of the Knudsen diffusivity equation, where the additional parameter d_g represents the diameter of the penetrant molecule.

Besides the permeability of the void, the other parameter in the three-phase Maxwell model for "sieve-in-a-cage" is the void size. For mixed matrix membranes with voids larger than a few nanometers, scanning electron microscopy (SEM) can give an estimate of the size of the average voids. However, Ångstrom-sized voids are below the resolution of the SEM, thus equipment with higher resolution such as TEM or AFM could be utilized to determine such void size.

2.2.2.3 Application of Three Phase Maxwell Model to Matrix Rigidification

The modified three phase Maxwell model can be extended to include the rigidification of the matrix surrounding the sieve particles. In this case, there are two tunable parameters, the permeability and the thickness of the interfacial region. The permeability of the polymer in the rigidified region near the sieve is assumed to be decreased by a chain immobilization factor, β:

$$P_I = \frac{P_C}{\beta} \qquad (2.17)$$

The obtained P_I is incorporated into the first application of the Maxwell model as the continuous phase, thus the effective permeability of the combined phase accounts for the rigidified effect. Permeabilities in the amorphous regions of semi-crystalline polymers are treated in a similar manner in literature.[30,31] For the gas molecules tested in this work (O_2, N_2, CO_2, CH_4), β has been found to typically take a value near 3. The thickness of the interface ℓ_I is the other variable in the model, and is more difficult to evaluate. Previous work assumed interface thickness of 0.75μm with 5μm sieves to fit the observed data.[25] AFM could be employed to provide more accurate determination of this parameter. In practice, the model is usually fit to the experimental results with void thickness as an adjustable parameter.

There has been limited literature available on the relationship between the thickness of the interface and the size of the particles. However, it can be envisioned that the size of interface surrounding one particle shrinks with decreasing particle size but the overall polymer/particle interface present in a particular membranes increases. Thus the aforementioned non-ideal morphologies are more pronounced with the smaller sieves.[32]

2.3 CRITERIA FOR MATERIALS SELECTION

The successful development of mixed matrix membranes requires both proper material selection as well as tailoring the properties of the two components to achieve optimal performances. Indeed, the selection of material combinations predetermines the ultimate separation efficiencies of the composite membranes. This has been demonstrated by a number of researchers who attempted to combine a variety of zeolites with rubbery and glassy polymers. Their studies yielded membranes that failed to exhibit selectivity enhancement even in the absence of defects.[33,34]

When designing a mixed matrix system for separating a certain gas pair, the molecular sieving phase must provide precise size and shape discrimination ability to distinguish the molecules. The dimensions of the gas molecules examined in this work are listed in Table 2.1 and 2.2. For example, in order to separate O_2 and N_2, the appropriate sieves must enable excellent size discrimination between O_2 (3.75Å×2.68 Å) and N_2 (4.07Å × 3.09Å). Silicalite which possesses pore size of 5.2Å is a poor candidate for this separation task because the pore dimension is substantially larger than both the gas molecules.[35] The same rule applies to zeolite 5A who does not provide molecular sieving ability in this case.[13] On the other hand, zeolite 4A offers an appropriate structure that allows O_2 to diffuse through unimpeded, while nitrogen must forgo a degree of freedom to transit through the pores.[36] Moreover, zeolites with three-dimensional networks are generally preferred for gas separation since they offer less restricted diffusion paths. Zeolite 4A has a three-dimensional pore network which adds merits to its application in O_2/N_2 separation in addition to the ideal sized framework.

Table 2.1 Kinetic diameters of gas molecules determined from the Lennard-Jones interaction potential[36]

Gas	Kinetic Diameter
O_2	3.46
N_2	3.64
CO_2	3.30
CH_4	3.80

Table 2.2 Molecular dimensions of spherocylindrical O_2 and N_2 molecules determined from the Kihara interaction potential [37]

Gas	Length (Å)	Width (Å)
O_2	3.75	2.68
N_2	4.07	3.09

Matrix polymer selection fixes minimum membrane performance in the absence of defects. Although rubbery polymers, such as silicone rubber, conform more readily to zeolites than glassy polymers, they typically exhibit high permeabilities and low selectivities and therefore push the overall performance of mixed matrix membranes considerably below the upper bond trade-off curve. As a result, the attractive polymer matrix materials are generally glassy with relatively lower permeability and much higher selectivities. Indeed, addition of zeolites or another highly selective media would only improve the already industrially acceptable properties, if defects can be eliminated. Last but not the least, the matrix polymers shall be easily spun into asymmetric hollow fibers to achieve the lab-scale to industrial scale transition.

Aside from selection of the individual components for a composite system, the combined properties of polymer and sieve must also be taken into account. The Maxwell model introduced in the previous section serves as an excellent tool to predict and optimize potential polymer/sieve pairs. It was shown that a maximum exists in the expected selectivity increase, which is often referred to as 'matching of materials'.[38] This concept can be interpreted in a qualitative way. If the permeability of the polymeric phase is substantially larger than the sieving phase, gas molecules are likely to transport through the polymers by taking the least-resistance path. As a result, the sieves are 'starved' and unable to contribute to selectivity improvement. Nonetheless, it is unnecessary to choose a polymer significantly less permeable than the zeolite because it restricts the productivity of the membrane. An optimal exists when the permeability of the fast gas is slightly lower in the polymer phase than the sieves. In this case, the fast gas can permeate through either phase without strong inclination while the slow gas experiences a longer path because it has to avoid the zeolites. Essentially, the mixed matrix effect is to make fast gas transport faster and slow gas even slower. By properly selecting material combination, optimal performances can be achieved for various separation tasks.

It is noteworthy that the intrinsic affinity between polymer and sieve is another important factor in achieving a good mixed matrix membrane. Prior work attempted to use AFM to measure the adhesion force between various polymers and glass substrate.[25,26] The data were, however, too scattered to discern distinctive trends. Nevertheless, even without strong intrinsic interaction, it is still probable to create desirable composite membranes by properly tailoring the interface to promote the

compatibility. The following chapters will elaborate efforts done in this work to address this matter.

2.4 LITERATURE SURVEY OF MIXED MATRIX MEMBRANES

Mixed matrix membranes (MMMs) have been actively pursued in industry and academia for gas separation in the past 20 years. So far as the MMMs are concerned, the principal improvement in separation properties is expected to capitalize on the positive effect induced by the addition of inorganic phase, such as zeolites[39,40], carbon molecular sieves [41,42], activated carbons[43], silica[44,45]. The potential fields to employ MMMs have been widely investigated, including air separation (O_2/N_2), natural gas purification (CO_2/CH_4), hydrogen recovery (H_2/CO_2, H_2/N_2 and H_2/CH_4), and hydrocarbon separations (ethylene/ethane, *i*-pentane/*n*-pentane and *n*-butane/CH_4), etc. There are usually two forms of MMMs, dense films and asymmetric hollow fibers. The progress on each of them will be briefly reviewed in the subsequent sections.

2.4.1 Mixed Matrix Dense Film

The first attempt to create composite membranes comprising zeolites and polymers were made by Barrer and James in 1960.[46] Their study observed voids present at the polymer/zeolite interface when preparing mixture of a finely powdered polymer and zeolite crystals. Such voids were hypothesized to be the main cause of the deteriorated membrane performance. Paul and Kemp found that addition of 5A zeolite in silicone rubber substantially increase the time lag of CO_2 and CH_4.[47] Kulprathipanja mixed silicalite to cellulose acetate and observed a slight change in $\alpha_{O2/N2}$ from 2.99 to 3.63.[48] Jia et al incorporated silicalite into silica rubber and obtained very small improvement

even at 70wt% of solid concentration.[34] The lack in substantial selectivity enhancement is due to the poor material selection.

The preparation of composite membranes from a glassy polymer by a solution-casting process was investigated by Duval, who reported interfacial voids present in silicate filled cellulose acetate, Ultem® and poly (4-methyl-1-pentene) membranes.[49] The authors proposed that the stress occurring during the solvent evaporation step led to delamination of the polymer from zeolite surfaces. Vankelecom et al postulated that because of the highly stiff chains of the polyimide compared to flexible elastomer, the close packing achieved in the bulk polymer was disturbed in the vicinity of zeolite particles, resulting in the voids.[50] Other possible causes for the void formation include repulsive force between polymer and filler[25] and different thermal expansion coefficients for polymer and particle[51]. By far, the void-type morphology or 'sieve-in-a-cage' is still the most commonly encountered problem in dense mixed matrix study and thus the biggest challenge to be overcome.

A number of innovative techniques were developed to reduce or eliminate the aforementioned void-type morphology. Pechar et al used poly (imide siloxane) copolymer to prepare MMMs with the intention that the flexible siloxane component would provide flexibility and promotes good contact with the zeolite surface.[52] Several researchers suggested fabricating or processing MMMs at temperatures above the T_g of the glassy matrix.[53] The basic idea of this method is to avoid the stress induced during the transition from the rubbery state to glassy state and thus reduce the possibility of chain delamination resulted from such stress accumulation. Mahajan et al developed a sieve priming protocol to promote the interaction between polymer and zeolites.[54] It was

performed by coating the zeolite particles with a layer of polymers before the bulk polymer solution was added to create the final mixed matrix dope. The resultant PVAc/4A films exhibited enhanced selectivity over neat polymer for the separation of O_2/N_2 even at 40vol% sieve loading. The priming protocol was further investigated by Vu et al with Matrimid® and Ultem® films containing carbon molecular sieves.[55]

In addition to the above approaches using the intrinsic physical properties of the materials, another category of modification by tailoring the properties of the matrix or the sieve surface chemistry has been exploited. Mahajan et al incorporated a plasticizer into a high T_g polymer to increase the flexibility of the matrix.[25] A rubbery state was thus maintained during membrane formation process. The resultant MMMs were expected to show improved interface as well as selectivity. Nonetheless, it was found that the addition of plasticizer considerably changed the properties of the polymer matrix, rendering it less attractive than the commercial polyimides. Duval promoted adhesion between the modified silicalite surface and a polyetherimide matrix by use silane coupling agents to eliminate non-selective interfacial voids.[56] Mahajan et al also modified the sieve surface chemistry by applying silane coupling agent (APDEMS, for instance) as an interfacial compatilizer.[57] The covalent bonds formed between the polymer and sieves have been demonstrated to generate defect-free membranes with enhanced gas separation selectivities. Guiver et al reported higher selectivity for H_2/CO_2 separation with polysulfone MMMs containing APTES modified zeolite 3A.[58] Most recently, a new surface treatment was developed based on a two-step reaction sequence.[59] Such a treatment creates nanostructures on zeolite surfaces and it is believed that the dramatic increase in the topological roughness on the sieve surface provides enhanced adhesion at

the polymer/sieve interface. More detail regarding this new technique will be elaborated in the upcoming chapters.

The preceding discussions focus on the strategies to promote interfacial interaction between polymeric and inorganic phase. Upon the formation of intimate contact between polymer and particles, a new phenomenon was observed by Moaddeb[60] and Mahajan[25], where they identified decreased permeabilities and slightly higher selectivities exhibited by the composite materials relative to the Maxwell model prediction. This effect is referred to as 'matrix rigidification'. The depression in permeability is believed to be caused by immobilization or tethering of polymer chains in the vicinity around the solid particles while the slightly higher selectivity is attributed to the more rigid chains in the interfacial region.

Another non-ideal morphology in mixed matrix system was discovered by Moore et al in a subsequent study.[61] The characteristic transport property is considerable reduction in permeability while no enhancement in selectivity. It can be induced by non-ideal penetrants, such as water, organic solvent molecules or coupling agents. A systematic investigation was devised by the authors who utilized pressure-decay gas sorption system to characterize the dynamic sorption as well as equilibrium uptake of the zeolites.

Contrary to the above research where effort was directed towards making best use of the superb selectivity of the zeolites or carbon molecular sieves, a different class of investigations was conducted which involves the use of non-porous, nano-sized particles.[19] The function of the fillers is to systemically manipulate the molecular packing of the polymer chains, hence enhancing the separation properties of glassy polymeric membranes. In the work by Merkel[62] and He[63] where non-porous, nano-sized fumed

silica was incorporated into poly (4-methyl-2-pentyne) (PMP), the transport of *n*-butane/CH_4 was tremendously enhanced in both permeability and selectivity. Similar effects were also observed with poly (2,2-bis (trifluoro methyl)-4,5-difluoro-1,3-dioxole-co-tetrafluoroethylene) (AF2400)].[64] Current study on reserve-selective membranes attempts the incorporation of nano-sized metal oxide to substantially modify the matrix properties.[65]

2.4.2 Asymmetric Mixed Matrix Membranes

The demand for higher productivity on an industrial scale implementation led to the formation of asymmetric membranes or composite membranes with a thin selective skin layer on a relatively open-celled porous support to substitute the thicker flat dense film. Unfortunately, as membrane thickness is reduced the probability of transmembrane defects increases dramatically, thereby leading to difficulties in supporting and packaging commercially viable amounts of membrane area. The key improvement for large-scale application of membrane technology was the development of ultra-thin, integrally skinned asymmetric cellulose acetate membranes for reverse osmosis by Loeb and Sourirajan.[66] The key to this achievement was the invention to allow drying asymmetric cellulose acetate membranes without collapse of the porous substructure and destruction of the selective skin.[67] In the late 1970s, Henis and Tripodi developed the revolutionary concept of the multicomponent ('caulked') membrane that could be formed from essentially any glassy material.[68] A caulked asymmetric membrane consists of an integrally-skinned structure, coated with a very thin layer (< 1mm) of another highly permeable polymeric material such as silicone rubber. The primary function of the coating is to plug any defects in the selective skin layer. Implementation of the caulking

process to repair the small number of pinholes and other defects that undermined the intrinsic selectivity of the membrane simplified processing and handling enormously. Therefore it represented the major breakthrough regarding the practicality of membrane technology for gas separation with advanced membrane materials.

Composite asymmetric membranes typically consist of a very thin selective coating applied to either a symmetrically porous membrane or an integrally skinned asymmetric membrane having a micro-porous skin layer. The most attractive aspect of asymmetric membranes is their potential for minimizing material cost, because only the selective layer must be comprised of a more expensive high-performance polymer.[69] Incorporation of highly selective zeolites or carbon molecular sieves into the thin skin layer can further enhance the separation performance of such materials. Currently most of the mixed matrix hollow fibers are produced via a dual-layer co-extrusion technology. Ekiner and Kulkarni produced Ultem® hollow fibers containing 4A type zeolites whose selectivity for O_2/N_2 range from 8.1 to 8.5.[70] Miller et al formed composite fibers with ZSM-5 type zeolites for the separation of *p*-xylene from *m*-xylene and achieved selectivity as high as 4, in contrast to ~1 with most polymeric membranes.[71] In both patents, the zeolites were primarily dispersed in the thin skin layer with neat polymer as substructure.

The non-ideal morphologies identified in dense mixed matrix films are also highly relevant to asymmetric membranes. A major hurdle to the successful fabrication of mixed matrix hollow fibers is the lack of optimal polymer-sieve interaction, which compromises the performance of the selective skin layer. The techniques developed in dense film field have been attempted in fiber forms. Modification of sieve surface via silane coupling agents has been reported to improve the interfacial adhesion in hollow fibers.[72] A few

post-treatment approaches were attempted which improved the performance of fibers.[73,74] Recent work by Husain introduced a novel surface modification method via the use of thionyl chloride and a Grignard reagent.[75] Such a treatment is hypothesized to have suppressed nucleation of the hydrophilic polymer lean phase around the particles. This topic will be exploited in depth in Chapter 5.

2.5 REFERENCES

[1] Koros, W.J.; Fleming, K. G. *Membrane-based gas separation.* J. Membr. Sci. **1993**, *83*, 1.

[2] Mitchell, J.K. *Journal of the Royal Institution of Great Britain* **1831**, *IV*, 101.

[3] Graham, T. *Philosophical Magazine* **1866***, 32,* 401.

[4] von Wroblewski, S. *Wied. Annalen der Physik*, **1879**, *8*, 29.

[5] Wijmans, J.G.; Baker, R. W. *J. Membr. Sci*. **1995**, *107*, 1.

[6] Baker, S.A. *J. Membr. Sci*. **1994**, *94*, 1.

[7] Paul, D. R. *Separation and Purification Methods* **1976**, *5*, 33.

[8] Ghosal, K.; Freeman, B.D. *Polymers for Advanced Technologies* **1994**, *5*, 673.

[9] Neogi, P. *Diffusion in polymers*; Marcel Dekker: New York, 1996.

[10] Barbari, T.A. *J. Poly. Sci. Part B: Polym. Phys.* **1997**, *35*, 1737.

[11] Paul, D.R.; Koros, W. J. *J. Polym. Sci., Polym. Phys.* **1976**, *14*, 675.

[12] Yampolskii, Y.; Pinnau, I.; Freeman, B. D. *Materials Science of Membranes*; John Wiely & Sons: Chichester, 2006.

[13] Yang, R. T. *Gas Separation by Adsorption Processes*; Butterworths Publications: Massachusetts, 1987.

[14] Koros, W. J.; Hellums, M. *Transport Properties, in Encyclopedia of Polymer Science and Engineering, 2nd edition*; John Wiley & Sons: New York, 1989.

[15] Paul, D. R.;Yampolskii, Y. *Polymeric Gas Separation Membranes*; CRC Press: Boca Raton, FL, 1994.

[16] Singh, A. *Membrane Materials with Enhanced Selectivity: An Entropic Interpretation,* Ph.D thesis: The University of Texas at Austin, 1997.

[17] Alentiev, A. Y.; Yampolskii, Y. P. *J. Membr. Sci.* **2000**, *165*, 201.

[18] Freeman, B. D. *Macromolecules* **1999**, *32*, 375.

[19] Merkel, T. C.; Freeman, B. D.; Spontak, R. J.; He, Z.; Pinnau, I.; Meakin, P.; Hill, A. J. *Science* **2002**, *296*, 519.

[20] He, Z.; Pinnau, I.; Morisato, A. *Desalination* **2002**, *146*, 11.

[21] Petropoulos, J. H. *J. Polym. Sci: Polym. Phys. Edi*. **1985**, *23*, 1309.

[22] Maxwell, J. C. *A Treatise on Electricity and Magnetism*; Clarendon press: Oxford, 1873.

[23] Michaels, A.S.; Parker, R. B. *J. of Polym. Sci.* **1959**, *41*, 53.

[24] Bouma. R. H. *J. Membr. Sci.* **1997**, *128*, 141.

[25] Mahajan, R. Formation, *Characterization and Modeling of Mixed Matrix Membrane Materials*, Ph.D Thesis: the University of Texas at Austin, 2000.

[26] Moore, T. T. *Effect of Materials, Processing, and Operating Conditions of The Morphology and Transport Properties of Mixed Matrix Membranes*; Ph. D thesis: The University of Texas at Austin, 2004.

[27] Knudsen, M. *Annalen der Physik* **1909**, *28*, 75.

[28] Moore, T. T.; Koros, W. J. *J. Mole. Stru*. **2005**, *739*, 87.

[29] Suh, S. H.; MacElroy, J. M. D. *Mol. Phys.* **1986**, *58*, 445.

[30] Michaels, A.S.; Bixler, H. J.; *J. Polym. Sci.* **1961**, *50*, 393.

[31] Michaels, A.S.; Vieth, W. R.; Barrie, J. A. *J. Appl. Phys.* **1963**, *34*, 13.

[32] Tantekin-Ersolmaz, S.B. *J. Membr. Sci*. **2000**, *175*, 285.

[33] Duval, J.M.; Kemperman, J. B.; Folkers, B. *J. Appl. Polym. Sci.* **1994**, *54*, 409.

[34] Jia, M.; Peinemann, K. V.; Behling, R. D. *J. Membr. Sci*. **1991**, *57*, 289.

[35] Flanigen, E.M.; Bennett, R.; Grese, R. W.; Cohen, R. L. *Nature* **1978**, *271*, 512.

[36] Breck, D.W. *Zeolite Molecular Sieves: Structure, Chemistry, and Use*. Robert E. Krieger Publishing Co, Inc: Malabar, FL, 1974.

[37] Singh, A.; Koros, W. J. *Ind. Eng. Chem. Res*. **1996,** *35*, 1231.

[38] Zimmerman, C. M.; Singh, A.; Koros, W. J. *J. Membr. Sci*, **1997**, *137*, 145.

[39] Vankelecom, I. F. J. *J. Phys. Chem. B* **1997**, *101*, 2154.

[40] Berry, M.B. *Microporous Mesoporous Mater*. **2000**, *39*, 205.

[41] Vu, D. Q.; Koros, W. J.; Miller, S. J. *J. Membr. Sci.* **2003**, *211*, 335.

[42] Vu, D.Q., Koros, W. J.; Miller, S. J. *Ind. & Eng. Chem. Res*. **2002,** *41*, 367.

[43] Ji, W.; Sikdar, S. K.; Hwang, S. T. *J. Membr. Sci.* **1995**, *103*, 243.

[44] Fragiadakis, D.; Pissis, P.; Bokobza, L. *Polymer* **2005**, *46*, 6001.

[45] Cornelius, C.J.; Marand, E. *Polymer* **2002**, *43*, 2385.

[46] Barrer, R. M.; James, S. D. *J. Phys. Chem.*, **1960**, *64*, 421.

[47] Paul, D. R.; Kemp, D. R. *J. Polym. Sci., Polym. Symp.* **1973**, *41*, 79.

[48] Kulprathipanja, S.; Neuzil, R. W.; Li, N. N. *U. S.* 1988, Us. p. 7 pp. Cont. of U.S. Ser. No. 697,990.

[49] Duval, J. M.; Folkers, B.; Mulder, M. H. V.; Desgrandchamps, G.; Smolders, C. A. *J. Membr. Sci.* **1993**, *80*, 189.

[50] Vankelecom I. F. J.; Mercks, E.; Luts, M.; Uytterhoeven J. B. *J. Phys. Chem.* **1995**, *99*, 13187.

[51] Li, Y.; Chung, T. S.; Cao, C.; Kulprathipanja, S. *J. Membr. Sci*. **2006**, *275*, 17

[52] Pechar, T. W.; Kim, S.; Vaughan, B.; Marand, E.; Baranauskas, V.; Riffle, J. *J. Membr Sci.* **2006**, *277*, 210.

[53] Duval, J. M. *Adsorbent Filled Polymeric Membranes;* Ph. D thesis: The Netherlands, University of Twente. 1995.

[54] Mahajan, R. ; Burns, R.; Schaeffer, M.; Koros, W. J. *J. Appl. Poly. Sci*. **2002**, *86*, 881.

[55] Vu, D. Q.; Koros, W. J.; Miller, S. J. *J. Membr. Sci.* **2003**, *211*, 311.

[56] Duval, J. M.; Kemperman, A. J. B.; Folkers, B.; Mulder, M. H. V.; Desgrandchamps, G.; Smolders, C. A. *J. Appl. Poly. Sci.* **1994**, *54*, 409.

[57] Mahajan, R.; Koros, W. J. *Ind. Eng. Chem. Res*. **2000**, *39*, 2692.

[58] Guiver, M. D.; Robertson, G. P.; Dai, Y.; Bilodeau, F.; Kang, Y. S.; Lee, K. J. *J. Polym. Sc: Polym. Chem.* **2003**, *40*, 4193.

[59] Shu, S.; Husain, S.; Koros, W. J. *J. Phys. Chem. C* **2007**, *111*, 652.

[60] Moaddeb, M.; Koros, W. J. *J. Membr. Sci.* **1997**, *125*, 143.

[61] Moore, T. T.; Vo, T.; Mahajan, R.; Kulkarni, S.; Hasse, D.; Koros, W. J. *J. Appl. Polym. Sci*. **2003**, *90*, 1574.

[62] Merkel, T. C.; Freeman, B. D.; Spontak, R. J.; He, Z.; Pinnau, I.; Meakin, P.; Hill, A. J. *Chem. Mater*. **2003**, *15*, 109.

[63] He, Z.; Pinnau, I.; Morisato, A. *Desalination* **2002**, *246*, 11.

[64] Merkel, T. C.; Bondar, V.; Nagai, K.; Freeman, B. D.; Yampolskii, Yu. P. *Macromolecules* **1999**, *32*, 8427.

[65] Freeman, Benny D.; Matteucci, Scott; Lin, Haiqing. *Metal oxide nanoparticles filled polymers.* U.S. Pat. Appl. Publ. 2007, US 2007137477.

[66] Loeb, S.; Sourirajan, S. *Adv. Chem. Ser*. **1962**, *38*, 117.

[67] Vos, K. D.; Burris, F. O. *Ind. Eng. Chem. Res. Dev.* **1969**, *8*, 84.

[68] Henis, J. M. S.; Tripodi, M. K. *J. Membr. Sci.* **1981**, *8*, 233.

[69] Pinnau, I.; Koros, W. J. *Ind. Eng. Chem. Res*. **1991**, *30*, 1837.

[70] Ekiner, O. M.; Kulkarni, S. S. *Porcess for Making Hollow Fiber Mixed Matrix Membranes*; US patent 6663805, 2003.

[71] Miller, S. J.; Munson, C. L.; Kulkarni, S. S.; Hasse, D. J. *Purification of p-Xylene Using Composite Mixed Matrix Membranes*. US Patent 6500233, 2002.

[72] Husain, S. *Mixed Matrix Dual Layer Hollow Fiber Membranes for Natural Gas Separation*; Ph.D thesis: Georgia Institute of Technology, 2006.

[73] Li, Y.; Chung, T. S.; Huang, Z. *J. Membr. Sci.* **2006**, *52*, 2898.

[74] Jiang, L. Y.; Chung, T. S.; Kulprathipanja, S. *AIChE J*. **2006**, *52*, 2898.

[75] Husain, S.; Koros, W. J. *J. Membr. Sci*. **2007**, *288*, 195.

CHAPTER 3
MATERIALS AND EXPERIMENTAL PROCEDURES

The present work involves formation and characterization of mixed matrix membranes comprising organic polymers and inorganic inserts, as well as surface modification of the fillers to promote compatibility with the polymer matrix. This chapter will first introduce all the materials used in this study, followed by the experimental procedures used to create and test the membranes. Moreover, the experimental protocols utilized to modify the fillers will be presented. A summary of the complementary techniques employed to characterize the morphological, elemental and structural information of the materials will be provided at the end of this chapter.

3.1 MATERIALS

3.1.1 Polymers

The polymers used in this research were purchased from industrial suppliers. There are three polymers that have been investigated in the current work: Polyvinyl acetate or PVAc (M_w=500,000 Aldrich, Milwaukee, WI) is a rubbery polymer with a T_g of 35ºC; Ultem® (M_w =56,000, GE Plastics; Pittsfield, MA) is a glassy polyetherimide with a T_g of 215ºC; Matrimid® 5218 (Vantico; Brewster, NY) is a glassy polyimde with a T_g of 305 ºC. The molecular structures and gas transport properties of the polymers are shown in Figure 3.1 and Table 3.1, respectively.

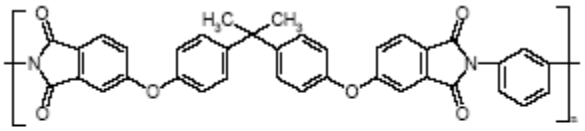

BPADA-mPDA (Ultem®)

2,2-bis[4-(3,4-dicarboxyphenoxy)phenyl] propane dianhydride - 1,3-phenylenediamine

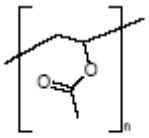

Poly (vinyl acetate)

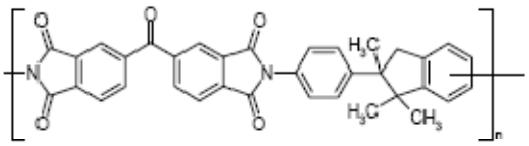

BTDA-DAPI (Matrimid®)

3,3′,4,4′-benzophenonetetracarboxylic acid dianhydride - 5(6)-amino-1-(4′aminophenyl)-1,3,3-trimethylindane

Figure 3.1 Molecular structures of the polymers used in this work.

Table 3.1 Gas transport properties of the polymers used in this work (permeation data are collected at 35ºC with upstream pressure of 65 psia)

Polymers	Permeability, Barrer		Selectivity		Density
	O_2	CO_2	O_2/N_2	CO_2/CH_4	g/cm^3
PVAc	0.5 (0.54*)	Uncertain**	6 (6.2-6.3*)	Uncertain**	1.19
Ultem®	0.4	1.4	7.5	38	1.28
Matrimid®	2	10	6.9	35.5	1.2

* The transport property of PVAc has been observed to shift over time. The numbers in the bracket were obtained after 3 years of storage in the drawer. It is hypothesized that oxidation and hydrolysis are the possible causes of the change.

** PVAc is known to plasticize under very low partial pressure of CO_2, therefore it is difficult to obtain CO_2/CH_4 separation performance without the influence of plasticization.

3.1.2 Inorganic Fillers

This work explores both micro-porous zeolites and non-porous silica particles as the dispersed phase. Zeolite 4A was primarily used as the molecular sieving material. It has a LTA (Linde Type A) structure, which is a 3-dimensional pore network of interconnected cages that is ideally suited to the separation of O_2/N_2 and CO_2/CH_4. The larger particles with average diameters of ~5μm were obtained from Advanced Specialty Gas Equipment (Middlesex, NJ). A second batch of zeolite 4A was provided by ChevronTexaco Energy Technology Company (Richmond, CA), the average diameter ofwhich is ~100nm. The framework structure of zeolite 4A and cell parameters are shown in Figure 3.2 and its transport properties are listed in Table 3.2. In addition to the molecular sieves, non-porous silica was also investigated as an insert phase. It was obtained from Dr. C. P. Wong's lab in Materials Science & Engineering department. The manufacturer is most likely Nissan Chemicals (Japan). Non-porous silica does not facilitate selective transport of gas molecules thus it is incorporated into the matrix to examine the properties in the interfacial regions.

Cell Parameters:
a = 11.919Å b = 11.919 Å c = 11.919 Å
alpha = 90.000º beta = 90,000 º gamma = 90.000º
volume = 1693. 24 $Å^3$ R_{DLS}= 0.0026

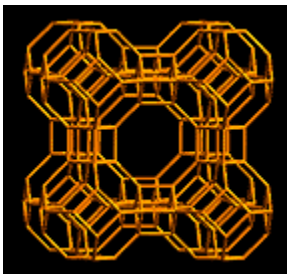

Figure 3.2 Framework structure of LTA zeolite and its cell parameters[1]

Table 3.2 Gas transport properties of zeolite 4A [2]

Zeolite	Permeability, Barrer		Selectivity	
	O_2	CO_2	O_2/N_2	CO_2/CH_4
4A (LTA)	0.77	15	37	340

3.1.3 Solvents

Several solvents are used in this work to dissolve polymers, prepare zeolite suspensions, modify sieve surface chemistry and act as inert liquid environments for reactions to take place. These solvents include dichloromethane ($MeCl_2$), N-methyl pyrrolidinone (NMP), toluene, methanol, ethanol (EtOH), iso-propanol (IPA), butanol, chloroform ($CHCl_3$) and tetrahydrofuran (THF). All of these solvents were purchased from Aldrich (Milwaukee, WI). When zeolites were involved, only anhydrous solvents with sure seal® bottles were used to prevent contamination caused by moisture.

3.1.4 Penetrants

Pure gases (O_2, N_2, CO_2, CH_4) of 99.999% purity were obtained from Air Products (Allentown, PA).

3.1.5 Other Reagents

3.1.5.1 Silane Coupling Agents

Organofunctional silanes are commonly used as adhesion promoters between organic polymers and mineral substrates under a variety of circumstances. The silane adhesion promoter, or 'coupling agent', may function as (i) a finish or surface modifier; (ii) a primer or sizing agent; or (iii) an adhesive, depending on the thickness of the bonding material at the interface.[3] An aminosilane γ-aminopropyldimethylethoxysilane (Gelest;

Morrisville, PA) was selected to modify the zeolite surface to enhance adhesion with the polymer matrixes. The structure of this reagent is shown in Figure 3.3. The ethoxy group on one end undergoes a hydrolysis process in solution before the silane reacts with the hydroxyl groups that are ubiquitous on zeolite surfaces.[4] The amine group on the other end can further react with the imide group in the polymer through a ring opening reaction as illustrated in Figure 3.4.[5] Such a reaction creates covalent bonds between the sieve and polymer phases and thus enhances the affinity.[6]

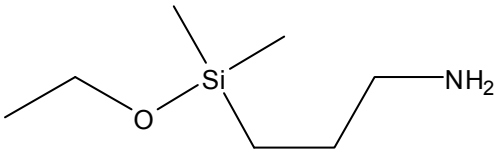

3-aminopropyldimethylethoxysilane

Figure 3.3 Structure of γ-aminopropyldimethylethoxysilane (APDMES)

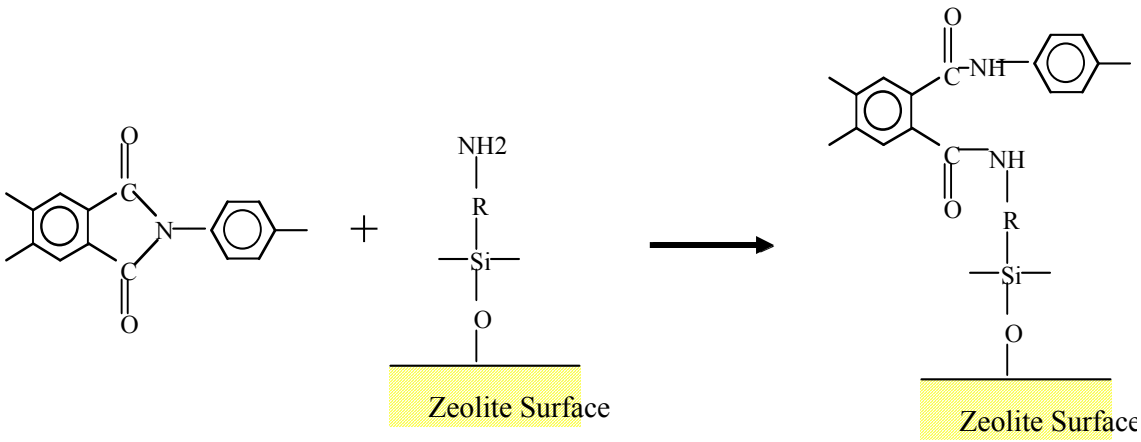

Figure 3.4 Illustration of the reaction between polyimides and aminosilane coupling agents

3.1.5.2 Grignard Reagent

Organomagnesium compounds, commonly called Grignard reagents are prepared by adding an alkyl halide to magnesium shavings being stirred in diethyl ether or THF under

anhydrous conditions. This work uses a Grignard reagent, methylmagnesium bromide, as a surface modifier. It reacts with 2-propanol and generates methane and solid precipitates containing $MgBr_2$ and $Mg(OH)_2$. This reaction will be exploited in detail in Chapter 6. The reagent is a 3.0M solution in diethyl ether (Aldrich, Milwaukee, WI**).** In a reaction involving Grignard reagents, it is important to ensure that no water is present, which would otherwise cause the reagents to decompose rapidly. It is also noteworthy that these chemicals degrade quickly over time, thus use of fresh reagents is highly recommended when performing sieve treatments. Furthermore, this material is extremely flammable and corrosive, therefore proper safety procedures must be followed. The structure of methylmagnesium bromide is shown in Figure 3.5.

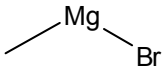

methyl magnesium bromide

Figure 3.5 Chemical structure of methyl magnesium bromide

3.1.5.3 Thionyl Chloride

Thionyl chloride whose structure is demonstrated in Figure 3.6 was used in this work as a zeolite modification reagent. The original intention of its implementation was to chlorinate the sieve surface, as reported by a number of researchers who successfully observed direct Si-Cl bonds with thionyl chloride treated silica/silicate materials.[7-9] Nevertheless, it was discovered that the reaction takes a different path in the current study with aluminum-containing zeolites. More detailed discussion with regard to this point will be presented in Chapter 6 and 7. Thionyl chloride, ReagentPlus, 99.5%, low iron (Fe < 5ppm) was purchased from Sigma-Aldrich (Milwaukee, WI). Careful handling of this

material is required because it is highly volatile, corrosive and reacts violently with water.

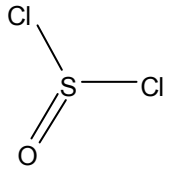

thionyl chloride

Figure 3.6 Chemical Structure of thionyl chloride

3.2 EXPERIMENTAL PROCEDURES

This section will detail the experimental procedures used to (i) create neat and mixed matrix dense films; (ii) modify the sieve surface chemistry or morphology to enhance the interaction with the polymers; and (iii) the major techniques used to measure the properties of membranes such as permeability and solubility, along with complementary characterization methods to explore elemental and structural information of materials.

3.2.1 Membrane Formation

This section outlines the protocols used to create both pure polymeric and mixed matrix dense film membranes.

3.2.1.1 Formation of Pure Polymeric Dense Films

3.2.1.1.1 Preparation of Casting Solution

All the polymers were dried in a vacuum oven at approximately 120°C over night prior to use. The polymers were placed in a Petri dish covered with an aluminum foil while drying. Small holes were made on the foil to allow vapors to to be liberated.

A 40-mL vial with PTFE septa (I-Chem, Fisher Scientific, Pittsburgh, PA) was obtained and rinsed with the appropriate solvent to be used to dissolve the polymer. The

dried polymer was transferred into the vial by a spatula quickly to minimize moisture re-adsorbing into the materials. A proper amount of solvent to make a certain concentration of solution was pre-calculated and measured using either a volumetric column or a syringe. The concentration of polymer determines the final viscosity of the solution. For casting a pure polymeric film, either dilute (6-8wt%) or more concentrated solutions (20-25wt%) can be used. Nonetheless, the formation of mixed matrix dense film requires high viscosity dope to prevent the particles from settling. After the solvent was added into the vial and mix with the polymer, the vial was capped tightly with a Teflon®-coated septum cap and further sealed with parafilm® (VWR, Menasha, WI) to prevent volatile solvent evaporation. The vial was then agitated by hand to help partially dissolve the polymer and placed on a roll mill. Paper towels or Kimwipes® were used as cushions to maintain a snug environmental for the vials. The solution was allowed to rotate on the roller until the polymers were completely dissolved (typically one day for the polymers used in the present work). It was allowed to sit to release any air bubbles trapped in the solution. When very viscose dopes were prepared, it may be necessary to de-gas the polymer solution in a vacuum oven to remove gas bubbles.

3.2.1.1.2 Film Casting

The casting substrate can be either a glass or Teflon® plate. Usually a glass plate treated with a silane Glassclad® 18 (United Chemical Technologies, Horsham, PA) was used when making Ultem® or Matrimid® membranes while Teflon® plate was utilized primarily when casting PVAc films. There are a few other alternatives such as Teflon® coated aluminum foil or Teflon® coated vinyl (BYTAC®, Norton Performance Plastics Corporation, Wayne, NJ). Yet most of the PVAc films produced in this work were cast

on a pure Teflon® substrate. All casting surface was cleaned using soap water and acetone before use. It is also important to keep the flat surface horizontally leveled. This could be done by adjusting the heights of the four corners of the leveling base (Paul Gardener Company, Pompano beach, FL). A bubble leveler was used to facilitate the adjustment.

Solution evaporation casting can be done by using either a casting knife or a casting ring. The first approach was used in this work because the high viscosity nature and solid content of mixed matrix dope make it difficult to pass the syringe. A doctor knife (Paul Gardener Company, Pompano beach, FL) was the primary tool to draw cast films on various substrates. It has two clearances, 10 mil and 12 mil, both of which are used in the current work. In addition to the aforementioned apparatus, a glove bag (Aldrich, Milwaukee, WI) was used in film casting throughout this work. It provided a closed and controlled environment for the casting process.

All the necessary elements (casting substrate, polymer solution, casting knife, a bottle of appropriate solvent and a Petri dish) were placed in the glove bag before casting. The bag was then purged with nitrogen for 3 times to eliminate the air originally present inside. Then ~20mL of solvent was poured into the Petri dish and allowed to reach saturation within the glove bag (this usually takes 40min with toluene and 20min with dichloromethane). The purpose of this step was to create a saturated environment and reduce the solvent evaporation rate when the nascent film was formed. After that, the casting knife was placed near the top edge of the casting surface and polymer solution was poured across the front edge of the casting knife. The solution was drawn slowly towards the end of the substrate. The nascent film was allowed to sit in the glove bag for

overnight to let most of the volatile solvent evaporate. After the film vitrified, it was taken out of the glove bag and dried in a vacuum oven for at least overnight. The temperature used to dry PVAc films was usually 110 ºC - 120ºC (180ºC - 200ºC) was used on a few occasions) and Ultem® films were usually annealed under 230ºC. The final step was to remove the films from oven and mask them into permeation systems or store in sample bags.

3.2.1.2 Formation of Mixed Matrix Dense Film

The procedure to create mixed matrix dense films was very similar to that used for pure polymeric films. The major difference lies in the formation of casting dopes. In addition to the preparation of a pure polymer solution as mentioned in the previous section, a sieve dispersion was needed to incorporate zeolites into the membranes. A proper amount of zeolites/silica (to form 15wt%, 30wt% and 40wt% solid loading films) was first dried in a vacuum oven under 200ºC for overnight then dispersed in the corresponding solvent via a sonicator (model VC 50, Sonics & Materials Inc, Newtown, CT) for 2 min. This was followed by a 'priming' step where 10wt% of the bulk polymer solution required to make the final films was mixed with the sieve dispersion and placed on the roll mill for overnight. The purpose of this operation was to prime the sieve surface with a thin layer of polymers which is considered to facilitate the adsorption of bulk polymers when they are introduced later. The rest of the polymer solution was added to the mixture and roll for overnight again. A homogeneous suspension would be obtained afterwards and was ready for film casting.

The rest of the experimental was performed in the same fashion as described in the 'Film Casting' section. It is important to maintain a low humidity inside the glove bag as the zeolites can adsorb moisture quickly.

3.2.2 Sieve Surface Modification

Modification of inorganic surfaces has been widely explored in literature to increase the hydrophobicity, compatibility with organic phases, functionality of the material, etc. Sieve surface modification was exploited in this work in order to enhance the adhesion between the inorganic fillers and polymeric continuous phases to eliminate the interfacial voids. It was an important step in formation of successful mixed matrix membranes. Three approaches were attempted and the procedures will be discussed individually below.

3.2.2.1 Silanation

Silanation of sieve surface was regularly performed in mixed matrix membrane formation. Samples of 5-10g of dry molecular sieves were dried at 150ºC under vacuum before the treatment. Meanwhile a mixture of iso-propanol and DI water (95:5 by volume) was prepared and stored in a plastic beaker. Thereafter 5mL of γ-aminopropyldimethylethoxysilane (APDMES) was added to this H_2O/isopropanol solution and allowed to hydrolyze for 5 minutes. This amount of coupling agent is typical for treating 5-10g of solids and is in very large excess. Zeolites were then added and dispersed in the solution using a sonication horn (Ultra 1000, Dukane, Leesburg, VA) for a total of 30 minutes in 5 minutes' bursts with 5 minutes rest periods. An ice bath was often used to prevent the solution from excess heating. The silanation reaction took place at this stage where the hydroxyls on sieve surface react with the hydroxyls in the

coupling agents. Finally the sieves were collected via high pressure filtration or centrifugation and dried in the oven at 150ºC for 12-24 hours under vacuum.

One additional step carried out after silanation was to adsorb a certain amount of polymers on silanated sieves and enable the ring opening reaction shown in Figure 3.4. This protocol is often referred to as 'sizing'. It was conducted by first dispersing proper amount of silanated sieves (~ 8-10 wt%) in a certain solvent, followed by sonication to create a homogeneous suspension. Such a solution was heated to 150ºC when dried polymer was added to make a 0.2 – 0.3 wt% polymer solution. The mixture was maintained at 150ºC for 5 hours with constant stirring. When NMP was the solvent, a nitrogen sweep was utilized to prevent oxidation. In the end the sieves were collected via centrifuge and dried at 150ºC overnight under vacuum.

3.2.2.2 Hydrophobization of Sieve Surface by Alcohols

Alcohols with different chain lengths were investigated to hydrophobize the zeolite surface. Samples of 5g of zeolite 4A were placed in a three-neck reaction flask and dried at 150ºC for 24 hours in a vacuum oven. Anhydrous alcohols of 100mL volume were transferred via dry lines into the flask. A condenser was connected to the center neck of the flask and water was kept running throughout the treatment. The entire experimental set up was placed in an oil bath, above a hot plate enabled with magnetic stirring. The reaction temperature varied with different alcohols but generally it was controlled at 50ºC above the boiling point of the alcohols. Once the boiling point was reached, the liquid was allowed to reflux inside the system for 48 hours while a magnetic stir bar was used to keep a homogeneous dispersion. Upon the end of the reaction, heat was turned off and a dry nitrogen sweep was employed to evaporate the remaining alcohols. The sieves were

later collected and rinsed with the corresponding alcohol for three times, with subsequent drying at 150ºC for 24 hours in a vacuum oven.

3.2.2.3 Grignard Treatment

The original procedure of this novel treatment was first developed by Husain.[10] Zeolite 4A, which is an aluminosilicate (Advanced Specialty Gas Equipment, Middlesex, NJ) with a characteristic 5μm cubic form, was selected as the model dispersed phase. Samples of 5g of 4A particles were placed in a three-neck reaction flask. All the particles and the glassware used in the treatment were first dried in a vacuum oven at 150ºC for 24hr, followed by flame-drying of the glassware with a propane torch prior to the treatment. Then amount of 80mL of anhydrous toluene (99.8%, Aldrich) and 20mL of thionyl chloride (99.5%, low ion solution, Aldrich) were added to the reaction flask, which contained the 4A powders. Both liquids were transferred carefully through a dry transfer line to maintain a moisture-free environment. This dispersion was kept in a sonication bath (Model 1510, Branson) for 12-16 hours, after which toluene and extra thionyl chloride were evaporated by a constant nitrogen sweep through the system. Vacuum was used to facilitate the removal of residual thionyl chloride from the molecular sieves. Thereafter 80mL of anhydrous toluene and 15mL of methyl magnesium bromide (3.0 M solution in diethyl ether, Aldrich) were added to the reaction flask in the same manner as described above. The dispersion was again kept in a sonication bath for 12-16 hours. When the reaction was finished, extra methyl magnesium bromide was quenched by anhydrous 2-propanol (99.5%, Aldrich) and the particles were collected and rinsed with 2-propanol three times followed by abundant de-ionized water for several times. The same treatment procedure applies to pure silica particles as well. It is

important to keep a moisture-free environment because both thionyl chloride and the Grignard reagent are very sensitive to water hence possible degradation of reagents could occur if there is considerable amount of water adsorbed on the glassware or molecular sieves.

3.3 MEMBRANE TESTING TECHNIQUES

Gas permeation and sorption experiments are two essential techniques utilized to characterize gas separation membranes. Permeation tests measure the permeability and selectivity of a membrane while sorption tests determine the solubility of gas in a certain material.

3.3.1 Gas Permeation Test

3.3.1.1 Experimental Apparatus

A schematic of the permeation system is illustrated in Figure 3.7. The system is enclosed in an insulated box for temperature regulation. A heating tape is used as the heat source and a fan is used to circulate air inside the box. All the parts are made of stainless steel fittings from Swagelok® (Solon, OH).

The system is basically composed of three parts: upstream (7), cell (8) and downstream (2), all of which are connected via tubing and valves to a vacuum pump. Pressure transducers (Dresser Instruments, Stratford, CT; MKS Instruments, Andover, MA) were connected to the volume compartments and the signals were recorded with a data acquisition board (KCPI-3107, Keithley, Lake Mary, FL). Labview (National Instruments, Austin, TX) was utilized as the data acquisition software.

The membrane was masked in a customized cell (8) that consists of two stainless steel plates. A piece of porous metal is inserted in the downstream part as mechanical support

for the membrane. The up and down sides of the cell are connected to the feed and permeate volumes respectively.

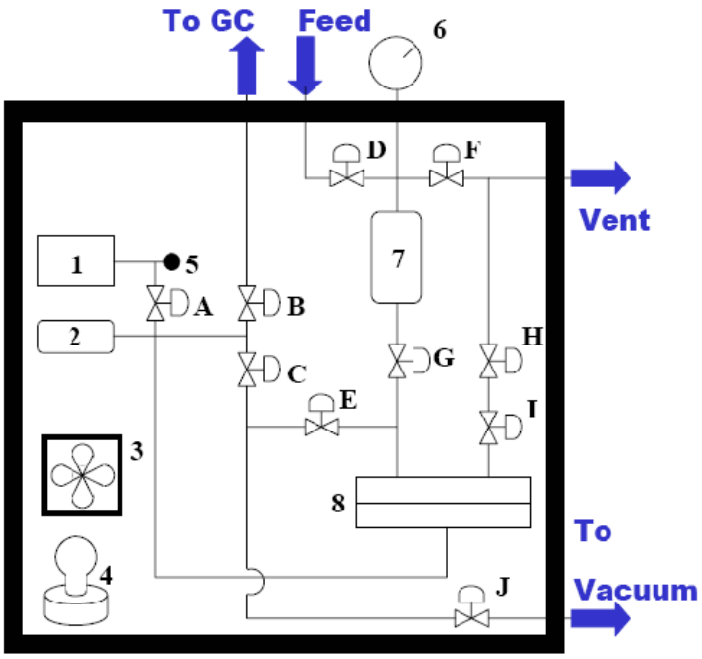

Figure 3.7: Schematic of the permeation system. (1) Downstream Pressure Transducer, (2)Permeate Reservoir, (3) Fan, (4) Heater, (5) Rupture Device, (6) Upstream Pressure Transducer, (7) Feed Reservoir, (8) Permeation Cell, (A) Downstream Pressure Transducer Isolation Valve, (B) GC Valve, (C) Downstream Vacuum Valve, (D) Feed Valve, (E) "Middle" Valve, (F) Vent Valve, (G) Cell Isolation Valve, (H) Retentate (Metering) Valve, (I) Retentate Shutoff Valve, and (J) Vacuum Shutoff Valve. Adapted from reference 2.

3.3.1.2 Film Masking

The detail regarding the design of permeation cells and masking films to permeation systems can be found elsewhere.[11] Essentially a 'sandwich' type mask was made by placing a piece of film between two pieces of adhesive backed aluminum tape (Avery Denison Specialty Tape Division; Pasadena, CA). The area of the film being tested varies according to the properties of the materials. A smaller area (less than ½" diameter) was often used with relatively permeable materials and vice versa. This 'sandwich' is further

placed on a porous piece of metal at the bottom side of the permeation cell while two pieces of filter paper (Fisher; Pittsburg, PA) were utilized to support the membrane. Occasionally epoxy was placed on top of the sandwich at the membrane/aluminum tape interface to prevent leaking.

3.3.1.3 Experimental Procedure

After the cell was installed in the system, the entire system was evacuated for 24 hours by exposing the feed, permeate volumes along with the cell to vacuum. A leak test was then performed to measure the intrinsic leak rate of the atmospheric gases into the down stream reservoir. Only leak rate less than 5% of the expected permeation rate can be considered acceptable. All the valves should be kept closed when doing a leak test. Thereafter the feed gas was introduced into the upstream reservoir and rapidly purged through the vent valve three times to flush out any remaining air molecules. The feed gas was then allowed to reach thermal equilibrium in the volume for at least half an hour. After that, the gas was exposed to the upper side of the cell, which is also the upper side of the membrane being tested. The pressure change in the downstream reservoir due to permeation through the membrane was recorded continuously. When the permeation was finished, the entire system was evacuated again to allow additional tests with other gases. If multiple gas molecules were to be tested, carbon dioxide was always the last feed gas since it could induce plasticization which can substantially change the properties of the materials.

3.3.2 Gas Sorption Test

Pressure decay sorption was the primary method used in this work to measure the solubility of gas molecules in polymers or zeolites. The sorption experimental apparatus is illustrated in Figure 3.8. It is composed of two gas reservoirs made of Swagelok® fittings interconnected by long handle valves. Pressure transducers are used to record the pressure changes in the reservoirs. The entire set up is immersed in a water bath circulated by a temperature regulator [Fisher Scientific, Pittsburgh, PA]. When molecular sieves are the examined sorbent, small volumes are specially designed to yield a reasonable signal/noise ratio.

To perform the sorption measurements, samples were first placed in the sample cell and sealed with gasket. Both the two reservoirs were evacuated for 24 hours to remove gas pre-sorbed into the materials. Gas was introduced into the feed reservoir and allowed to reach thermal equilibrium for half an hour. Then the interconnection valve B was quickly opened for 3 seconds to allow gas to expand into the cell reservoir. The pressure in the cell started to decay due to gas being sorbed by the sample, which was monitored continuously. Once the sample reached equilibrium with the gas phase, a mole balance before and after the expansion gave the amount sorbed into the sample. Compressibility factors available from NISTL must be used to account for the non-ideality of the gas phase under high pressures.[12] The kinetic sorption curve can be obtained by plotting the pressure in the cell against time. This information is particularly important when analyzing zeolite sorption to identify whether the pores are clogged or not.

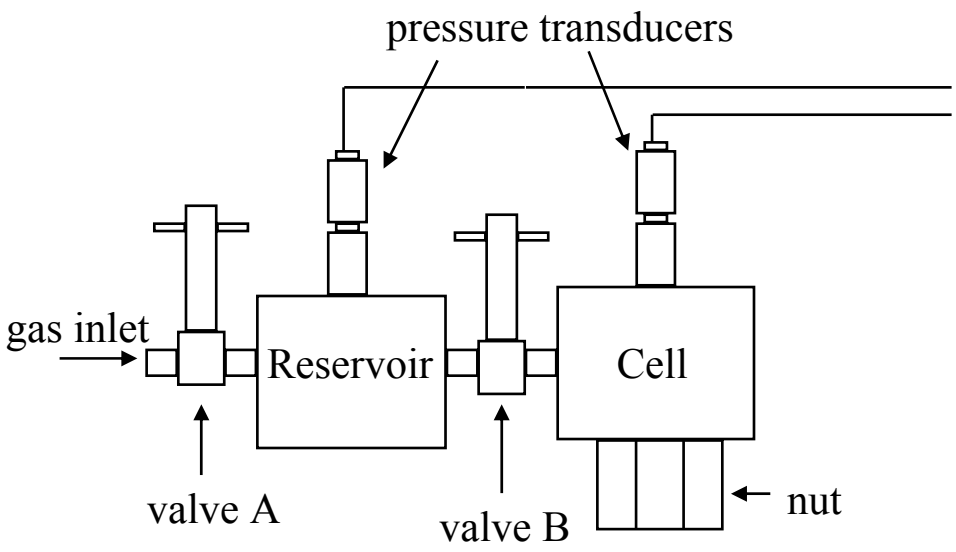

Figure 3.8 Schematic of a pressure decay sorption apparatus.

3.4 COMPLEMENTARY CHARACTERIZATION TECHNIQUES

A number of complementary characterization techniques were used to analyze the properties of materials and the elemental, structural changes concurring with various treatments.

3.4.1 Scanning Electron Microscopy (SEM)

Pieces of dried films were submerged in liquid nitrogen for 2 minutes before they were shear fractured by a pair of tweezers. Cross sections were mounted onto metal sample stages via conductive carbon tape, followed by sputter coating with a thin layer of gold (Model P-S1, ISI, Mountain View, CA). When particles were subjected to SEM examination, they were first dispersed in either ethanol or water and a few drops of such dispersion were placed on the sample mounts. No gold sputtering was used for powder samples. The images were obtained with SEM JEOL 1530, equipped with a thermally assisted field emission gun operating at 10 keV.

3.4.2 X-ray Photoelectron Spectroscopy (XPS)

XPS spectra were collected using a Surface Science model SSX-100 ESCA Spectrometer equipped with an electron gun and a monochromator. The system uses an Al Kα source (hν = 1486.6 eV). Ejected photoelectrons are detected by a hemispherical analyzer that provided high sensitivity and resolution. The operating pressure in the analyzing chamber was below 5×10^{-9} Torr. For each sample, spectra were collected in such a way that the photoemission angle was varied from 70° to 20° at an interval of 5° (forward), and back from 20° to 70° at an interval of 5° (backward), and three more rounds of forward and backward.

3.4.3 Solid-State NMR Measurements.

The details with regard to the relationship between solid-state NMR spectra and structures of zeolites and silicates can be found in Appendix A. ^{29}Si NMR spectra were recorded on a Bruker DSX-300 spectrometer equipped with a 7mm MAS probe with resonance frequencies of 59.6 MHz. Magic angle spinning was carried out at a rotation speed of 5 kHz. Single π/2 radio frequency pulses (pulse length 5μs) were used with a repetition time of 10s. ^{29}Si chemical shifts were referenced to 3-(Trimethylsilyl)-1-Propanesulfonic acid, sodium salt (0 ppm). ^{27}Al MAS spectra were obtained at 78.2 MHz by using the same spectrometer. The ^{27}Al chemical shifts were referenced to the external $Al(H_2O)_6^{3+}$ in saturated aqueous aluminum chloride solution. Before being packed into the NMR MAS rotors, all the samples were equilibrated in the saturated water vapor of an NH_4Cl solution. The measurements were performed with a spin rate of 6.5 kHz, 0.6 μs excitation pulse, 0.2sec recycle delay.

3.4.4 X-ray Diffraction (XRD)

X-ray diffraction yields insightful information on the crystallinity and structural integrity of crystalline samples. The data were collected with Ni-filtered Cu Kα radiation on a PanAlytical X'Pert PRO apparatus. The samples were pressed into a sample holder with a microscope slide. Precautions were taken to avoid preferred orientation. The data were recorded by step-scanning at 0.02° 2θ per step from 5° to 70° 2θ, where θ is the Bragg angle, and a counting time of 1s for each step.

3.4.5 Nitrogen Adsorption

Nitrogen adsorption measurements were implemented in this work to characterize the surface areas, pore volumes and pore size distribution of molecular sieves. The samples were degassed at 300°C for 18 hours under vacuum to remove pre-sorbed gas. The measurements were carried out on a Micromeritics ASAP 2020 (Micromeritics, Norcross, GA) at 77K. Both micropores and mesopores could be detected using this apparatus.

3.4.6 Miscellaneous

Mechanical Analysis (DMA) tests were performed on a dynamic mechanical analyzer (model 2980, Texas Instrument) under room temperature. Three films were examined for each type of pure or composite films.

Thermal Gravimetrical Analysis (TGA) was conducted on a Netzsch STA 409 PC TGA (Burlington, MA). Samples can be heated either under nitrogen or air up to a maximum of 1500°C.

Zeta-potential measurements were conducted on a Zetasizer® Nano ZS™ (Malvern, Worcestershire, United Kingdom). A very dilute solution of zeolites in solvent was prepared by dispersing ~0.05g of zeolite sample in 20mL solvent. It is essential to use

extremely dilute solution for the laser in the equipment to detect the movement of a single particle.

3.5 REFERENCES

[1] International Zeolite Association http://www.iza-structure.org.

[2] Moore, T. T. *Effect of Materials, Processing, and Operating Conditions of The Morphology and Transport Properties of Mixed Matrix Membranes*; Ph. D thesis: The University of Texas at Austin, 2004.

[3] Mittal, K. L.; Pizzi, A. Adhesion promotion techniques: technological applications; M. Dekker: New York, 1999.

[4] Plueddemann, E. P. *Silane Coupling Agents*, 2nd edition. Plenum Press: New York, 1991.

[5] Shang, X.Y.; Zhu, Z. K.; Yin, J.; Ma, X. D. *Chem. Mater*. **2002**, *14*, 71.

[6] Anschel, M.; Murphy, P. D. *J. Adhesion Sci. Tech*. **1994**, *8*, 787.

[7] Bansal, A.; Lewis, N. S. *J. Phys. Chem. B* **2001**, *105*, 10266.

[8] Bansal, A.; Li, X.; Yi, S. I.; Weinberg, W. H. Lewis, N. S. *J. Phys. Chem. B* **2001**, *105*, 10266.

[9] Sunseri, J. D.; Gedris, T. E.; Stiegman, A. E.; Dorsey, J. G. *Langmuir* **2003**, *19*, 8608.

[10] Husain, S. *Mixed Matrix Dual Layer Hollow Fiber Membranes for Natural Gas Separation*, Ph.D Thesis: Georgia Institute of Technology, 2006.

[11] Moore, T. T.; Damle, S.; Williams, P. J.; Koros, W. J. *J. Membr. Sci*. **2004**, *245*, 227.

[12] Zimmerman, C.M., *Advanced gas separation membrane materials: Hyper rigid polymers and molecular sieve-polymer mixed matrixes,* Ph.D Thesis: the University of Texas at Austin. 1998.

CHAPTER 4
INVESTIGATION AND COMPARISON OF SIEVE SURFACE MODIFICATION APPROACHES

4.1 BACKGROUND OF ADHESION IMPROVEMENT IN COMPOSITE MATERIALS

Composites filled or reinforced with fibers or powders constitute a broad domain of applications.[1-8] For example, improvements of the tensile strength, impact resistance, and also of electrical properties and aging characteristics strongly depend on adhesion between the matrix and the filler and on stability of the interfaces exposed to humidity, solvents, or temperature cycling.[9] Because of the large contribution of interfaces in a typical fiber- or powder-filled composite, any beneficial changes in surface characteristics of the filler and the resulting enhanced interaction with the matrix usually have dramatic effects on the performance of the materials. Inherent incompatibility of components is difficult to avoid, especially when a component of very different characteristics is incorporated into a matrix to tailor its properties. Good adhesion and stability of an interface help distribute stress, so better control and tailoring of the nano-scale interfacial regions to optimize the desired properties can enable the creation of improved composite materials.

Prior work to control interfacial compatibility in composite materials has considered various approaches including use of coupling agents to covalently bond the two phases;[10,11] surface-initiated polymerization with pre-formed particles;[12,13] and in situ synthesis of particles within pre-fabricated polymer matrices.[14] Use of coupling agents is usually limited to a specific polymer/filler pair because the selection of coupling agents

depends on the detailed chemical structure of the polymeric matrix. While the other two methods can solve some specialty problems, a generally applicable approach involving the blending of pre-made particles into pre-synthesized polymer is even more attractive. Such an approach provides full synthetic control over both the filler and the matrix, and has the ability to generate diverse composite materials.

4.2 MIXED MATRIX MEMBRANES WITH PVAC

4.2.1 Mixed Matrix Film Characterization

PVAc was explored in the present work as a control case due to its high chain flexibility (T_g=35ºC*)* and known affinity for silicate surfaces.[15] This material has been shown to form desirable interfaces with zeolites without any surface modification.[16] In this work, zeolite 4A was mixed with PVAc to fabricate mixed matrix membranes as control experiments to demonstrate the mixed matrix effect. Films with various sieve loadings were formed and characterized by O_2/N_2 permeation tests, the results of which are illustrated in Figure 4.1. The permeation of CO_2/CH_4 was not examined herein because PVAc plasticizes at CO_2 pressure of ~5 psig, rendering it unsuitable for CO_2 and CH_4 separation.

It is apparent that selectivity enhancement was successfully achieved with PVAc/4A combination. The films with 15wt% and 30wt% of solid contents all showed selectivities approaching the Maxwell model prediction. The flexibility of PVAc enables the chain segments to conform onto the sieve surfaces relatively easily as to form a void-free interface. Moreover, the potential hydrogen bonds formed between these two materials further contribute to the creation of desirable membranes. As the concentration of sieves increases, the amount of interfacial region in a membrane is enlarged and any defect at

the interface would greatly impact the performance of a membrane. The success rate of films annealed under 120ºC is fairly low. The discoveries made in the subsequent section indicated 200ºC was a more optimal condition for annealing PVAc based composites. Thus the 40wt% films illustrated in Figure 4.1 were all annealed 200ºC. The films with 40wt% sieve loading exhibited "partially defective" properties with slightly higher permeabilities and lower selectivities than the model values. It is believed that such films have a large portion of interfaces intact with small amount of defects present. It is noteworthy that the measured permeabilities of the defect-free membranes are usually lower that the theoretical values, which is believed to be caused by 'matrix rigidification' effect as introduced earlier in Chapter 1. The polymer chains surrounding the particles become immobilized due to conformation or tethering to solid surface, thus leading to a reduced permeability in the interfacial zones. There may be argument that 'matrix rigidification' could induce an enhancement in selectivity. In order to test this hypothesis, a control step was performed by combining PVAc with zeolite 3A, which is impermeable to either O_2 or N_2. In this case, any deviation from the Maxwell model prediction would be due to the 'rigidified region'. As indicated in the graph, PVAc-3A films only exhibited decreased permeabilities relative to the predicted values while negligible changes in selectivity was observed as compared to neat polymer. It is thereby hypothesized that since the rigidified chains affect both the gas molecules in a similar manner, the selectivity should not be altered much.

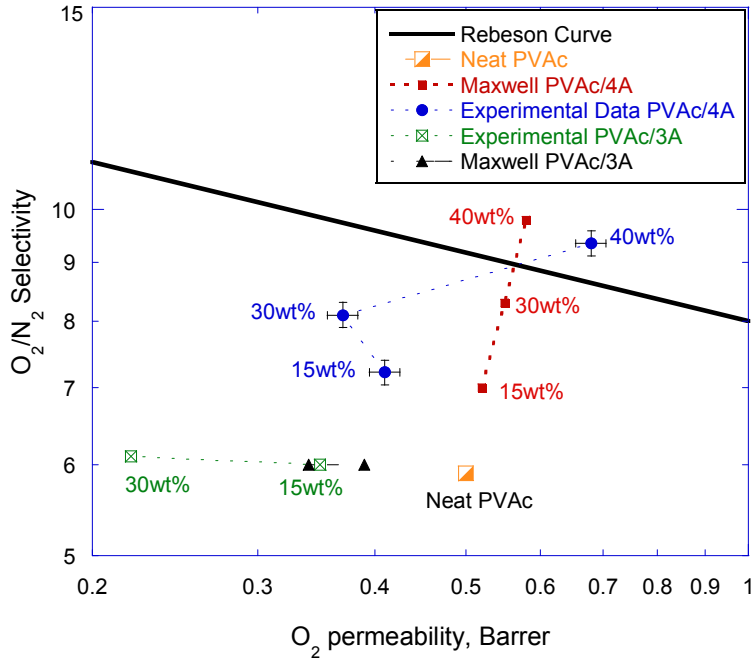

Figure 4.1 O_2/N_2 transport properties of PVAc containing 15wt%, 30wt% and 40wt% zeolite 4A and PVAc containing 15wt%, 30wt% zeolite 3A membranes, all tested at 35ºC and 65 psia upstream pressure.

4.2.2 Effect of Annealing Temperature on PVAc Composite Films

Another interesting study was conducted to investigate the effect of annealing temperature on the properties of PVAc. The basic idea is that the contact angle between a liquid and a substrate is indication of the adhesion between the two materials. Lower contact angle suggests stronger interaction and vice versa. It is also known that when a polymer is above its glass transition temperature, its behavior becomes similar to a fluid. If the contact angle between a polymeric 'fluid' and a zeolite could be obtained, the interactive affinity can be evaluated. In order to measure the contact angle between a polymer and a zeolite, a spherical PVAc particle (~2mm in diameter) was placed on a glass substrate that was selected to serve as a surrogate for zeolite surface. The polymer

was heated to a series of temperatures above its glass transition (35ºC) under vacuum for overnight and allowed to cool gradually. The contact angles were measured afterwards and the plot of contact angle vs. annealing temperature is depicted in Figure 4.2. Representative images of PVAc particle on a glass substrate during a contact angle measurement are displayed in Figure 4.3. Although the T_g of PVAc is close to room temperature and it is believed that these two materials have favorable interactions, the contact angle of PVAc on glass did not start to drop until around 150ºC as shown in the graph. This decreasing tendency continues till 250ºC upon which the contact angle stays stable. The graph suggests that the PVAc sphere did not start to 'melt' or become 'fluid-like' until 150ºC and it became essentially a 'fluid' around 250ºC. This conclusion was drawn based on the fact that above this temperature the contact angle no longer changes, which indicates the intrinsic interaction at equilibrium between a liquid-state PVAc sphere and the glass substrate. It is proposed in view of the observations made here that a higher annealing temperature (above 150ºC) may increase the adherence between PVAc and zeolites because the chains behave close to a fluid and thereby the attachment to a solid surface is presumably easier to occur than when they are in the solid-state.

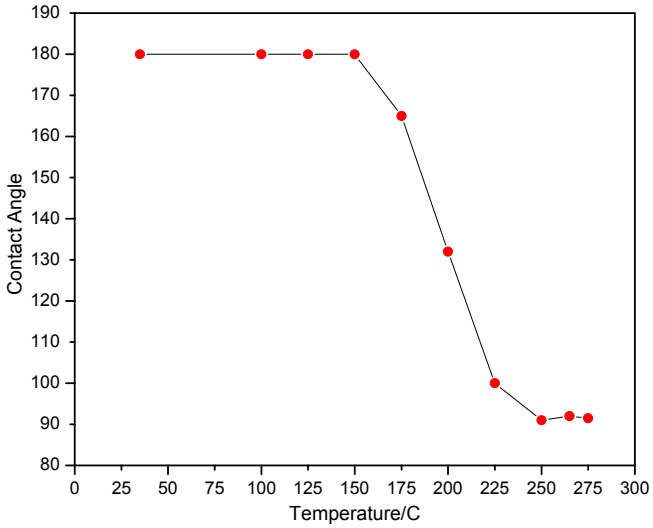

Figure 4.2 The contact angle of a PVAc sphere on a glass substrate under different temperatures.

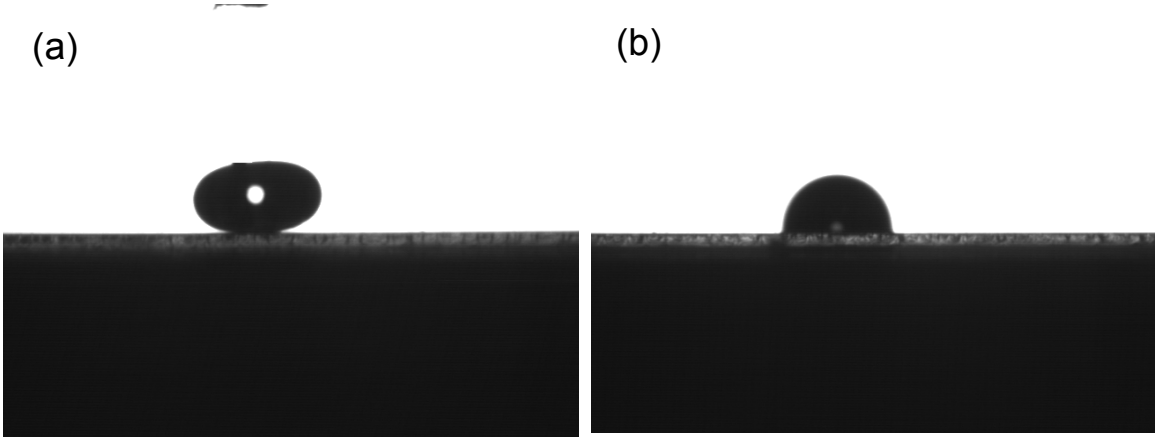

Figure 4.3 Representative images of a PVAc sphere on a glass substrate during a contact angle measurement: (a) PVAc dried at 50ºC under vacuum; (b) PVAc dried at 200ºC under vacuum.

Another important factor that needs to be considered when bringing up the annealing temperature is the stability of the polymer. Evidently the polymer should be stable under the appropriate annealing temperature without any degradation. A TGA test was performed on PVAc to find out the proper temperature range and the result is shown in

Figure 4.4. According to the plot, PVAc stays stable under 240ºC thus any temperature below this point should be proper for annealing this particular polymer.

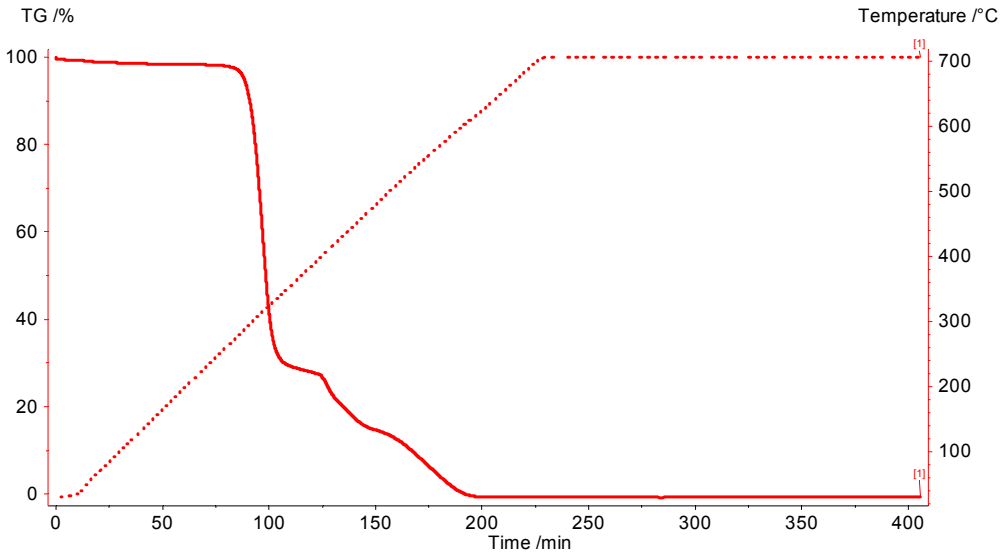

Figure 4.4 TGA test of neat PVAc heated in air up to 700ºC.

Based on the preceding findings, annealing temperature of 200ºC was considered a good condition. Mixed matrix films of PVAc containing zeolite 4A at 15wt% and 30wt% were annealed under this temperature and characterized via permeation experiments. Table 4.1 summarizes the obtained results. Desirable mixed matrix effect was achieved in both films. It is interesting to notice that the permeability at 30wt% is even lower than those shown in Figure 4.1 which were annealed under 120ºC. In other words, the degree of chain rigidification is probably more pronounced in films annealed under higher temperature.

The aforementioned discoveries may be of special interest to high zeolite loading membranes where good chain conformation at the interface is critical to obtain a defect-free and measurable film. Limited work has been done in the present study with regard to

this issue but it would be interesting to perform a further investigation of the annealing temperature on membrane performances. Moreover, it would be valuable to apply the same principle used with PVAc to other polymers, such as Ultem® and Matrimid®, to seek for optimal annealing temperatures of composite films based on an array of polymeric matrixes.

Table 4.1 Transport properties of PVAc/4A films annealed under 200ºC (tested at 35ºC and 65 psia upstream pressure)

Sieve Loading	Predicted P_{O2}	Observed P_{O2}	Predicted $\alpha_{O2/N2}$	Observed $\alpha_{O2/N2}$
15wt%	0.53	0.48	6.9	6.8
30wt%	0.56	0.31	8.4	8.7

4.3 MIXED MATRIX MEMBRANES WITH ULTEM®

Unlike PVAc, Ultem® is a polyether imide material with rigid backbones (T_g =215ºC). In addition, the hydrocarbon rings in this polymer do not favor the silanol rich zeolite surface due to the hydrophobic – hydrophilic interaction. These facts coupled together determine that Ultem® is unable to conform well to bare zeolite surfaces and thereby the membranes formed with Ultem® and unmodified zeolites all showed 'sieve-in-a-cage' morphology.[17] Consequently, tailoring the sub-optimal interfaces in Ultem® mixed matrix membranes is highly desired as to eliminate the voids which are detrimental to membrane performances. Zeolite surface modification was exploited in this work in order to

promote the interfacial adhesion between the matrix and fillers and formulate membranes with anticipated selectivity improvements.

Three approaches were attempted and studied in this work and the experimental results will be presented in this section. A most effective method will be selected and investigated in depth in later chapters.

4.3.1 Silanation of Zeolite Surface

The use of silane coupling agent to enhance interfacial adhesion in mixed matrix membranes was first reported by Mahajan, where the authors employed an aminosilane γ-aminopropyldimethylethoxysilane (APDMES) to modify the zeolite surface to improve affinity with the polymer matrixes.[18] In order to replicate their previous work and compare this surface modification method with others inspected in this study, APDMES was applied to zeolite 4A and Ultem® mixed matrix membranes were formed with such modified sieves.

4.3.1.1 Membrane Characterization

The permeation data of Ultem®/silanated 4A membranes are depicted in Figure 4.5. All the films either at 15 wt% or 30 wt% sieve loading exhibited depressed permeability as compared to the prediction by the Maxwell model, indicating the absence of voids in these composites. It is, however, surprising that the selectivity improvement is rather limited. Although the selectivity values are all beyond neat Ultem®, none of the films fulfilled the theoretical enhancement. This trend is consistent with Moore's discovery where the author obtained reduced permeabilities with Ultem®/ silanated 4A membranes without full improvements in selectivity.[19] It was proposed therein that the sonication horn used in the surface modification treatment may have driven iso-propanol molecules

into zeolite pores and thus 'clogged' or 'partially clogged' the micropores. In Mahajan's earlier work, ethanol was utilized as the solvent to disperse the solids and coupling reagent, and no such phenomenon was observed. The smaller dimension of ethanol makes it easier to be removed afterwards by heating while the larger IPA molecule may have remained in the zeolite pores and difficult to be extracted.[19] According to the results displayed in Figure 4.5, the sieves used in the current work appear to be partially clogged otherwise no selectivity increase would have occurred at all.

The above analysis suggests that the implementation of silane coupling agent promotes the polymer/sieve adhesion while at the same time the experimental procedure induces another undesirable effect, the blockage or partial blockage of zeolite pores. Subsequent section aims to elucidate the changes in modified zeolites and seek proof for the above hypothesis.

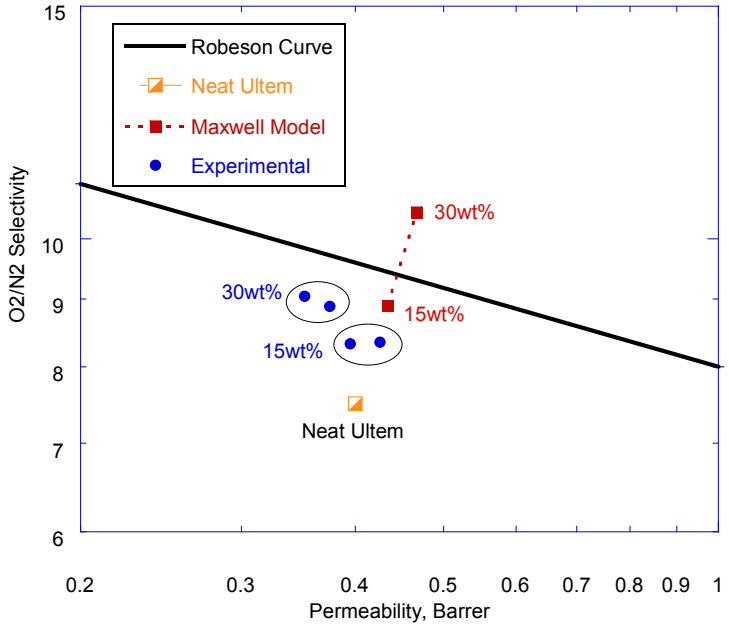

Figure 4.5 O_2/N_2 transport properties of Ultem® containing zeolite 4A modified via APDMES. (all tested at 35ºC and 65 psia upstream pressure)

4.3.1.2 Zeolite Characterization

XPS and TGA were utilized to characterize the silane modified sieves in order to illustrate the formation of covalent bonds between APDMES and zeolite surface, as well as any possible changes that accompanied the reaction. Figure 4.6 depicts the XPS spectra of silanated zeolite 4A and a control sample of the same batch of treated sieves after drying in air under 700ºC in TGA. The purpose of high temperature burning is to decompose the organic linkages that potentially have bonded to zeolites. Obviously strong C 1s intensity was detected on silane treated sieves (Figure 4.6a), inferring organic components attached to the surface. The analyzed C concentration is ~11 atom% on these powder samples. Moreover, a weak N 1s peak appeared at 400eV, which presumably is introduced by the amine groups in the silane coupling agent. After the surface functionalized zeolites were heated in air up to 700ºC, the C 1s peak diminished to negligible base value, accompanied by the disappearance of the N 1s signal (Figure 4.6b). The most likely scenario speculated from the above findings is that the silane linkages were decomposed during the burning off process.

Additionally, TGA revealed an interesting phenomenon associated with the silanated sieves. As shown in Figure 4.7, the total weight loss of modified sample (~7 wt%) upon air drying is considerably less than the untreated zeolites (~22.5 wt%). It is difficult to distinguish the percentage of weight loss attributed to moisture removal and decomposition of surface organic components. But according to XPS data, silane linkages were indeed burnt off, thus the 7wt% loss includes both water evaporation and degradation of organics. The sharp reduction in weight loss can be resulted from two facts: (1) The presence of silane chains on zeolites largely increases the hydrophobicity

of such surfaces and significantly reduced moisture adsorption; (2) The pores of silanated zeolites are partially 'clogged', leading to decreased adsorption capacity of water molecules. The second presumption can tentatively explain the permeation results where only partial selectivity enhancement was acquired, concurring with great depression in flux.

O_2 physisorption measurements generated further proof for the 'pore blockage' phenomenon. The data illustrated in Table 4.2 show an obvious decrease in surface area after silanation, most likely attributed to the strongly adsorbed iso-propanol molecules taking up available sorption sites. O_2 adsorption was utilized in these tests instead of N_2 adsorption because the diffusion rate of N_2 into zeolite 4A pore is extremely slow at 77K (literally considered 'inaccessible' to the pores). This issue will be elaborated in section 5.5.2. Precautions were taken to prevent any potential safety hazards involved in using liquid O_2.

Table 4.2 Oxygen physisorption measurement results of neat and silanated zeolite 4A samples (5μm).

Zeolite 4A	Surface Area (cm^2/g)
Pristine	356.0
Silanated	270.4

In conclusion, characterization of neat and modified sieve samples revealed that silane coupling agent successfully reacted with surface silanols and created covalent bonds with zeolite surface. Nonetheless, the sieves are likely to be partially clogged by the large solvent molecules during the treatment, leading to reduction in the selectivity of

membranes constituting such sieves. Aside from these facts, another disadvantage related to the utilization of silanes is that the selection of coupling agents is dependent on the specific chemical structures of the polymer matrix. Therefore, different silanes need to be chosen in order to suit various types of polymers.

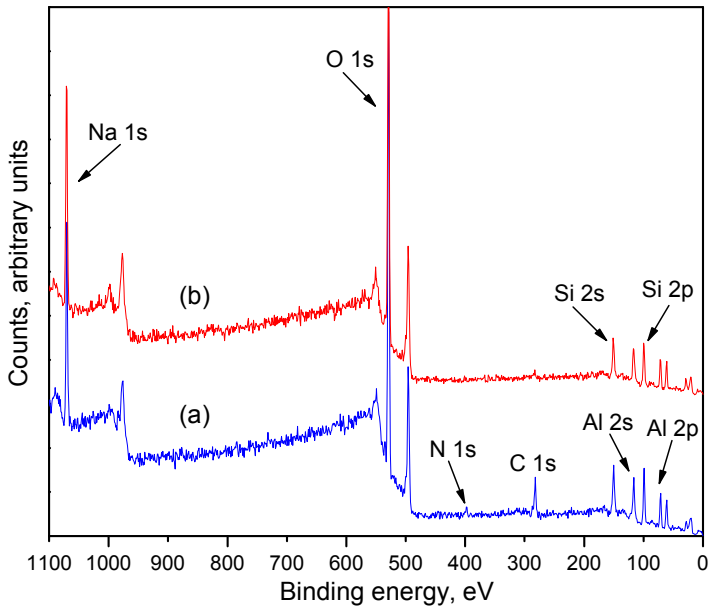

Figure 4.6 XPS surface survey spectra of zeolite 4A: (a) silane modified sieves; (b) the same batch of sample in (a) after TGA test in air under 700ºC.

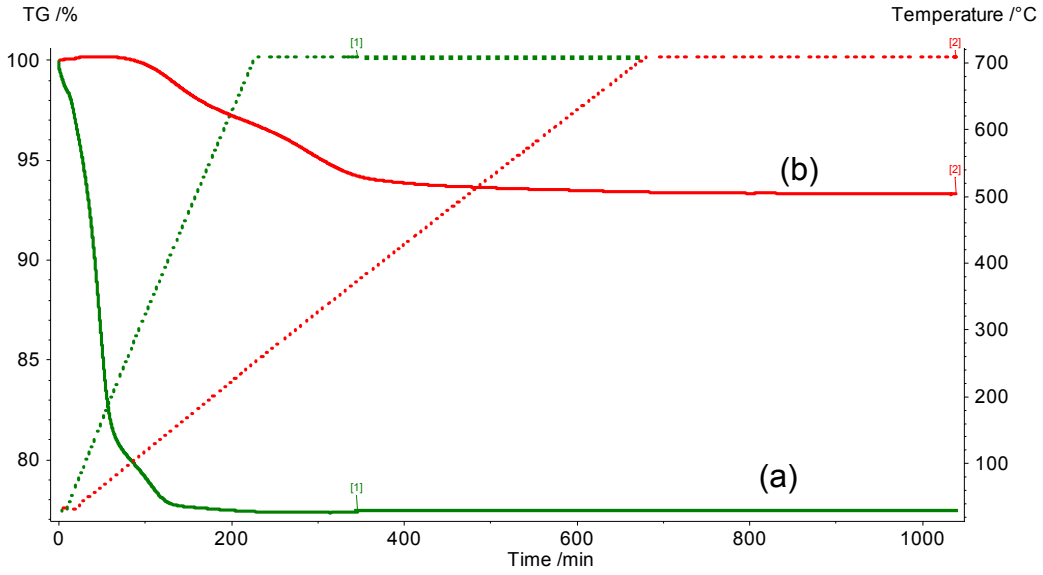

Figure 4.7 TGA results of two zeolite 4A samples (5μm): (a) neat zeolites; (b) silane treated zeolites.

4.3.2 Hydrophobization of Sieve Surface via Alcohols

Prevention of water adsorption at the polymer-sieve interface is important in order to avoid the 'plugged sieve' morphology. And it is particularly significant for asymmetric hollow fibers because they undergo a water quench bath in the standard spinning procedure. Nucleation of a water rich phase at the sieve surface could promote local phase separation, further leading to a 'sieve-in-a-cage' morphology.[20] If the sieve surface could be rendered hydrophobic, these problems would possibly be avoided. Hydrophobizing the sieve surface was studied hereby to improve the sieve's immunity to moisture. Reaction of zeolite surface with alcohols proceeds via an etherification process where the surface silanols (Si-OH) are converted to ether groups. The functionalization process is illustrated in Figure 4.8. The 'capping' of hydrophobic groups will break the surface hydroxyl network to reduce adsorption of moisture on the sieve surface. Increased hydrophobicity is anticipated to reduce local phase separation due to the

presence of water molecules and thus increase the adsorption of polymers on sieve surfaces.

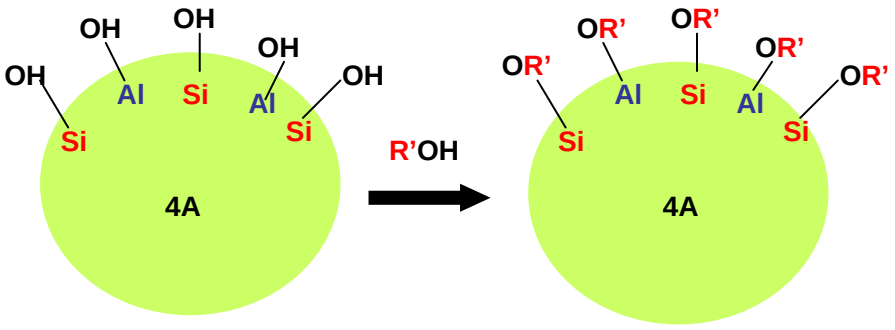

Figure 4.8 Reaction of zeolites surface silanol groups with alcohols.

One factor which could determine the prospects of this technique is the choice of an appropriate alcohol for the treatment. The criteria for selecting a proper alcohol are to provide adequate hydrophobicity to exclude water and to form a favorable interface with the polymer. Several alcohols of different chain length including methanol, ethanol and 1-propanol were considered as the modification reagents. Mixed matrix membranes comprising the modified zeolites were formulated and tested.

4.3.2.1 Membrane Characterization

Permeation measurements were conducted to test the gas separation performances of composite films constituting alcohol modified zeolites. As shown in Figure 4.9, at 15wt% solid concentration, the film comprising ethanol treated sieves exhibited transport properties close to the model prediction. The other two types of films, on the other hand, both demonstrated higher permeability and lower selectivity than theoretical values, which is characteristic of leaky interface morphology. When the sieve content increases to 30wt%, all the composite films delivered larger flux without any enhancement in selectivity. This clearly implies the failure of proper attachment of polymer chains at

interfaces. Moreover, the membrane containing 40wt% methanol treated zeolites showed very poor transport property. It is believed that this film is defective with holes that largely deteriorate the membrane selectivity. In a word, the modified sieves did not provide adequate improvements to achieve good membrane material.

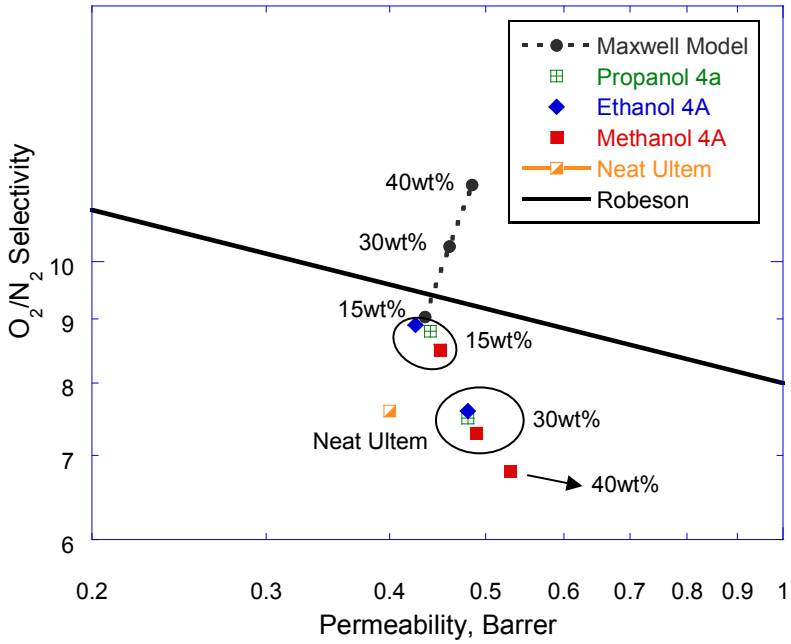

Figure 4.9 O_2/N_2 transport properties of Ultem® containing zeolite 4A modified via three different alcohols: methanol, ethanol and 1-propanol. (all tested at 35ºC and 65 psia upstream pressure)

4.3.2.2 Zeolite Characterization

The unsatisfactory results presented in Figure 4.9 could be caused by the failure of surface modification reactions. To test this possibility, characterization of zeolites treated via alcohol etherification process was performed on XPS and solid-state NMR to illuminate the possible changes occurring at the sieve surface.

Figure 4.10 depicts the XPS surface survey spectra of zeolite 4A modified via different alcohols. All the three treated samples showed higher C concentrations relative to the pristine sample. The detected C concentration on methanol treated sieves is ~8.9 atom% and ~12.9 atom% on ethanol treated counterparts. This corresponds to a higher C intensity in Figure 4.10c than Figure 4.10b. It was originally anticipated that the 1-propanol treated sieves would deliver the highest surface C content. Nonetheless, the detected C concentration is ~9.1 atom% on such sieve surface, consistent with weaker C peak intensity in Figure 4.10d than Figure 4.10c. It is possible that as the chain length of alcohol molecule increases, it becomes more difficult for the etherification reaction to take place. The bulkier groups are likely to yield larger hinderance that prevents the alcohol molecules from approaching the sieve surface; or the chains will have to rotate and bend in order to fit onto the surface via certain orientations. This hypothesis could possibly explain the smaller C concentration on 1-propanol treated sieves. The discovery indicates that the hydrophobicity of modified sieve surface does not necessarily increase with bigger alcohol molecules in this treatment and a 'trade-off' relationship may exist between the size of modification agents and the yield of surface etherification reaction.

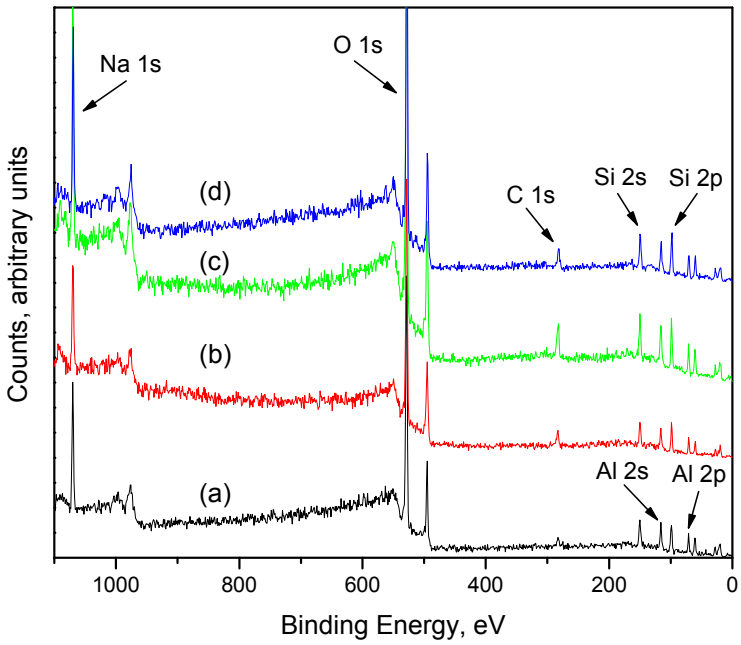

Figure 4.10 XPS survey spectra of surface modified zeolite 4A through alcohol etherification process: (a) fresh 4A; (b) methanol modified 4A; (c) ethanol modified 4A; (d) isopropanol modified 4A.

In addition to XPS, ^{13}C solid-state NMR was employed to confirm the successful bonding of ether groups to the sieves. The obtained spectra are illustrated in Figure 4.11. As anticipated, ether groups were detected in the treated samples. These results combined with XPS data provide strong proof of the success of surface modification reactions. Therefore, the lack of improvements in membrane performance is not due to the failure in treatments. The ether groups presumably have increased the surface hydrophobicity, but the lack of favorable interaction still exists and results in deficient membranes.

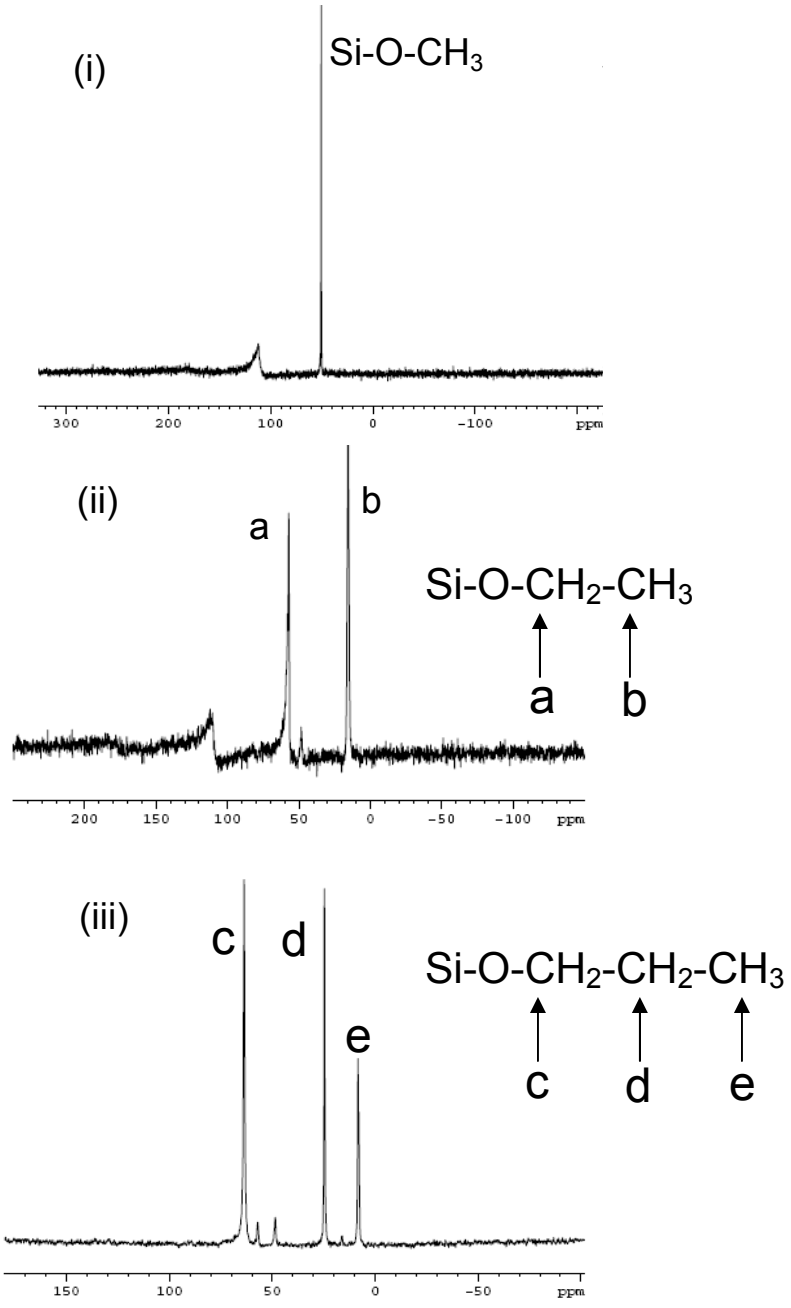

Figure 4.11 ^{13}C solid-state NMR spectra of modified zeolite 4A: (i) methanol treated sieves; (ii) ethanol treated sieves; (iii) 1-propanol treated sieves. The peaks are designated to the corresponding carbon atoms in the ether groups as shown along in the figure.

4.3.3 Grignard Surface Treatment

A new sieve surface modification method was most recently invented by Husain.[21] Such treatment involves two steps: reaction of zeolites with thionyl chloride, followed by exposure to methyl magnesium bromide (a Grignard reagent) and iso-propanol. The detailed chemistry underlying this chemical process will be elaborated in Chapter 6.

Mixed matrix dense films of Ultem® incorporated with this type of modified sieves were formulated and their gas separation performances were measured using permeation experiments. Figure 4.12 depicts the obtained results. This graph will be discussed in detail in Chapter 5 along with systematic characterization of dense films including SEM imaging, mechanical analysis, etc. In any case, the unmodified zeolites resulted in membranes with only higher flux and no improvement in selectivity. On the other hand, the samples containing surface modified zeolites all exhibited successful selectivity enhancement inferring much better interfacial adhesion is provided by such fillers. Even at higher sieve loading of 40wt% where most films containing fresh or modified sieves using the other two approaches failed to be tested, membranes with Grignard treated zeolites yielded desirable separation properties. The underlying mechanism of why such treated sieves enabled better interaction between polymer and fillers will be proposed and explored in Chapter 5.

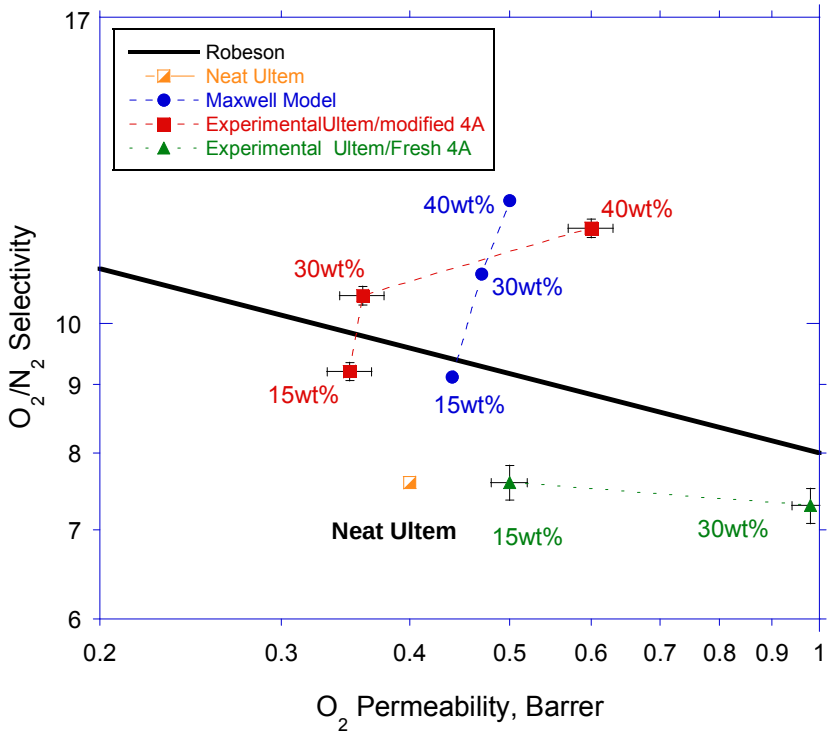

Figure 4.12 O_2/N_2 separation properties of Ultem® composite films, pure gas tests, 35°C, upstream pressure of 65psia.

4.4 CONCLUSIONS

The previous section summarizes three surface modification approaches inspected in this work to improve interfacial adhesion in mixed matrix membranes. Silanation of sieve surface provided improved interfacial attachment while the treatment blocked or partially blocked the micropores of zeolites simultaneously. And the selection of silane coupling agents is dependent on the specific chemical structures of polymer matrixes. Furthermore, the cost of silane coupling agents is quite high (~$200/5g), which makes this approach economically unattractive. Hydrophobizing the sieve surface via alcohols is

a simple and cost-effective method. However, negligible improvements in transport properties were found with the modified sieves. The newly developed Grignard treatment showed highest efficacy in promoting the compatibility between Ultem® and zeolite 4A even at 40wt% solid concentration and it did not show any sign of pore-blockage which makes this method the most promising candidate among the three for sieve surface modification.

The rest of the thesis will focus on systematic investigation of the Grignard treatment including detailed characterization of the mixed matrix membranes comprising sieves modified via this approach, exploration of the underlying mechanism of the demonstrated improvements (Chapter 5), elucidation of the detailed chemistry involved in this specific and complex process (Chapter 6 and 7), as well as methods to extend it to other inorganic materials to enable it a general strategy for interfacial adhesion enhancement in composite materials (Chapter 8).

4.5 REFERENCES

[1] Zhang. J.; Hou, L. Y.; Xu, L.; Xu, Z. L. *Chem. Mater*. **1999**, *11*, 3177.

[2] Molenkamp, W. C.; Watanabe, M.; Miyata, H.; Tolbert, S. H. *J. Am. Chem. Soc*. **2004**, *126*, 4476.

[3] Raghavan, S. R.; Riley, M. W.; Fedkiw, P. S.; Khan, S. A. *Chem. Mater*. **1998**, *10*, 244.

[4] Clark, J. H.; Macquarrie, D. J.; *Chem Commun*. **1998**, 853.

[5] Wright, A. P.; Davis, M. E.; *Chem. Rev*. **2002**, *102*, 3589.

[6] Lu, X.; Manners, I.; Winnik, M. A. *Macromolecules* **2001**, *34*, 1917.

[7] Teshima, K.; Sugimura, H.; Takai, O. *Langmuir* **2003**, *19*, 8331.

[8] Jeong, H. K.; Nair, S.; Vogt, T.; Dickinson, C.; Tsapatsis, M. *Nature Materials* **2003**, *2*, 53.

[9] Mittal, K. L.; Pizzi, A. *Adhesion Promotion Techniques*; Marcel Dekker: New York, 1999.

[10] Wall, J. S.; Hu, B.; Siddiqui, J. A.; Ottenbrite, R. M. *Langmuir* **2001**, *17*, 6027.

[11] Xie, X. L.; Tang, C. Y.; Zhou, X. P. *Chem. Mater*. **2004**, *16*, 133.

[12] Wang, J. Y.; Chen, W.; Liu, A. H.; Lu, G.; Yang, B. *J. Am. Chem. Soc*. **2002**, *124*, 13358.

[13] Perruchot, C.; Khan, M. A.; Kamitsi, A.; Armes, S. P.; Patten, T. E. *Langmuir* **2001**, *17*, 4479.

[14] Gomes, D.; Nunes, S. P.; Peinemann, K. V. *J. Membr. Sci*. **2005**, *246*, 13.

[15] Reed, J. S. *Principles of Ceramics Processing*; Wiley: New York, 1995.

[16] Mahajan, R.; Koros, W. J. *Ind. Eng. Chem. Res*. **2000**, *39*, 2692.

[17] Mahajan, R. *J. Appl. Poly. Sci.* **2002**, *86*, 881.

[18] Mahajan, R. Formation, *Characterization and Modeling of Mixed Matrix Membrane Materials*, Ph.D Thesis: the University of Texas at Austin, 2000.

[19] Moore, T. T. *Effect of Materials, Processing, and Operating Conditions of The Morphology and Transport Properties of Mixed Matrix Membranes*; Ph. D thesis: The University of Texas at Austin, 2004.

[20] Husain, S.; Koros, W. J. *J. Membr. Sci*. **2007**, *288*, 195.

[21] Husain, S. *Mixed Matrix Dual Layer Hollow Fiber Membranes for Natural Gas Separation*; Ph.D Thesis: Georgia Institute of Technology, 2006.

CHAPTER 5
MIXED MATRIX MEMBRANES WITH SURFACE MODIFIED ZEOLITE 4A BY THE HALIDE/GRIGNARD ROUTE

5.1 OVERVIEW

As discussed in the preceding chapter, the newly developed Halide/Grignard reaction sequence has most effectively promoted the interfacial compatibility in mixed matrix membranes. This chapter presents the characterization results of composite membranes containing zeolite 4A modified by this specific chemical treatment. SEM imaging reveals that a new surface morphology that resembles 'whiskers' appears on the modified sieves. Poly vinyl acetate (PVAc) and Ultem® composites containing this type of modified particles exhibit defect-free interfaces. DMA reveals that such composites have higher moduli as compared to those embedded with non-treated fillers with the same loadings. Furthermore, these materials also show impressive enhancements in gas permselectivity. The dramatic increase in the topological roughness (physical heterogeneity) on the sieve surfaces is proposed to provide improved interaction at the interface via induced adsorption and physical interlocking of polymer chains via multiple contact points in the nanoscopic inorganic whisker structure. XPS and TGA yielded useful information that quantitatively supports the above hypothesis. The presented strategy has potential to be extended to many other polymeric composites for a variety of applications, where tailoring polymer-solid interface compatibility is important.

5.2 MORPHOLOGICAL CHARACTERIZATION OF ZEOLITES AND COMPOSITE MEMBRANES

Figure 5.1a and 5.1b show the surface morphology of the as-received 4A particles of average diameters of 5μm and 200nm, respectively. Figure 5.1c and 5.1d represent the modified counterparts. These scanning electron microscopy (SEM) images clearly show that the surfaces of the sieves are changed significantly after the treatment. A new morphology that resembles inorganic whiskers or asperities was formed on the outer surface of the particles. Due to the difference in the size of the zeolite particles, the surface structure resembles 'whisker' on a 5μm sieve while it appears 'cotton balls' on 200nm crystals. The zeolites used in the subsequent sections were all 5μm particles. The results of membranes constituting submicron samples will be addressed in Appendix B along with the explanation why such sieves were less studied. The length of the inorganic morphology is estimated to be around 50nm and the width of these asperities appears to be one to two orders of magnitude smaller than the length, thus high aspect ratio structures exist on the surfaces. The significance of this scaling will be discussed in a later section. It is anticipated that the detailed dimensions of these features are adjustable via control of the treatment conditions. Efforts have been directed towards exploring this possibility and the results will be presented in chapter 8. Base on the surface characterizations of the modified particles, such as XPS and XRD, magnesium hydroxide was detected as the component of this inorganic whisker structure. The characterization results will be presented in chapter 6.

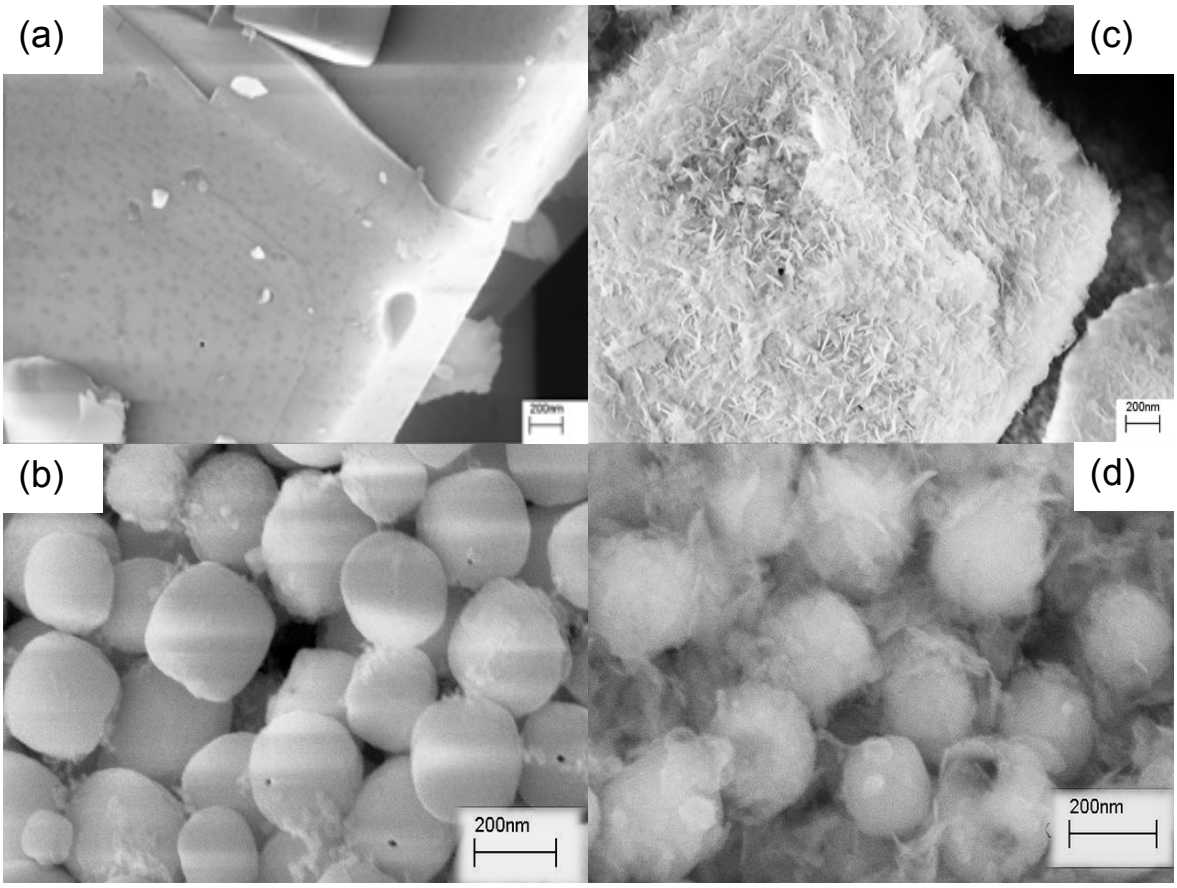

Figure 5.1 Representative Scanning Electron Micrographs (SEM): (a) unmodified 5μm 4A; (b) unmodified 200nm 4A; (c) modified 5μm 4A with the inorganic surface morphology; (d) modified 200nm 4A with the inorganic surface morphology.

When the modified particles were incorporated into a commercially available polymeric matrix Ultem® to form composites, the resultant films exhibited better interaction at the interface. The film composed of Ultem® and unmodified 4A had apparent voids between polymer and particles (Figure 5.2a), indicating poor adhesion between the two phases. These undesirable voids were eliminated in the films embedded with the modified particles bearing the whisker surface morphology (Figure 5.2b), implying enhanced interaction at the interfacial regions. No obvious defects could be observed even at high magnification as shown in Figure 5.2c, at least within the resolution of the SEM apparatus. This improvement evidently suggests that this

nanoscale whisker morphology stabilizes the polymer chains at the interface and promotes compatibility between polymer and filler particles. Since the resolution of SEM is inadequate to observe Ångstrom-sized defects, finer characterizations are needed to demonstrate that the interface is indeed intact at such small dimensions. DMA and gas permeation tests will be able to detect the mechanical and gas transport properties of these materials and thus yield insightful information with regard to this issue.

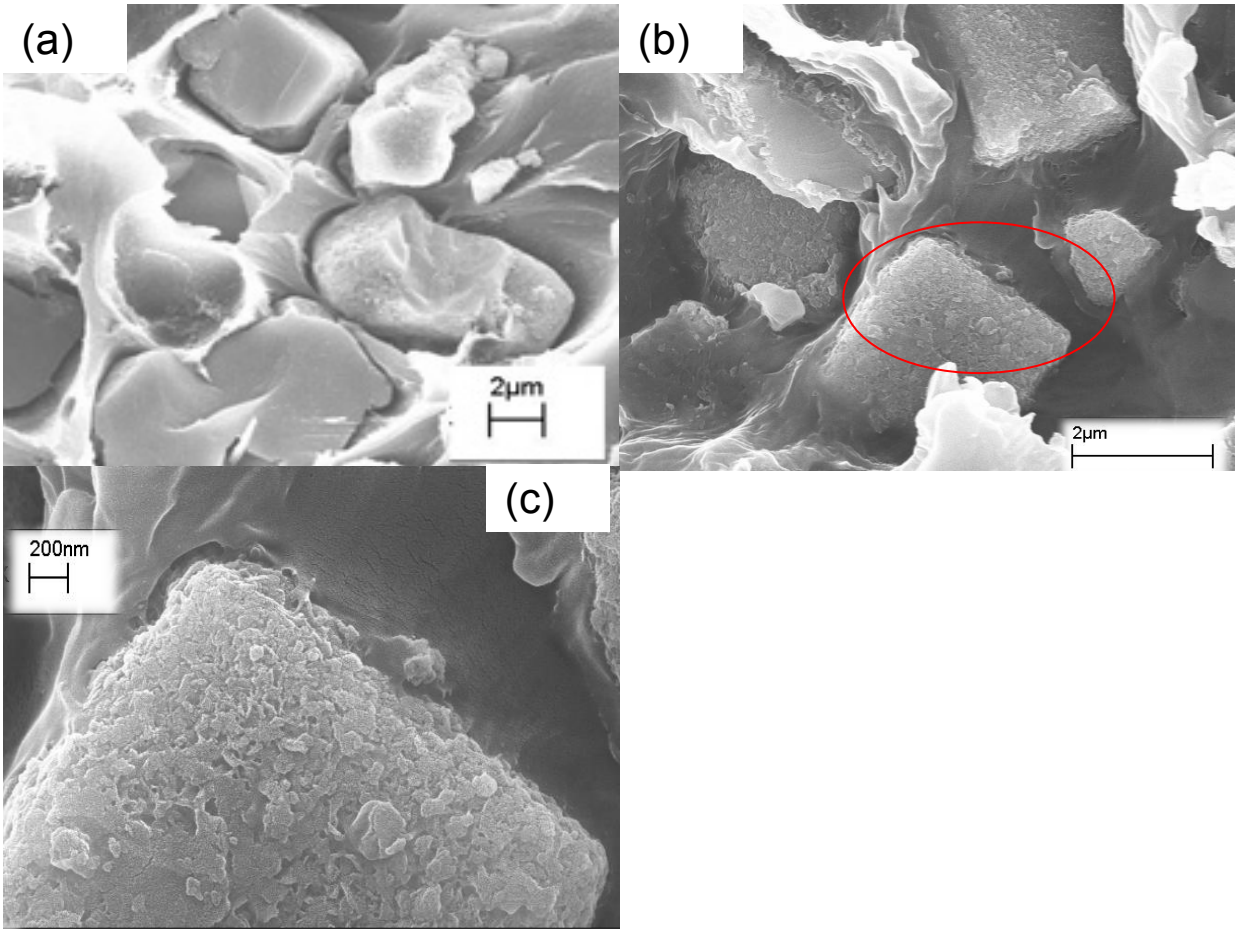

Figure 5.2 Representative Scanning Electron Micrographs (SEM): (a) unmodified 5μm 4A in Ultem®; (b) modified 5μm 4A in Ultem®; (c) higher magnification image of the circled region in (b).

5.3 MECHANICAL PROPERTIES OF MIXED MATRIX MEMBRANES

Besides Ultem®, polyvinyl acetate (PVAc) composites were also explored to demonstrate the versatility of this method with different kinds of polymers. Impressive changes were observed in the mechanical strength of both PVAc and Ultem® composites containing the modified 4A fillers.

Dynamic Mechanical Analysis (DMA) for the PVAc based composite films constituting either unmodified or modified 4A particles (both at 15wt% sieve loading) revealed increased elastic moduli over pure PVAc, as displayed in Figure 5.3a. This trend suggests that the incorporation of 4A fillers into PVAc formed good mixed matrix materials with improved mechanical property. The fact that the PVAc/fresh 4A films have higher moduli than neat polymer films is expected since PVAc is a very flexible polymer with a glass transition temperature (T_g) of 35ºC, and it is known to have affinity for silicate surfaces.[1] Thermodynamically, it is likely that the acetate groups in PVAc may interact favorably with the natural silanols on the unmodified 4A surfaces.[2] Therefore it is relatively easy for PVAc chains to adhere well to zeolite surface and form a desirable interface without any modification. Even accounting for this fact, it is evident that the moduli of PVAc/modified 4A films are even higher than their counterparts comprising pristine 4A, suggesting even better adhesion is enabled by the modified sieves with nanostructured surfaces.

In Ultem® based films the situation is completely different as illustrated in Figure 5.3b. The Ultem® composite films loaded with unmodified and modified 4A fillers (both at 15wt% sieve loading) exhibited markedly different properties. The Ultem®/unmodified 4A films had elastic moduli even less than the neat polymer, reflecting the apparent voids

at the interfacial regions (Figure 5.2a) due to poor adhesion. On the other hand, Ultem®/modified 4A films showed higher elastic moduli than the neat polymer, pointing to the presence of strong interaction between Ultem® and the sieves with nanostructures on the outer surface. This difference in the adhesion behavior of Ultem® with the two types of particles is believed to reflect the intrinsic nature of the rigid polyimide backbone of Ultem®, which has a T_g of 215ºC. Low chain flexibility impedes adsorption ability onto a particle surface to form defect-free interface. Moreover, the weak affinity of the Ultem® backbone for the silanol rich native 4A surfaces tends to lead to poor adhesion. Thus the void-containing interfacial morphology of Ultem® and unmodified 4A is believed to be caused by the intrinsically less favorable interaction between the comparatively smooth particle surface and rigid polymer chain. The nanoscale inorganic whiskers on the modified particle surface are believed to greatly enlarge the contact area and serve as interlocking points to stabilize the polymer chains, so the void morphology is eliminated even in the absence of highly favorable energetic interaction. This hypothesis will be explored in more detail in section 5.5. In any case, the DMA test results are consistent with the SEM observations in Figure 5.2 and further confirm that the interfacial adhesion is promoted by the modified fillers whose surfaces consist of inorganic nanostructures.

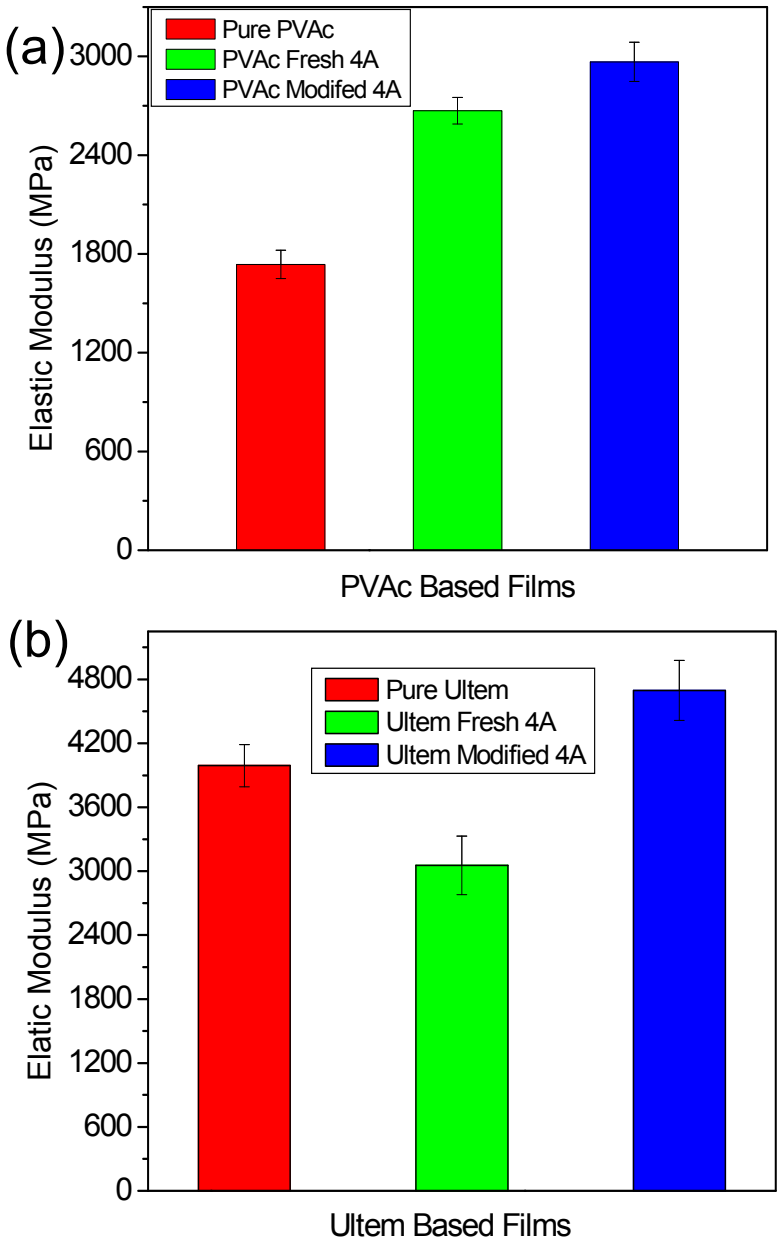

Figure 5.3 DMA test results of two sets of films: (a) neat PVAc, PVAc containing pristine 4A (15wt% sieve loading) and PVAc containing modified 4A particles (15wt% sieve loading); (b) neat Ultem®, Ultem® containing pristine 4A (15wt% sieve loading) and Ultem® containing modified 4A particles (15wt% sieve loading). Statistical ANOVA analysis was performed to evaluate the significance of the variance. For PVAc based films, the three groups showed F of 240.6 and p-value of 0.0043; and for Ultem® based films, the three groups showed F of 62.14 and p-value of 0.0159. Since both the p-values were less than 0.05, the null hypothesis could be rejected.[3]

5.4 GAS SEPARATION PERFORMANCES OF COMPOSITE FILMS WITH ZEOLITE 4A

Gas transport measurements are used in this study as another probe for the interfacial morphologies in composite membranes. Transport is very sensitive to defects due to the sub-nanometer difference in the size of typical gas molecules, so it is ideally suited to probe the interfacial integrity between the inorganic and polymer phases. In addition to the improvement in mechanical properties, remarkable changes have been observed in gas transport properties of composite films using the modified particles with nano-structured surface morphology. Zeolite 4A is a well known molecular sieve with a pore diameter of 3.8Å and a 3-dimensional pore network of interconnected cages that is ideally suited to the separation of O_2/N_2, and it has been estimated to have a very attractive oxygen permeability of 0.75 Barrers and an ideal O_2/N_2 selectivity of roughly 40, which is much above the performance properties of polymers. Similarly attractive performance is expected for the CO_2/CH_4 pair based on their relative sizes (3.3 Å minimum dimension for CO_2 and 3.8 Å for CH_4). Unfortunately, pure defect free zeolite membranes are extremely difficult and expensive to fabricate into large area applications. Thus mixed matrix membranes offer a promising alternative to make better use of the superb properties of zeolite 4A.

5.4.1 Permeation Measurements of PVAc Mixed Matrix Films

PVAc has been shown to form favorable interface with 4A particles due to its intrinsic flexibility and affinity for silicates,[1,2] but this polymer is not suitable for practical industrial gas separation because it is hard to process into hollow fibers and it can be easily plasticized by CO_2. Thus PVAc based composite films were only tested with O_2 and N_2 and the results are illustrated in Figure 5.4. The experimental results of PVAc

with unmodified 4A can be found in Chapter 4. All the composite films comprising modified 4A particles exhibited improved selectivities and reduced permeabilities relative to the Maxwell model prediction. It is important to notice that at 40 wt% solid content, the permeabilities continued to decrease; while 'partially defective' films with higher flux than theoretical prediction were obtained with the untreated zeolite samples as shown in Chapter 4. In addition, the success rate of films at such higher filler loading is much higher than those obtained with unmodified forms. Generally the decrease in permeability values is believed to be attributed to a 'matrix rigidification' effect. In the case of Grignard treated sieves, there may be another aspect associated with the impermeable inorganic layers on the sieve surface that have potentially added transport resistance to gas molecules and further depressed the permeability. In any case, this discovery is indicative of defect-free interfaces in such membranes, consistent with the desirable selectivity enhancement observed here.

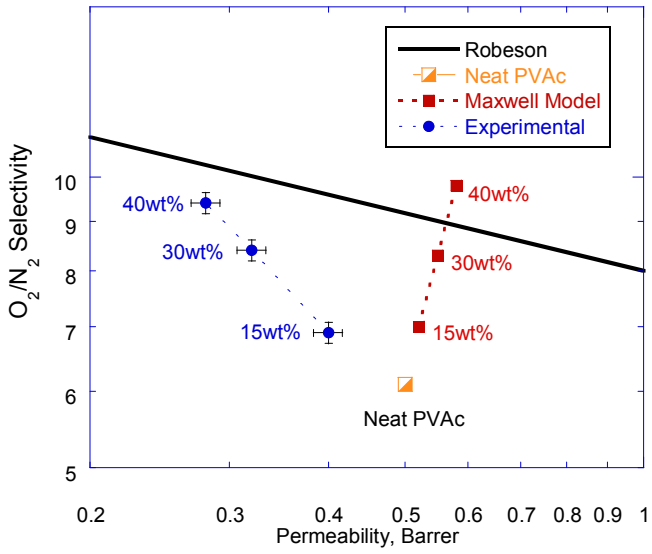

Figure 5.4 Gas transport properties of PVAc composite films containing modified zeolite 4A using the halide/Grignard treatment, tested at 35ºC and upstream pressure of 65 psia.

5.4.2 Permeation Measurements of Ultem® Mixed Matrix Films

Ultem® has great advantages over PVAc in its membrane formability and resistance to plasticization; however, it presents other challenges due to difficulty in creating defect-free interfaces.[4,5] Pure gas permeation experiments were performed to measure the gas transport properties in Ultem® based films and the results are reported in Figure 5.5. Figure 5.5a depicts the separation performance for oxygen/nitrogen. The bold line is the "upper bond tradeoff curve", which sets the upper limit for the separation performance of the available solution-processable polymeric materials.[6] The transport property of neat Ultem® lies below this curve. The blue dots represent the theoretical transport properties of Ultem®/4A films predicted by the Maxwell Model. The red squares and green triangles are the experimental data obtained for the composite films containing modified 4A particles and pristine 4A, respectively. The numbers designate the percentage of filler loadings in the polymer matrix by mass.

It is apparent that the Ultem®/fresh 4A films yielded no improvement in separation efficiency with O_2/N_2 selectivity equivalent to the neat polymer. This could be easily explained by the fact that the voids existing between polymer and fillers (Figure 5.2a) provide a free bypass for the gas molecules. They allow both oxygen and nitrogen molecules to transport directly through the voids without entering the selective micropores in the zeolites. In other words, 4A zeolites didn't participate in differentiating O_2 or N_2; therefore, no selectivity enhancement was observed. On the other hand, significant selectivity improvement was achieved by incorporating the modified 4A particles with the special surface morphology into Ultem® matrix. As indicated on the plot, at sieve loadings of 15wt% and 30wt%, the selectivity values obtained by

experiments approach the Maxwell Model predictions, and considerably exceed the neat polymer. This improvement further supports the absence of defects at the interface even at Ångstrom-scale and thus better adhesion is present in the composites containing modified fillers. The permeabilities of these films are relatively lower than model predictions, which is believed to be caused by immobilization of polymer chains due to adsorption onto the particle surfaces.[7,8] Moreover, a filler effect due to the impermeable nature of the inorganic $Mg(OH)_2$ whiskers may also contribute to this flux depression. At 40 wt% loading, the selectivity is a bit lower than the model value but still impressively higher than the property of neat Ultem®. At higher loading of fillers, more interfaces exist in a composite film, and any difficulty of maintaining a completely defect-free material becomes more pronounced. These films are considered to be 'partially' defective with a great proportion of interfaces intact while some defects present at certain minor regions. The separation performance for CO_2 and CH_4 follows the same trend as in the preceding discussions and is shown in Figure 5.5b.

In conclusion, the enhancement in gas separation efficiency of composite films is strong proof that the nanoscale whisker structure on the filler surface has largely improved the effective compatibility at the interface between the organic and inorganic phases. Furthermore, due to the size of the gas molecules themselves, this improvement also gives evidence that the defects were eliminated at Ångstrom scale. All previous results shown by SEM images, elastic moduli and gas separation properties illustrate the significant potential to use this new surface tailoring approach to nanoscopically engineer advanced materials.

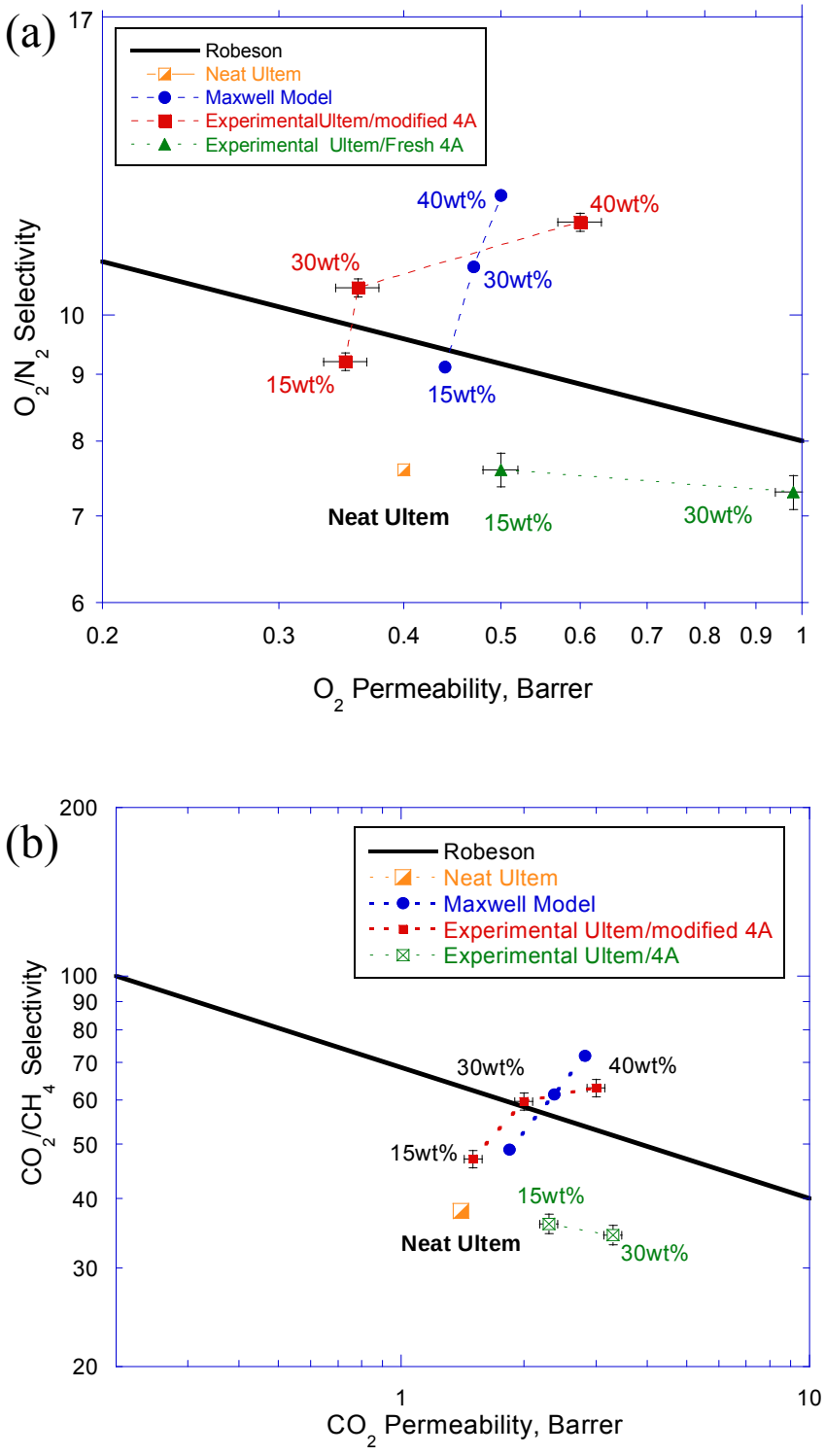

Figure 5.5 Gas transport properties of Ultem® composite films: (a) separation performance for O_2/N_2 at different filler loadings; (b) separation performance for CO_2/CH_4 at different filler loadings. (pure gas tests, 35°C, upstream pressure of 65 psia).

5.4.3 Permeation Measurements of Matrimid® Mixed Matrix Films

Matrimid® is the most challenging polymer in the present research. The structure of this material is even more rigid that Ultem® (T_g = 310ºC) and the hydrocarbon rings in this polymer intrinsically lack favorable interaction with hydroxyls on zeolite surface. In the past, attempts to formulate Matrimid® mixed matrix membranes all ended up with defective materials generating higher permeability and equal selectivity relative to the neat polymer. A Matrimid® film with ~15 wt% modified zeolite content was produced and tested via permeation experiment herein. Table 5.1 illustrates the transport properties of this sample. For both the gas pairs of O_2/N_2 and CO_2/CH_4, the experimental data showed depressed permeabilities below the Maxwell model prediction and selectivities even slightly higher than the theoretical value. The findings demonstrated the great potential of the Grignard treatment in its application to a variety of polymers, regardless of the specific chemical structures. This approach appears more effective than silane coupling agent in the case of Matrimid® because previous investigators found a 'leaky interface' morphology with silanated zeolite 4A in Matrimid®.[9]

Table 5.1 Gas transport properties of Matrimid® mixed matrix film (15 wt% zeolite content), tested at 35ºC and upstream pressure of 65 psi.

Membrane	O_2 Permeability, Barrer	O_2/N_2 Selectivity	CO_2 Permeability, Barrer	CO_2/CH_4 Selectivity
Neat Matrimid®	2.1	6.7	11.3	35
Maxwell Model	1.91	7.12	11.7	41.1
Experimental	1.89	7.7	9.17	41.2

5.5 HYPOTHESIS ON ADHESION ENHANCEMENT ENABLED BY THE INORGANIC SURFACE MORPHOLOGY

All the preceding results suggest that formation of nanoscale structures on the surfaces of particles promotes the interfacial adhesion in the resultant mixed matrix membranes. A few ideals are proposed herein to qualitatively explain how such nanostructures are believed to enhance the interfacial attachment in a composite system.

5.5.1 Surface Roughness Induced Polymer's Adsorption

A schematic vision of the scenario enabled by the inorganic whisker morphology is depicted in Figure 5.6. For typical polymers, the preferred conformation state is as random coils. However, the surfaces of the pristine zeolite particles are comparatively smooth with few irregularities (Figure 5.1a and 5.1b). When a polymer chain adsorbs onto this type of surface, it must significantly deform in order to adhere via the formation of 'loops, trains and tails', [10] which are obviously much more ordered configurations than the initial random coils. In this case, the entropy penalty of a polymer's adsorption onto a solid surface, ΔS_1, is considerable. Nevertheless, in case of a heterogeneous particle surface, a polymer coil need not change original conformation too much to adhere; therefore the entropy penalty, ΔS_2, is substantially lower as compared to the situation of a smooth particle surface.[11,12] The inorganic whisker morphology created in our experiment represents a very disordered surface topography where polymer chains can entangle into the whiskers without much change in configuration, and may even show a favorable mixing entropy with the nanoscale entities comprising the morphology. The free energy of adsorption can be represented as

$$\Delta G = \Delta H - T\Delta S$$

If an adequately negative enthalpy of interaction (ΔH) offsets a negative entropy change, adsorption can still occur ($\Delta G<0$). This is presumably the situation with PVAc, which has intrinsic affinity towards silicate particles via the formation of hydrogen bonds. On the other hand, for Ultem® system, the less favorable enthalpic interaction (ΔH) is presumably unable to overcome the entropy penalty if Ultem® chains adsorb onto smooth 4A surfaces. Thus effective adsorption does not occur under such circumstances ($\Delta G>0$), consistent with the voids present at the interface (Figure 5.2a). The whisker morphology created via the treatment can significantly minimize the entropy penalty and enable Ultem®'s adsorption within such whisker structures ($\Delta G<0$), as shown by the void-free interface (Figure 5.2b). In conclusion, adsorption onto a heterogeneous particle surface is much more favored based on the ability to mitigate the entropy penalty effect.

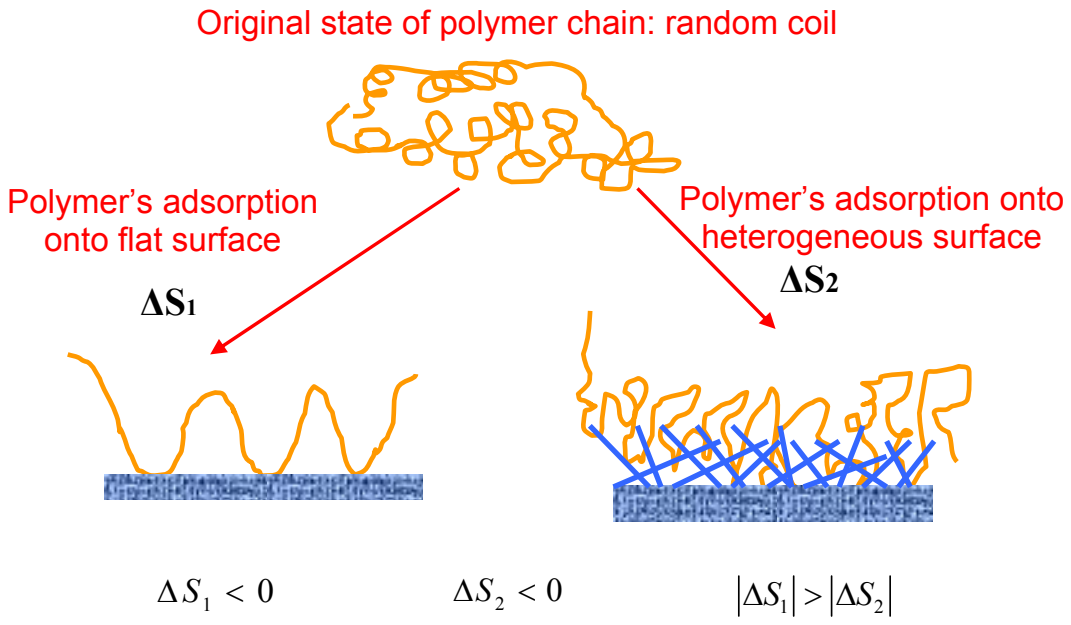

Figure 5.6 Polymer's adsorption onto a flat, ordered surface versus its adsorption onto a heterogeneous surface with random nanostructures. ΔS_1 designates the entropy change of a polymer chain to adsorb onto a flat surface and ΔS_2 symbolizes the entropy change of the same chain to adsorb onto a whisker structure.

5.5.2 Physical Interlocking: Multiple Points of Attachment

Once on the surface, the polymer chains are often more difficult to remove than they were to attach in the first place. The cause is related to multiple points of attachment. If one considers hydrogen bonding, for example, at 5 kcal/mol, then one such bond is rather easy to break. To break two such bonds is more complicated than just having 10kcal/mol available, because both bonds need to be broken *simultaneously*, or, the second bond needs to be broken before the first one reforms. In the case of several such bonds, it often proves difficult to debond all of them at the same time. Hence the kinetics of debonding is much slower than the kinetics of bonding in the first place.[13]

According to this theory, the whiskers bring another advantage of stabilizing the chains at interface by creating multiple points of attachment. N_2 physisorption tests were performed to measure the BET surface areas of various zeolite 4A samples and the results are summarized in Table 5.2. It should be noted that for this measurement, only submicron particles can yield reasonable data while the 5μm crystals are unable to be characterized by N_2 adsorption. This phenomenon has been well documented in literature. Breck et al reported that the pores of large zeolite 4A particles are literally 'inaccessible' to N_2 molecules at 77.35K due to the uniform Si/Al=1 framework and the charge compensation ions.[14,15] The diffusion coefficient is so small that the adsorption process takes extremely long time to complete. Contrary to this discovery, nano-sized 4A crystals have a Si/Al ratio higher than unity and therefore less charge compensation ions exist in the framework, leading to a larger pore size accessible by liquid N_2.[16-18] The data shown in Table 5.2 revealed a substantial increase in surface areas after the Grignard treatment for both batches of submicron zeolite 4A. This increase is apparently attributed to the

presence of surface nanoscale entities. Clearly, in such a case, the contact areas between polymer and fillers are greatly augmented by these inorganic structures. It is known that during the formation of membranes, stress forms when solvent evaporates from membranes and such stress can cause delamination of polymer chains from the sieve surface.[19] The whiskers serve as effective interlocks between sieve and polymer to grab tightly and stabilize the contact of polymer chains and thus prevent the delamination. A schematic vision is illustrated in Figure 5.7.

Table 5.2 BET surface areas of submicron zeolite 4A before and after Grignard treatment, measured by Nitrogen Physisorption tests.

Zeolite 4A	$A_{unmodified}$ cm^2/g	$A_{modified}$ cm^2/g
Batch 1*	338.0	563.5
Batch 2**	378.0	620.4

* Batch 1 was provided by Chevron Energy Corporation a few years ago. The batch number is C2286-43.
** Batch 2 was provided by Chevron Energy Corporation most recently, batch number unavailable.

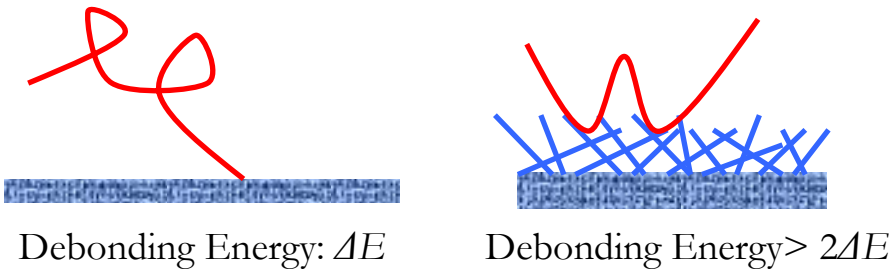

Figure 5.7 Illustration of multiple points of contact enabled by the whisker structure on sieve surface.

5.5.3 Dimension Similarity

Furthermore, it is important to point out that the length scale of the inorganic whisker structure also plays a crucial role in achieving the improvement. The length of such whiskers formed in our experiment is around 50nm, with apparent aspect ratio well above 10. A high magnification image of the surface structures is displayed in Figure 5.8. This structure provides a dimension that is close to the scaling of a polymer chain in the present study. The 'diameter' of a linear polymer molecule is roughly given by its root-mean-square (r.m.s) end to end length, which for many carbon backbone polymers is given approximately by

$$\left\langle r^2 \right\rangle^{1/2} / nm = 0.06 M^{1/2}$$

Where M=molecular weight. [20,21] This approximation can be used to roughly calculate the dimensions of PVAc and Ultem® chains in this work. For PVAc, Mw = 500,000, the approximate r = 42.2 nm; for Ultem®, Mw = 56,000, the approximate r = 15.0 nm. This closeness in dimensions of the whiskers and polymer chains makes adsorption even easier, because the chains can relax in an environment similar to their native configurations. It is hypothesized that a finer surface morphology such as needles or whiskers is more desirable than mild surface roughness such as holes, pits or chunky pieces. It would be ideal if the treatment conditions could be properly controlled to generate fine inorganic surface structures. Nonetheless, the detailed relationship between different treatment conditions and the surface morphology requires more in-depth investigation to be defined.

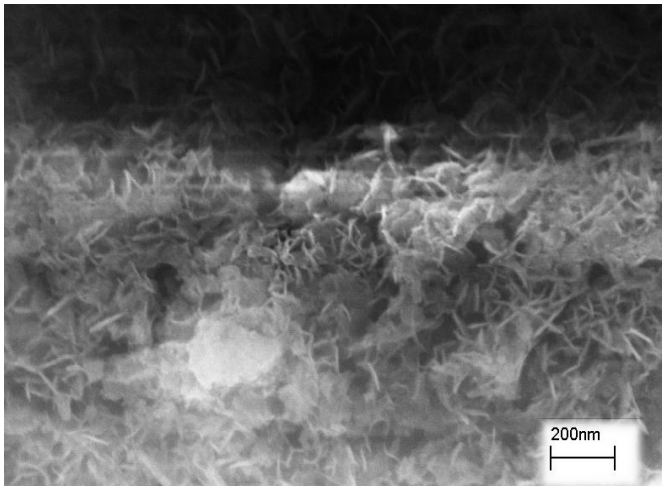

Figure 5.8 A high magnification SEM image of the 'whisker-like' surface structures on zeolite 4A surface.

5.6 QUANTITATIVE MEASUREMENTS OF POLYMER'S ADSORPTION ON SIEVE SURFACE

The preceding discussions proposed hypothesis on why the nanostructures help promote the adsorption of polymer chains onto such surfaces. This section aims to quantitatively measure polymer's adsorption on different solid surfaces, thereby providing proof to these assumptions. Experimentally, unmodified zeolite 4A and the modified counterparts with roughened surface morphology were dispersed in dilute PVAc/toluene solution and Ultem®/dichloromethane solution, respectively. The particles were then collected via centrifuge, repeatedly rinsed with the solvent for three more times, followed by drying under vacuum at 100ºC overnight. It is assumed that the mobile polymer segments on the solid surface would be easily dissolved by the solvent during rinse, so only the strongly adsorbed or mobilized chains will remain on the particle surfaces. Although theoretically speaking, after abundant rinse, the solvent should be able to extract all the chains from the solid surface, limited times of rinse (three used here) is presumably unable to dissolve all the adsorbed segments. The difficulty in

removing polymers from a solid surface is another indication of the strength of adhesion. It is noteworthy that only submicron zeolite 4A was investigated in this section because the much higher surface areas would enable a larger adsorption capacity and the changes in surface elemental compositions or weight loss will be more pronounced than the micron-sized counterparts.

5.6.1 XPS Analysis

The dried powders after dispersing in polymer solutions were analyzed using XPS to reveal the surface elemental compositions and the spectra are illustrated in Figure 5.9 and 5.10. It was found that C is present on both the polymer doped particle surfaces due to the adsorbed polymer segments (Figure 5.9b and 5.9d). On the other hand, C is absent from both samples of unmodified 4A (Figure 5.9a) or Grignard treated 4A that has not been exposed to polymer solutions (Figure 5.9c). Furthermore, the atomic concentrations of C vary on different surfaces. For zeolite 4A after being dispersed in PVAc solution, ~18 atom% is present on the unmodified particles while ~32 atom% was detected on the roughened sieves.

Similar trend can be observed in the case of Ultem® (Figure 5.10). About 48 atom% of C exists on the roughened 4A (Figure 5.10d) versus ~20 atom% detected on neat 4A (Figure 5.10b) after exposure to polymer solution. Besides larger C concentration, a stronger N signal was found on roughened zeolite surface (Figure 5.10d) which is introduced by the imide groups in Ultem®, while the N peak intensity in Figure 5.10b is very low inferring much less polymers have adsorbed on such smooth surfaces. These discoveries reflect the fact that the modified zeolites bearing the nanoscale structures

have promoted the adsorption of polymers onto solid surfaces, regardless of the chemical structures of the macromolecules.

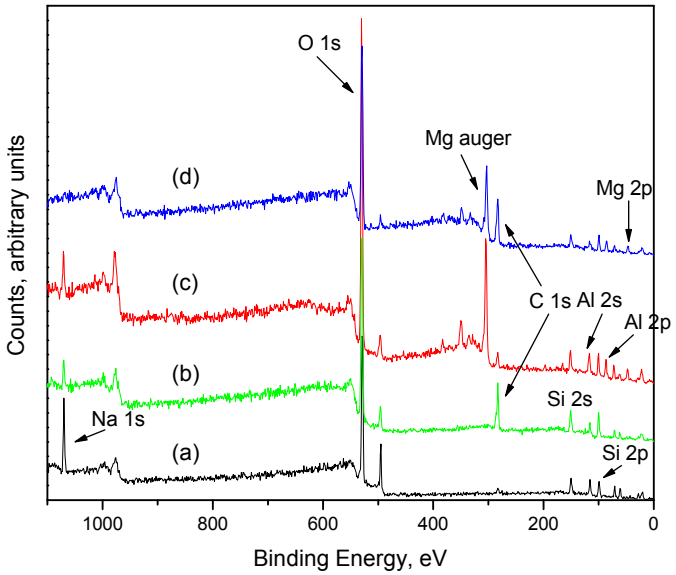

Figure 5.9 XPS spectra of zeolite 4A samples: (a) unmodified 4A; (b) unmodified 4A after dispersing in PVAc; (c) Grignard treated 4A; (d) Grignard treated 4A after dispersing in PVAc.

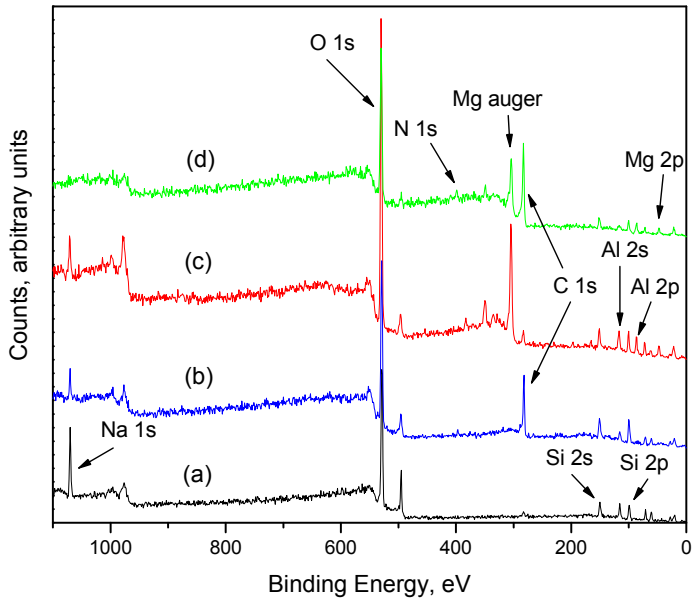

Figure 5.10 XPS spectra of zeolite 4A samples: (a) unmodified 4A; (b) unmodified 4A after dispersing in Ultem®; (c) Grignard treated 4A; (d) Grignard treated 4A after dispersing in Ultem®.

5.6.2 TGA Characterization

Thermal Gravimetric Analysis (TGA) was utilized in this study to provide further evidence of the induced adsorption of polymers onto disordered surfaces. The powders after being dispersed in polymer solutions and dried to remove residual solvent were heated in air under high temperatures in a TGA furnace. The purpose of such operation is to degrade the polymers adhering to the particle surfaces, so the weight loss can be used to indicate the amount of polymers originally present on the solid surface.

A few control experiments were performed before inspecting the polymer doped sieves. Pure $Mg(OH)_2$ crystals were dried in air at temperatures up to 700ºC to reveal the conversion temperature from hydroxide to oxide. As shown in Figure 5.11, the crystals start to lose water from around 290ºC and the dehydration is completed around 320ºC.

The eventual loss in weight is ~31wt% which corresponds well with the stoichiometric value of 31.03wt%. This dehydration effect should be observed in all the modified samples with $Mg(OH)_2$ on the surfaces. Moreover, neat 4A and Grignard treated 4A underwent the same drying process to set the backgrounds for their polymer dispersed counterparts. As depicted in Figure 5.12a, the intrinsic loss caused by removal of moisture in zeolite 4A is ~14 wt%. About ~2 wt% higher loss was associated with the Grignard treated sample, which presumably is related to the extra dehydration effect in the range of 290ºC - 320ºC. In other words, dehydration of surface $Mg(OH)_2$ components resulted in a higher weight loss in the Grignard treated sample.

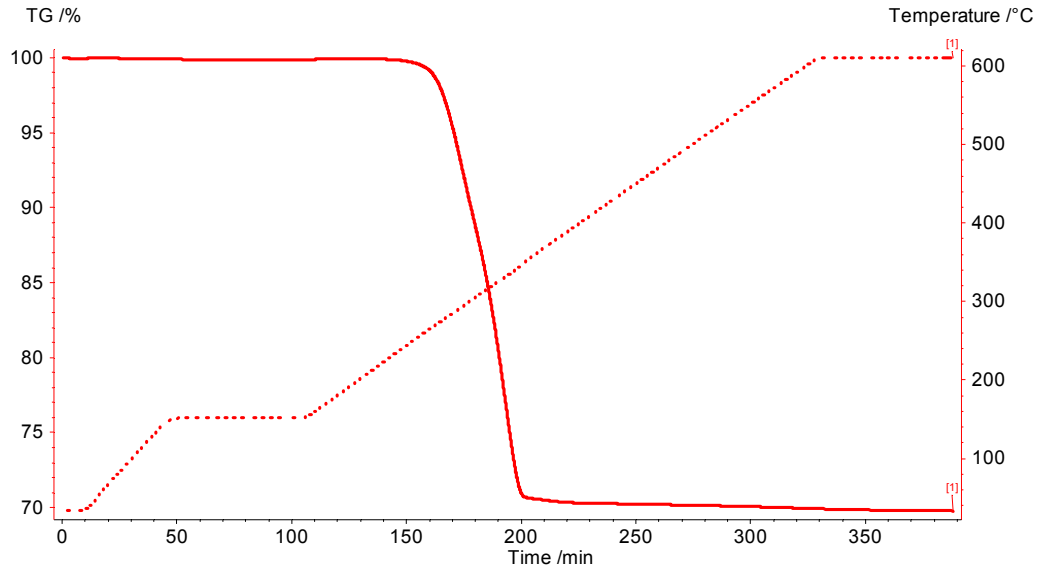

Figure 5.11 Thermal Gravimetric Analysis (TGA) curve of pure $Mg(OH)_2$ crystals.

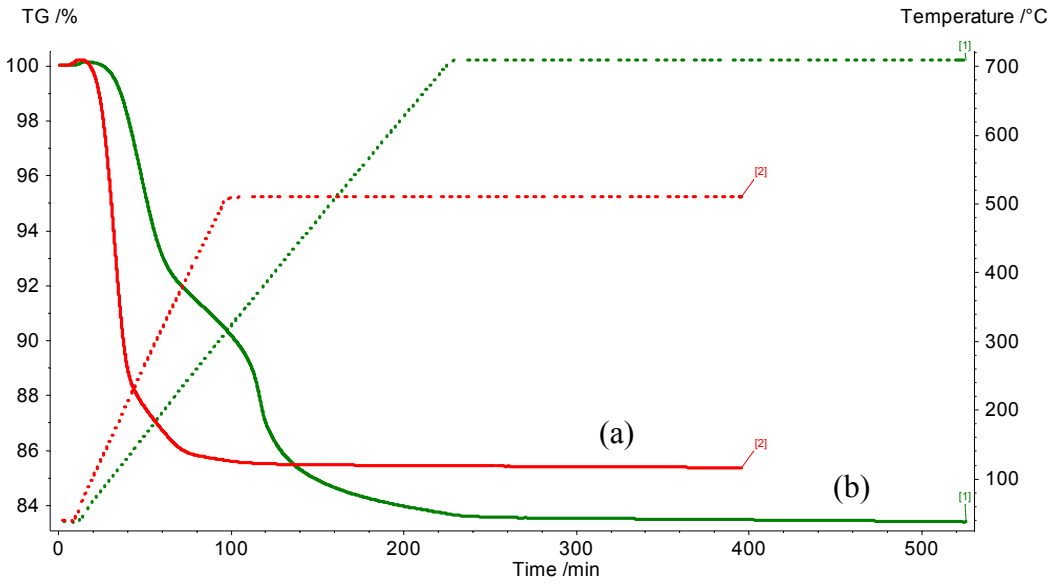

Figure 5.12 Thermal Gravimetric Analysis (TGA) results of zeolite 4A samples: (a) neat 4A; (b) Grignard treated 4A.

Figure 5.13 depicts the TGA results of 200nm zeolite 4A sieves after dispersing in PVAc/toluene solution. As explained earlier, the advantage of submicron sieves lies in the fact that the much higher surface areas should enable a larger adsorption capacity and the effect of weight loss would thus be more articulated in the burn off process. The initial weight loss occurring below 200ºC is believed to be due to the evaporation of water pre-adsorbed in zeolites, accounting for ~14% of total weight loss in both samples. Zeolites are microporous material that can adsorb significant amount of water in the internal pores. PVAc started to degrade from around 220ºC, causing a further weight loss above this temperature. The conversion from $Mg(OH)_2$ to MgO was manifested in the modified sieves within the range of 290ºC - 320ºC, which is designated to a change in the curvature within that region. The ultimate polymeric loss detected with the unmodified 4A is ~3.5% while ~15% was observed with the modified sieves. The numbers were

obtained by subtracting the base values (indicated by previous tests in Figure 5.12) from the ultimate loss in the polymer doped samples. The difference between (a) and (b) implies that more polymers were burnt off from the modified sieves than the unmodified counterparts. In other words, more chain segments adsorbed on the modified particles in the first place.

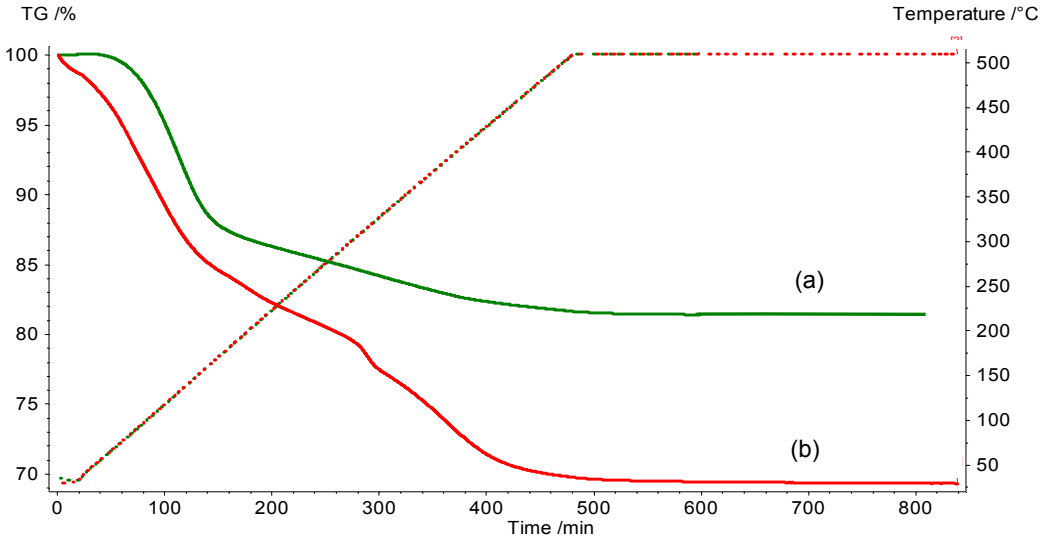

Figure 5.13 Thermal Gravimetric Analysis (TGA) results of 200nm zeolite 4A samples: (a) unmodified zeolites after dispersing in PVAc solution; (b) modified zeolites after dispersing in PVAc solution.

Similar experiments were carried out with zeolite 4A powders after dispersing in Ultem® solutions and the results are illustrated in Figure 5.14. A higher isotherm temperature (700ºC) was used for Ultem® because it has a higher degradation temperature and it was found that the decomposition was not complete when TGA was performed up to 500ºC. Both the samples demonstrated a weight loss of ~18% below 200ºC, probably related to the removed water content. The slight change in curvature between 290ºC and 320ºC was caused by the additional dehydration of $Mg(OH)_2$

accompanying the decomposition of Ultem®. A much higher polymeric loss occurred with the modified sample bearing disordered surfaces as opposed to the pristine form having smooth surfaces. These observations are in accordance with the earlier discovery where larger polymeric weight loss was associated with the modified particles after dispersing in PVAc solution. These results combined together further support that surface heterogeneity enables induced adsorption of polymer chains. This phenomenon is not limited by the chemical nature of polymers as it is manifested in both the cases of PVAc and Ultem®.

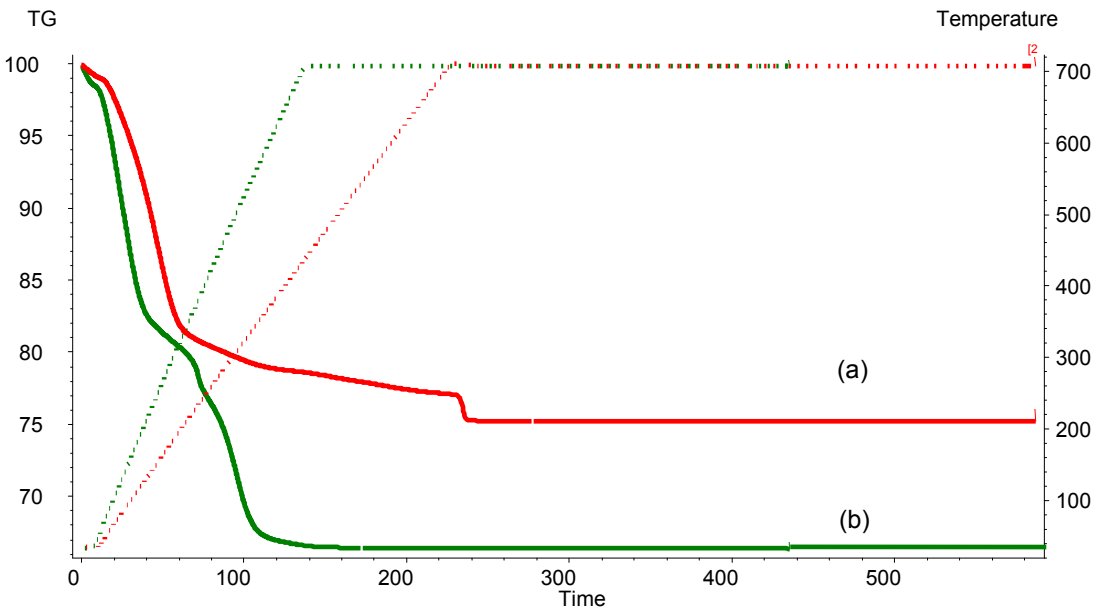

Figure 5.14 Thermal Gravimetric Analysis (TGA) results of 200nm zeolite 4A samples: (a) unmodified zeolites after dispersing in Ultem® solution; (b) modified zeolites after dispersing in Ultem® solution.

XPS analysis was performed on the samples which underwent TGA to double check that all the polymers were burned off from the particle surface. The resultant spectra are illustrated in Figure 5.15 and Figure 5.16. It is obvious that the C peaks diminished

completely following the TGA tests, which is a consequence of the fact that all the adsorbed polymers were degraded and converted to gaseous products.

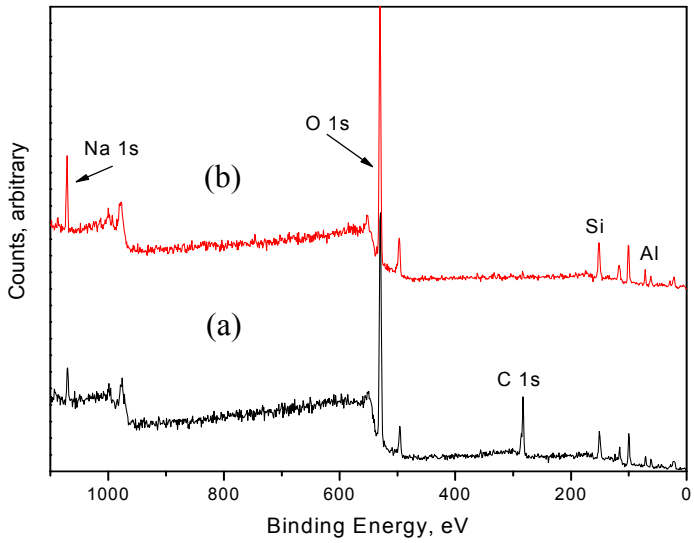

Figure 5.15 XPS surveys of unmodified 0.2µm zeolite 4A samples: (a) after dispersing in dilute PVAc solution; (b) sample (a) after TGA test in air under 500ºC.

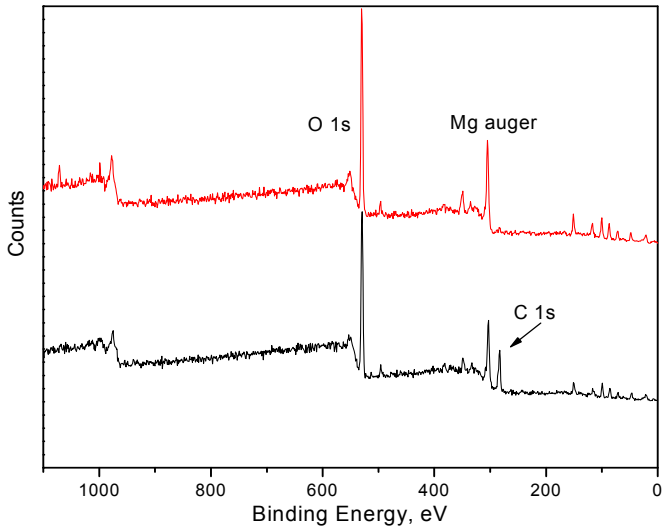

Figure 5.16 XPS surveys of Grignard modified 0.2µm zeolite 4A samples: (a) after dispersing in dilute Ultem® solution; (b) sample (a) after TGA test in air under 700ºC.

To summarize the preceding discussions, XPS and TGA characterizations yielded quantitative measures of polymers' adsorption on zeolite surfaces. The obtained results reveal that stronger adsorption occured on the modified, roughened particle surfaces as compared to the unmodified, smooth surfaces. Thus these findings provide further evidence of the assumptions made in section 5.5.

5.7 FEATURES OF THIS STRATEGY

A great advantage of this approach is that it can potentially be generalized and is not confined to a particular polymer/filler system. Unlike the utilization of coupling agents which depends on the chemical structure of a polymer matrix, the current approach need not be complicatedly tailored to a specific polymer/particle pair since the thermodynamic entropy effect and physical interlocking are universal. This approach appears potentially applicable in many occasions in which similar roughened morphologies can be created on filler surfaces. Once the surface patterns are achieved, the modified fillers could be incorporated into the desired polymer matrixes to form void-free composites. A possible avenue in this regard might be deposition of an outer layer of disordered carbon nanotubes on a glassy carbon to form new composite materials. This topic could be interesting and useful to inspect.

5.8 CONCLUSIONS

In summary, this chapter reports a general strategy to enhance the interfacial adhesion in polymeric composites by creating nanoscale morphologies on the surfaces of particles. The surface morphology, which appears as inorganic whiskers, was achieved by treating silicate particles (zeolites 4A) with thionyl chloride, followed by subsequent reaction

with methyl magnesium bromide (a Grignard reagent). Polymeric composites containing this type of modified particles exhibit defect-free interfaces. DMA revealed that such composites have higher moduli than those constituting non-treated fillers with the same loadings. Furthermore, gas permeation measurements demonstrated that these materials also show impressive enhancements in gas separation efficiency. Ideas were proposed to qualitatively explain why such nanoscale structures contribute to improved adhesion at the interfaces. The surface roughening effect is believed to have contributed to the enhancement via thermodynamically induced adsorption and physical interlocking in the whisker structure. The entanglement can therefore effectively stabilize contact between the polymer and inorganic fillers. XPS and TGA measurements generated more insightful information which quantitatively supports the above assumptions. A great advantage of this methodology is that it need not be confined to a specific material pair, since the thermodynamic principle and physical interlocking mechanism provided by the inorganic whiskers are universal and potentially applicable in occasions where similar nanoscopic morphologies can be created on the filler surfaces. Thus the presented strategy has potential to be extended to many other polymeric composites for a variety of applications, where tailoring polymer solid interface compatibility is important.

5.9 REFERENCES

[1] Mahajan, R.; Koros, W. J. *Ind. Eng. Chem. Res*. **2000**, *39*, 2692.

[2] Reed, J. S. *Principles of Ceramics Processing*; Wiley: New York, 1995.

[3] Johnson, R. A. *Miller and Freund's Probability and Statistics for Engineers*; Prentice-Hall: Englewood Cliffs, 1994.

[4] Vankelecom, I. F. J.; Merckx, E.; Luts, M.; Uytterhoeven, J. B. *J. Phys. Chem*. **1995**, *99*, 13187.

[5] Duval, J. M.; Kemperman, A. J. B.; Folkers, B.; Mulder, M. H. V.; Desgrandchamps, G.; Smolders, C. A. *J. Appl. Polym. Sci*. **1994**, *54*, 409.

[6] Robeson, L. M. *J. Membr. Sci*. **1991**, *62*, 165.

[7] Tsagaropoulos, G.; Kim, J. S.; Eisenberg, A. *Macromolecules* **1996**, *29*, 2222.

[8] Moore, T. T.; Koros, W. J. *J. Molec. Struc*. **2005**, *739*, 87.

[9] Mahajan, R. Formation, *Characterization and Modeling of Mixed Matrix Membrane Materials*, Ph.D Thesis: the University of Texas at Austin, 2000.

[10] Tanford, C. *Physical Chemistry of Macromolecules*; John Wiley & Sons: New York, 1961.

[11] Douglas, J. F. *Macromolecules* **1989**, *22*, 3707.

[12] Baumgartner, A.; Muthukumar, M. J. *Chem. Phys.* **1991**, *94*, 4062.

[13] Sperling, L. H. *Introduction to Physical Polymer Science*; John Wiley & Sons: New York, 2001.

[14] Breck, D. W. *Zeolite Molecular Sieves: Structure, Chemistry, and Use*; Wiley: New York, 1973.

[15] Breck, D. W.; Eversole, W. G.; Milton, R. M.; Reed, T. B.; Thomas, T. L. *J. Am. Chem. Soc*. **1956**, *78*, 5963.

[16] Rakoczy, R. A.; Traa, Y. *Microporous and Mesoporous Materials* **2003**, *60*, 69.

[17] Reed. T. B.; Breck, D. W. *J. Am. Chem. Soc*. **1956**, *78*, 5972.

[18] Wang, H.; Huang, L.; Holmberg, B. A.; Yan, Y. *Chem. Commun*. **2002**, 1708.

[19] Moore, T. T. *Effect of Materials, Processing, and Operating Conditions of The Morphology and Transport Properties of Mixed Matrix Membranes*; Ph. D thesis: The University of Texas at Austin, 2004.

[20] Flory, P. J. *Statistical Mechanics of Chain Molecules*; Hanser Publishers: New York, 1989.

[21] Hunter, R. J. *Foudations of Colloid Science*; Clarendon Press: Oxford, 1991.

CHAPTER 6
EXPLORATION OF THE UNDERLYING CHEMISTRY OF THE GRIGNARD TREATMENT

6.1 OVERVIEW

As presented in the preceding chapter, a two-step reaction sequence, dealumination via thionyl chloride followed by reaction with a Grignard reagent, has created a nano-scale morphology that appears as significantly roughened outer surfaces on zeolite 4A particles. This chapter is devoted to exploit the underlying chemical mechanism involved in the formation of such surface nanostructure.

XPS and XRD measurements revealed that the inorganic entities are composed of $Mg(OH)_2$ crystals. Furthermore, solid state ^{29}Si and ^{27}Al NMR and XPS surface analysis revealed that thionyl chloride partially removes aluminum from the zeolite 4A framework and yields NaCl and $AlCl_3$. Precipitation of these extracted inorganic salts on the surfaces of zeolite particles occur. Subsequently, methyl magnesium bromide is reacted with 2-propanol in a quenching process that generates $Mg(OH)_2$. The previously deposited NaCl and $AlCl_3$ nano-particles on zeolite surfaces are believed to function as heterogeneous nuclei for the growth of $Mg(OH)_2$ crystals which thereby create the nano-structured surface morphology. The modified particles are shown in chapter 5 to provide enhanced interfacial adhesion in polymeric composites.

6.2 INITIAL HYPOTHESIS

The application of a halide/Grignard chemical treatment on an aluminum-containing zeolite was originally proposed by Husain,[1] whose work was inspired by similar chemical processes being used on porous silica or silicate materials to attach alkyl moieties to the

silicon surface. Bansal et al developed a two-step procedure where the H-terminated Si surface was first chlorinated radically by PCl_5 and subsequently quenched with a Grignard reagent at 80°C for 30 min to 8 days to form Si-C bonds.[2-4] Sunseri et al studied complete methylation of silica surfaces using thionyl chloride as a chlorination reagent, along with subsequent methylation by methyl lithium.[5] Clark et al employed CCl_4 to make chlorinated silica followed by reaction with a Grignard reagent.[6] Terry et al used chlorine gas under ultraviolet excitation to replace H on the H-Si (111) surface, followed by immersion in alkyl lithium solution.[7] Vassylyev et al reported surface modification of ZSM-5 type zeolites using a combined $SiCl_4$ and Grignard reagent route.[8] In addition, research has discovered that by direct exposure of porous silica to Grignard reagents, Si-C bonds could be created as well.[9]

According to the aforementioned studies, the original hypothesis of applying halide/Grignard treatment to SSZ-13 zeolites was to methylate the zeolite surface thus improve the hydrophobicity of the sieves. The reaction was assumed to proceed via the following mechanism:

$$\langle Si\rangle - OH + SOCl_2 \rightarrow \langle Si\rangle - Cl + SO_2 + HCl \qquad (6.\ 1)$$

The chlorinated surface can further react with a suitable Grignard reagent to directly bond the alkyl group to the silicon surface as follows:

$$\langle Si\rangle - Cl + RM \rightarrow \langle Si\rangle - R + MCl \qquad (6.\ 2)$$

where RM is the organometallic (Grignard) reagent.

Nevertheless, our work presented here will demonstrate that with the presence of aluminum in zeolite framework, the reactions will proceed via a different path from the

equations 6.1 and 6.2. The subsequent sections aim to illustrate this matter and illuminate the detailed mechanisms involved in this complicated chemical process.

6.3 CHARACTERIZATION AND IDENTIFICATION OF SURFACE NANOSTRUCTURE

The morphologies of the surface structures can be found in Figure 5.1. This section summarizes the characterization results to identify the compound that comprises the nanoscale entities.

6.3.1 XPS Elemental Characterization

X-ray photoelectron spectroscopy was conducted to reveal the changes in the surface elemental compositions of the particles and the results are shown in Figure 6.1. Figure 6.1a depicts the XPS survey of untreated zeolite 4A, where the major peaks correspond to the four elements of this material: Na, O, Si and Al. After the two-step treatment, new peaks of Mg (~15 atom% atomic concentration) were detected on the sieve surfaces as shown in Figure 6.1b. Evidently the Mg containing species is attributed to the new surface structure. Since there is negligible change in the carbon concentration on the surface as compared to the base value on the unmodified particles, these whiskers are very likely to be an inorganic material. Two control steps were conducted to test this possibility. Firstly, the treated 4A powders were dried in air at 400ºC for 24 hours, followed by XPS analysis. Figure 6.1c illustrates the XPS spectrum for this sample and negligible change was observed as compared to the sample before air drying (Figure 6.1b). This suggests that the Mg-containing compound is probably inorganic in nature otherwise air drying at 400ºC would have led to the degradation of common organic species. The second control test was to disperse the treated 4A sample in a dilute

hydrochloride acid solution (0.1M) for 30 seconds. The sieves were then collected by centrifuge and rinsed repeatedly with de-ionized water. XPS spectrum for these HCl washed sieves is shown in Figure 6.1d. The intensities of Mg peaks for this sample diminished drastically and only ~1.8 atom% of Mg concentration was detected on the surface, as opposed to the original ~15 atom% before the acid washing. This etching test further implies that it is highly possible that the surface-magnesium containing compound is an inorganic substance, such as magnesium oxide or magnesium hydroxide. Nevertheless, to further prove this hypothesis, powder X-ray pattern was utilized to precisely identify this compound. In addition to zeolite 4A, pure silica particles were treated using the same halide/Grignard route. The reason for studying pure silica will be addressed later along with the XRD results. XPS survey for such treated silica also revealed the presence of Mg concentration on silica surfaces after the treatment, as can be seen in Figure 6.1e.

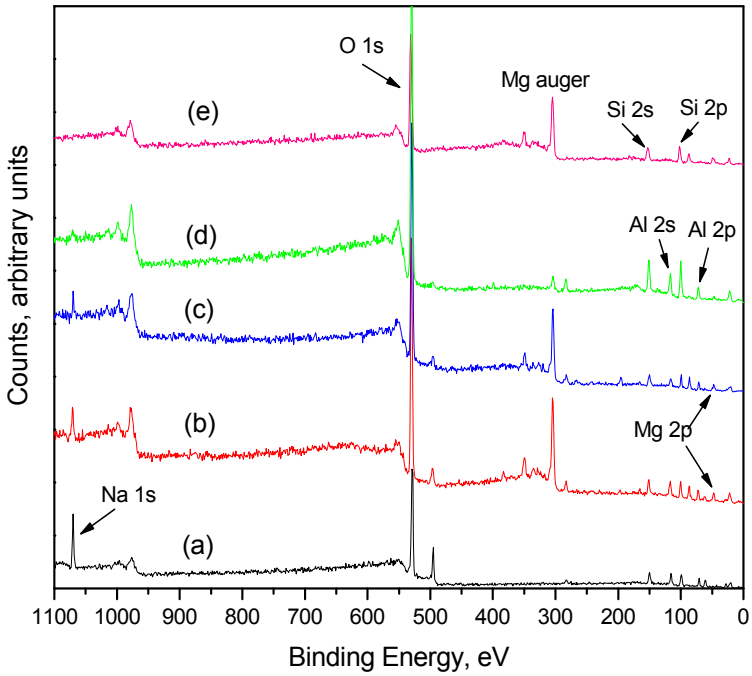

Figure 6.1 X-ray photoelectron survey spectra of zeolite 4A and pure silica particles after the surface treatment: (a) untreated zeolite 4A; (b) zeolite 4A treated by the halide/Grignard route; (c) same sample in (b) dried in air under 400ºC for 24 hours; (d) same sample in (b) after exposure to dilute HCl solution; (e) pure silica particles treated using the same chemical process. The major peaks detected are Na 1s (1072 eV), O 1s (531 eV), Si 2s (151 eV), Si 2p (99 eV), Al 2s (118 eV), Al 2p (73 eV), Mg 2p (50 eV).

6.3.2 X-ray Diffraction

Powder X-ray diffraction was performed to further identify the Mg-containing compound on the particle surfaces. Initial attempts to measure the modified zeolite 4A particles didn't yield any useful information. No difference was observed between the unmodified 4A and the modified counterparts. It may seem surprising at first but after careful consideration, it is not hard to explain the absence of diffraction peaks supposedly yielded by the surface nano-structure. Zeolite 4A is a very crystalline material, therefore it generates a number of peaks with high intensities in an XRD test. These strong peaks

of 4A tend to overwhelm the weak peaks produced by the Mg containing species on the surface since the amount of such nano-structure in the entire powder sample is very small as compared to the bulk 4A particles.

In order to avoid the interference caused by the fine crystallinity of zeolite 4A, pure silica was treated using the same procedure as described earlier. The great advantage of silica lies in the fact that it is an amorphous material, therefore only an amorphous peak will show up in an XRD analysis without any additional diffraction signals. This will allow us to observe the diffraction peaks generated by the small amount of nano-structures on silica surface. XPS test exhibited the existence of Mg concentration on the treated silica particle surfaces as well (Figure 6.1e). The XRD diffractogram of such modified silica is shown in Figure 6.2. The broad peak from 15º to 30º is the amorphous region of silica. It is evident that the other peaks are produced by the surface magnesium compound. After careful indexing with the standard XRD powder patterns, it was found that these peaks correspond perfectly to magnesium hydroxide $Mg(OH)_2$. This finding explains the previous observations that the surface structure can resist air drying at 400ºC but subject to HCl acid etching in an aqueous solution. Clearly $Mg(OH)_2$ could be dissolved by HCl to form water soluble $MgCl_2$ and thereby the surface structure was destroyed. In conclusion, work has identified that the surface nano-structure is comprised of $Mg(OH)_2$ crystals.

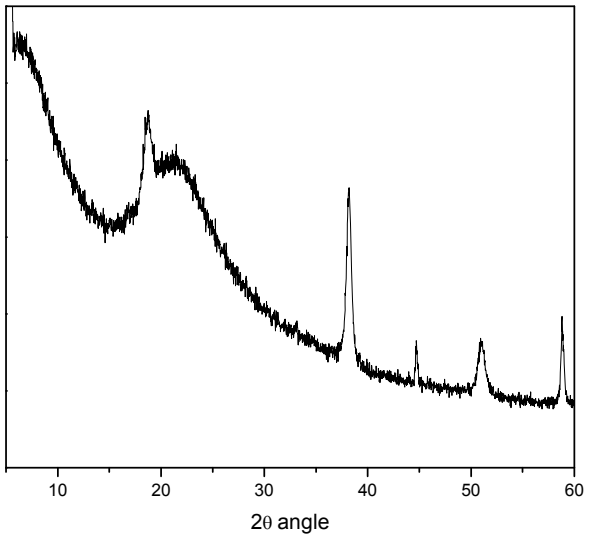

Figure 6.2 X-ray diffractogram of modified silica via the thionyl chloride/ Grignard chemical treatment described in the present study.

6.3.3 Zeta Potential Measurements of Zeolites

Zeta-potential measurement was used in this work primarily to characterize the stability of zeolite particles in solvents. The fundamental theories with regard to double layers and surface potential can be found in Appendix C. The measurements were conducted on a Zetasizer® Nano ZS™ (Malvern, Worcestershire, United Kingdom). A variety of zeolite 4A samples were subjected to this test in NMP and the results are summarized in Table 6.1.

The neat zeolites exhibited a zeta potential of -30mV. After the 2-step treatment, the surface potential reversed to a positive value of 127mV. This inversed sign indicated that the surface is rich in positive ions. It is possible that $Mg(OH)_2$ disassociates in NMP and produces Mg^{2+} which remains on the particle surface and renders the zeta potential positive. The absolute value of 127mV suggests high stability of particles in this solvent, because of the strong electrostatic repulsion among particles. This effect is particularly

distinct with the submicron batch of 4A, which has severe agglomeration in the unmodified form. The Grignard treatment increased the surface charge to 130.5mV (sample #5), significantly enhancing the stability of such sieves.

Two control experiments were performed. The Grignard modified sieves were calcined in air under 400ºC and zeta potential was collected for this sample. Negligible change (134.5mV) was detected, consistent with the inorganic nature of the nanostructures. Additionally, after the Grignard modified sieves were dispersed in a 0.1M HCl for 30 seconds, the zeta potential dropped to -50 mV. Most likely $Mg(OH)_2$ was dissolved by HCl solution and led to subsequent destruction of the surface morphology.

To summarize, zeta potential measurement offers useful insights with regard to the stability of zeolites in a certain solvent, as well as the changes in the surface charges caused by the modification procedures. It is interesting to observe charges on zeolite surface in an organic solvent because a majority of the literature reports involve an aqueous environment. Further inspection was carried out to reveal the underlying mechanism and ideas were proposed in Appendix C.

Table 6.1 Zeta-potential measurement results of various zeolite 4A samples

Zeolite	Zeta Potential in NMP(mV)
# 1 Neat 4A (5 μm)	-30.0
# 2 Modified 4A by 2-step Grignard treatment (5μm)	127.0
# 3 Sample 2 calcined in air at 400ºC	134.5
# 4 Sample 2 etched by HCl	-50.1
# 5 Modified 4A by 2-step Grignard treatment (0.2μm)	130.5

6.4 Exploration of the Formation Mechanism of $Mg(OH)_2$ Nanostructures

The proposed formation mechanism of the surface morphology development is explored in this section. Since there are two reaction steps involved in the treatment, they are investigated individually to reveal the changes occurring in each step.

6.4.1 Reaction Step One: Thionyl Chloride Treatment

In this section, zeolites were only treated with thionyl chloride. Solid state ^{29}Si NMR and ^{27}Al NMR were utilized to reveal the possible structural changes after this reaction. Figure 6.3a and 6.3b illustrate the corresponding ^{29}Si MAS NMR spectra for the untreated and treated zeolite 4A. A single sharp peak at -90 ppm was detected for the unmodified sample, which is assigned to the inherent uniform Si (4Al) framework of zeolite 4A. In other words, each SiO_4^{4-} tetrahedron is surrounded by four AlO_4^{5-} tetrahedral units. After exposure to thionyl chloride for 12 hours in a sonication bath, a new peak at -96 ppm showed up in the treated sample. This peak corresponds to the Si (3Al) blocks, which infers some aluminum was removed from the framework of zeolite 4A after this reaction. ^{27}Al MAS NMR provided further evidence for such dealumination reaction. Figure 6.3c depicts the ^{27}Al NMR spectrum of the untreated 4A. A single, relatively narrow signal is seen with a chemical shift at 60ppm corresponding to tetrahedrally coordinated aluminum in zeolite framework. Figure 6.3d shows the ^{27}Al NMR spectrum of the sample after reacting with thionyl chloride for 12 hours. Unlike the fresh 4A sample, there are two peaks present: the one at 60 ppm corresponding to aluminum still remaining in tetrahedral sites and the other with a chemical shift of around 0 ppm corresponding precisely to Al in octahedral coordination. The latter peak is clearly generated by aluminum that has been removed from the zeolite framework. To

summarize, these solid state NMR spectra indicate that thionyl chloride has partially removed aluminum from 4A structure. This reaction has been reported in literature to occur at elevated temperatures, above 300ºC.[10] However, in our case it was induced by constant sonication under room temperature. More detail regarding the effect of sonication on such dealumination reaction can be found in chapter 7.[11]

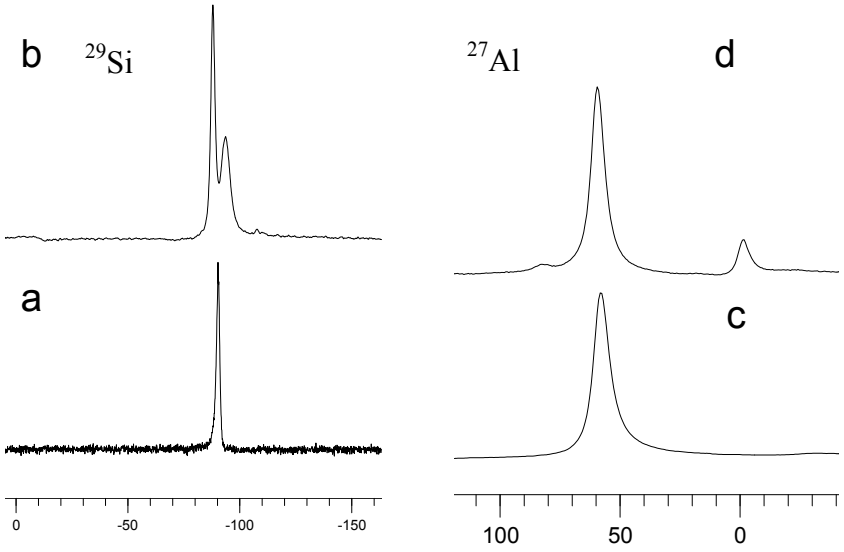

Figure 6.3 Solid state NMR spectra: (a) ^{29}Si NMR spectrum of unmodified zeolite 4A; (b) ^{29}Si NMR spectrum of zeolite 4A after 12hr reaction with thionyl chloride; (c) ^{27}Al NMR spectrum of the same sample in (a); (d) ^{27}Al NMR spectrum of the same sample in (b).

XPS surface analysis was employed to examine the products of the dealumination reaction by thionyl chloride and Figure 6.4 summarizes the results. Figure 6.4a demonstrates the surface survey of the fresh zeolite 4A sample, which consists of Na, O, Si and Al. After the thionyl chloride treatment, substantial chlorine concentration was detected on the surfaces of the sieves (Figure 6.4b). Strong peaks at 271 eV (Cl 2s) and 200 eV (Cl 2p) appeared, indicating that this procedure yielded Cl-containing species on the sieve surfaces. The chlorine concentration is attributed to NaCl and $AlCl_3$, which are

by-products of the dealumination reaction.[10,11] A significant increase in the sodium concentration was observed at 1072 eV (Na 1s), which can be readily explained by the production of NaCl during the dealumination process. Our observation here is in accordance with literature reports where researchers suggested the yield of NaCl after dealumination of sodium-containing zeolites,[12,13] which in our case is sodium-containing zeolite 4A. In addition to the increase in sodium concentration, the intensity of Al 2p peak is higher than that on the fresh 4A surface, which infers the enrichment of Al-containing substance on the treated zeolite surfaces. As shown earlier in Figure 6.3d, ^{27}Al NMR also detected non-framework aluminum species in this sample. These two results together imply the presence of $AlCl_3$ on the surfaces of the thionyl chloride treated sieves, which agrees well with Fejes and co-workers' observations.[10]

To summarize the first reaction, thionyl chloride acts as a dealumination reagent and partially removes aluminum from zeolite 4A framework. The two by-products of this reaction, NaCl and $AlCl_3$ precipitate on the particle surfaces afterwards. The significance of these two salts in the formation of the final nano-morphology will be discussed in the subsequent section.

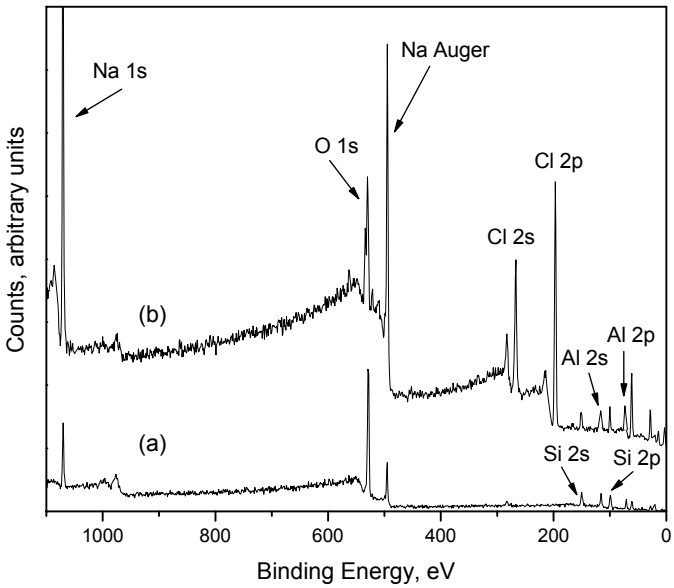

Figure 6.4 X-ray photoelectron spectra of 4A samples: (a) untreated zeolite 4A; (b) 4A after reaction with thionyl chloride. The major peaks detected are Na 1s (1072eV), O 1s (531eV), Si 2s (151eV), Si 2p (99eV), Al 2s (118eV), Al 2p (73eV), Cl 2s (271eV), Cl 2p (200eV).

6.4.2 Reaction Step Two: Grignard Reagent

Obviously the Grignard reagent used in this work (methylmagnesium bromide) provided the source of magnesium for the surface $Mg(OH)_2$ morphology, because it is the only magnesium containing compound used throughout the treatment. But how such a nanostructure was formed needs to be explored. Work described in this section aims to reveal this underlying chemical mechanism.

6.4.2.1 How Magnesium Hydroxide Is Produced

The first attempt is to identify through which process $Mg(OH)_2$ crystals are produced. There is an important step in our experimental procedure which is to quench the Grignard reagent with 2-propanol. During this process, large amount of gas was released,

accompanied by the formation of a white precipitate. This Grignard reaction is described to proceed via the following mechanism:[14,15]

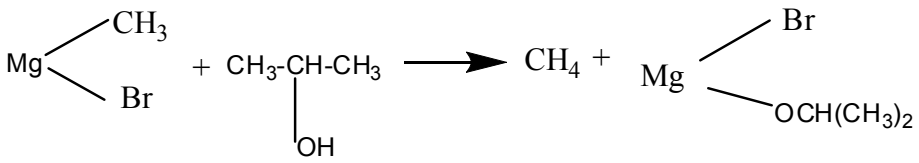

Scheme 6.1. Reaction mechanism of methyl magnesium bromide with 2-propanol.

The liberated gas observed in our quenching process is methane. However, the basic magnesium halide is only described as 'tends to separate from the liquid phase as a white precipitate' without defining what this precipitate actually consists of. However, this product is critical in our study because it is possible that such precipitate contains $Mg(OH)_2$, the compound that comprises the surface morphology.

To explore this possibility, small amount of methyl magnesium bromide solution was mixed with 2-propanol. Excess amount of 2-propanol was added in order to ensure no methyl magnesium bromide remained since it is a highly flammable and corrosive reagent. The white precipitate generated from this reaction was collected by centrifuge, followed by drying under vacuum for 24 hours. Elemental analysis by XPS and X-ray powder diffraction were conducted to examine the composition of such white powder. Three elements were detected by XPS survey (Figure 6.5a): O, Mg and Br, which could possibly comprise $MgBr_2$, $Mg(OH)_2$/MgO. The powder diffraction pattern, on the other hand, generated a series of strong peaks corresponding well to $MgBr_2$, as shown in Figure 6.6a. It was also noted that there were a few weak peaks at 2θ values of 38º and 51º which couldn't be assigned to $MgBr_2$. Nevertheless, the intensities of these peaks were

too small to index this material precisely. In order to eliminate the peaks yielded by $MgBr_2$ in XRD test, further control was done to reveal the other substance which generated the weak peaks at 2θ of 38º and 51º. The white precipitate collected from the Grignard/2-propanol reaction was dispersed in de-ionized water, in order to dissolve $MgBr_2$ as it is a water soluble salt. It was observed that although most of the white precipitate was dissolved immediately, there was small amount of white powder insoluble in water. This remaining powder was collected by centrifuge and rinsed with abundant de-ionized water, followed by drying. Again, XPS and XRD were performed to identify this powder sample, whose results are displayed in Figure 6.5b and 6.6b. It is clear that the Br peaks disappeared completely because all the $MgBr_2$ was dissolved by water. The insoluble powder is composed of Mg and O, whose XRD pattern corresponds perfectly to $Mg(OH)_2$ diffraction pattern (Figure 6.6b). This experiment also explains why it was difficult to observe $Mg(OH)_2$ peaks in an XRD test for the bulk reaction precipitate. As was observed, the majority of such precipitate is $MgBr_2$ which itself is a crystalline salt. Thus the high intensity peaks of $MgBr_2$ are likely to have overwhelmed the peaks yielded by the small amount of $Mg(OH)_2$. This phenomenon is similar to the previous zeolite 4A case, where the bulk 4A peaks covered the weak signals from the small amount of surface nanostructures.

The above investigations show that during the quenching process of methyl magnesium bromide with 2-propanol, $MgBr_2$ and $Mg(OH)_2$ are both produced and precipitated from the liquid phase. In our study, toluene was the liquid phase in which the solids were dispersed. The most likely scenario is that $MgBr_2$ and $Mg(OH)_2$ precipitated from toluene and encapsulated the zeolite particles. Later these zeolites were rinsed with

de-ionized water in the experimental procedure and $MgBr_2$ was dissolved away from the particle surfaces. The finally collected particles after water rinsing only had $Mg(OH)_2$ remaining on the surface, which comprises the nanomorphology as shown in Figure 5.1.

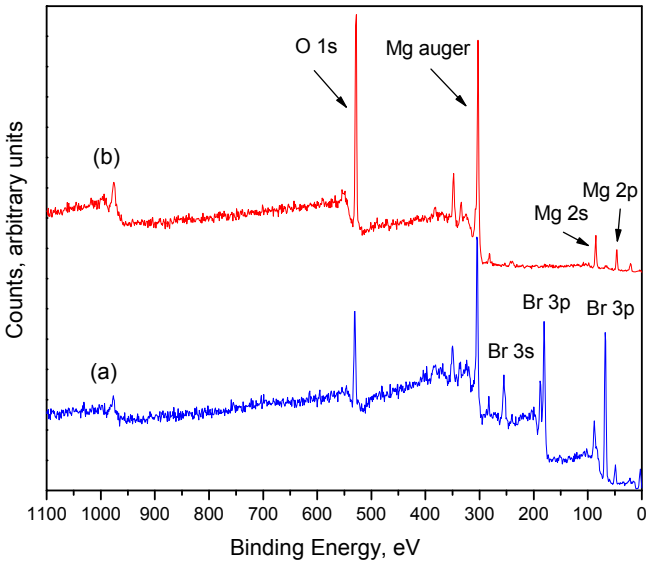

Figure 6.5 XPS analysis of the products from the reaction of methyl magnesium bromide with 2-propanol: (a) the white precipitates collected after the reaction; (b) same sample in (a) after rinsed with de-ionized water. The major peaks detected are O 1s (531 eV), Br 3s (256eV), Br 3p (182eV), Br 3d (70eV), Mg 2s (89eV), Mg 2p (50 eV).

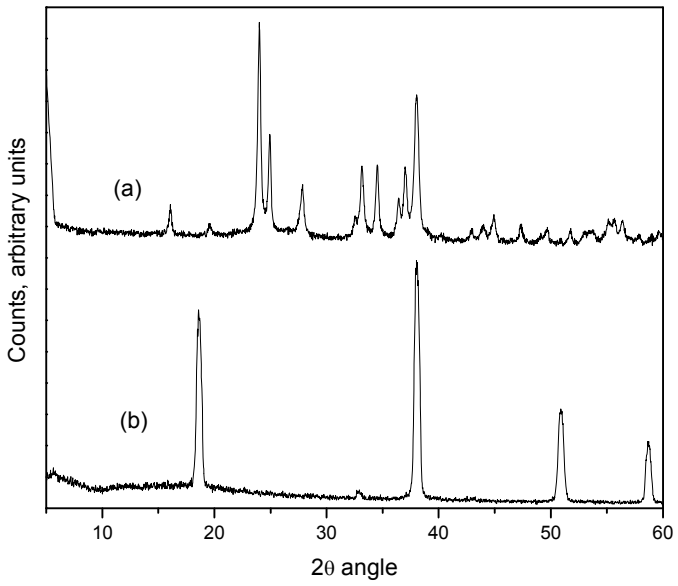

Figure 6.6 XRD diffraction patterns of the products from the reaction of methyl magnesium bromide with 2-propanol: (a) the white precipitates collected after the reaction; (b) same sample in (a) after rinsed with deionized water.

6.4.2.2 How the Specific Surface Morphology Was Created

After determined the chemical process that produced $Mg(OH)_2$, efforts were directed towards identifying how the specific surface morphology was formed. It was intuitive to assume that during the reaction of Grignard reagent with 2-propanol, this surface structure was created because this process yielded $Mg(OH)_2$, the component of such morphology. A control experiment was conducted to test this assumption, which was to expose zeolite 4A only to methyl magnesium bromide and 2-propanol without the preceding thionyl chloride step. SEM images were taken for these treated sieves and XPS was used to analyze the surface elemental composition, the results of which are shown in Figure 6.7. As can be seen in Figure 6.7a, no apparent surface morphology was observed as compared to the significantly roughened surfaces of sieves treated with the two-step

sequence (Figure 6.1). However, XPS still detected the presence of Mg concentration on these sieve surfaces (Figure 6.7b), which implies that Grignard/2-propanol reaction yielded $Mg(OH)_2$ but it did not have a specific crystalline morphology. The large 'chunks' in Figure 6.7a are likely to be some big $Mg(OH)_2$ crystals. These findings excluded the hypothesis that Grignard reagent/2-propanol reaction itself created the roughened surface morphology. In other words, in order to form the specific surface pattern as shown in the previous chapter Figure 5.1, both reaction steps must be involved.

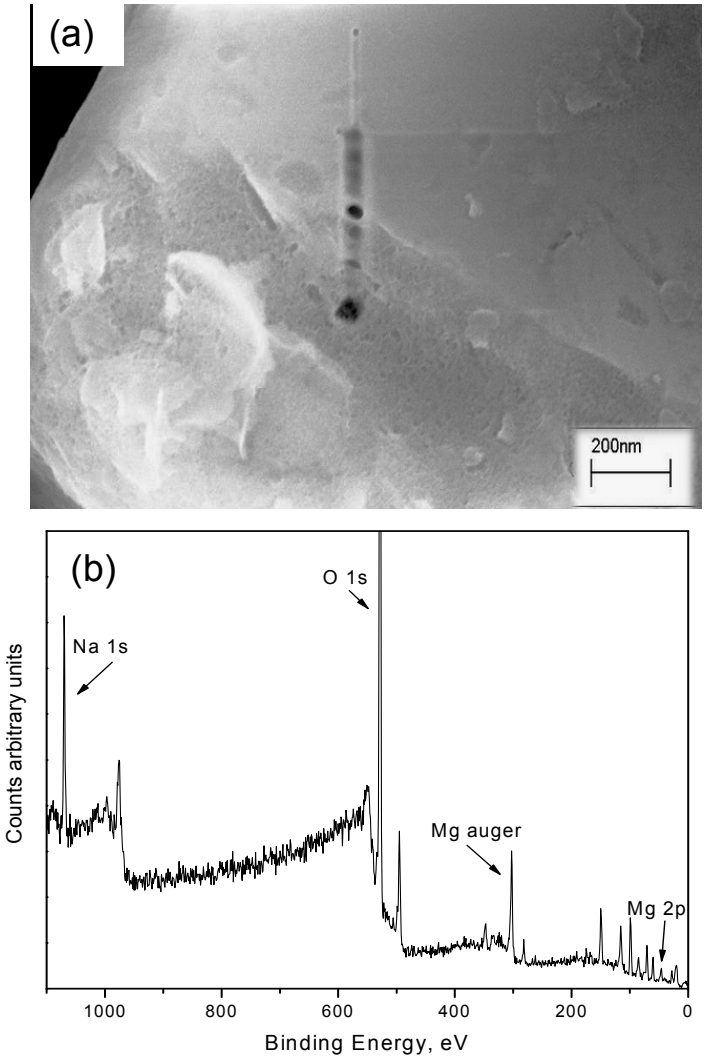

Figure 6.7 Sieve characterization results: (a) Representative SEM image of zeolite 4A particle treated only with methyl magnesium bromide/2-propanol; (b) XPS surface survey

of sample (a). The major peaks detected are Na 1s (1072 eV), O 1s (531 eV), Si 2s (151 eV), Si 2p (99 eV), Al 2s (118 eV), Al 2p (73 eV), Mg 2p (50 eV).

As was discussed in section 6.4.1, the direct result of the thionyl chloride reaction is that NaCl and $AlCl_3$ are generated and deposit on the surfaces of 4A particles. Without these salts, $Mg(OH)_2$ still precipitate on zeolite surfaces, but it does not have a defined crystal morphology. Therefore, it is hypothesized here that NaCl and $AlCl_3$ function as heterogeneous nuclei for the formation of $Mg(OH)_2$ fine crystals, thereby enabling $Mg(OH)_2$ to grow easily on the zeolite surface.[16] This process could have led to the specific 'whisker-like' crystal morphology. The proposed mechanism is illustrated in Figure 6.8. An experiment was performed to test this presumption. After the first reaction with thionyl chloride, zeolites were rinsed with abundant de-ionized water so that the NaCl and $AlCl_3$ were dissolved away. These rinsed particles were collected and dried, followed by exposure to methyl magnesium bromide and 2-propanol. No distinctive surface morphology was seen on such resultant particles. The SEM images were similar to Figure 6.8a. This observation provided further evidence that lack of surface nuclei (NaCl and $AlCl_3$) caused the absence of the distinctive morphology of $Mg(OH)_2$ on zeolite surfaces.

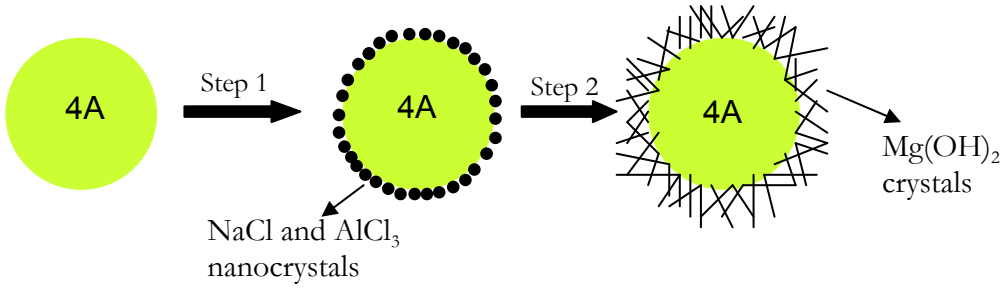

Figure 6.8 Illustration of the formation mechanism of the distinctive crystal morphology of $Mg(OH)_2$ on zeolite 4A surfaces.

Another possibility is that the nanostructure formed on zeolite 4A belongs to MgAl species. This hypothesis was ruled out by a few facts. First, although the products of dealumination reaction are NaCl and $AlCl_3$, the concentration of Na is much higher than Al which can be observed in Figure 6.4b. Hence, the majority of the surface after dealumination was covered with NaCl and to a small extent, $AlCl_3$. Moreover, later work involves directly depositing NaCl onto silica/silicate particle surfaces, followed by the Grignard reaction. Similar surface nanostructure was obtained, and XRD confirmed it is composed of $Mg(OH)_2$ crystals. This information will be included in chapter 8. In principle, by intentionally depositing nuclei on the surfaces of particles, it should be feasible to create similar nanostructures on the particles surfaces using the Grignard reaction. Forthcoming chapters will explore the above proposed mechanism and approach using surface seeding on materials other than zeolite 4A. It is expected that this chemical process could be extended to a broad array of inorganic materials.

6.5 EFFECT OF THE MODIFIED PARTICLES ON INTERFACIAL ADHESION

In chapter 5, the effect of such modified zeolites has been demonstrated[7,8] When incorporated into polymer matrixes, these particles provided greatly enhanced adhesion at the interfaces, thus formed defect-free polymeric composites with improved mechanical strength as well as gas separation efficiencies. The dramatic increase in the topological roughness (physical heterogeneity) on the sieve surfaces is believed to provide stronger interaction at the interfaces via induced adsorption and physical interlocking of polymer chains in the nano-scopic surface structure.

6.6 CONCLUSIONS

A two-step reaction sequence, dealumination via thionyl chloride followed by reaction with a Grignard reagent, created a nanoscale morphology that appears as significantly roughened outer surfaces on zeolite 4A particles. XPS and XRD measurements revealed that such surface nano-structures are composed of $Mg(OH)_2$ crystals. The formation mechanism of this specific surface morphology was explored. It was discovered by solid state ^{29}Si and ^{27}Al NMR and XPS surface analysis that thionyl chloride partially removes aluminum from the zeolite 4A framework and yields NaCl and $AlCl_3$. Precipitation of these extracted inorganic salts on the surfaces of zeolite particles occur. Subsequently, methyl magnesium bromide is reacted with 2-propanol in a quenching process and generates $Mg(OH)_2$. The previously deposited NaCl and $AlCl_3$ nano-particles on zeolite surfaces are believed to function as heterogeneous nuclei for the growth of $Mg(OH)_2$ crystals and creates the nano-structured surface morphology. The modified particles are shown in previous work to provide enhanced interfacial adhesion in polymeric composites.

6.7 REFERENCES

[1] Husain, S. *Mixed Matrix Dual Layer Hollow Fiber Membranes for Natural Gas Separation*, Ph.D Thesis: Georgia Institute of Technology, 2006.

[2] Bansal, A.; Li, X.; Lauermann, I.; Lewis, N. S.; Yi, S. I.; Weinberg, W. H. *J. Am. Chem. Soc*. **1996**, *118*, 7225.

[3] Bansal, A.; Lewis, N. S. *J. Phys. Chem. B* **2001**, *105*, 10266.

[4] Bansal, A.; Li, X.; Yi, S. I.; Weinberg, W. H. Lewis, N. S. *J. Phys. Chem. B* **2001**, *105*, 10266.

[5] Sunseri, J. D.; Gedris, T. E.; Stiegman, A. E.; Dorsey, J. G. *Langmuir* **2003**, *19*, 8608.

[6] Clark, J. H.; Williamson, C. J. *J. Mater. Chem*. **1993**, *3*, 575.

[7] Terry, J.; Linford, M. R.; Wigren, C.; Cao, R.; Pianetta, P.; Chidsey, C. E. D. *J. Appl. Phys*. **1999**, *85*, 213.

[8] Vassylyev, O.; Hall, G. S.; Khinast, J. G. *J Porous Mater*. **2006**, *13*, 5.

[9] Kim, N. Y.; Laibinis, P. E. *J. Am. Chem. Soc*. **1998**, *120*, 4516.

[10] Fejes, P.; Kiricsi, I.; Hannus, I.; Kiss, A.; Schobel, G. React. *Kinet. Catal. Lett.* 1**980**, *14*, 481.

[11] Shu, S.; Husain, S.; Koros, W. J. *Ind. Eng. Chem. Res.* **2007**, *46*, 767.

[12] Anderson, M. W.; Klinowski, J. *J. Chem. Soc., Faraday Trans*. **1986**, *82*, 1449.

[13] Klinowski, J.; Thomas. J. M.; Fyfe, C. A.; Gobbi, G. C.; Hartman, J. S. *Inorg. Chem*. **1983**, *22*, 63.

[14] Fieser, L. F. Fieser, M. *Organic Chemistry*; Reinhold: New York. 1956.

[15] Bruice, P. Y. *Organic Chemistry*; Pearson Prentice Hall: Upper Saddle River, NJ. 2007.

[16] Mullin, J. W. *Crystallization*; Butterworth-Heinemann: Oxford, 2001.

CHAPTER 7
SONICATION ASSISTED DEALUMINATION OF ZEOLITE 4A USING THIONYL CHLORIDE

7.1 PREVIEW

Work in the previous chapter showed that during the reaction of zeolite 4A with thionyl chloride, aluminum was extracted from zeolite framework and produced $AlCl_3$ and NaCl Similar phenomena were reported in literature at more elevated temperatures as opposed to the ambient conditions used in this study. This chapter aims to perform an in-depth inspection of this surprising observation.

The dealumination of zeolite 4A by thionyl chloride was investigated near room temperature in the liquid phase with and without the assistance of sonication. The structural changes observed by ^{29}Si and ^{27}Al solid-state NMR showed that the experimental condition, that is, in the presence or absence of sonication, significantly affected the efficiency of the dealumination process of zeolite 4A. Successful dealumination was achieved with the assistance of sonication at room temperature while simple stirring led to negligible changes. It was also found that the degree of dealumination could be tailored by the duration of sonication to generate zeolites with various Si/Al ratios. XPS surface elementary analysis detected chlorine rich sieve surfaces after the sonication treatment, which is attributed to $AlCl_3$ and NaCl, the by-products of the dealumination reaction. These results confirmed that sonication accelerated dealumination reaction under ambient conditions. XRD tests, unit cell calculation and nitrogen physisorption analysis revealed partial loss in framework integrity after the treatment. This new procedure allows convenient preparation of

alumina-deficient zeolites of a wide range of Si/Al ratios under ambient conditions. The dramatic local heating resulted from ultrasound is proposed to explain the unusual observation of dealumination by thionyl chloride near room temperature.

7.2 BACKGROUND OF ZEOLITE DEALUMINATION

Zeolites, which offer stability and activity combined with a high selectivity, have attracted considerable interest due to their important applications in catalysis. Such materials can be synthesized in a very wide range of compositions with Si/Al ratio varying from unity in zeolite A, to over 1000 in materials belonging to the highly siliceous ZSM series.[1] The stability of zeolites is closely related to the framework Si/Al ratio, a higher ratio leading to increased stability. Nevertheless, several industrially important zeolites can be synthesized only with relatively low SiO_2/Al_2O_3 ratio, thus it is desirable to remove further tetrahedral aluminium from the zeolite framework by subsequent treatments.[2] An essential step in the preparation of an active, stable zeolite catalyst often involves the modification of the as-synthesized material. Dealumination, the removal of framework aluminum atoms without severely disrupting the crystalline structure of zeolites, is an important process that allows adjustments in the Si/Al ratio of zeolites, hence their acidity and catalytic properties.[3] For example, the dealumination of zeolite Y not only improves its hydrothermal stability but also influences its catalytic cracking properties.[4] Lee et al. have reported the use of a highly dealuminated mordenite for the alkylation of biphenyl with propylene to form 4,4'-diisopropylbiphenyl (DIPB).[5]

Dealumination of a zeolite was first reported by Barrer and Makki who progressively removed aluminum from natural clinoptilolite by washing it with hydrochloric acid of different strengths.[6] Subsequent dealumination studies were carried out primarily on

commercially important mordenite and Y zeolites.[7,8] In general, aluminum-deficient zeolites can be prepared by two following methods: i. Thermal or hydrothermal treatment of the ammonium-exchanged form of zeolites. This involves heat-treatment of zeolites in the presence of steam.[9] The hydrothermal approach results in partial framework dealumination, but the aluminum remains in the zeolites cages or channels as detrital material and the process is time consuming. ii. Chemical extraction with suitable reagents. This approach includes: (a) washing with mineral acids such as HCl,[10] oxalic acid,[11] or citric acid.[12] These reagents may involve a loss of the initial crystallinity, especially at higher degrees of dealumination. (b) reaction in the vapor phase at high temperatures such as silicon tetrachloride,[13] thionyl chloride,[14] and other halides and oxyhalides.[15] Such a treatment can be carried out with a variety of reagents and results in the removal of aluminum from the zeolites in a volatile form. Nevertheless, it requires higher temperature reaction conditions and is usually performed in a flow type tube reactor under a dry stream of nitrogen. Therefore this treatment is relatively inconvenient as compared to a potential chemical treatment which can be achieved in the liquid phase under ambient conditions, as well as retaining the initial crystallinity of the parent zeolite to a large extent.

Despite extensive study of dealumination of zeolites by various methods, to our knowledge, there hasn't been any report in the literature regarding dealumination of a zeolite using an acid halide near room temperature. Besides, dealumination of zeolite A is not as thoroughly explored in the literature as that of modenite and zeolite Y, but it is also an important material due to its selective sorptive and catalytic properties[16] and ion exchange capacity.[17] Therefore, this current work attempts to address an effective

procedure using thionyl chloride to prepare aluminum-deficient zeolite A in the liquid phase near room temperature while maintaining high levels of zeolite crystallinity. Sonication was employed to assist the dealumination reaction in the liquid phase near bulk room temperature. The effect of duration of sonication was also studied to explore a way to adjust the Si/Al ratio in this new procedure. ^{29}Si and ^{27}Al solid-state NMR was used to monitor the structural changes occurring in the dealumination process. X-ray photoelectron spectroscopy (XPS) was used to probe the chlorine species formed during thionyl chloride treatment and X-ray diffraction analysis to examine the crystallinity of the zeolites.

7.3 EXPERIMENTAL

Dealumination. Samples of 5-7g of 4A particles were placed in a three-neck reaction flask. All the particles and the glassware used in the treatment were first dried in a vacuum oven at 150 ºC for 24 hr, and the glassware was also flame-dried with a propane torch prior to the treatment. An amount of 20mL of anhydrous toluene (99.8%, Aldrich) and 20 mL of thionyl chloride (99.5%, low ion solution, Aldrich) were added to the reaction flask. Both liquids were transferred carefully through a dry transfer line to maintain a moisture-free environment. This dispersion was kept in a sonication bath (Frequency 40KHz, Model 1510, Branson) for 12hr, 24hr or 48hr, after which toluene and extra thionyl chloride were evaporated by constant nitrogen sweep through the system. During constant sonication, the temperature of the water bath increased to 40ºC. As a comparison, the same amount of 4A was also treated with the procedure described above, but only with magnetic stirring under the same temperature and for the same reaction length. The particles were further rinsed with anhydrous toluene three times and

collected by filtration. To characterize the chlorine-containing species formed after dealumination, a control step was performed, which was to rinse the treated sieves with de-ionized water in contrast to anhydrous toluene. This step can dissolve the salts potentially generated in the dealumination reaction.

Ion Exchange. Samples of 2g of zeolites were dispersed in 70 cm^3 of $CaCl_2$ solution (1M). Ion exchanged was carried out at 60 ºC for 5 hours under vigorous stirring. After washing repeatedly with deionized water, the samples were dried at 120 ºC under vacuum.

7.4 SOLID STATE NMR STRUCTURAL CHARACTERIZATION

^{29}Si NMR has proved to be especially useful in the structural characterization of dealuminated zeolites, since it provides direct information on the composition and Si, Al distribution of the tetrahedral framework, independently of the presence of non-framework Al species.[18] The ^{29}Si chemical shifts fall into five distinct ranges, depending on whether a given SiO_4^{4-} tetrahedron is linked, by oxygen bridges, to four, three, two, one or no AlO_4^{5-} tetrahedra; these ordering notes are denoted Si(4Al), Si(3Al), Si(2Al), Si (1Al) and Si (0Al) respectively. ^{27}Al NMR, on the other hand, allows a clear distinction between tetrahedral framework Al and octahedral non-framework Al. Therefore, the degree of framework dealumination and the amount of non-framework aluminum in dealuminated zeolites can be determined by ^{29}Si and ^{27}Al NMR.[19]

7.4.1 ^{29}Si NMR Measurement

Figure 7.1 shows the corresponding ^{29}Si MAS NMR spectra for the parent and various dealuminated forms of zeolites 4A. A single sharp resonance peak at -90 ppm was detected for both parent 4A (Figure 7.1a) and 4A that was treated with thionyl chloride

under stirring condition for 24 hr (Figure 7.1b). This peak is assigned to the inherent uniform Si(4Al) framework of zeolite 4A. In other words, each SiO_4^{4-} tetrahedron is surrounded by four AlO_4^{5-} tetrahedral units. This is clear evidence that negligible dealumination occurred when the reaction was performed in a stirring system under ambient temperature. On the other hand, Figure 7.1c, 7.1d and 7.1e qualitatively demonstrated that progressive dealumination was successfully achieved under room temperature with the presence of sonication in the treatment. Figure 7.1c gives the spectrum for the material that was treated for 12 hr with sonication. The relative peak intensities of the aluminium-rich Si(4Al) units decreased and a new shoulder which presents Si(3Al) blocks appeared at -96 ppm in the spectrum. After a longer reaction time of 24 hr, the intensities of Si(4Al) and Si(3Al) structures diminished, accompanied by a considerable increase in the lower aluminium units Si(2Al), Si(1Al) and Si(0Al), as indicated by Figure 7.1d. The stepwise changes suggest that the number of SiO_4^{4-} tetrahedra joined to AlO_4^{5-} tetrahedra decreased in favor of SiO_4^{4-} tetrahedra connected to more of such similar tetrahedra. Furthermore, after 48hr of treatment in the presence of sonication, the sample only yielded a single sharp peak at -110 ppm, attributable to pure siliceous unit Si(0Al), ie, Si(4Si) ordering of tetrahedra, to the exclusion of all other configurations. The peak is narrow, which implies high homogeneity and crystallinity. To summarize the preceding discussions, it is concluded that with the assistance of sonication, it is viable to generate aluminum-deficit zeolites using thionyl chloride under ambient reaction conditions. It is also important to note that by varying the duration of sonication, zeolites can be dealuminated to various degrees, thus allowing the production of zeolites with potentially a wide range of Si/Al ratios.

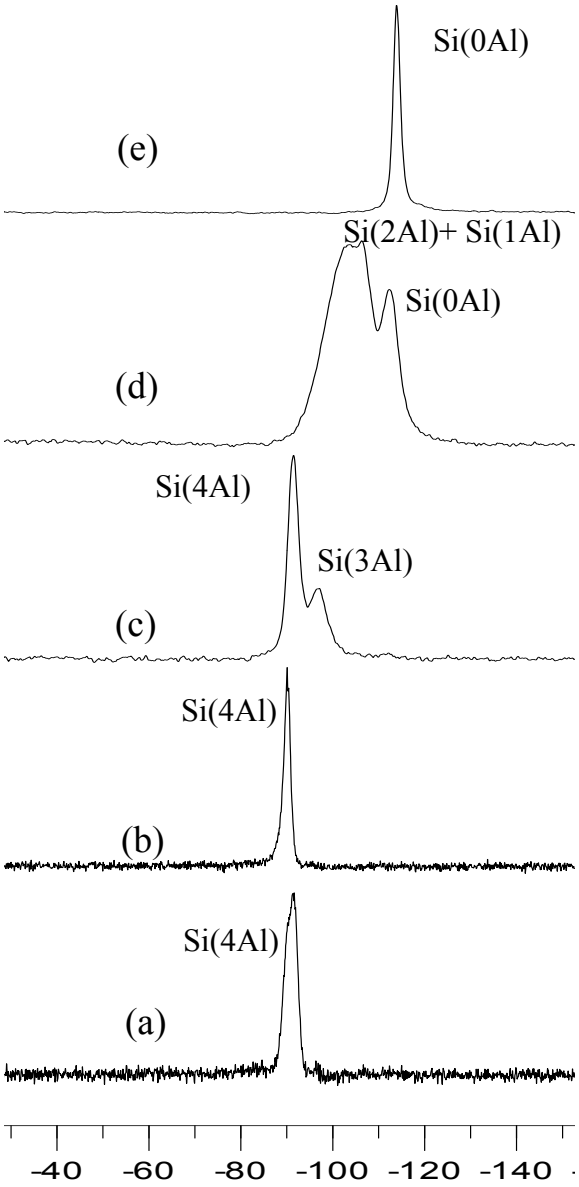

Figure 7.1 ^{29}Si MAS-CP NMR spectra of parent zeolites and the dealuminated counterparts: (a) parent zeolite 4A; (b) 4A after treatment with thionyl chloride for 24 hr in a stirring system under room temperature; (c) 4A after treatment with thionyl chloride for 12 hr with continuous sonication under room temperature; (d) similar sample as in (c), but with 24 hr sonication; (e) similar sample as in (c), but with 48 hr sonication.

7.4.2 ^{27}Al NMR Measurement

Further characterization using ^{27}Al MAS NMR was performed to investigate this reaction. Figure 7.2a displays the ^{27}Al spectrum of the parent 4A. A single, relatively

narrow signal is seen with a chemical shift of 60ppm corresponding to tetrahedrally coordinated aluminum. After 24 hours' treatment with thionyl chloride in a stirring system, there was no structural change observed in the resulting sieves as shown by Figure 2b. Figure 2c gives the ^{27}Al spectrum of the sonication treated sample, the ^{29}Si spectrum of which was shown in Figure 1c. There are two peaks: the one at 60 ppm corresponding to aluminum still remaining in tetrahedral sites and another one with a chemical shift of around 0 ppm corresponding unmistakably to Al in octahedral coordination. The latter peak is clearly generated by aluminum that has been removed from the framework. Thus it further supports the fact that sonication induced dealumination process under room temperature. Upon washing, the octahedral peak disappeared as shown by Figure 7.2d. According to the reaction mechanism proposed by Fejes et al for dealumination of zeolites by phosgene,[14] $AlCl_3$, where Al exists in octahedral coordination, is produced in the dealumination process. This can possibly explain the appearance of octahedral peak in Figure 7.2c. Also $AlCl_3$ can readily be dissolved by water, which is in agreement with the fact that the octahedral peak disappeared after water rinsing (Figure 7.2d). Further evidence for the existence of $AlCl_3$ is indicated in XPS results, as discussed in a later section.

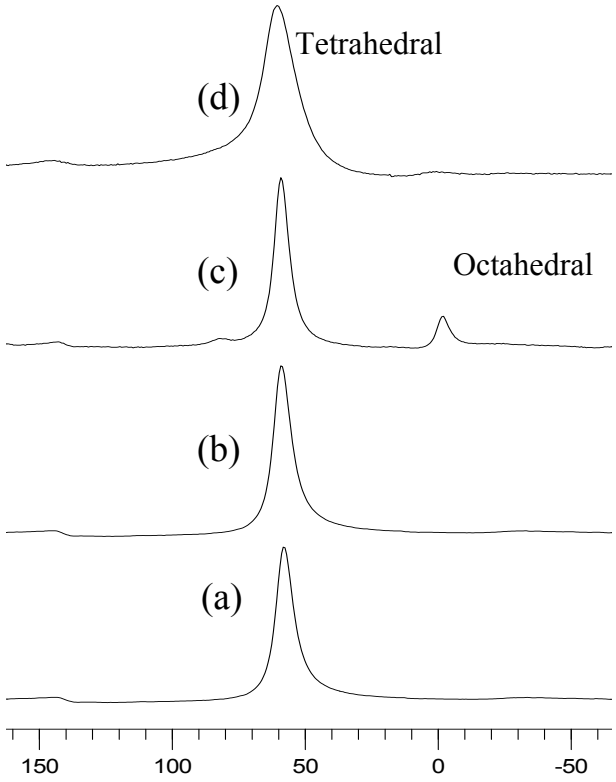

Figure 7.2 ^{27}Al MAS NMR spectra of: (a) parent zeolite 4A; (b) zeolite 4A after thionyl chloride treatment with stirring for 24hr under room temperature; (c) zeolite 4A after thionyl chloride treatment with sonication for 12 hours under room temperature; (d) sample (c) after extensive washing with water.

7.5 XPS SURFACE ELEMENTAL ANALYSIS

XPS surveys of the surface elemental compositions of various 4A samples yielded additional information with regard to the products of the dealumination. The results are depicted in Figure 7.3. Figure 7.3a illustrates the surface survey of parent 4A which consists of Na, O, Si and Al. After thionyl chloride treatment for 24 hr under room temperature in a stirring system, negligible change was observed in the surface elemental composition of the treated sieves, as shown in Figure 7.3b. However, substantial chloride was detected on the surfaces of the sieves that underwent the same treatment but with sonication. The XPS survey spectra (Figure 7.3c) showed strong peaks at 271 eV (Cl 2s)

and 200 eV (Cl 2p), indicating that this procedure yielded chlorine containing species on the sieve surfaces. Also a significant increase in the sodium concentration was observed at 1072 eV (Na 1s). The chlorine concentration is presumably attributed to NaCl and $AlCl_3$, which are by-products of the dealumination reaction. However, in the literature Fejes didn't predict the generation of NaCl after the reaction since H-type mordenite was investigated in their study and this type of zeolite doesn't contain sodium ions.[18] Our observation here is consistent with other literature reports where researchers suggested the yield of NaCl after dealumination process of sodium-containing zeolites.[1, 20] Besides, the intensity of Al 2p peak was higher than that on the parent 4A surface. As discussed in the previous section, ^{27}Al NMR also detected non-framework aluminum species in this sample. These two results together imply the presence of $AlCl_3$ on the surfaces of the sonication treated sieves, which agrees with Fejes' observation.[14] The chlorine, sodium and aluminum concentrated zeolite surface provides further evidence to the fact that dealumination reaction was achieved with the assistance of sonication. As a control step, the dealuminated 4A zeolites were washed repeatedly with de-ionized water, followed by XPS examination. It was found that the chlorine peaks disappeared after the rinsing step, and the intensity of Na 1s and Al 2p peaks also diminished significantly, which can be readily explained by the fact that NaCl and $AlCl_3$ were dissolved by water. The spectrum for this sample is shown in Figure 7.3d.

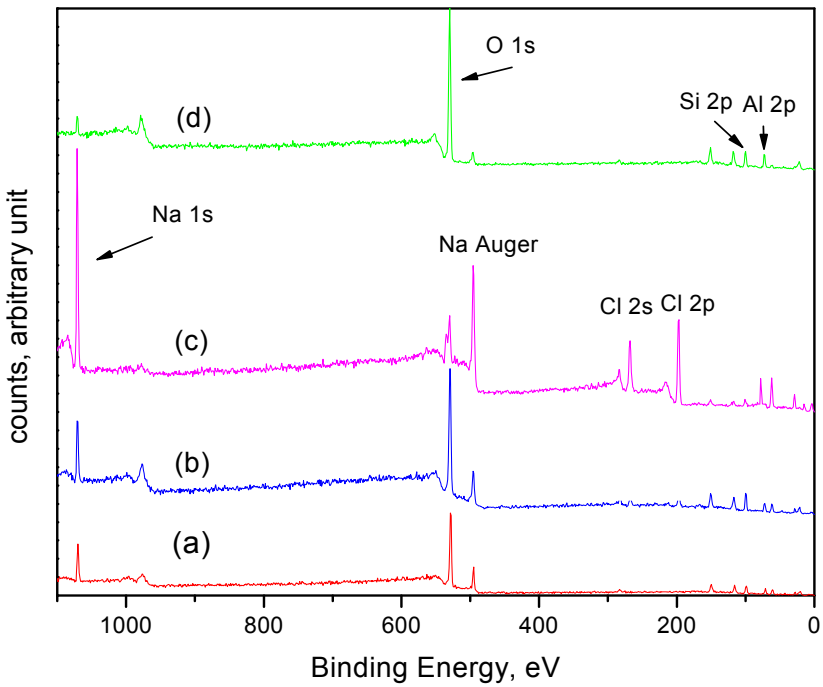

Figure 7.3 X-ray photoelectron survey spectra of various 4A samples: (a) pristine zeolite 4A (b) 4A after treatment with thionyl chloride for 24 hr in a stirring system (c) 4A after treatment with thionyl chloride for 24 hr with constant sonication (d) sample (c) after washing with abundant water. The major peaks detected are Na 1s (1072eV), O 1s (531eV), Si 2s (151eV), Si 2p (99eV), Al 2s (118eV), Al 2p (73eV), Cl 2s (271eV), Cl 2p (200eV).

The Si/Al ratios of the various treated zeolite 4A samples were evaluated by XPS to provide a quantitative measure of the degrees of dealumination. All the end products were rinsed repeatedly with de-ionized water to dissolve the by-products on the surface before the XPS measurements. As indicated by the results listed in Table 7.1, the Si/Al ratio in the final product gradually increased with increasing treatment duration. This observation agrees well with the NMR spectra discussed earlier, which again confirmed that sonication induced the dealumination process of zeolite A.

Table 7.1 X-ray photoelectron elemental analysis of Si/Al ratios in various zeolite A samples

Sample ID	Si/Al
Parent Zeolite 4A	1.0
Zeolite 4A treated for 24hr with constant stirring	1.03
Zeolite 4A dealuminated for 12hr with constant sonication	1.21
Zeolite 4A dealuminated for 24hr with constant sonication	9.33
Zeolite 4A dealuminated for 48hr with constant sonication	negligible Al detected

7.6 X-RAY DIFFRACTION MEASUREMENT

7.6.1 XRD Spectra

The effect of dealumination on the integrity of the zeolites was first analyzed by X-ray powder diffraction (Figure 7.4). After treatment with thionyl chloride for either 24 hr or 48 hr, the samples yielded diffraction patterns corresponding well to the parent zeolites. The products are evidently crystalline, which suggests the structural integrity was satisfactorily retained after dealumination. The intensities of peaks in Figure 7.4b and 7.4c seem lower than Figure 7.4a and there could be two possible reasons for this change. Firstly, the structure factors depend upon the framework alumina content as well as upon the cation content. The dealuminated samples contain less aluminum and the Na^+ cations were removed from the framework as indicated by previous XPS results. In this case, the dealuminated end products don't have the same composition as the parent zeolites, thus it is not precise to evaluate the degree of crystallinity of dealuminated samples by direct comparison of peak heights in XRD powder pattern.[1,21] Secondly, the decrease in peak

intensities could be due to actual loss of crystallinity in the zeolites. The latter possibility will be further explored by unit cell calculation and nitrogen physisorption measurements.

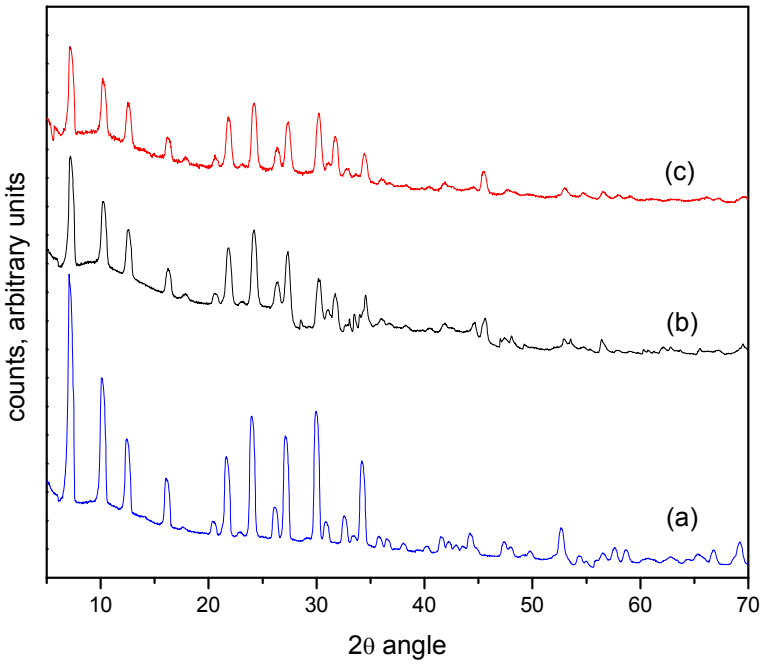

Figure 7.4 X-ray diffraction patterns of zeolite 4A and its dealumination forms: (a) parent 4A; (b) 4A dealuminated for 24 hr with constant sonication; (c) 4A dealuminated for 48 hr with constant sonication.

7.6.2 Determination of Unit Cell Size

The unit cell size was determined by indexing the acquired XRD diffractograms. PowderX was used to index the powder XRD patterns and unit cell calculation. Lapod was used to perform unit cell refinement. The results are displayed in Table 2. The data suggested that the unit cell was subjected to gradual contraction upon dealumination. This trend infers a possible 'partial loss' of the framework crystallinity during the dealumination process. In addition, the removal of sodium cations from the zeolites could also have contributed to the decrease in lattice parameter

Table 7.2 Lattice constant of zeolite NaA and its dealuminated forms

Sample ID	Unit Cell Size (Å)
Parent 4A	12.28
4A Dealuminated for 24hr	12.23
4A Dealuminated for 48hr	12.20

7.7 NITROGEN PHYSISORPTION ANALYSIS

The surface area of the material was examined by nitrogen physisorption to provide more information regarding the framework integrity (Table 3). Because the two sodium cations locate in or near the eight-membered ring pores and reducing the effective size of the pore opening to less than 3.1 Å, zeolite NaA is known not to adsorb nitrogen at 77K.[16, 22] Therefore all the zeolite samples were converted to CaA forms before characterization by nitrogen adsorption at 77K.[21] The pore size of zeolite CaA is 5Å which is accessible by nitrogen molecules.[22]

As expected, the pores of the Ca^{2+} exchanged zeolite A were accessible to nitrogen. The BET surface areas and micropore volumes of the ion exchanged sieves are reported in Table 7.3. Both the BET surface areas and micropore volumes decreased after the treatment for either 24hr or 48hr. This decreasing trend may be attributed to the formation of mesopores when aluminum was removed from the framework, as suggested by Jones and co-workers.[23] In Rakoczy' study where ammonium acetate was used as the dealumination agent for zeolite A, at a Si/Al ratio of 2.5, only 20% of crystallinity was retained from the parent zeolite A.[21] Although our method is also accompanied by a partial loss in framework integrity, the damage to the framework is milder than the

previous method and most importantly, it allows preparation of zeolite A with higher Si/Al ratios.

Table 7.3 Nitrogen physisorption data for parent zeolite A and different dealuminated counterparts

Sample ID	BET surface area (m^2/g)	t-plot $V_{micropores}$ (cm^3/g)	reference
Parent Zeolite CaA	421.3	0.281	this study
Zeolite A dealuminated for 24hr with constant sonication	347.1	0.239	this study
Zeolite A dealuminated for 48hr with constant sonication	293.8	0.203	this study
Zeolite CaA		0.297	Breck[29]

Several reaction mechanisms have been suggested to explain the framework stabilization of zeolites upon dealumination: a) Formation of new Si-O-Si bonds at the hydroxyl nests by elimination of water;[3] b) Silica transport and insertion into vacancies left by dealumination;[24] c) The so-called T-jump reaction mechanism assumes that the vacancies created by framework dealumination gradually migrate from the interior of the zeolite crystal to its surface, by exchanging places with neighboring T atoms.[25] To our knowledge, there hasn't been any report regarding which of the above proposed mechanisms occurs in the case of dealumination by thionyl chloride. Zeolite A which is used in our study has a Si/Al of 1, which means in order to get a pure siliceous A, a large amount of aluminum needs to be removed and thus vacancies are created. Locally dissolved silica species could have migrated to the vacancies to heal the defects, as suggested by Jones et al.[23] Also as indicated by our XPS results, the by-products of this reaction are concentrated on the surfaces of the sieves. This fact implies that T-jump

mechanism may also operate under the conditions described here by enabling the reaction products to migrate from the interior of the crystal to its surface. Thus multiple mechanisms could be possible in the present study.

7.8 THE EFFECT OF SONICATION

The literature of dealumination by an acid halide reports elevated temperatures, above 300°C.[14] Nevertheless we have shown that with the assistance of sonication, dealumination by thionyl chloride can be achieved under ambient conditions of around 40°C. We here propose a hypothesis to qualitatively explain this unusual phenomenon. The chemical effect of high-intensity ultrasound results primarily from acoustic cavitation: the formation, growth, and implosive collapse of bubbles in liquids.[26-28] During bubble collapse, intense shock waves are generated and propagate through the liquid at velocities above the speed of sound.[29, 30] Unusual sonochemical effects are induced by these shock waves, most importantly, high velocity collisions among solid particles suspended in such liquids.[29] These collisions result in extreme heating at the point of impact, which can lead to effective local melting and dramatic increases in the rates of many solid-liquid reactions.[31] It has been shown that the peak effective temperatures reached during interparticle collisions can reach up to 2600°C on the local spot.[29]

Based on these facts, it is suggested that in the reaction system of our study, the interparticle collisions could have caused dramatic local heating between particles. Thionyl chloride could have been vaporized at the interface under such high temperature and functioned as a dealumination reagent. And the NaCl and $AlCl_3$ yielded from the reaction could have migrated to the surfaces of the particles, and upon contact with the

cold toluene at the solid-liquid interface, the salts solidify and precipitate on the crystal surfaces, according to XPS results. The effect of ultrasound also explains why dealumination didn't occur with simple stirring under room temperature because there is no such dramatic local heating phenomenon present in the stirring case. It is envisioned that this new procedure can be extended to other types of zeolites to generate aluminum-deficient forms and by controlling the duration of sonication, different Si/Al ratios can be achieved. It could also be interesting to apply sonication to other chemical reagents such as silicon tetrachloride, which traditionally have been used in gas-solid reactions to dealuminate zeolites.

7.9 CONCLUSIONS

The dealumination of zeolite 4A with thionyl chloride was studied with and without the presence of sonication. Solid-state ^{29}Si and ^{27}Al MAS NMR spectroscopies were utilized for a qualitative determination of the degree of dealumination. The ^{29}Si and ^{27}Al NMR results showed that sonication has effectively facilitated the process of dealumination near room temperature while simple stirring caused negligible changes in zeolite structure. Also the degree of dealumination was found to depend on the duration of sonication. XPS surveys detected chlorine rich surfaces on the sonication treated zeolites, which is attributed to NaCl and $AlCl_3$, by-products of the dealumination reaction. The Si/Al ratios obtained from XPS tests also showed an increasing trend with longer treatment time. These results strongly support the fact that sonication has induced dealumination under ambient conditions. Partial loss in crystallinity was observed by XRD tests, unit cell calculation and nitrogen physisorption analysis. Nevertheless, this new procedure allows relatively convenient preparation of aluminum-deficient zeolites

with potentially a wide range of Si/Al ratios under ambient conditions. The dramatic local heating resulted from ultrasound has presumably caused the unusual phenomenon of dealumination using thionyl chloride under bulk room temperature.

7.10 REFERENCES

[1] Anderson, M. W.; Klinowski, J. *J. Chem. Soc., Faraday Trans*. **1986**, *82*, 1449.

[2] Bekkum, H.; Flanigen, E. M.; Jansen, J. C. Eds. *Introduction to Zeolite Science and Practice*; Elsevier: New York, 1991.

[3] Whyte, T. E.; Betta, R. D.; Derouane, E. G.; Baker, R. T. K. *Catalytic Materials: Relationship Between Structure and Reactivity*; American Chemical Society: Washington, D.C, 1984.

[4] Chen, N. Y.; Garwood, W. E.; Dwyer, F. G. *Shape Selective Catalysis in Industrial Applications*, 2nd ed.; Dekker: New York, 1996

[5] Lee, G. S.; Maj, J. J.; Rocke, S. C. *Catal. Lett*. **1989**, *2*, 243.

[6] Barrer, R. M.; Makki, M. B. *Can. J. Chem*. **1964**, *42*, 1481.

[7] Chen, N.Y.; Smith, F. *Inorg. Chem*. **1976**, *15*, 295.

[8] Triantafillidis, C. S.; Vlessidis, A. G.; Evmiridis, N. P. *Ind. Eng. Chem. Re*s. **2000**, *39(2)*, 307.

[9] Parikh, P. A.; Subrahmanyam, N.; Bhat, Y. S.; Halgeri, A. B. *J. Mol. Catal*. **1994**, *88*, 85.

[10] Maache, M.; Janin, A.; Lavalley, J. C.; Joly, J. F. *Zeolites* **1993**, *13*, 419.

[11] Apellian, M. R.; Fung, A. S.; Kennedy, G. J.; Degnan, T. F. *J. Phys. Chem.* **1996**, *100*, 16577.

[12] Xie, Z. K.; Chen Q. L.; Zhang C. F.; Bao J. Q.; Cao Y. H. *J. Phys. Chem. B* **2000**, *104*, 2853.

[13] Weitkamp, J.; Sakuth, M.; Chen, C.; Ernst, S. *J. Am. Soc.; Chem. Commun*. **1989**, 1908.

CHAPTER 8
GENERALIZATION OF THE GRIGNARD TREATMENT

8.1 OVERVIEW

Based on the understanding of the underlying chemistry involved in the Grignard treatment, this chapter is dedicated to generalizing this highly specific treatment to inorganic materials other than zeolite 4A. Pure silica (Si/Al=∞) was studied as a model filler system to represent the other end of the aluminosilicate material spectrum. Similar nanostructured surfaces can be achieved via a heterogeneous nucleation process presented here. Efforts were exerted towards tailoring the morphologies of the inorganic surface structures. It was found that finer surface nuclei is desirable to generate 'whisker-like' $Mg(OH)_2$ crystals. SEM imaging, gas permeation tests and XPS surface analysis showed that modified silica particles with considerable surface roughening enabled improved interfacial adhesion in a polymeric composite. It is envisioned that this technique can be implemented to modify various inorganic materials regardless of their Si/Al ratios, thereby generating a broad array of polymeric composites with enhanced interaction between polymers and dispersed inserts.

8.2 INITIAL ATTEMPT WITH PURE SILICA

Non-porous silica particles with a characteristic diameter of 3 μm were primarily used as the filler phase (Figure 8.1a and 1b). Another category of nano-sized porous silica was used as a control to replicate the literature data. The results of this study are summarized in Appendix D. The first attempt was to treat the non-porous particles using the standard protocol as described in Chapter 3: reaction with thionyl chloride followed by exposure

to methyl magnesium bromide and 2-propanol.[15] Nevertheless, no apparent morphology was observed on these treated silica surfaces, when compared to the unmodified counterparts. Representative SEM image is shown in Figure 8.1c and 1d. This observation was indeed anticipated based on the formation mechanism of the surface morphology proposed at the end of Chapter 6.[18] Specifically, the surface nano-structure observed with zeolite 4A is believed to form via a heterogeneous nucleation process, where NaCl and $AlCl_3$ are extracted from zeolites during dealumination reaction and function as the nuclei for the growth of $Mg(OH)_2$ crystals in the second step. Since pure silica does not contain aluminum or charge compensation Na^+ ions, thionyl chloride clearly can not extract inorganic compounds through the same dealumination reaction applicable for zeolite 4A, whose framework is composed of SiO_2, Al_2O_3 and charge compensation Na^+ ions. Surface characterization results of these modified silica using XPS and XRD were reported in Chapter 6. $Mg(OH)_2$ was detected to be present on such silica surface, however, it doesn't have a distinctive crystalline shape. The lack of surface nuclei presumably has caused the absence of defined patterns on silica surfaces because $Mg(OH)_2$ could not grow via the same heterogeneous nucleation mechanism.

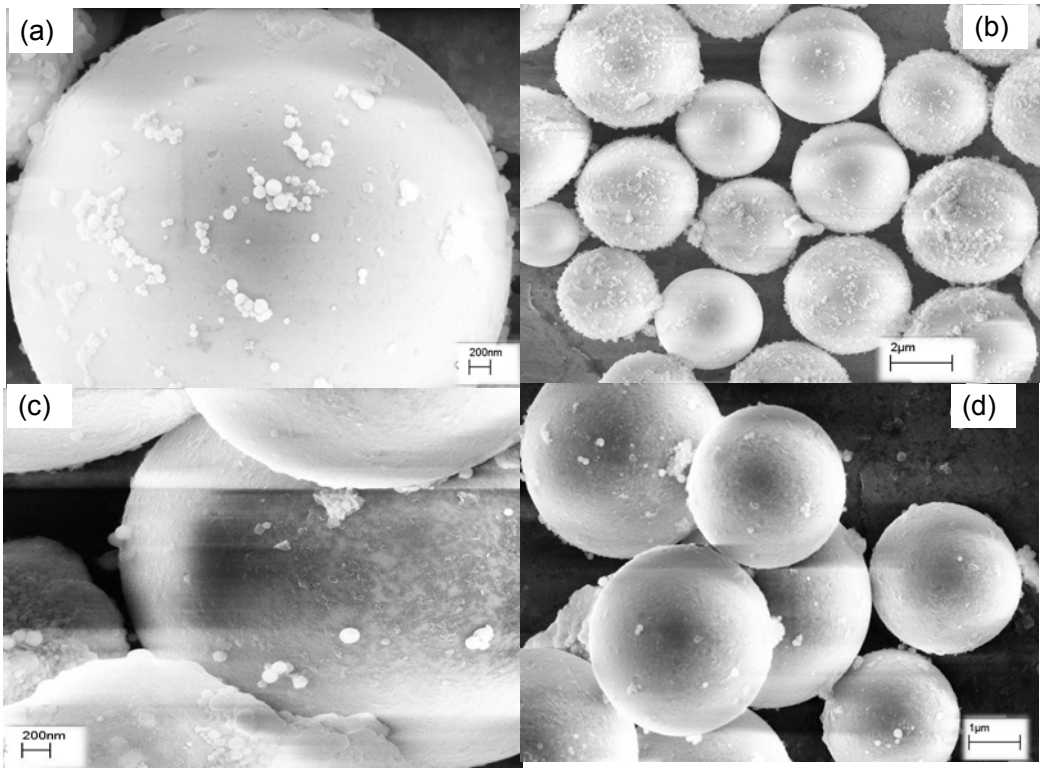

Figure 8.1 Representative SEM micrographs of silica: (a) and (b) as-received silica; (c) and (d) silica treated via the standard two-step reaction sequence.

8.3 CREATION OF NANOSTRUCTURES ON SILICA SURFACES

In order to create roughened surface morphology on silica particles, 'surface seeding' was devised to intentionally deposit nuclei on such surfaces from external sources. Two approaches were pursued and will be discussed individually below.

8.3.1 Surface Seeding via Zeolite 4A

The first attempt to deposit seeds on silica surfaces involved simply mixing a small amount (5wt%) of zeolite 4A crystals into silica powders. In principle, 4A will produce NaCl and $AlCl_3$ in the dealumination reaction with thionyl chloride. These salts will presumably be transferred to silica surfaces under the sonication field used to maintain a homogeneous particle dispersion in a solvent. Later these salts could function as heterogeneous nuclei for the crystallization of $Mg(OH)_2$ to form certain crystal patterns.

A schematic of this process is illustrated in Figure 8.2. Silica powders mixed with 5wt% zeolite 4A were treated using the standard protocol as described in Chapter 3.[15] Such modified particles were examined under SEM and the representative image is displayed in Figure 8.3. Obviously, a roughened surface morphology was obtained on silica surfaces with the seeding process. X-ray Photoelectron Spectroscopy (XPS) and X-ray Diffraction (XRD) identified the surface structure is composed of $Mg(OH)_2$, consistent with previous observations. The characterization results are shown in Figure 8.5b and 8.6a.

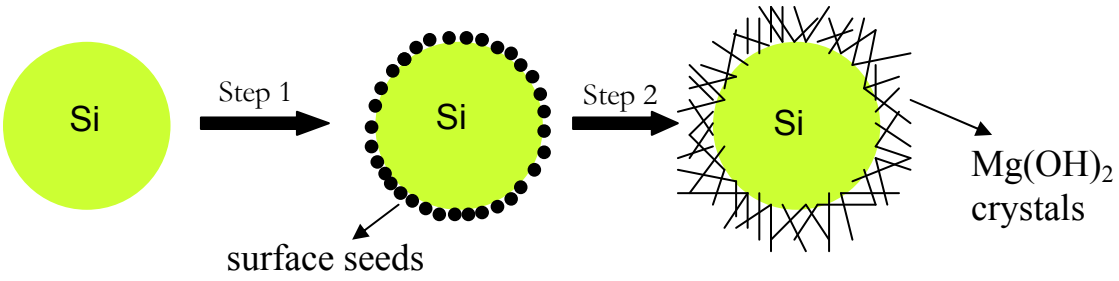

Figure 8.2 Illustration of the surface seeding approach by depositing nuclei from external source thus forming $Mg(OH)_2$ crystals on silica surfaces.

8.3.2 Surface Seeding via Direct Deposition of NaCl in Aqueous Solution

Based on the hypothesis made in Chapter 6, the major role of zeolite 4A is to produce NaCl and $AlCl_3$ which can further function as surface nuclei for the growth of $Mg(OH)_2$ crystals. It is hypothesized here that if one could deposit NaCl or $AlCl_3$ on silica surface, regardless of the method used, it should be possible to create $Mg(OH)_2$ of distinctive patterns. A simple way to precipitate inorganic salts on particle surfaces is to disperse the particles in the corresponding salt aqueous solution, followed by evaporation of water, after which the salts will deposit on the particle surfaces.

Experimentally NaCl was directly deposited on silica surfaces in an aqueous solution without using thionyl chloride or zeolite 4A. The modified seeding was performed by first dispersing silica powders in a NaCl solution, followed by filtration to collect the particles. These powders were subsequently dried under vacuum at 100ºC overnight to remove water. Since the silica used in the present study is non-porous, only the outer surface will adsorb a thin layer of liquid while dispersing in NaCl solution. Later salt particles will precipitate on the surfaces of silica when water evaporates, which will presumably enable the heterogeneous crystallization of $Mg(OH)_2$. This type of NaCl 'seeded' silica was only exposed to methyl magnesium bromide and 2-propanol, without the preceding thionyl chloride reaction. The experimental procedure was the same as used in the second step of the standard Grignard treatment. The resultant particle morphology is demonstrated in Figure 8.4. It is obvious that similar roughened surface structure was successfully created on silica surfaces with this much simplified process. Moreover, XPS and XRD confirmed the surface structure is composed of $Mg(OH)_2$ as demonstrated in Figure 8.5c and Figure 8.6b. This procedure avoids the use of thionyl chloride, simplified the surface modification process and is also a cost-effective approach.

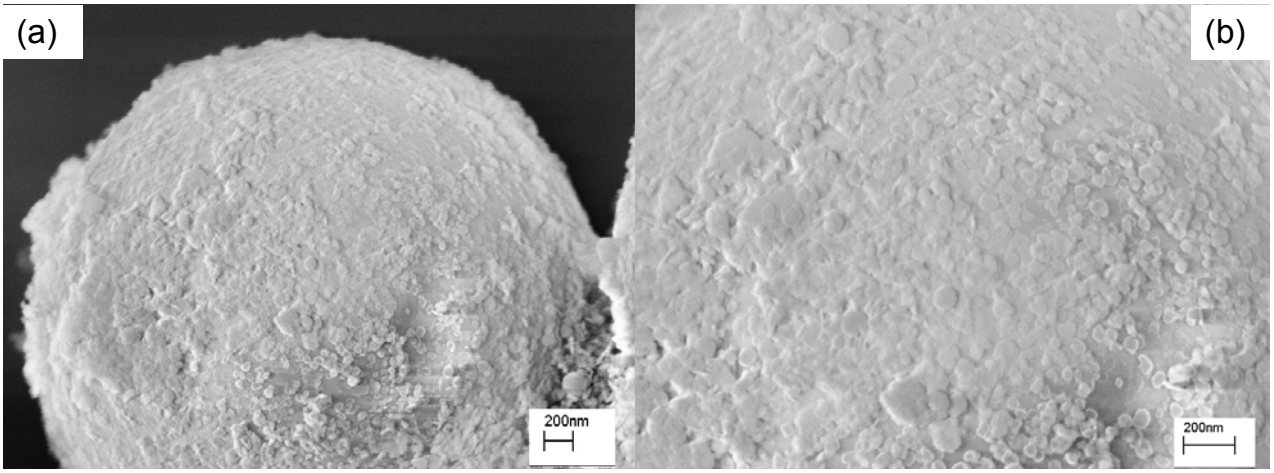

Figure 8.3 Representative SEM micrographs of silica particles: (a) modified silica using the standard two-step sequence with the presence of 5wt% zeolite 4A; (b) higher magnification image of the surface morphology.

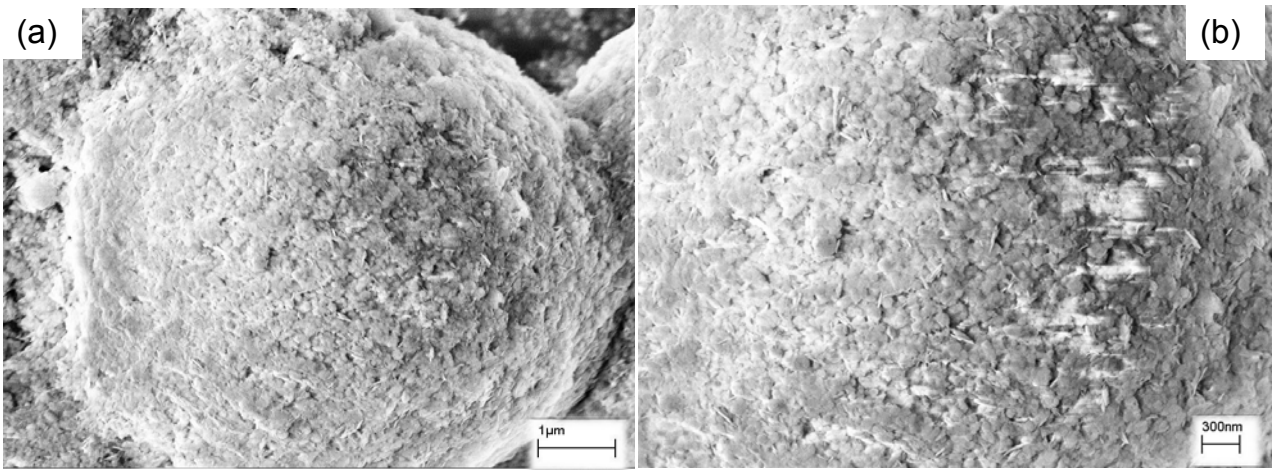

Figure 8.4 Representative SEM micrographs of silica particles: (a) NaCl seeded silica after exposure to methyl magnesium bromide and 2-propanol; (b) higher magnification image of the surface morphology.

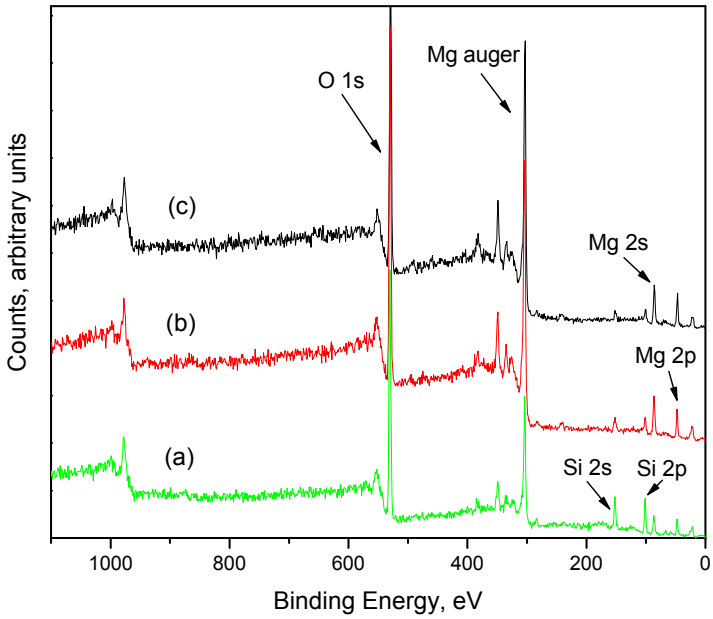

Figure 8.5 XPS surface survey of silica samples: (a) silica treated via the standard two-step sequence; (b) silica mixed with 5wt% zeolite 4A and treated via the standard two-step sequence; (c) NaCl seeded silica after exposure to methyl magnesium bromide and 2-propanol.

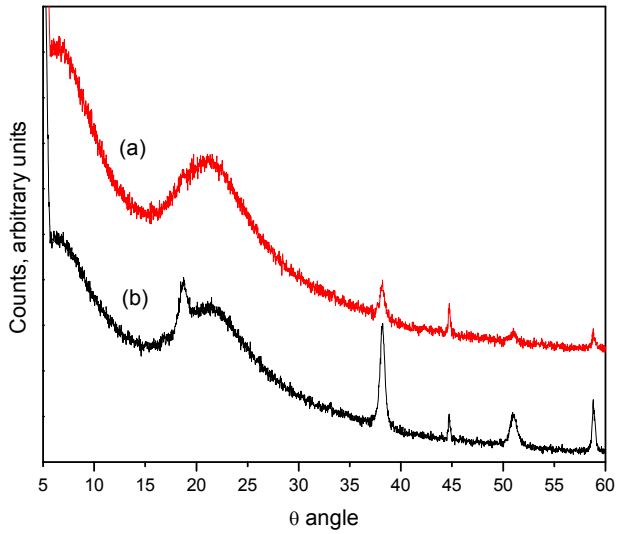

Figure 8.6 XRD spectra of silica samples: (a) silica mixed with 5wt% zeolite 4A and treated via the standard two-step sequence; (b) NaCl seeded silica after exposure to methyl magnesium bromide and 2-propanol.

8.4 CHARACTERIZATION OF MIXED MATRIX FILMS WITH SILICA

8.4.1 Interfacial Morphologies

Pure silica and its various modified forms were incorporated into Ultem® to form composite films. SEM was implemented to visually examine the interfacial morphologies in these composites and the results are illustrated in Figure 8.7 and 8.8. Figure 8.7 clearly show that Ultem® containing neat silica (Figure 8.7a and 8.7b) and silica modified via the standard 2-step treatment procedure (Figure 8.7c and 8.7d) exhibited voids between the fillers and polymer. This is believed to be due to the poor adhesion between the inorganic and organic phases. On the other hand, the silica particles with considerably roughened surfaces resulted in intact interfaces without any voids, as displayed in Figure 8.8. The absence of voids indicates that the nanoscale surface structures have effectively improved the interfacial compatibility between the inorganic fillers and organic polymer. Furthermore, these discoveries suggest an important point, which is the presence of $Mg(OH)_2$ on the particle surface does not necessarily guarantee a defect-free interface; roughened surface morphology is critical in achieving this goal. In other words, *surface chemistry is not the only element that contributes to the adhesion improvements observed in this study*. As described in the previous section, all the modified silica particles have similar concentrations of $Mg(OH)_2$ on their surfaces, inferring similar surface chemistry. However, only those bearing substantially roughened surface morphology generated membranes with desirable interaction between the inserts and polymer. The dramatic increase in the topological roughness on the particle surfaces is believed to provide improved interaction at the interface via induced adsorption and physical interlocking of polymer chains on such particle surfaces.[20,21]

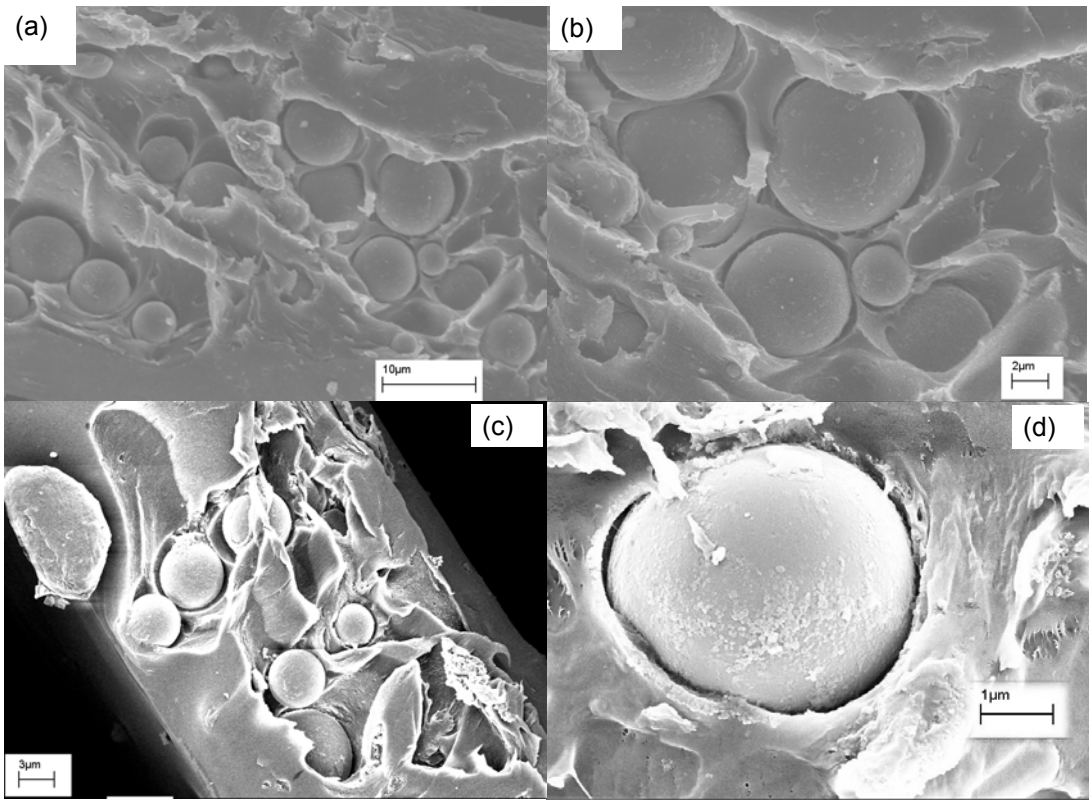

Figure 8.7 Ultem® composite films containing various silica forms showing 'sieve-in-a-cage' morphology: (a) and (b) neat silica; (c) and (d) modified silica using the standard 2-step treatment protocol.

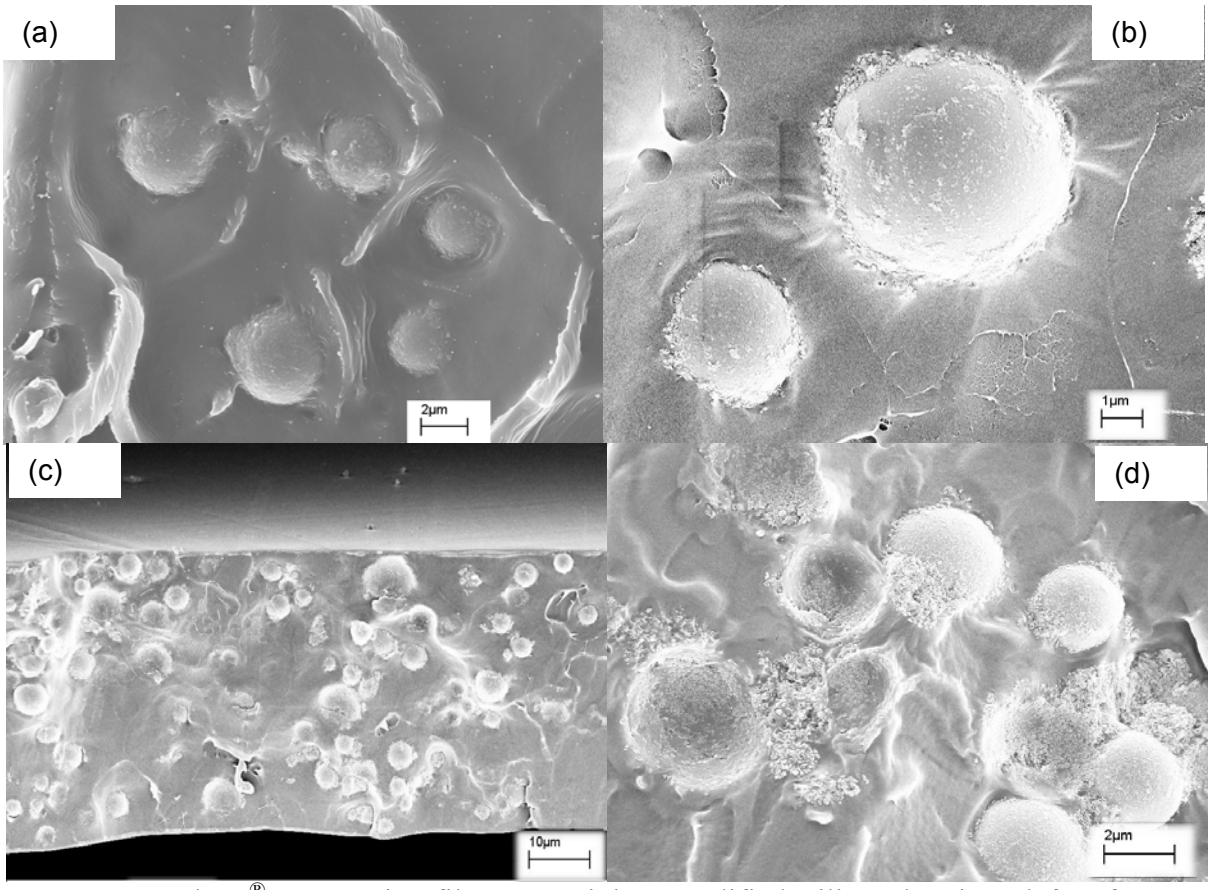

Figure 8.8 Ultem® composite films containing modified silica showing defect-free interfaces: (a) and (b) modified silica with the presence of 5wt% zeolite 4A; (c) and (d) 0.5M NaCl solution seeded silica after exposure to methyl magnesium bromide and 2-propanol.

8.4.2 Gas Transport Properties

Gas transport measurements are used in this study as another probe for the interfacial morphologies in composite films. Because gas transport is very sensitive to sub-nanometer defects by virtue of the 3-4 Å characteristic size of gas molecules, it is ideally suited to probe the interfacial integrity between the inorganic and polymer phases. Moreover, since gas molecules such as O_2 and N_2 differ in size by only roughly 0.2 Å, comparing their transport properties provides an exquisitely sensitive probe of interfacial morphology available by no other means. The Maxwell model was utilized to predict the theoretical transport properties of Ultem®/silica films. Unlike the micro-porous zeolites,

the silica particles used in this work are non-porous, and impermeable to either O_2 or N_2, nor do they provide any size discrimination of O_2 over N_2. As a result, when performing the calculation with the Maxwell model, the permeabilities of O_2 and N_2 through silica are regarded as 0 and selectivity as unity. Theoretically the selectivity of such composite films should equal to the neat polymer Ultem® because non-porous silica doesn't affect selectivity of the composite system. Yet the gas permeability values will be excellent indicators for the interfacial morphologies since any deviation from the model prediction will be caused by the non-ideal changes at the polymer-silica interfaces.

8.4.2.1 PVAc Based Mixed Matrix Membranes

PVAc was studied as a control case to illustrate the mixed matrix concepts. The high flexibility of the chain segments and the known affinity towards silicate materials make this material a favorable case for mixed matrix study. Mixed matrix membranes with various silica particles were formed and characterized by O_2 and N_2 permeation experiments, the results of which are illustrated in Table 8.1.

It is interesting to notice that although PVAc and zeolite 4A can form an intact interface without any sieve modification, neat silica and PVAc produced membranes with higher permeabilities than the model prediction, suggesting void-type morphologies at the interface. It is known that the acidity of hydroxyls on silicate surface increases with the aluminum content.[23] As a result, the surface silanols of zeolite 4A (Si/Al =1) are much more acidic than those of silica (Si/Al=∞), which could explain the strong affinity between PVAc and 4A and much weaker interaction between PVAc and silica. The modified silica via the standard 2-step Grignard treatment yielded membranes with higher flux than Maxwell Model value too, inferring that the presence of surface

$Mg(OH)_2$ component does not necessarily eliminate the interfacial defects. The two types of seeded silica which have disordered surface structures resulted in membrane permeabilities lower than the theoretical value, implying the 'matrix rigidification' effect is present in such films. In other words, the fillers and polymer matrix are well adhered to each other and the interface is void-free. The above observations suggest the important role of particle surface roughness in achieving satisfactory adhesion improvement in mixed matrix membranes.

Table 8.1 Gas transport properties of PVAc composite films with 15wt% solid (pure gas tests, 35°C, upstream pressure of 65 psi). Three films were tested with each filler and the permeabilities reported here are averaged values with standard deviation less than 3.9%.

Membranes	O_2 Permeability, Barrer	O_2/N_2 Selectivity
Neat PVAc	0.53	6.2-6.3*
Maxwell Model (15wt%)	0.44	6.2-6.3
Unmodified silica	0.54	6.2
Modified silica using standard 2-step procedure	0.50	6.1
Modified silica using 2-step procedure with the presence of 5wt% zeolite 4A	0.43	6.3
0.5M NaCl seeded silica after exposure to Grignard reagent	0.39	6.3

* The selectivity of PVAc was found to shift after 3 years' storage in the lab. The literature value of PVAc O_2 permeability is 0.5 barrer and O_2/N_2 selectivity of 5.9-6.0.

8.4.2.2 Ultem® Based Mixed Matrix Membranes

Ultem® is another polymeric matrix examined in this work. It is more challenging to form a good mixed matrix membrane due to limited chain motion and lack of favorable interaction with inorganic surfaces. Pure gas permeation experiments with O_2 and N_2

were conducted to measure the gas transport properties in Ultem® based films and the results are shown in Table 8.2. The two types of films shown in Figure 8.7 both demonstrated much higher permeabilities than the model prediction, which agrees well with the void-type interface. Voids existing between polymer and fillers provide a free bypass for the gas molecules and allow both O_2 and N_2 to transport directly through the voids, thus causing a much higher flux. Contrary to the above findings, the two sets of films shown in Figure 8.8 exhibited reduced permeabilities relative to the model values, which is believed to be due to immobilization of polymer chains via adsorption onto particle surfaces.[25,26] The results imply that the interfaces in such films are intact without any defects even at an Ångstrom scale. To summarize, the difference in the permeabilities of composite films provide further evidence that the particles with roughened surface structures greatly promoted adhesion at the interfacial regions and led to defect-free composites.

Table 8.2 Gas transport properties of Ultem® composite films with 15wt% solid (pure gas tests, 35°C, upstream pressure of 65 psi). Three films were tested with each filler and the permeabilities reported here are averaged values with standard deviation less than 4.3%.

Membranes	O_2 Permeability, Barrer	O_2/N_2 Selectivity
Neat Ultem	0.4	7.6
Maxwell Model	0.34	7.6
Unmodified silica	0.56	7.5
Modified silica using standard 2-step procedure	0.54	7.5
Modified silica using 2-step procedure with the presence of 5wt% zeolite 4A	0.32	7.6
0.5M NaCl seeded silica after exposure to Grignard reagent	0.30	7.6

When the solid concentration was increased to 30wt% in the films, the interfaces started to fail to some extent. The permeation data are summarized in Table 8.3. The neat silica and silica modified via the 2-step sequence again resulted in membranes with much higher permeabilities than the Maxwell model prediction, reflecting poor adhesion at the interfacial regions. It is interesting to notice that the permeabilities are, however, lower than the corresponding films with 15wt% solids. There are two factors affecting the flux in this case, the enlarged interfacial areas due to higher concentration of fillers and increased transport resistance due to incorporation of impermeable silica inserts. These two factors tend to oppose each other because larger interfacial areas suggest more defects which can lead to higher flux, while the presence of more impermeable silica most likely depresses the permeability. Therefore, the reduced permeabilities at 30wt% silica loading relative to 15wt% are believed to be a result of two competing trends.

The composite films embedded with two types of surface roughened silica exhibited higher flux than theoretical prediction too, indicating the existence of defects in such membranes. Nonetheless, the fact that their permeabilities are lower than the first two samples containing silica without substantial surface roughness infers better adhesion is provided by these modified silica. Furthermore, the films including NaCl seeded silica yielded the lowest permeability, which is in accordance with the finest surface structure as displayed in Figure 8.4. In chapter 5 where intact interfaces were obtained with zeolite 4A even at 30wt% loadings, the surface structures are of even smaller dimensions and appear to have a much higher aspect ratio with 'needle-like' shape. These observations imply that finer surface morphology is likely to enable better interfacial adhesion. Therefore, in order to improve interfaces at higher solid contents, it is desirable to tailor the morphology of $Mg(OH)_2$ structures to even smaller dimensions. Efforts made to explore this assumption will be elaborated in a subsequent section.

Table 8.3 Gas transport properties of Ultem® composite films with 30wt% solid (pure gas tests, 35°C, upstream pressure of 65 psi). Three films were tested with each filler and the permeabilities reported here are averaged values with standard deviation less than 5.0%.

Membranes	O_2 Permeability, Barrer	O_2/N_2 Selectivity
Neat Ultem	0.4	7.6
Maxwell Model	0.29	7.6
Unmodified silica	0.48	7.5
Modified silica using standard 2-step procedure	0.49	7.5
Modified silica using 2-step procedure with the presence of 5wt% zeolite 4A	0.43	7.6
0.5M NaCl seeded silica after exposure to Grignard reagent	0.40	7.6

8.5 QUANTITATIVE MEASURE OF POLYMER'S ADSORPTION ON SILICA SURFACES

Quantitative experiments were carried out to demonstrate the stronger adsorption of polymer chains onto roughened silica surfaces as opposed to smooth surfaces. Two characterization techniques (XPS and TGA) were employed, and results from these analysis will be discussed separately below.

Three types of silica were inspected herein: (1) unmodified silica; (2) silica treated via the standard 2-step protocol; (3) surface seeded silica after Grignard modification with roughened surface morphology as shown in Figure 8.4. The particles were first dispersed in dilute PVAc/toluene solution and Ultem®/dichloromethane solution (3wt%), respectively. Afterwards they were collected via centrifuge, repeatedly rinsed with the

corresponding solvent for 3 more times, followed by drying under vacuum at 100ºC overnight. It is assumed that the mobile polymer segments on the solid surface would be easily dissolved by the solvent during rinse, only the strongly adsorbed or mobilized chains will remain on the particle surfaces. Theoretically speaking, after an abundant rinse, the solvent should eventually be able to extract all the chains from the solid surface. However, limited times of rinse (three used here) is presumably insufficient to dissolve all the adsorbed segments. The difficulty in removing polymers from a solid surface is another indication of the strength of adhesion. The two modified silica, which bear similar surface chemistry but discrete physical morphologies, are expected to generate useful information with regard to whether the effect of surface chemistry (enthalpy) or surface roughness (entropy) plays a greater role in enhancing polymers' adsorption in this study.

8.5.1 XPS Analysis

The powders after being dispersed in polymer solutions and subsequently dried to remove solvents were analyzed using XPS to reveal the surface elemental compositions and the spectra are illustrated in Figure 8.9 and 8.10.

Figure 8.9 summarizes the XPS survey spectra obtained with Ultem® dispersed particles. It was found that C is present on all the silica surfaces because of the adsorbed polymers. Nevertheless, the atomic concentrations of C differ in the investigated samples. The detected C concentration is ~50 atom% on the roughened silica versus ~29 atom% on the other modified counterpart without distinctive surface morphology, and ~20 atom% was observed on neat silica sample. These numbers correspond well to the much

higher peak intensity at 280eV in Figure 8.9c than 8.9a and 8.9b. In addition to larger C concentration, a higher N signal was obtained on roughened silica surface (~5%) which is introduced by the imide groups in Ultem®. The N peak intensity in Figure 8.9a and 8.9b, on the contrary, is negligible inferring much less polymers have adsorbed on such smooth surfaces. The same trend can be observed in Figure 8.10 which presents the XPS results of PVAc dispersed particles. The C concentration is again much higher on the roughened particle surface, implying stronger polymer adsorption has occurred with such type of surfaces.

The disparity between the two modified samples suggested that the presence of $Mg(OH)_2$ is not the only reason for enhanced adsorption of polymers on modified particle surfaces. Indeed, the presence of more polymer chains on the surface roughened particles point to the fact that the nanostructures help grab and stabilize the chain segments at polymer/filler interface to prevent them from easily extracted by solvents. Therefore physical heterogeneity outweighs change in surface chemistry in this case.

Moreover, N_2 physisorption tests discovered a substantial increase in the BET surface area of the roughened silica compared to the two other counterparts. The results are summarized in Table 8.4. These discoveries imply that the contact areas between polymer and fillers are greatly augmented by the presence of nanoscale entities. At the end of Chapter 5, it is hypothesized that these nanoscale inorganic structures serve as effective interlocks between inserts and polymer to stabilize the polymer chains at interfaces via multiple points of contact.

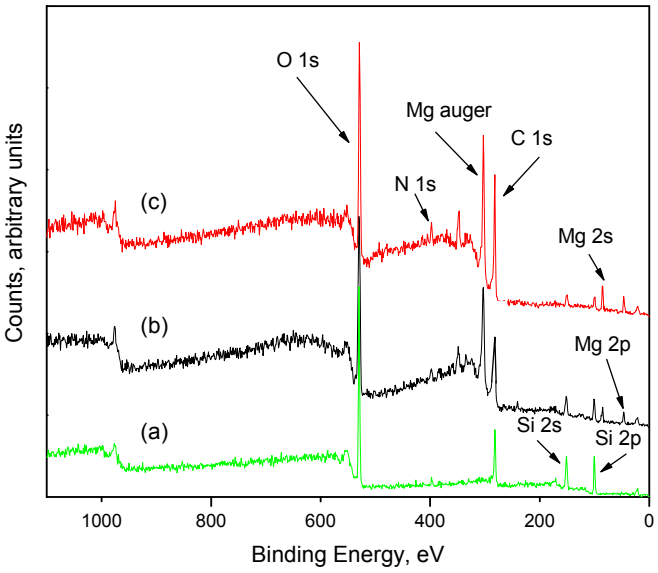

Figure 8.9 XPS surface analysis of silica after dispersed in Ultem® dilute solution and rinsed with dichloromethane: (a) pure silica; (b) modified silica via the standard 2-step sequence; (c) seeded silica after Grignard treatment with roughened surface morphology. The major peaks detected are O 1s (531 eV), N 1s (398 eV), C 1s (285 eV), Si 2s (151 eV), Si 2p (99 eV), Mg 2s (89 eV), Mg 2p (50 eV).

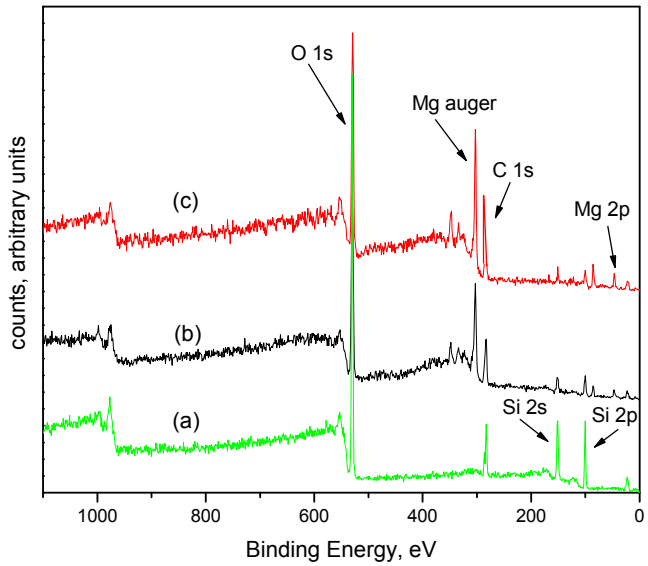

Figure 8.10 XPS surface analysis of silica after dispersed in PVAc dilute solution and rinsed with toluene: (a) pure silica; (b) modified silica via the standard 2-step sequence; (c) seeded silica after the Grignard treatment with roughened surface morphology. The

major peaks detected are O 1s (531 eV), C 1s (285 eV), Si 2s (151 eV), Si 2p (99 eV), Mg 2s (89 eV), Mg 2p (50 eV).

Table 8.4 BET surface areas of various silica samples measured by nitrogen physisorption tests

Sample ID	BET Area (m^2/g)
Neat Silica	3.0
Modified Silica Via the Standard 2-step Sequence	11.8
Seeded Silica After the Grignard Treatment	101.5

8.5.2 TGA Characterization

Thermal Gravimetric Analysis (TGA) was utilized in this study to provide further proof of the induced adsorption of polymers onto disordered surfaces. The dried powders after dispersed in polymer solutions are heated in air under high temperatures in a TGA furnace. The purpose of such operation is to oxidize and degrade the polymers attached to the particles, and the weight loss indicates the amount of removed polymers, in other words, the amount of polymers originally present on the surfaces.

A series of control experiments were conducted before the inspection of polymer doped samples. Neat silica and the two types of modified silica were dried in air up to 700ºC and the results are shown in Figure 8.11. Unlike zeolite 4A which adsorbs considerable amount of moisture due to its microporous structure, silica particles used in this work are nonporous in nature and thus unable to adsorb as much water as zeolitic materials. Additionaly, the absence of Al from silica renders this material less hydrophilic. As a result, there is very small change in weight loss below 150ºC in these samples, contrary to ~14wt% loss occurring with zeolite 4A shown earlier in Chapter 5. It

is also discovered in Chapter 5 that the conversion temperature from $Mg(OH)_2$ to MgO is within the range of 290ºC - 320ºC. This dehydration effect was manifested in the two modified samples, where a sharp weight loss was observed between 290ºC and 320ºC, accounting for the removed water from $Mg(OH)_2$. The slightly higher weight loss associated with seeded silica after the Grignard treatment suggests more $Mg(OH)_2$ is present on such particle surface. The difference may be due to random precipitation of $Mg(OH)_2$ on a smooth particle surface as opposed to heterogeneous crystallization with the presence of nuclei (NaCl in this case).

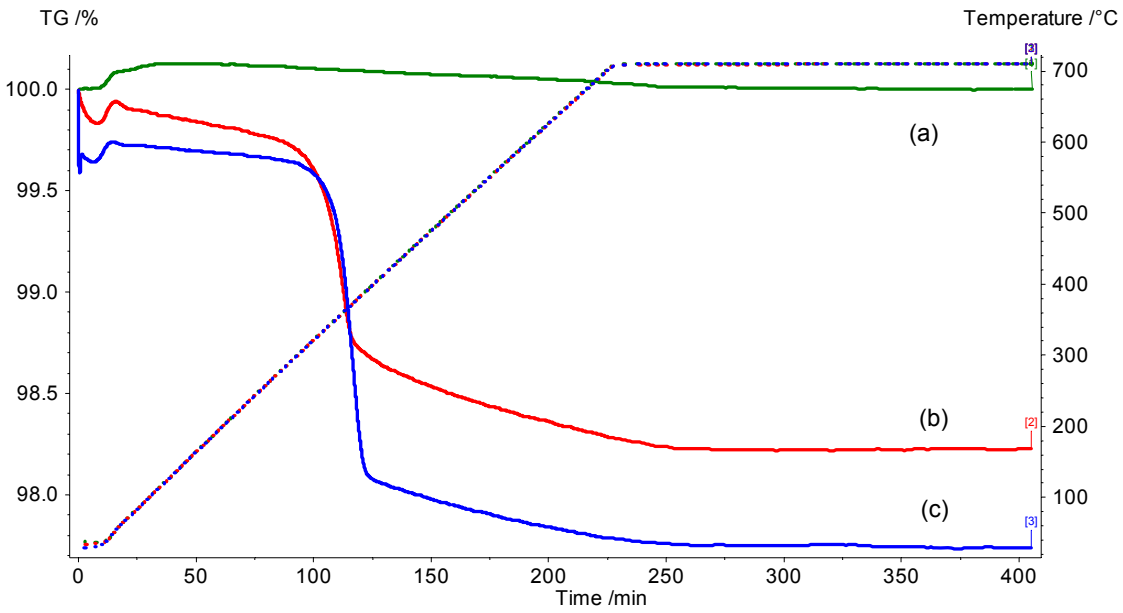

Figure 8.11 Thermal Gravimetric Analysis (TGA) results of 3µm silica samples: (a) unmodified silica; (b) modified silica using the standard protocol; (c) seeded silica after the Grignard treatment.

Figure 8.12 demonstrates the TGA results of silica samples doped with PVAc. The polymer started to degrade from around 250ºC, causing an apparent weight loss above this temperature in all samples. In the range of 290ºC - 320ºC, both the two modified

samples exhibited a sharp drop in weight, which can be designated to the dehydration of $Mg(OH)_2$ present on the particle surfaces. It needs to be pointed out that the degradation of PVAc is also taking place within this scope, accompanied by the dehydration of surface inorganic entities. It is noteworthy that the absolute value of polymeric weight loss observed with 3μm silica is much less than that obtained with 0.1μm zeolite 4A in Chapter 5. The submicron sieves have much larger surface areas that offer a larger adsorption capacity, thereby the effect of weight loss in a TGA test is more pronounced. The final detected polymeric loss is evidently highest in the most roughened sieves (seeded and Grignard treated) as compared to the other two counterparts. The difference suggests that larger number of chains adsorbed on the particles with surface nanostructures in the first place. An interesting comparison to draw is between the two types of modified silica, one having large pieces of $Mg(OH)_2$ crystals and the other with nanoscale $Mg(OH)_2$ structures. These two samples have similar surface chemistry but very different morphologies. The fact that stronger adsorption occurred with surface roughened silica infers that the enthalpic interaction brought by the presence of $Mg(OH)_2$ on the particle surface does not contribute to the full enhancement; surface roughness plays a critical role in achieving the improved adhesion observed in this study.

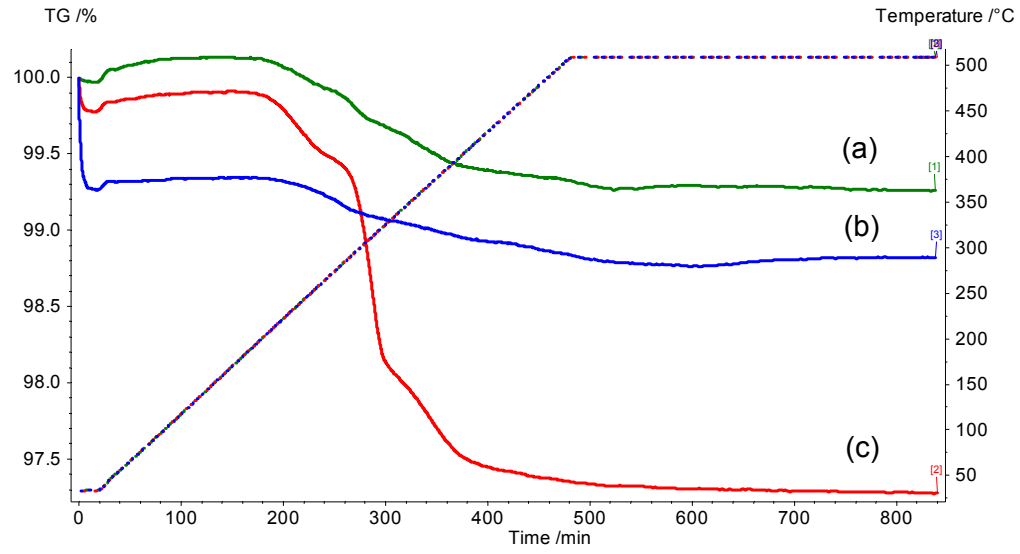

Figure 8.12 Thermal Gravimetric Analysis (TGA) results of 3μm silica samples: (a) unmodified silica after dispersing in PVAc solution; (b) 2-step modified silica after dispersing in PVAc solution; (c) seeded and Grignard treated silica after dispersing in PVAc solution.

Similar tendency was observed in Figure 8.13 which displays the TGA curves of various silica particles after dispersing in Ultem® solutions. It is obvious that almost no polymer's adsorption occurred with the unmodified, smooth silica particles, or the pre-adsorbed chains were easily extracted by solvent during rinse. It suggests very weak intrinsic affinity between silica and Ultem®. The observation here is different from the previous case with PVAc where small amount of PVAc was found to adsorb on neat silica surface (Figure 8.11a). This could result from hydrogen bonds formed between the carbonyls in PVAc and the hydroxyls on silica surfaces. Very few such bonds can form between Ultem® and silica, which presumably explains the absence of chain attachment with neat silica. On the other hand, about 4.2% polymeric weight loss was related to surface roughened silica particles, implying induced adsorption caused by the surface structures. The highest weight loss associated with the sample bearing nanostructured

surfaces again implies that surface roughness has greatly promoted adsorption and helped stabilize the contact between polymer and fillers. Moreover, the discrepancy between the two types of modified silica reflects the greater significance of surface roughness as compared to surface chemistry enabled by this specific treatment.

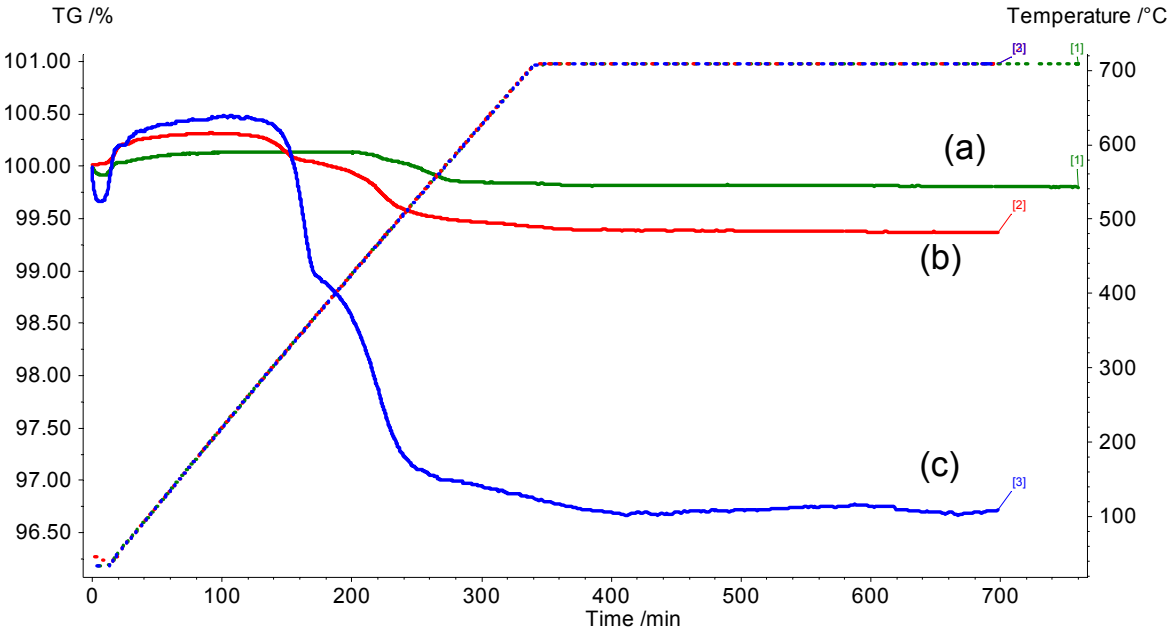

Figure 8.13 Thermal Gravimetric Analysis (TGA) results of 3µm silica samples: (a) unmodified silica after dispersing in Ultem® solution; (b) 2-step modified silica after dispersing in Ultem® solution; (c) seeded and Grignard treated silica after dispersing in Ultem® solution.

It is noteworthy that all the samples upon finishing of TGA were subjected to XPS tests and it was confirmed that no C remained on the surface of such samples. These findings verify that all the polymer chains were decomposed during the thermal analysis.

To summarize the preceding discussions, XPS and TGA yielded quantitative measures of polymers' adsorption on particle surfaces from a macroscopic view. The obtained results reveal that enhanced polymer chain adherence takes place on the modified, roughened particle surfaces as compared to the unmodified, smooth surfaces.

Furthermore, the presence of $Mg(OH)_2$ component on the surface itself does not account for the full enhancement in interfacial affinity. Indeed the nanoscale, disordered entities have substantially promoted the adsorption of polymers and stabilize the chains at the polymer/filler interfaces.

8.6 TAILORING THE MORPHOLOGY OF $MG(OH)_2$ SURFACE STRUCTURES

8.6.1 Hypothesis on Varied Surface Structures

It was noted that the surface morphologies created on silica surfaces through the 'seeding' process do not resemble exactly those formed on zeolite 4A surface. The $Mg(OH)_2$ crystals shown in Figure 8.3 and 8.4 appear as spherical particles rather than whisker-shaped morphologies obtained with 4A. An assumption is proposed here to explain the cause of difference in the surface patterns.

The essential difference between zeolite 4A and silica with regard to the Grignard treatment is the number of available surface nuclei present on the particle surfaces. The disparity in the density of surface seeds is believed to have caused the different morphologies of $Mg(OH)_2$ crystals observed in this study. In the case of zeolite 4A, each zeolite particle is able to produce $AlCl_3$ and NaCl in the reaction with thionyl chloride and the sieve surface is densely covered by very fine seeds after the dealumination reaction. When $Mg(OH)_2$ starts to form later, the crystals have to grow in the direction away from the particle surface due to the lack of space in the adjacent surface regions where other $Mg(OH)_2$ crystals are also forming on the nuclei. While in the case of silica particles, the density of surface seeds is much lesser than pure 4A system because only 5wt% of 4A was introduced to produce seeds or limited amount of NaCl was adsorbed from an aqueous solution. When $Mg(OH)_2$ crystals start to form on such silica surfaces,

they have enough space to grow into the vicinities on the surface and eventually form chunky crystals or spheres. A schematic of this proposed mechanism is depicted in Figure 8.14. According to this assumption, in order to create 'whisker' or 'needle' like crystals, it is desirable to have very fine nuclei densely covered on the particle surfaces.

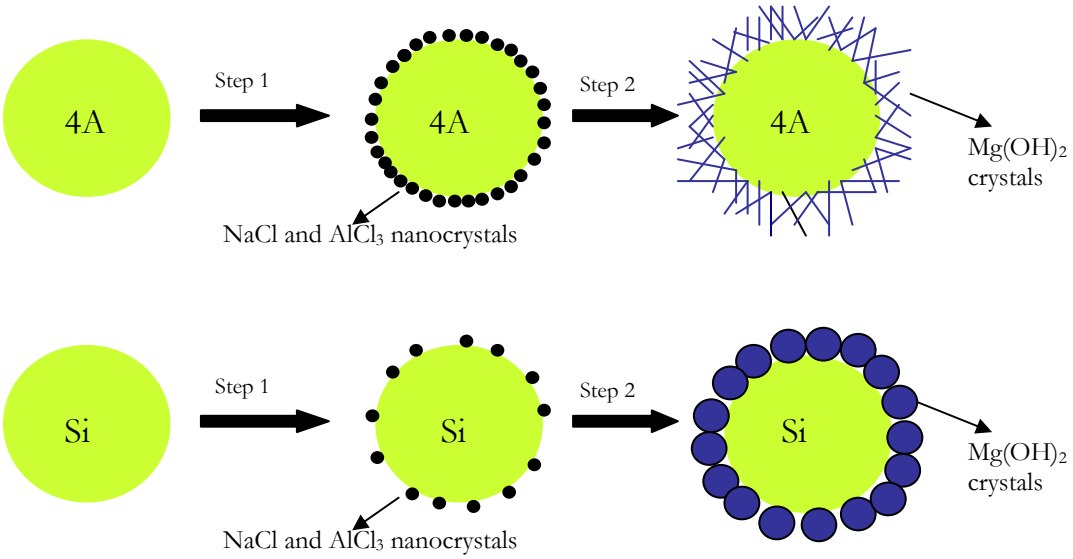

Figure 8.14 Illustration of the effect of different densities of surface seeds on the final morphologies of $Mg(OH)_2$ created on the particle surfaces.

8.6.2 Approaches to Tailor the Surface Morphologies

Work in the previous section shows that by intentional precipitation of nuclei on silica surfaces, it is viable to create distinctive patterns of $Mg(OH)_2$ crystals on the particle surfaces. Based on the hypothesis in Figure 8.14, the density of surface nuclei essentially determines the final morphology of $Mg(OH)_2$ crystals. Thereby, by varying the concentrations of nuclei present on silica surface, it is presumably viable to form different crystalline morphologies. This section addresses exploration of this possibility and the results are presented below.

8.6.2.1 Varying the Amount of Zeolite 4A

When silica is seeded by the introduction of zeolite 4A, the number of available nuclei is in proportional to the amount of zeolite crystals mixed with silica powders. Different weight percentages of zeolite 4A ranging from 2.5wt% to 10wt% were added to silica system and the resultant surface morphologies are displayed in Figure 8.15. With 2.5wt% of 4A crystals in the system, only large pieces of $Mg(OH)_2$ crystals were formed on silica surface as displayed in Figure 15a and 15b. With increased 4A loading to 5wt%, the crystals became nanoscale spheres, which can be seen in Figure 15c and 15d. At even higher 4A concentration of 10wt%, the finest crystal morphology was obtained which started to resemble 'needles' with higher aspect ratio (Figure 15e and 15f). These observations are strong proof of the previous speculation that the population of nuclei available on the surfaces determines the final morphology of $Mg(OH)_2$ crystals.

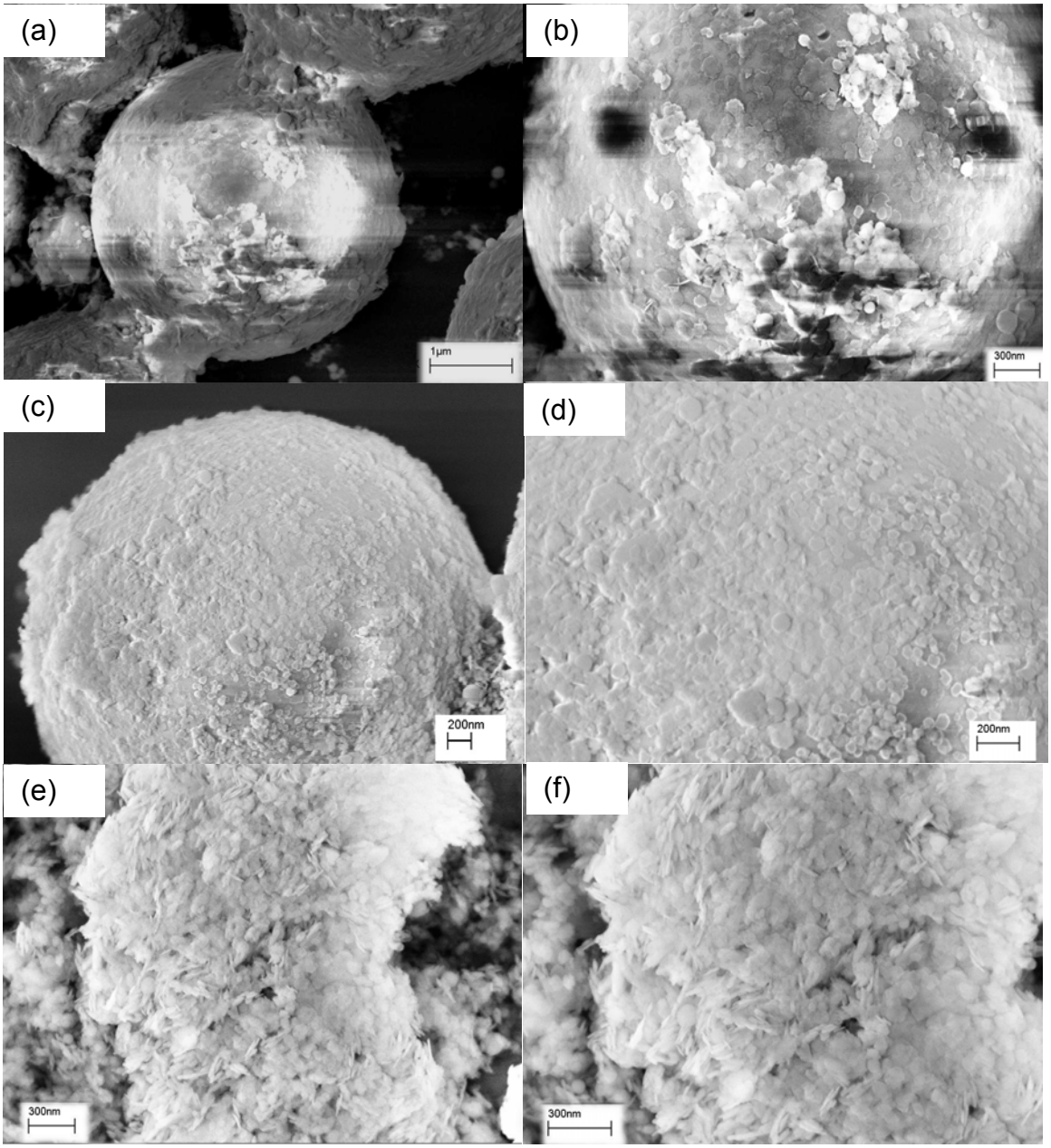

Figure 8.15 Representative SEM micrographs of treated silica particles (3μm in diameter): (a) and (b) silica (with 2.5wt% of 4A) after the Grignard treatment; (c) and (d) silica (with 5wt% of 4A) after the Grignard treatment; (e) and (f) silica (with 10wt%) of 4A after the Grignard treatment.

8.6.2.2 Varying the Concentration of NaCl Seeding Solution

Work in the previous section shows that by properly tailoring the amount of zeolites, the patterns of surface structures can be adjusted. The other approached devised in this work to precipitate nuclei on silica surfaces is to immerse silica particles in NaCl aqueous solution, followed by evaporation of water. It is easy to change the concentrations of NaCl solutions in which the silica particles are dispersed, and thereby adjust the number of nuclei deposited.

NaCl solutions of different concentrations (0.25M, 0.5M and 3M) were used in this study as seeding solutions. The resultant morphologies on silica are displayed in Figure 8.16. At low concentration of NaCl solution, only sparsely distrubuted $Mg(OH)_2$ crystals were obtained after the Grignard treatment, as shown in Figure 8.16a and 8.16b. The morphology of such crystals is either chunky pieces or sphere-like solids. When the concentration of seeding solution increased to 0.5M, the surface became densely covered with $Mg(OH)_2$. The size of such crystals is smaller than the previous case, obtained with 0.25M seeding solution. This discovery implies that increasing number of nuclei present on surface leads to finer $Mg(OH)_2$ morphologies. It is, however, surprising that the silica seeded by 3M NaCl solution delivered surface morphology similar to those seeded by 0.5M solution. Different batches were made and the results are duplicable. It was originally supposed that higher NaCl concentration shall produce smaller dimensions of $Mg(OH)_2$, and 3M solution should create even finer surface structures than 0.5M solution. Nonetheless, it is possible that silica surface has a capacity to adsorb certain amount of ions in aqueous solution and it has already reached equilibrium at 0.5M

concentration. The change from 0.5M to 3M will not increase the number of ions adsorbed on the surface and hence the formed NaCl solids after water evaporates.

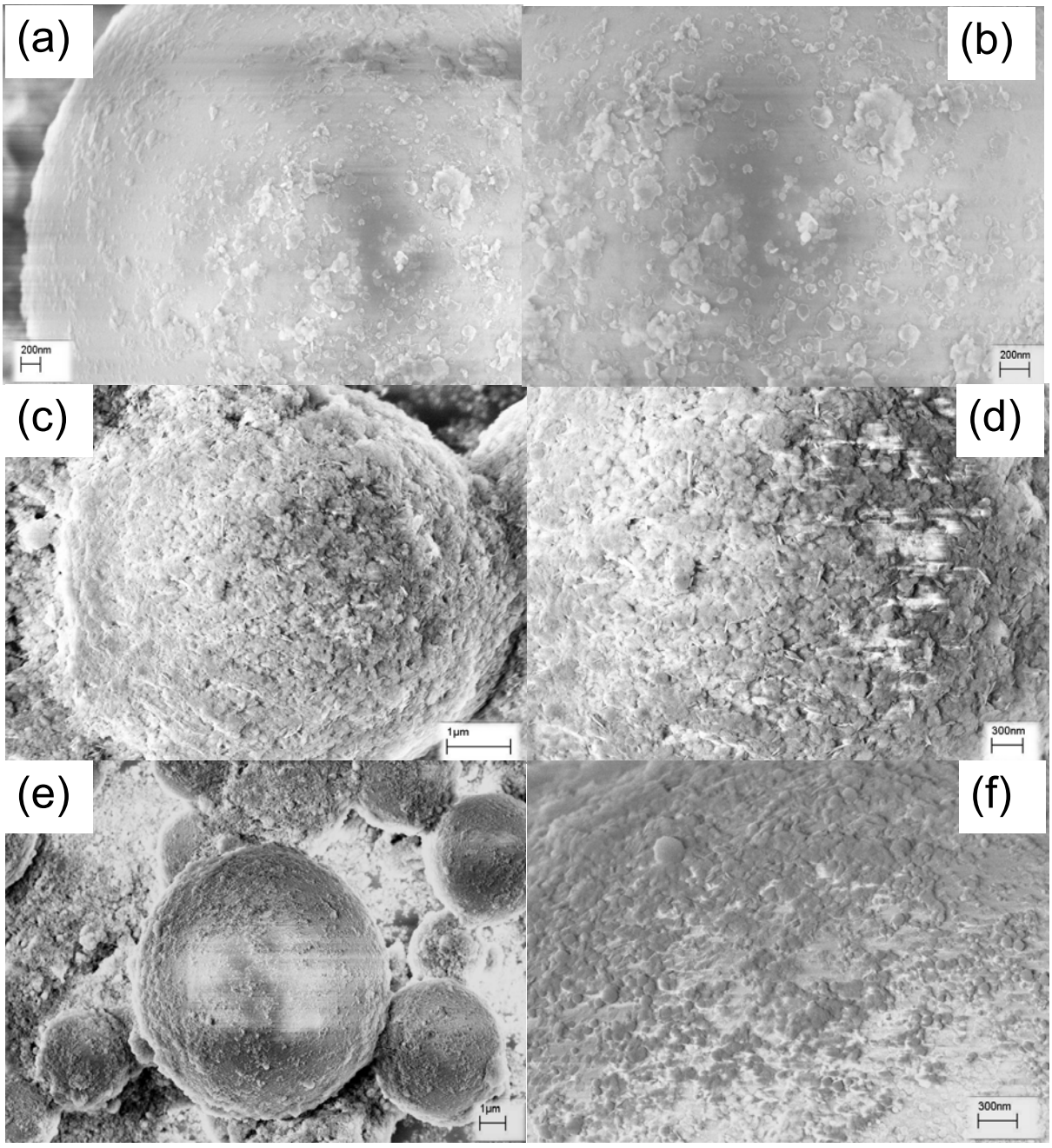

Figure 8.16 Representative SEM micrographs of various treated silica particles: (a) and (b) silica seeded in 0.25M NaCl solution after exposure to Grignard reagent; (c) and (d) silica seeded in 0.5M NaCl solution after exposure to Grignard reagent; (e) and (f) silica seeded in 3M NaCl solution after exposure to Grignard reagent.

The three types of silica shown in Figure 8.16 were incorporated into Ultem® matrix to produce mixed matrix membranes. The properties of membranes should yield insightful information with regard to the effect of different degrees of surface roughness on the adhesion improvement between the fillers and polymer. The permeation data are tabulated in Table 8.5. It is evident that all the modified fillers led to lower flux than films containing unmodified silica. Nonetheless, the films with silica seeded by 0.25M NaCl solution showed the highest flux among the three modified forms and the permeability is higher than the Maxwell model prediction. This discovery indicates that mild surface roughness as obtained in Figure 8.16a and 8.16b is not sufficient to provide significant adhesion enhancement so as to ensure a defect-free composite membrane. A highly disordered surface structure with entities of nanoscale dimensions is more effective in achieving desired improvements in mixed matrix membranes.

Table 8.5 Gas transport properties of Ultem® composite films with 15wt% solid (pure gas tests, 35°C, upstream pressure of 4.5atm). Three films were tested with each filler and the permeabilities reported here are averaged values with standard deviation less than 4.1%.

Membranes	O_2 Permeability, Barrer	O_2/N_2 Selectivity
Neat Ultem	0.4	7.6
Maxwell Model	0.34	7.6
Unmodified silica	0.56	7.5
0.25M NaCl seeded silica after exposure to Grignard reagent	0.49	7.5
0.5M NaCl seeded silica after exposure to Grignard reagent	0.30	7.6
3M NaCl seeded silica after exposure to Grignard reagent	0.31	7.6

8.6.2.3 Modified NaCl Seeding with Cold Methanol Facilitated Precipitation

The discoveries made in the preceding section offer further proofs for the nucleation hypothesis, yet a new challenge came up which is related to the capacity of silica surface to adsorb ions in an aqueous solution. The transition from 0.5M to 3M NaCl seeding solution did not lead to a smaller dimension of surface structure. This phenomenon is likely to be caused by the saturation of ions on silica surface. As mentioned earlier, in order to create 'whisker' or 'needle' like morphology, it is highly desirable that large population of very fine nuclei is present. In earlier experiments, the precipitation of NaCl solids was achieved by evaporation of water at 100ºC, which could have resulted in the formation of large NaCl crystals rather than nanoscale salts. In an effort to create finer seeds on silica surface, cold methanol was used to 'quench' or facilitate the precipitation of NaCl. The melting point of methanol is –97 °C therefore liquid methanol can be kept under very low temperature. In addition, the solubility of NaCl in methanol is only 1.39g/100g methanol. The basic idea is that when frozen methanol is added to NaCl solution, the precipitation of salt will be greatly accelerated. Indeed, very fine NaCl crystals will be generated and deposit on the silica surface, which can later be the heterogeneous nuclei for the formation of $Mg(OH)_2$ crystals. And these finer nuclei are assumed to produce crystals of small dimensions.

The modified seeding procedure is described hereby. Amount of 50mL of methanol was stored in the freezer for at least two days. Samples of ~5g of silica are dispersed in 3M NaCl solution. The dispersion was kept on a shaker for 2 hours, after which centrifuge was used to collect the particles. The liquid in the centrifuge tube was then decanted. At this moment, cold methanol was immediately added into the centrifuge tube.

The particles at the bottom of the tube were re-dispersed in methanol using a sonication horn. The frozen methanol should presumably extract the water layer from silica surface and yield large number of fine NaCl crystals. The seeded silica was collected via filtration followed by drying under vacuum at 150ºC for overnight. Afterwards, the dried powders were treated by Grignard reagent and iso-propanol using the standard experimental protocol. The final product was examined via SEM to reveal the surface morphology and representative images are displayed in Figure 8.17.

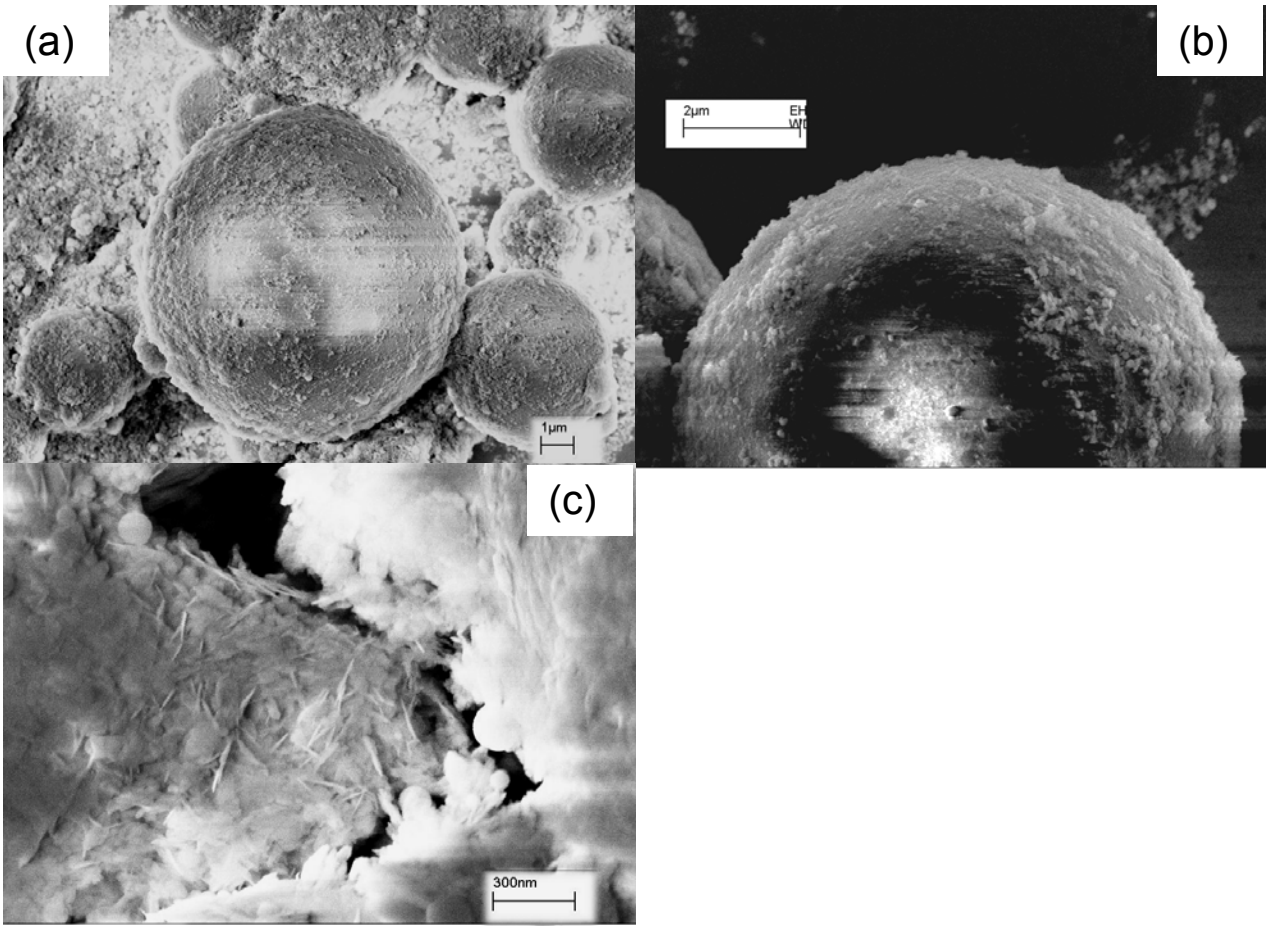

Figure 8.17 Representative SEM micrographs of surface modified silica. These particles were first seeded by 3M NaCl solution facilitated with cold methanol. Afterwards, they were exposed to methyl magnesium bromide and iso-propanol.

Instead of the anticipated 'needle-like' crystals, the acquired surface morphology is still quite similar to the previous case where 3M NaCl solution was used to seed the silica under room temperature. Nonetheless, there are certain regions where the crystals started to bear the shape of whiskers, as shown in Figure 8.17c. These results may seem surprising at first glance, but after careful consideration of the experimental procedure, it is not difficult to explain the possible causes of the absence of fine crystals. Firstly, the methanol used was stored in a freezer where the temperature can only reach as low as -5ºC. Such temperature may not be low enough to induce a rapid precipitation of salts. Furthermore, a sonication horn was employed to re-disperse the particles in liquid methanol, during which the local heating caused by sonication could have warmed up the solution and thereby increased the growth rate of NaCl to form larger crystals. Such large nuclei are possible to eventually yield spherical or cubic $Mg(OH)_2$ morphologies, rather than high aspect ratio shapes. Nevertheless, when methanol was added to the centrifuge tube, on the surfaces of those silica that were in touch with the frozen methanol before sonicator was introduced to re-disperse the particles, rapid precipitation may have taken place. This assumption could tentatively explain the fact that at limited areas, 'whisker-like' structure was observed as exhibited in Figure 8.17c.

In an effort to reduce the dimension of $Mg(OH)_2$ component and create high aspect ratio structures, a few changes were made to improve the surface seeding:

(i) In order to further reduce the temperature of methanol, the alcohol was stored in a plastic tube which was then immersed in liquid nitrogen. Solid methanol soon started to form and the mixture of liquid methanol and solid methanol has a temperature of -98ºC,

which is the melting point of this substance. This procedure greatly reduced the temperature of methanol used to accelerate precipitation.

(ii) A saturated NaCl solution was prepared to replace the 3M NaCl solution as the seeding environment. It is anticipated that the introduction of frozen methanol will create a super-saturated condition out of the already saturated solution. Under such circumstances, the precipitation of very fine crystals is expected to happen and later deposit on silica surfaces.

(iii) In order to avoid the local heating caused by sonicator, the sieves were simply dispersed by hand shaking first and placed on a shaker for one hour before filtration was used to collect the solids.

The rest of the experimental is the same as described before. The surface morphology of treated silica sample is shown in Figure 8.18. Obviously there are needle shaped crystals appearing on the surface. In Figure 8.17 where needle-like crystals were also present, such morphology was only observed at very limited regions through out the sample. But in Figure 8.18 almost each particle surface is covered by some of these fine crystals suggesting the modified process generated larger number of $Mg(OH)_2$ whiskers. The majority of the inorganic structure, however, still resembles nanosized particles. The increase in the number of needle shaped crystals reflects that more finer nuclei were present in the formation stage of $Mg(OH)_2$. But only a limited portion of such small seeds existed as compared to the larger counterparts that produced the nanoparticles. It is presumed here that the frozen methanol (-98ºC) indeed created smaller-dimensional NaCl particles, which later precipitated on silica surfaces. Nonetheless, as the temperature of the system warmed up to room temperature during the filtration step used to remove

methanol and collect the solids, these pre-formed NaCl crystals may have aggregated and grown into bigger forms. Under this assumed circumstance, it would be helpful to use a freeze dryer to remove methanol at its melting point (-98ºC) instead of filtration at room temperature. This operation would presumably retain the fine seeds generated by frozen methanol and deliver more needle shaped $Mg(OH)_2$ crystals in the subsequent deposition.

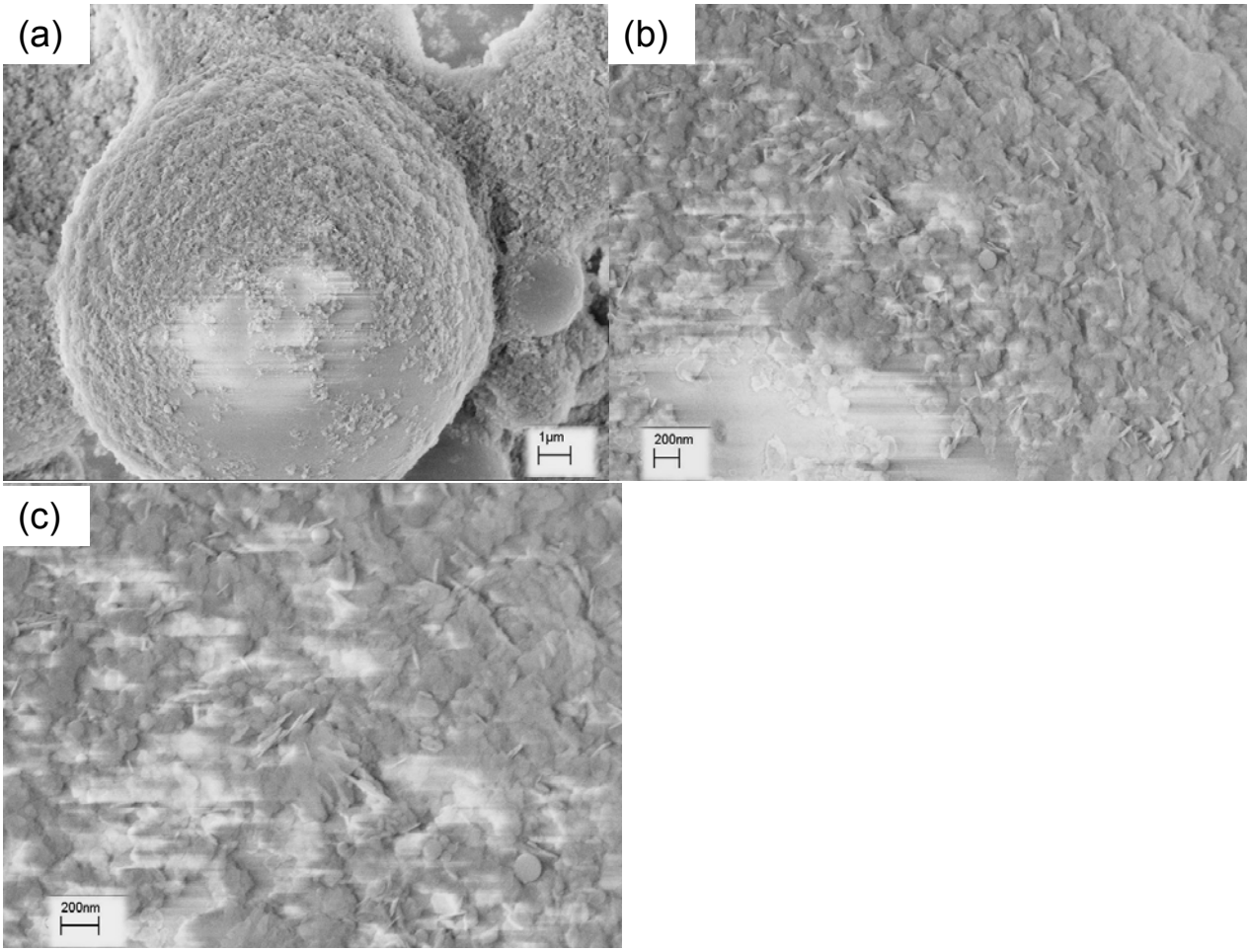

Figure 8.18 Representative SEM micrographs of Grignard treated silica using the modified surface seeding procedure.

8.7 REFERENCES

[1] Zhang. J.; Hou, L. Y.; Xu, L.; Xu, Z. L. *Chem. Mater.* 1999, 11, 3177.

[2] Molenkamp, W. C.; Watanabe, M.; Miyata, H.; Tolbert, S. H. *J. Am. Chem. Soc*. **2004**, *126*, 4476.

[3] Raghavan, S. R.; Riley, M. W.; Fedkiw, P. S.; Khan, S. A. *Chem. Mater*. **1998**, *10*, 244.

[4] Clark, J. H.; Macquarrie, D. J.; *Chem Commun*. **1998**, 853.

[5] Wright, A. P.; Davis, M. E.; *Chem. Rev*. **2002**, *102*, 3589.

[6] Lu, X.; Manners, I.; Winnik, M. A. *Macromolecules* **2001**, *34*, 1917.

[7] Teshima, K.; Sugimura, H.; Takai, O. *Langmuir* **2003**, *19*, 8331.

[8] Jeong, H. K.; Nair, S.; Vogt, T.; Dickinson, C.; Tsapatsis, M. *Nature Materials* **2003**, *2*, 53.

[9] Mittal, K. L.; Pizzi, A. *Adhesion Promotion Techniques*; Marcel Dekker: New York, 1999.

[10] Wall, J. S.; Hu, B.; Siddiqui, J. A.; Ottenbrite, R. M. *Langmuir* **2001**, *17*, 6027.

[11] Xie, X. L.; Tang, C. Y.; Zhou, X. P. *Chem. Mater*. **2004**, *16*, 133.

[12] Wang, J. Y.; Chen, W.; Liu, A. H.; Lu, G.; Yang, B. *J. Am. Chem. Soc*. **2002**, *124*, 13358.

[13] Perruchot, C.; Khan, M. A.; Kamitsi, A.; Armes, S. P.; Patten, T. E. *Langmuir* **2001**, *17*, 4479.

[14] Gomes, D.; Nunes, S. P.; Peinemann, K. V. *J. Membr. Sci*. **2005**, *246*, 13.

[15] Shu, S.; Husain, S.; Koros, W. J. *J. Phys. Chem. C* **2007**, *111*, 652.

[16] Husain, S.; Koros, W. J. *J. Membr. Sci*. **2007**, *288*, 195.

[17] Shu, S.; Husain, S.; Koros, W. J. *Ind. Eng. Chem. Res*. **2007**, *46*, 767.

[18] Shu, S.; Husain, S.; Koros, W. J. *Chem. Mater*. Submitted.

[19] Moore, T. T.; Damle, S.; Williams, P. J.; Koros, W. J. *J. Membr. Sci*. **2004**, *245*, 227.

[20] Douglas, J. F. Ma*cromolecules* **1989**, *22*, 3707.

[21] Baumgartner, A.; Muthukumar, M. J. *Chem. Phys.* **1991**, *94*, 4062.

[22] Maxwell, J. C. *A Treatise on Electricity and Magnetism*; Clarendon press: Oxford, 1983; Volume 2.

[23] Boumaa, R. H. B.; Checchettia, A.; Chidichimob, G.; Drioli, E. *J. Membr. Sci*. **1997**, *128*, 141.

[24] Moore, T. T.; Koros, W. J. *J. Molec. Struc*. **2005**, *739*, 87.

[25] Tsagaropoulos, G.; Kim, J. S.; Eisenberg, A. *Macromolecules* **1996**, *29*, 2222.

[26] Mahajan, R.; Koros, W. J. *Ind. Eng. Chem. Res*. **2000**, *39*, 2692.

CHAPTER 9
CONCLUSIONS AND RECOMMENDATIONS

9.1 SUMMARY AND CONCLUSIONS

Mixed matrix membranes that comprise domains of organic and inorganic components were developed to effectively surpass the polymeric 'upper bound trade-off' curve'. The validity of mixed matrix concept was demonstrated by previous investigators, yet a few non-ideal morphologies that undesirably affect membrane properties were discovered. Among these non-idealities, lack of intrinsic compatibility between the organic polymers and inorganic fillers is most detrimental to membrane performances and thus poses the biggest challenge to be overcome in order to fabricate successful composite membranes. Essentially, control of the nanoscale interface between the sieve and polymer in a composite membrane represents the key technical hurdle in transitioning from a lab-scale to a large manufacturing scale. Therefore the overarching goal of this research is to devise and explore approaches to enhance the performance of mixed matrix membranes by properly tailoring the sub-optimal interface. This work achieved a number of major advancements toward the objective, each of which is listed below and then discussed in more detail in the following paragraphs.

1. Developed and investigated three different approaches to promote interfacial adhesion between polymers and inserts in composite membranes. A comparison was drawn to evaluate these methods and the most effective strategy (Grignard treatment) was selected and further inspected.
2. Successfully formulated and characterized mixed matrix membranes comprising zeolites modified via the Grignard treatment. Achieved membranes with excellent

gas separation efficiency and mechanical properties. Proposed and exploited the basis of the improvements in polymer/sieve compatibility enabled by this specific process.

3. Examined and illuminated the detailed chemical mechanisms involved in the complex Grignard treatment through systematic characterization and carefully designed experiments.
4. Discovered and identified the effect of sonication on the dealumination of zeolites, which can potentially be applied to prepare zeolites with a variety of Si/Al ratios.
5. Created a technique to generalize the highly specific Grignard treatment to inorganic materials other than zeolite 4A and achieved membranes with improved interfacial adhesion.
6. Revealed the effect of surface nuclei density on the ultimate morphology of deposited nanostructures and how different surface morphologies influence polymer/filler interaction in composite membranes. Devised methods to tailor the morphologies of such structures to deliver better adhesion enhancement.

The understanding of various non-ideal morphologies and how they affect the transport properties of mixed matrix membranes is well established by previous researchers at the onset of the present work. Innovative ideas were proposed to solve these problems in order to improve the membrane performance. Nonetheless, the lack of inherent compatibility between polymers and fillers remains the key challenge to the successful formation of composite membranes. Chapter 4 summarizes the efforts made in

this work towards promoting the interfacial affinity in a composite membrane. Three different surface modification methods were investigated. It was found that the use of silane coupling agents improved the interfacial adhesion but induced pore blockage which limits the selectivity enhancement in mixed matrix membranes. Hydrophobizing via alcohols did not deliver satisfactory results in promoting membrane performances. The most recently developed Grignard treatment was shown to most effectively improve the interfacial adhesion and resulted in membranes with desirable properties even at 40wt% of sieve loading. Therefore this specific modification approach was selected as the focus of this research.

The investigation of mixed matrix membranes comprising zeolite 4A as the dispersed phase is described in Chapter 5. Detailed characterization including SEM, DMA and permeation tests indicate that the Grignard modified zeolites yielded defect-free membranes with impressive improvements in gas permselectivity and mechanical properties. The most distinctive feature of the modified sieves is that they have a significantly roughened outer surface that resembles 'whiskers' as compared to the smooth surface of untreated counterparts. The dramatic increase in topological roughness is proposed to provide improved interaction at the interface via induced adsorption and physical interlocking of polymer chains via multiple contact points in the nanoscale inorganic whisker structure. XPS and TGA study of polymer's adsorption on neat vs. modified sieves generated quantitative measures which support the above hypothesis. It is anticipated that this strategy has potential to be applied to a broader domain of composite materials where tailoring polymer-filler interface is important.

In order to fully understand the highly specific and complex Grignard treatment, substantial efforts were made towards revealing the underlying chemical mechanism involved in this process. A variety of characterization techniques were employed to illuminate the structural and elemental changes in sieves concurring with each reaction. It was discovered that thionyl chloride partially removes aluminum from the zeolite 4A framework and yields NaCl and $AlCl_3$. Precipitation of these extracted inorganic salts on the surfaces of zeolite particles occur. Subsequently, methyl magnesium bromide is reacted with 2-propanol in a quenching process that generates $Mg(OH)_2$. The previously deposited NaCl and $AlCl_3$ nano-particles on zeolite surfaces are believed to function as heterogeneous nuclei for the growth of $Mg(OH)_2$ crystals which thereby create the nano-structured surface morphology.

An interesting discovery was made along with the work described in the previous paragraph, which is related to the unusual dealumination of zeolite 4A near room temperature. Systematic inspection revealed that sonication induces dealumination under ambient conditions, contrary to the literature reports where similar reactions took place at much elevated temperatures. It was also found that the degree of dealumination could be adjusted by the duration of sonication to generate zeolites with various Si/Al ratios. The dramatic local heating by ultrasound was proposed to explain this abnormal phenomenon. This new procedure allows convenient preparation of alumina-deficient zeolites of a wide range of Si/Al ratios under ambient conditions.

Based on the understanding of the Grignard treatment, which is essentially a heterogeneous nucleation process, Chapter 8 presents work to explore the possibility of extending this highly specific method to inorganic materials other than zeolite 4A, hence

making it a more general strategy for surface modification. Silica was selected and investigated as another filler to represent the other end of aluminosilicate material spectrum. Surface 'seeding' via intentionally depositing nuclei on particle surface from an external source was devised to create similar morphology on silica surface. It was demonstrated that by properly tailoring the seeding process, the ultimate morphology of the surface structure can be modified. Furthermore, sieves with finer surface morphology resulted in stronger adsorption of polymers at the interface and generated better membranes than those with mild surface roughness. Thereby it is desirable to achieve 'needle' or 'whisker' shaped structures on the modified particle surfaces in order to stabilize the attachment of polymer segments at interface in membrane materials.

9.2 RECOMMENDATIONS FOR FUTURE WORK

The current work demonstrated great potential of a new surface modification strategy. Creation of nanostructures on the particle surface is envisioned to be able to apply to many other composite materials to tailor the sub-optimal interfaces. A few recommendations for future work are made and discussed below.

9.2.1 Exploration of Surface Seeding with a Variety of Zeolites

Work addressed in Chapter 8 explored the feasibility of extending the Grignard reagent to inorganic materials other than zeolite 4A (Si/Al=1). Preliminary results showed the viability of creation and tailoring of similar inorganic structures on silica (Si/Al=∞) surfaces. Silica with significantly roughened outer surface formed desirable interfacial contact with polymer matrix. Therefore, this technique is applicable to materials at the two ends of aluminum-silicate spectrum. Future efforts could extend this

technique to zeolites of a wide variety of Si/Al ratios, thus rendering it a general strategy for surface modification.

The idea of 'surface seeding' was inspired by study of Grignard treatment with zeolite 4A, yet it has not been directly applied to this particular zeolite. One could simply 'seed' the surface of zeolite 4A using NaCl solution, followed by exposing the particles to methyl magnesium bromide and 2-propanol, to avoid the preceding reaction of zeolites with thionyl chloride. It is expected that roughened surface morphology will appear after such an operation. Nonetheless, substantial difference exists between the nuclei (NaCl and $AlCl_3$) yielded by dealumination reaction and those deposited from an external source (NaCl solution). The inorganics extracted by thionyl chloride are very fine, nanoscale particles homogeneously distributed on zeolite 4A surface; while precipitation of NaCl from an aqueous solution tends to generate large, cubic shaped salts. This discrepancy in size and coverage of nuclei is likely to produce different morphologies of $Mg(OH)_2$ crystals eventually observed on the surface. Therefore, optimization of the salt seeding process is necessary to formulate 'needle' shaped structures, which have been proven to most effectively stabilize polymer chains at a solid surface. Use of lower temperature precipitation or addition of surfactants could be employed to approach this matter.

Another possible avenue to exploit with surface seeding is to use $AlCl_3$ solution rather than NaCl solution as the nuclei source. There have been arguments about the surface inorganic structure being a magnesium-aluminum complex because aluminum can potentially be incorporated into magnesium oxides to form new crystal complexes. This possibility was ruled out in the current study because the XPS detected considerably

larger concentration of NaCl than $AlCl_3$ after dealumination reaction. Nevertheless, it is probable that by seeding with $AlCl_3$, crystals of other morphologies will be obtained because magnesium-aluminum complex has different crystalline shapes from $Mg(OH)_2$. It is even possible to prepare a solution composed of NaCl and $AlCl_3$ mixture, the ratio of which is in accordance with the XPS results of dealuminated 4A. This seeding solution would be closest to the chemical environment after the dealumination reaction.

After careful understanding and control of the seeding technique, the Grignard treatment could be applied to other zeolites such as SSZ-13, CVX-7, ZSM-5, etc of different Si/Al ratios. Once the surface pattern is achieved, the sieves can be incorporated into various polymer matrices (Ultem®, Matrimid®, Torlon®, 6FDA based polymers) to create a broad domain of composite membranes for various separation implementations.

It is believed by the author that $Mg(OH)_2$ is not the sole candidate to formulate surface nanostructures. The chemical process used in this work generated this specific substance and its precipitation led to roughened surface morphology. In fact, different chemical processes can be devised to create and deposit materials that can form certain patterns, such as various oxides. The ultimate goal is to extend the essential concept derived from this study and make this strategy a really generalized method.

9.2.2 Combination of Silanation with Grignard Treatment

The utilization of silane coupling agents was shown in Chapter 4 to improve the affinity between polymers and inorganic fillers. Despite the fact that the treatment procedure may lead to pore blockage, this approach still has its merits and is worth further investigation. It is proposed that the sieves after the Grignard treatments could undergo a second modification by reacting with silane coupling agents. The hydroxyls

provided by $Mg(OH)_2$ surface structures can presumably react with silanes and form covalent linkages. This procedure could create 'double' interlocks between fillers and polymers: physical interlocking via the whisker structure and chemical bonding via the coupling agents. It is anticipated that greater improvements would be achieved through the dual treatments. This effect can be particularly pronounced in occasions where favorable interaction between $Mg(OH)_2$ and polymer matrix is absent; the presence of silanes on the other hand can compensate for the lack of intrinsic compatibility and ensure good contact.

A simple way to proceed with this hypothesis is to study the reaction of pure $Mg(OH)_2$ crystals with silane coupling agents. By careful characterization of the treated crystals, it is feasible to reveal the coverage of silane linkages on $Mg(OH)_2$ surface. These results could be used to guide later investigation with Grignard and silane 'double-treated' treated sieves.

Another issue that will possibly be encountered with regard to silane treatment is the selection of an appropriate solvent for dispersion of sieves and the couple agent. It was shown that sonication may have driven iso-propanol into zeolite pores and result in partially or completely 'clogged' zeolites with reduced or diminished selectivity. In order to prevent this undesirable phenomenon, it is recommended that alcohols of small molecular dimensions be used in future inspections, such as methanol and ethanol.

9.2.3 Differentiation of Entropic versus Enthalpic Effect Enabled by Grignard Treatment

A constant topic regarding the improvements resulted from Grignard treatment is whether the modified surface improves the entropic interactions between polymer and fillers or it functions via entropically inducing polymers' adsorption into random

configurations. The presented work by utilization of XPS and TGA to examine polymer's adsorption on various surfaces shed lights on this point. These measurements detected macroscopic properties, yet a more microsopic study is necessary to fully understand and control this process from a fundamental viewpoint.

AFM can be used to illuminate the intrinsic interaction (ΔH) between polymers and $Mg(OH)_2$ or polymers and zeolites. A simple approach would be to functionalize the AFM tip by doping the polymer onto the tip, followed by adhesion force measurements with an appropriate substrate. In this case, the substrate could be a $Mg(OH)_2$ or zeolite crystal. To avoid the interference of packing disorder and variance in surface roughness caused by multiple particles, it is ideal to use a single crystal with smooth surface for AFM study. The adhesion force obtained between polymer and zeolites will serve as a baseline. If the detected adhesion force between polymer and $Mg(OH)_2$ is much stronger than the inherent polymer-zeolite affinity, the enthalpic interaction plays a crucial role in promoting the confinement of polymers onto $Mg(OH)_2$ features. On the other hand, if the interaction between polymer and $Mg(OH)_2$ is close to or even less attractive than the intrinsic polymer-zeolite adhesion, ΔH is unlikely to account for the majority of improvements enabled by the inorganic whisker structures. The most likely scenario is that the combination of enthalpic and entropic effects offered the enhancements observed here If a material which has strong inherent adhesion with the polymer can be deposited via the formation of nanoscale surface structures, it will most efficiently promote the filler-polymer interaction.

The aforementioned AFM study will provide insightful findings to differentiate the significance of enthalpy versus entropy in Grignard treatment. It will also be interested to

look into sieves treated via silane coupling agents or dual treatments (Grignard plus silane) to illuminate the effect of silane linkages and surface roughness.

9.2.4 Effect of Annealing Temperature on Composite Membrane Formation

Preliminary work with PVAc presented in Chapter 4 laid the ground for examining the effect of annealing temperature on membrane formation. Contact angle measurement was shown to be an effective way of detecting polymer's interaction with an inorganic surface. Limited work was done in the current research to explore this matter. However, it is an interesting and important factor in determining the success of formulating a good membrane material.

Future research could apply the same principles illustrated in Chapter 4 to seek an optimal annealing condition for a certain composite membrane. By measuring the contact angle of a polymer with a glass substrate which serves as a surrogate for the zeolite surface, it is viable to reveal the interaction of polymer with an inorganic surface under various temperatures. Generally, beyond the melting point of a polymer, the contact angle starts to drop as temperature increases and ultimately reaches equilibrium. Nonetheless, TGA tests are necessary to determine the proper range of temperatures when polymers are stable. A variety of polymeric materials used to form mixed matrix membrane such as Ultem®, Matrimid®, Torlon® and 6FDA based polymers could be potential candidates for this study.

9.2.5 Miscellaneous Points

(1) Formation of Matrimid® mixed matrix membranes containing surface modified zeolites. Matrimid® has more attractive gas separation properties than Ultem® because it yields much higher flux with only small reduction in selectivity. Nonetheless, this

material is very challenging to form successful mixed matrix membranes due to its extremely rigid chains and lack of favorable interaction with zeolite surfaces. The new Grignard treatment has potential to generate desirable interface with this polymer. A potential challenge will be proper annealing of the membranes due to the high T_g of this polymer (305ºC).

(2) Mixed gas permeation tests of composite membranes. Current work focuses on using pure gas permeation to reveal the ideal selectivity of membranes. It is expected that mixed gas measurements will yield even higher selectivity for O_2/N_2 and CO_2/CH_4 due to the competitive transport phenomenon.

(3) Continuing study of mechanical properties of composite membranes. Work described in Chapter 5 demonstrated that DMA is a very useful technique in examining the elastic moduli of composite membranes. The obtained data can be employed to reveal the corresponding morphologies present at the interface. Future study could extend this methodology to hybrid films and hollow fibers bearing various filler loadings.

(4) Extending sieve surface modification to high zeolite loading membranes. The importance of interface in high zeolite loading membranes leaves no doubt. Current work generated 'partially' defective membranes at 40wt% of 4A in Ultem®. In order to create successful composite membranes at even higher solid content, sieve surface modification is a key step towards this goal. The combination of Grignard treatment and silanation may be promising to deliver double enhancement and hence ensure defect-free interfaces at such high sieve loadings.

(5) Exploration of Polymer-Sieve Interface via AFM. Aside from measuring the interaction between polymer and sieve, AFM can be utilized to probe the interfacial

regions between polymer and fillers in a composite membrane. The size of interface and degrees of chain rigidification will be especially interesting to examine. Precise determination of these two parameters will allow fundamental understanding of 'matrix rigidification' morphology and enable tailoring the Maxwell model to better predict membrane performance. A few more aspects worth inspection include how the particle size affects the size of interface and how the interface evolves with increasing sieve concentration in a membrane (possible overlapping at high loadings).

APPENDIX A FUNDAMENTALS OF ^{29}Si and ^{27}Al SOLID STATE NMR OF ZEOLITES

A.1 ^{29}SI SOLID-STATE NMR

The first ^{29}Si NMR spectrum of a soldium silicate was published in 1973[1], followed by a series of papers on this topic[2-4]. These studies clearly demonstrated that ^{29}Si NMR may contribute greatly to the knowledge of the complex nature of silicates owning to two fundamental features of the spectra: (i) characteristic and mostly well separated signals for the SiO_4 groups in different structural surroundings may be observed in the ^{29}Si NMR spectra; and (ii) from the signal intensities the relative concentrations of the different structural entities can be estimated. Therefore, detailed formation on the structure and the quantitative distribution of the various building groups and silicate species may be obtained from the ^{29}Si NMR spectra.

For the presentation of the structure of building units or silicate anions in the following the commonly used Q^n notation is adopted. In this notation, Q represents a silicon atom bonded to four oxygen atoms forming a tetrahedron. The superscript *n* indicates the connectivity, i.e. the number of other Q units attached to the SiO4 tetrahedron under study. Thus, Q^0 demotes the monomeric orthosilicate anion SiO_4^{4-}, Q^1 end-groups of chains, Q^2 middle groups in chains or cycles, Q^3 chain branching sites and Q^4 three dimensionally cross-linked groups. The degree of protonation is ignored in this description. A subscript denotes the number of equal Q^n units in the silicate species in question. For aluminosilicates the number of AlO_4 tetrahedra bound to the central silicon of a Q^n unit is given in parentheses, e.g. Q^n(mAl) means an SiO_4 group connected via

oxygen bridges to m Al and $n - m$ other Si atoms, where $n = 0 - 4$ and $m < n$. A schematic representation and some examples of the Q notation are shown in Figure A.1.

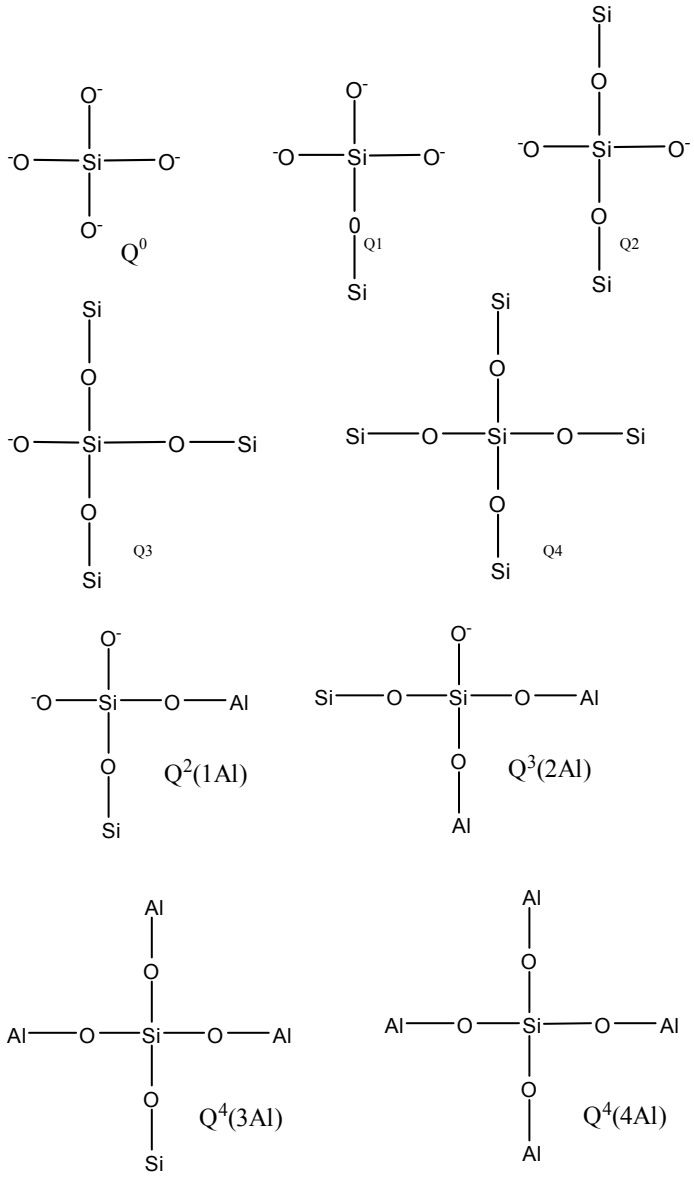

Figure A.1 Notation for building units and silicate anions. Top, Q^n units of silicates; bottom, examples of Q^n(mAl) units of aluminosilicates, adapted from reference 5.

A.2 ^{27}AL SOLID-STATE NMR

The clear distinction between four- and sixfold coordinated aluminum in AlO_4 and AlO_6 units is of considerable interest in structural studies of aluminosilicates, since both

units are present, e.g., in various types of layer silicates, and six-fold coordinated non-framwork aluminuium-oxygen compounds may occur besides AlO_4 after the thermal treatment of framework aluminosilicates, especially zeolites. ^{27}Al NMR is capable of unambiguously and , in general, quantitatively distinguishing between tetradedrally and octahedrally coordinated aluminium by clearly separated shift ranges of about +50 to +80 ppm for AlO4 and about -10 to +20 ppm for AlO_6. A typical ^{27}Al MAS NMR spectrum of an aluminosilicate (layer silicate margarite) containing both four- and sixfold coordinated Al is given in Figure A.2.

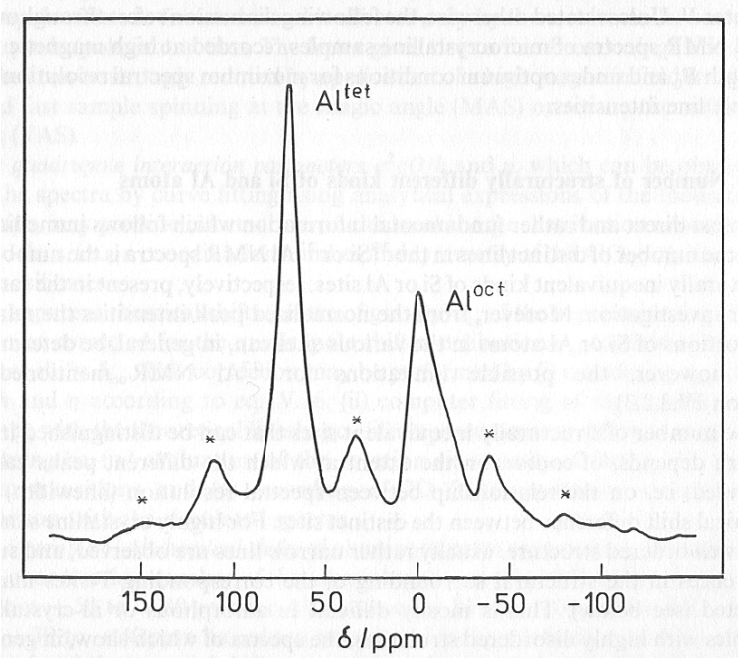

Figure A.2 ^{27}Al NMR spectrum of the layer aluminosilicate margarite. Altet and Aloct denote detrahedrally and octahedrally coordinated aluminium, respectively. Spinning side bands are marked by asterisks. Adapted from Reference 5.

REFERENCES

[1] Smith, K. A.; Kirkpatrick, J.; Oldfield, E.; Henderson, D. M. *Am. Mineral*. **1983**, *68,* 1206.

[2] Janes, N.; Oldfield, E. *J. Am. Chem. Sco*., **1985**, *107*, 6769.

[3] Grimmer, A. R.; Lampe, F. V.; Magi, M. Lippmaa, E. *Z. Chem*. **1983**, *23*, 344.

[4] Clayden, N. J.; Dobson, C. M.; Hayes, C. J.; Rodger, S. A. *J. Chem. Soc., Chem. Commun*. **1984**, 1396.

[5] Engelhardt, G.; Michel, D. *High-Resolution Solid-Stte NMR of Silicates and Zeolites*; John Wiley & Sons: New York, 1987.

APPENDIX B MIXED MATRIX MEMBRANES with NANOSIZED ZEOLITE 4A

B.1 MIXED MATRIX MEMBRANES COMPRISING NANOSIZED 4A

As shown earlier in Figure 5.1, a 'cotton ball' like morphology was observed with 100nm zeolite 4A after subjected to the 2-step Grignard treatment. Composite films comprising such modified sieves were produced and characterized.

Figure B.1 depicts the permeation results of PVAc composite films constituting neat vs. Grignard treated zeolite 4A. Although the larger version of 5μm zeolite 4A can form good mixed matrix material with PVAc matrix due to high chain flexibility and favorable interaction, the PVAc films containing neat 100nm 4A exhibited poor transport properties. At both 15wt% and 30wt% zeolite loading, the composites had much higher permeabilities than pure polymer accompanied by equal or even worse selectivities. The deterioration is due to the agglomerates present in such films. Submicron particles are known to aggregate severely without surface modification and the finer the particles are, the faster the rate of agglomeration is.[1] Pristine 100nm sieves were difficult to disperse in the solvent when preparing mixed matrix solution even with the assistance of a sonicator. The resulted composite films contain large particles even visible to naked eyes. Such aggregates can cause pinholes or channels in membranes which are highly detrimental to transport properties. On the other hand, PVAc comprising Grignard treated 100nm 4A generated completely different properties. The treated sieves were able to be dispersed in solution excellently without apparent aggregates. The increased stability is due to the higher surface potential as addressed in Chapter 6. The flux of these films was even lower than the Maxwell model inferring the absence of voids from these films. Nevertheless,

only slight increase in selectivity was observed despite the good adhesion at the interface at both 15 wt% and 30 wt% sieve loading. Similar tendency was found in Ultem® composite films embedded with fresh and Grignard treated 100nm 4A, as displayed in Table B.1. Increased permeability and poor selectivity were obtained with pristine zeolites while reduced permeability and slightly enhanced selectivity occurred with the Grignard modified counterparts. Given the fact that voids do not exit in the membranes, the deviation from the theoretical prediction is most likely resulted from the intrinsic properties of zeolites. Efforts made towards elucidating this information will be summarized in the subsequent section.

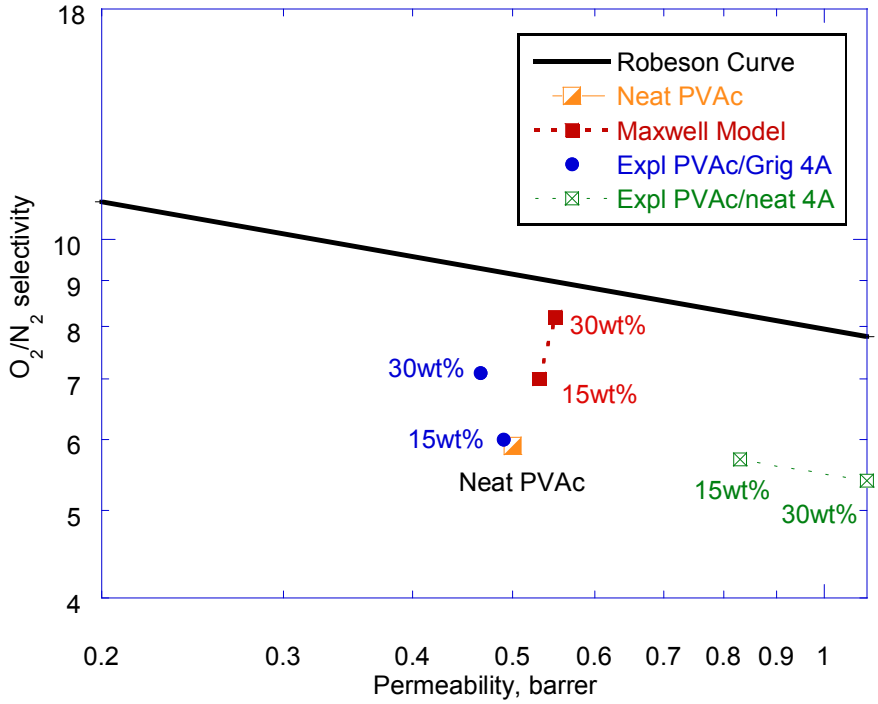

Figure B.1 O_2/N_2 transport properties of PVAc mixed matrix membranes containing unmodified and Grignard treated 100nm zeolite 4A at 15wt% and 30wt% solid concentrations. (tested at 35ºC and upstream pressure of 65 psia)

Table B.1 O_2/N_2 transport properties of Ultem® mixed matrix membranes containing unmodified and Grignard treated 100nm zeolite 4A at 15wt% filler content (tested at 35ºC and upstream pressure of 65 psia).

Membrane	O_2 Permeability Barrer	O_2/N_2 Selectivity	CO_2 Permeability Barrer	CO_2/CH_4 Selectivity
Neat Ultem	0.4	7.5	1.4	38
Maxwell Model	0.44	9.1	1.83	48.7
Expl 15wt% neat 4A	0.51	7.6	2.37	35
Expl 15wt% Grignard 4A	0.43	8.0	1.25	40.9

B.2 CHARACTERIZATION OF NANOSIZED ZEOLITE 4A

The separation performance described in the preceding section pointed that the intrinsic properties of this batch of submicron sieves may be different from the literature values. In an effort to explore the possible changes, a few techniques including XRD and N_2 physisorption were used to characterize the sieves.

The first hypothesis is that the Grignard treatment might have damaged the crystallinity of 4A thus leading to deteriorated selectivity. This phenomenon was not observed with 5 μm larger particles as shown in Chapter 5 but the much finer sieves may be more vulnerable to the dealumination by thionyl chloride. XRD was employed to examine the crystallinity of the treated sieves and the diffraction patterns were depicted in Figure B.2. Negligible changes were discovered according to the spectra, suggesting that the framework structure of zeolites was not damaged by the reagents under the conditions used in the treatment. Therefore loss of zeolite crystallinity is not the cause of poor separation properties.

Another possibility inspected is the presence of mesopores in zeolites. It was proposed by Hillock that the mesopores existing inside a zeolite crystal can significantly alter the transport behavior of gas molecules.[2] If the mesopores form a channel that traverses the interior of a zeolite particle, they allow gas molecules to directly bypass through such a path instead of transporting in the micropores. On the other hand, if the mesopores are all enclosed inside the crystal, they only increase the rate of transport without hurting the selective ability. In practice, both the two types of mesopores can form during the synthesize process and thus be present in same batch of zeolites. This assumption could be employed herein to tentatively explain the unexpected gas transport properties observed in Figure B.1. The most likely scenario is that this batch of submicron 4A contains both types of mesopores, which considerably change the intrinsic selectivity of such material. N_2 physisorption was utilized to probe this possibility and the results are illustrated in Figure B.3. In addition to the microporous domain less than 5Å, there is another big distribution of pores in the range of 20nm to 30nm as shown on the plot. It is, however, unable to tell from N_2 adsorption experiment whether these pores are enclosed or traverse, or the ratio of the two couterparts. Nevertheless, it illustrates that there are intrinsic defects within the zeolite material used in this work, whose transport properties are most likely altered as compared to the literature values of perfect crystals.

Based on the above findings, it was decided not to further pursue study of this batch of submicron zeolites due to its intrinsically defective nature.

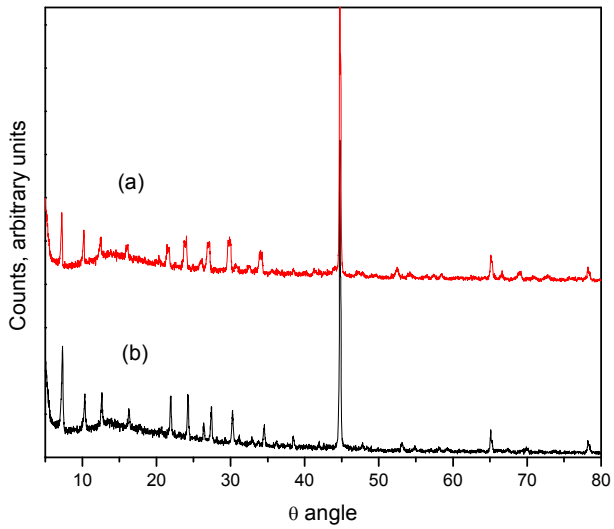

Figure B.2 XRD diffraction patterns of zeolite 4A samples: (a) neat 4A; (b) Grignard treated 4A.

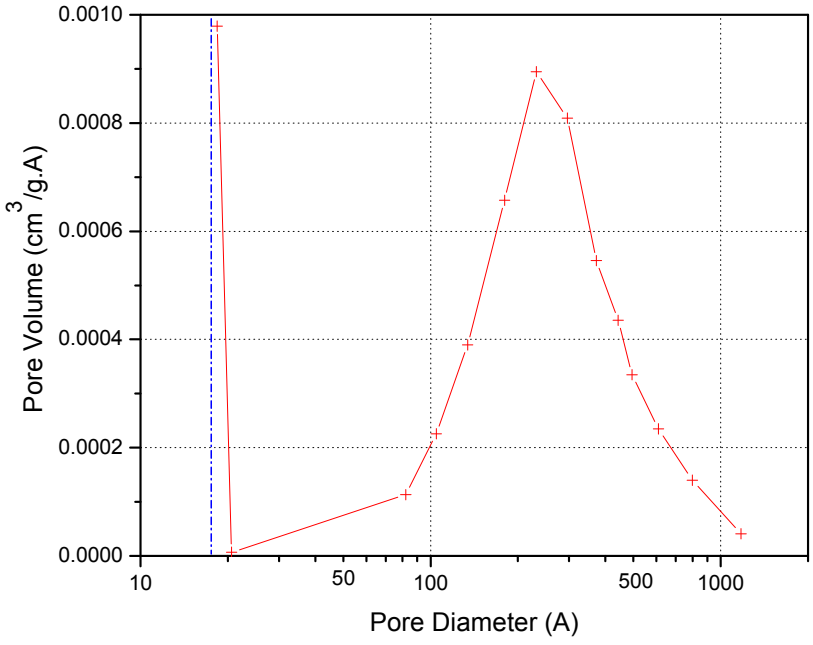

Figure B.3 BJH desorption curve dV/dD pore volume, measured on submicron zeolite 4A.

REFERENCES

[1] Hunter, R. J. *Foudations of Colloid Science*; Clarendon Press: Oxford, 1991.

[2] Hillock, A. M. W. *Crosslinkable Mixed Matrix Membranes for Natural Gas Purification*, Ph.D thesis: Georgia Institute of Technology, 2005.

APPENDIX C INVESTIGATION OF ZETA-POTENTIAL MEASUREMENTS FOR ZEOLITES

C.1 INTRODUCTION OF DOUBLE LAYER THEORY AND ZETA-POTENTIAL

The charge which develops at the interface between a colloidal particle and the liquid medium in which it is suspended may arise by any of several mechanisms. Among these are the dissociation of ionogenic groups on the particle surface and the differential adsorption from solution of ions of different charges into the surface region. The development of a net charge at the particle surface affects the distribution of ions in the adjacent interfacial region, resulting in an increased concentration of counterions - ions of charge opposite to that of the particle - close to the surface. Thus an electrical double layer is formed in the region of the particle-liquid interface.

The double layer (Figure C.1) may be considered to consist of two parts: an inner region which includes ions bound relatively strongly to the surface (including specifically adsorbed ions) and an outer, or diffuse, region in which the ion distribution is determined by a balance of electrostatic forces and random thermal motion. The potential in this region, therefore, decays as the distance from the surface increases until, at sufficient distance, it reaches the bulk solution value, conventionally taken to be zero.

When subjected to an electric field as in microelectrophoresis, each particle and its most closely associated ions move through the solution as a unit and the potential at the boundary between this unit i.e. at the surface of shear between the particle with its ion atmosphere and the surrounding medium, is known as the zeta potential ζ.[1]When a layer of macromolecules, whether a polyelectrolyte or an uncharged polymer, is adsorbed on the surface of the particle, this can alter the zeta potential simply because it shifts the

location of the shear plane further from the actual surface. Zeta potential is therefore a function of the surface charge of the particle, any adsorbed layer at the interface and the nature and composition of the surrounding medium in which the particle is suspended. It is usually, but not necessarily, of the same sign as the potential actually at the particle surface but, unlike the surface potential, the zeta potential is readily accessible by experiment. Moreover, because it reflects the **effective** charge on the particles and is therefore related to the electrostatic repulsion between them, zeta potential has proven to be extremely relevant to the practical study and control of colloidal stability and flocculation processes. Figure C.1 illustrates the distribution of ions near a solid surface and

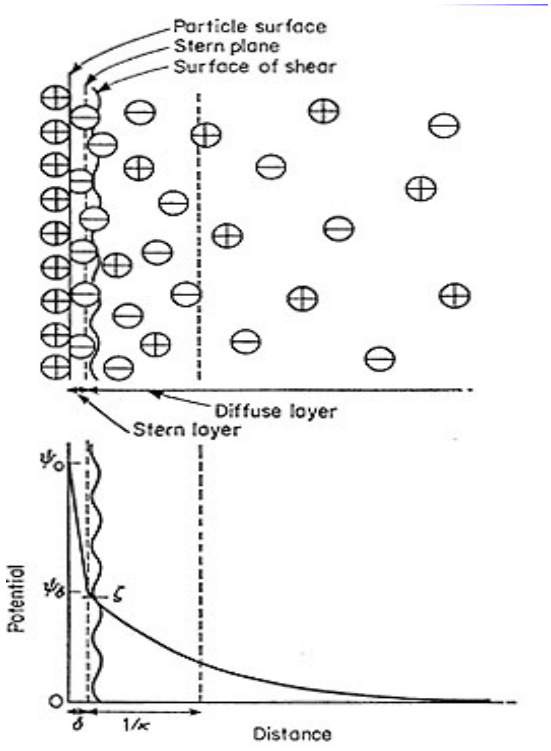

Figure C.1 Illustration of the double layers around a solid particle dispersing in a liquid. Adapted from reference 2.

C.2 EFFECT OF ORGANIC SOLVENT ON ZETA POTENTIAL

In the previous section, it was found that the zeta potential of unmodified zeolite 4A in NMP is -30mV. Nonetheless, it is a common practice in literature to report the zeta potential of oxides in aqueous solutions.[3,4] Figure C.2 illustrates how the pH of a solution can render the zeolite surface either positively or negatively charged. To our knowledge, very few resources can be found that deals with the zeta potential of zeolites in organic solvents. In an effort to explain the reason for negative surface charge of 4A in NMP, a mechanism is proposed in Figure C.3.

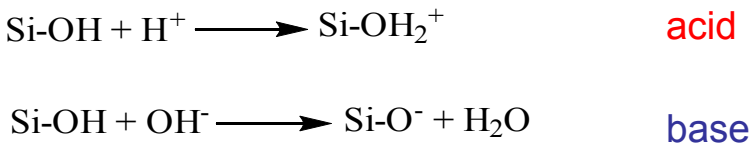

Figure C.2 The surface charges on silicate surface in different pH environment.

The carbonyl group in NMP is polarized where the oxygen atom is practically negative due to the higher polarization potential than the carbon atom. Therefore, the oxygen becomes an electron acceptor and readily attracts the hydrogen from the surface silanols of zeolites by formation of hydrogen bonds. The disassociation of silanols leave the zeolite surface negatively charged. This phenomenon is similar to the aqueous case where a basic solution delivers negative zeolite surface charge by taking the hydrogen.

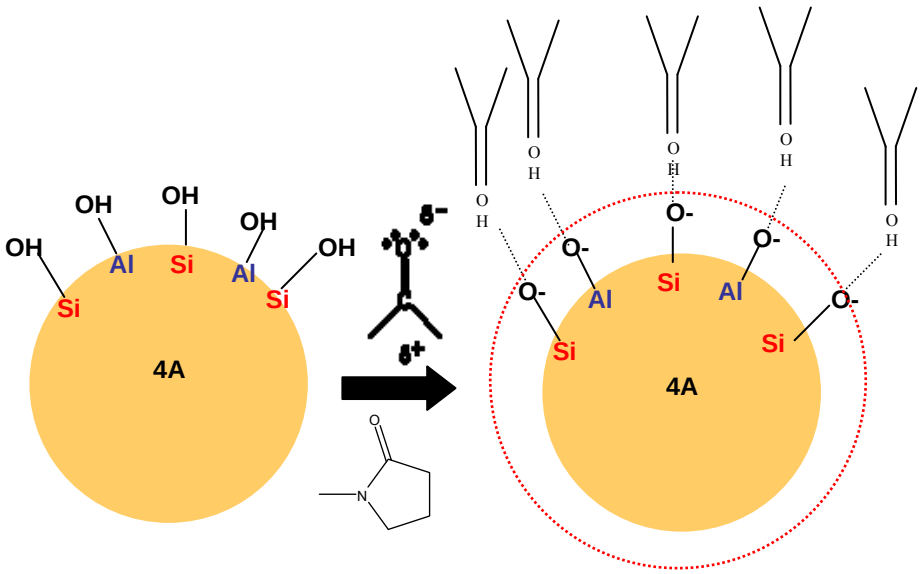

Figure C.3 Proposed mechanism of zeolite 4A surface charging in NMP.

According to the aforementioned hypothesis, zeta potential of zeolites should vary with the electronegativity of the polar groups in solvents. The more electronegative a group is, the higher surface potential is anticipated. To check this assumption a series of organic solvent were employed as the liquid phase and zeta potential of zeolite 4A was obtained in each of these solvents. Table C.1 displays the list of solvent inspected and the corresponding experimental results. Chloroform which bears three very electronegative atom Cl generated the highest absolute value of zeta potential, indicating largest amount of surface charges. The value decreases as the electronegativity of the polarized group in a solvent weakens, as demonstrated by NMP and THF. Moreover, no surface potential was detected with toluene or hexane, both of which do not contain any polarized functional groups in their structures. The tendency illustrated by these data provides strong proof to the mechanism proposed in the previous section. It could be helpful when choosing an appropriate solvent to disperse zeolites.

Table C.1 Zeta potential measurement results of zeolite 4A in various organic solvents.

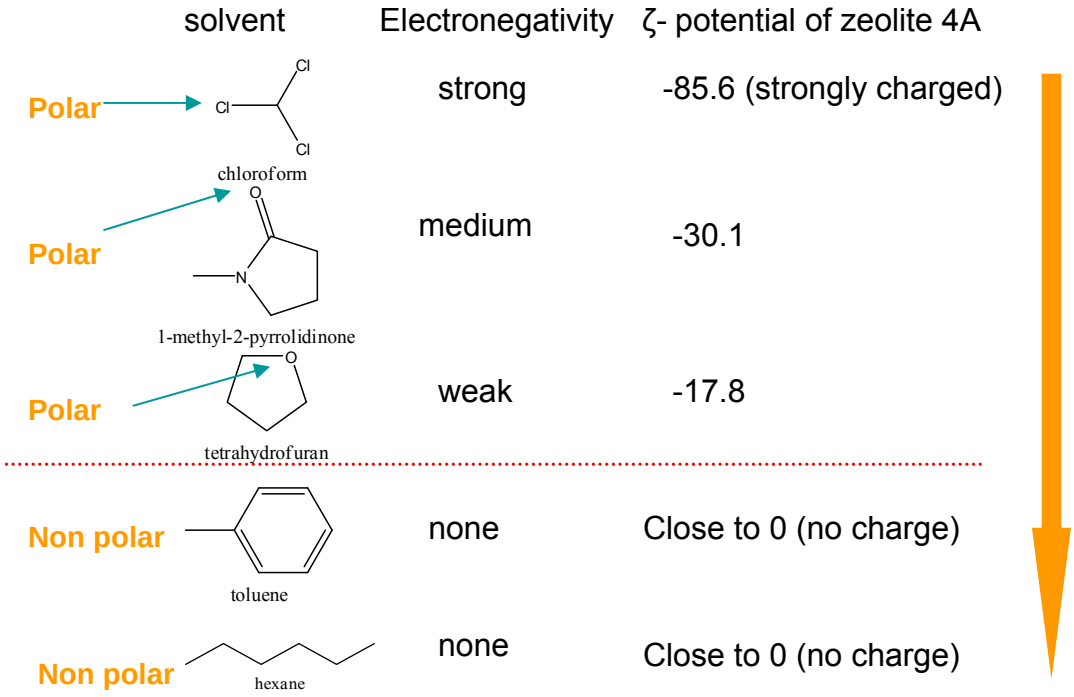

It is noteworthy that zeta potential is subjected to change upon the addition of polymer in the solution. This situation is the 'actual' environment in a mixed matrix dope or casting solution. Future work could extend this study to mixed matrix solutions to characterize the stability of particles and how macromolecules affect the surface potentials of particles in solutions.

REFERENCES

[1] Hunter, R.J., *Foundations of Colloid Science, Vol. 1*. 1986.

[2] Piirma, I., *Polymeric Surfactants*. *Surfactant Science Series*. *Vol. 42*; Marcel Dekker: New York, 1992.

[3] Beattie, J. K.; Djerdjev, A. M.; Gibb, S. E. *New Journal of Chemistry* **2003**, *27*, 1433.

[4] Kremer, S. P. B.; Kirschhock, C. E. A.; Rouxhet, P. G.; Jacobs, P. A.; Martens, J. A. *Studies in Surface Science and Catalysis* **2001**, *135*, 159.

APPENDIX D STUDY OF GRIGNARD TREATMENT ON NANOSIZED POROUS SILICA

As introduced earlier, the original purpose of the Grignard treatment was to methylate zeolite surface and thereby rendering it hydrophobic. The idea was inspired by reported work in which Bansal et al created direct Si-C bonds with mesoporous silica materials.[1-3] The primary inorganic silicate inspected in the present work is zeolite 4A. And it was found that no such Si-C bonds were formed after the same reactions. The detailed chemical mechanisms in this case were elaborated in Chapter 6. Nonetheless, in order to replicate the observations made by Bansal, a batch of nanosized mesoporous silica (Aldrich, product number 54,103-6) was studied and the results will be discussed below. Two treatment protocols were applied to this type of silica: (i) the standard 2-step protocol developed in this work; (ii) sample only exposed to the Grignard reagent. The latter operation is a control step to test the hypothesis whether Grignard reagent can directly react with mesoporous silica surfaces.

Figure D.1 and D.2 illustrates the ^{13}C and ^{29}Si solid state NMR spectra for various modified forms of silica, respectively. As indicated by Figure D.1, methyl groups were detected in both the modified silica samples, regardless of the treatment procedures. ^{29}Si NMR revealed more insightful information with regard to the forms of carbon in these two samples. After the first reaction of thionyl chloride, there is no change observed in silica structure. The resonance peaks at -93.6ppm and -102ppm in Figure D.2a reflect the intrinsic framework of this batch of silica, the structure of which is shown in Figure D.3.[5] It was initially hypothesized that Si-Cl peak would be seen here. However, the Cl atom is very sensitive to moisture and it might have associated with water in the air and produced

HCl, thus breaking the Si-Cl bond. This could tentatively explain the absence of Si-Cl peak after thionyl chloride reaction. After the 2-step sequence, the peak shifted to around -60ppm and doublets appeared in the spectrum Figure D.2b (located at -53 ppm and -61 ppm respectively). This region covers the typical chemical shifts for Si-C bonds. The presence of doublets is believed to be attributed to the carbon connected to the two types of framework silica as indicated in Figure D.3. This discovery suggests that direct Si-C bonds were formed after 2-step treatment developed in this work, consistent with Bansal's work.[1-3] Moreover, it is interesting to find Si-C bond in the silica sample modified only by the Grignard reagent (Figure D.2c), which implies it is able to directly react with silica silanols. Kim et al discovered similar effect with porous silicates.[4]

In addition to the aforementioned porous silica, non-porous silica (3μm) which was investigated in Chapter 8 was examined using the same methodology described above. Nonetheless, no carbon peak was obtained in ^{13}C NMR measurement, only substantial noise was present. Furthermore, no chemical shifts occurred after the Grignard treatment, relative to the inherent structure of silica as shown in Figure D.4. This finding obviously implies the absence of Si-C bonds in such treated sample. It is unclear yet why Grignard reagent was unable to perform the same reaction with non-porous silica as opposed to the porous counterparts. It is probable that the amorphous and crystalline structures result in considerable difference in the reactivity of surface silanols; and the much larger surface area offered by nanosized, porous silica certainly provides more articulated changes when subjected to any chemical treatment.

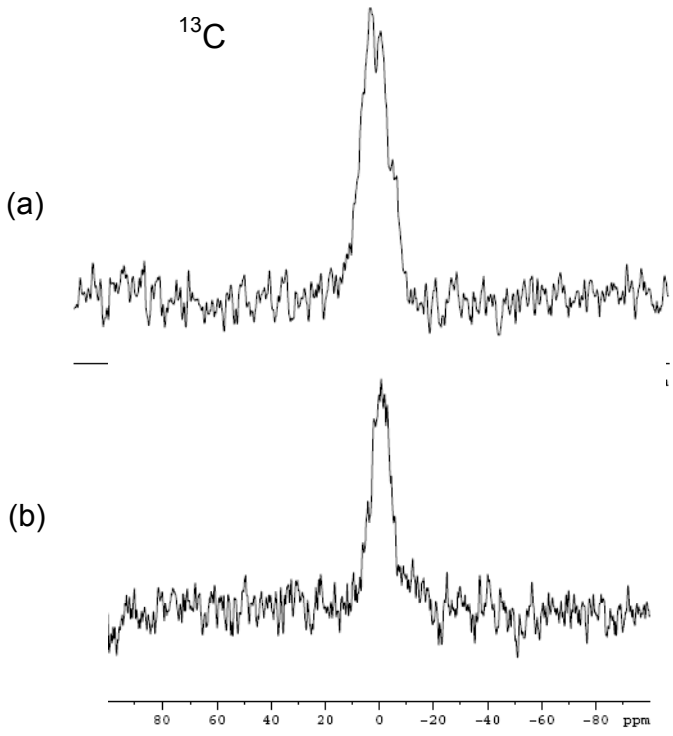

Figure D.1 ^{13}C solid state NMR spectra of nanosized porous silica samples: (a) silica after the standard 2-step reaction; (b) silica only exposed to Grignard reagent.

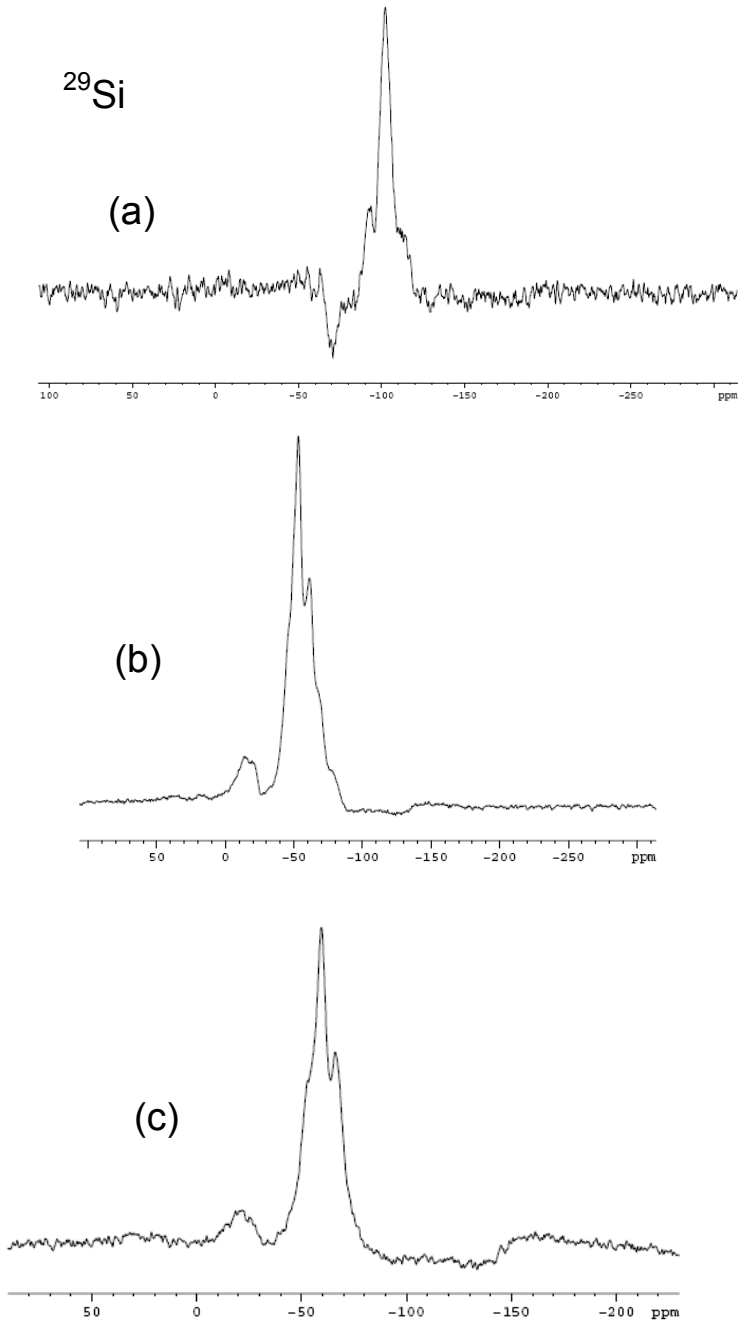

Figure D.2 ^{29}Si solid state NMR spectra of nanosized porous silica samples: (a) silica after thionyl chloride treatment; (b) silica after the 2-step Grignard treatment; (c) silica after exposure only to the Grignard reagent.

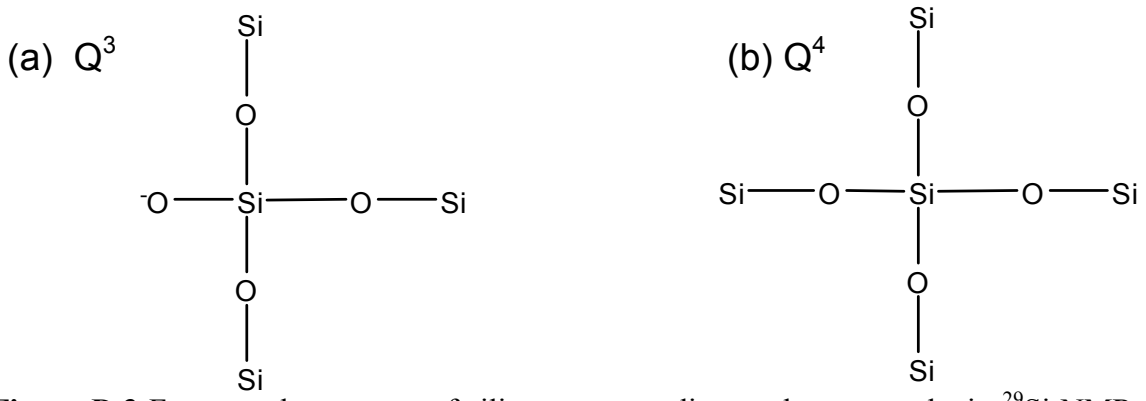

Figure D.3 Framework structure of silica corresponding to the two peaks in ^{29}Si NMR. (a) Q^3 group resonance peak at -93.6 ppm; (b) Q^4 group resonance peak at -102 ppm.

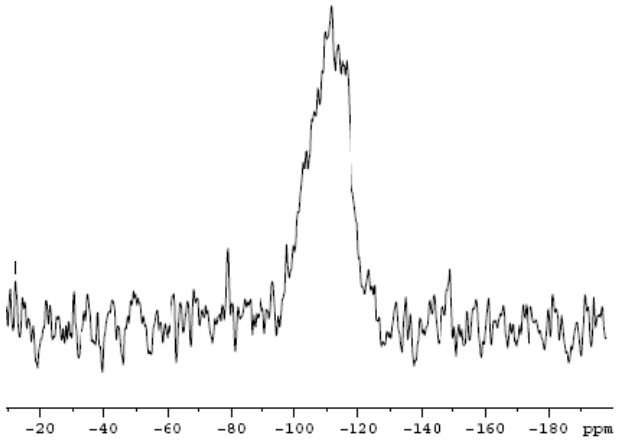

Figure D.4 ^{29}Si solid-state NMR of Grignard treated nonporous silica.

REFERENCES

[1] Bansal, A.; Li, X.; Lauermann, I.; Lewis, N. S.; Yi, S. I.; Weinberg, W. H. *J. Am. Chem. Soc*. **1996**, *118*, 7225.

[2] Bansal, A.; Lewis, N. S. *J. Phys. Chem. B* **2001**, *105*, 10266.

[3] Bansal, A.; Li, X.; Yi, S. I.; Weinberg, W. H.; Lewis, N. S. *J. Phys.Chem. B* **2001**, *105*, 10266.

[4] Kim, N. Y.; Laibinis, P. E. *J. Am. Chem. Soc*. **1998**, *120*, 4516.

[5] Engelhardt, G.; Michel, D. *High-Resolution Solid-Stte NMR of Silicates and Zeolites*; John Wiley & Sons: New York, 1987.